Stimuli-responsive Materials for Microfluidic Applications

Aishling Dunne, B.Sc

Thesis submitted for the Degree of Doctor of Philosophy

Principal Supervisors: Professor Dermot Diamond

Dr. Larisa Florea

secondary Supervisor: Dr. Aoife Morrin

Insight Centre for Data Analytics, National Centre for Sensor Research, School of Chemical Sciences, Dublin City University, Dublin, Ireland

Dublin City University August 2018

Declaration

I hereby certify that this material, which I now submit for assessment on the programme of study leading to the award of Doctor of Philosophy is entirely my own work, and that I have exercised reasonable care to ensure that the work is original, and does not, to the best of my knowledge, breach any law of copyright, and has not been taken from the work of others save and to the extent that such work has been cited and acknowledged within the text of my work.

Signed: _____

(Aishling Dunne)

Student ID No.: ___13211791_

Date: _____

Acknowledgements

Firstly I would like to say a huge thanks to Prof. Dermot Diamond for giving me this fabulous opportunity to work in this group. I will always be grateful for his guidance, support and for the many networking opportunities around the world to learn from so many leading scientists.

I also want to give a huge thanks to Dr. Larisa Florea for always believing in my scientific abilities, her willingness to share her vast knowledge and experience with me, her patience and for being such a huge support all the way through this process, I will always be very appreciative.

A big thanks goes to my fellow lab comrades both past and present. I would specifically like to thank Danielle Bruen, Jennifer Wilson, Wayne Francis and Alex Tudor, for all the science related discussions we've had, the chats, the stress-free distractions and all the fun we have had together over the last four years you have all made this an experience I will never forget.

To all those who have helped me in other ways within the Insight and NCSR centers, Thank you.

To my Mother and Father THANK YOU, for your unconditional love and belief in me when others thought I wouldn't even go to college, for always pulling me back up when I needed it, for all your encouraging words of wisdom and your undying support, I will never forget all you have done for me.

Thanks to my Husband, Darren for always being there for me, for being my best friend and for listening to all the science related problems that I was stressed about even if you didn't understand it properly.

To my granny Kitty, thank you for always helping me out in your own way and your support. To my Grandfathers Mick and Joe though you didn't see me get this far I know you would have been very supportive and proud.

Lastly, to my granny Rosie, I know you would have absolutely loved to go to college, you are my inspiration, this is for you!

Table of Contents

List of abbreviations

AA	Acrylic Acid
ACN	Acetonitrile
AMF	Alternating Magnetic Field
$CHCl_2$	Dichloromethane
DCC	Dicyclohexylcarbodiimide
DCM	Dichloromethane
DMAP	4-(Dimethylamino)pyridine
DI water	Deionised Water
DMAEMA	2-(Dimethylamino)ethyl methacrylate
DMSO	Dimethyl Sulfoxide
EtOH	Ethanol
EAM	Electro-adaptive Microfluidic
G″	Storage Modulus
G′	Loss Modulus
HCL	Hydrochloric Acid
IL	Ionic Liquid
LCST	Lower Critical Solution Temperature
LED	Light Emitting Diode
LOC	Lab on Chip
LVE	Linear Viscoelastic Range
MA	Maleic Anhydride
MAA	Methacrylic Acid
MC	Merocyanine Form
MC-H^+	Protonated merocyanine Form
M^{2+}	Divalent Metal Ion
MEOH	Methanol
NaOH	Sodium Hydroxide
NIPAAm	N-isopropyl Acrylamide
NMR	Nuclear Magnetic Resonance
NTf_2	bis(trifluoromethylsulfonyl)imide
p(NIPAAm)	Poly(N-isopropyl acrylamide)
P(HEMA-AA)	Poly(2-hydroxyethyl methacrylate-co-acrylic acid)
PAR	4-(2-pyridylazo)resorcinol
PDMS	Polydimethylsiloxane
PMMA	Poly(methyl methacrylate)

PMMA/PSA	Poly(methyl methacrylate)/ Pressure Sensitive Adhesive
PSA	Pressure Sensitive Adhesive
RIE	Reactive Ion Etching
ROMP	Ring-Opening Methathesis Polymerisation
SEM	Scanning Electron Microsocopy
SiO_2	Silicon dioxide, Silica
Si-ROMP	Surface Initiated- Ring-Opening Methathesis Polymerisation
SP	Spiropyran Form
SP-COOH	1'-(3-carboxypropyl)-3',3'-dimethyl-6-nitrospiro[2H-1]-benzopyran-2,2'-iodoline
SWCNT	Single-Walled Carbon Nanotubes
THF	Tetrahydrofuran
μTAS	Micro-Total Analysis Systems
UV	Ultraviolet
UEP	Unshared electron pair
VIS	Visible

Figure and Table Captions	
Chapter 1 (Literature Survey)	
Figure 1.1	Scheme demonstrating two methods of polymer brushes development (A) Grafting–to and (B) Grafting-from
Figure 1.2	Scheme showing the collapse and expansion of a hydrogel system
Figure 1.3	Schematic structure of spirobenzopyrans, representing the two orthogonal planes formed by two halves bonded in a spiro manner. The heterocyclic indoline part (**i**) and the benzopyran part (**ii**) of the spiropyran unit
Figure 1.4	Schematic structure of indolinespirobenzopyran (ISBP), showing the position of each atom. R' is typically CH_3, $(CH_2)_2COOH$ or phenyl while R represents a NO_2, OH or Cl group.
Figure 1.5	3D structures of the conversion of SP (left) to the MC (right) form upon UV light exposure and reversible switching from the zwitterionic MC form to the SP form upon visible light exposure.
Figure 1.6	Reversible isomerisation of spirobenzopyran (SP) to merocyanine (MC) and protonated merocyanine ($MC\text{-}H^+$).
Figure 1.7	Scheme indicating the two spatial interactions that may occur between the lone pairs on $N_{1'}$ and O_1 and antibonding (σ^*) between C_{spiro}-O and the heteroatoms. **(i)** ($n(N_1)$- $\sigma^*(C_{spiro}\text{-}O)$) is favoured compared to the Oxygen atoms lone pair (n_O) electrons interactions with the antibonding of the $C_{2',2}\text{-}N_{1'}$ bond ($\sigma^*_{C\text{-}N}$). **(ii)** ($n(O_1)$- $\sigma^*(C_{spiro}\text{-}N_1)$) determining a weakening of the $C_{spiro}\text{-}O_1$ bond and the strengthening of the $C_{spiro}\text{-}N_{1'}$ bond. (reproduced from[57]
Figure 1.8	Chemical structures of the orthogonal closed ring ISBP form and the probable merocyanine intermediate isomers (represented here by cis (C) or trans (T) configurations around the N-C=C-C, C=C-C=C and C-C=C-CO bonds) upon photo-excitation. (reproduced from [45])
Chapter 2	
Figure 2.1	Manufacture schematic: (i) patterned etch mask applied for RIE, (ii) RIE etch to define SI plates, (iii) deposit of SiO_2, (iv) deposit of Cr and Au, (v) deposit and pattern of PPy, (vi) pattern of Cr and Au, (vii) finished etching, (viii) free plates and hinge by etching SiO_2 (Adapted from Smela et al. [21]).
Figure 2.2	Schematic image of Si plate rotating on PPy/gold hinges; a) Bilayer PPy is reduced, plate lies flat. B) Bilayer PPy is partly oxidized, plate rotates out of the plane. (the electrochromic PPy is oxidised in both) (Adapted from E. Smela [28]).
Figure 2.3	Design and working principles of the stop valve incorporated into the microfluidic chip. (Adapted from Y. Tanaka et al.[29]).
Figure 2.4	Figure 2.4. Overview of the fabrication steps involved for the electro-adaptive microfluidic system, including electrode deposition onto the VHB acrylic elastomer, stacking of these actuators, casting of the PDMS passive layer, activating the PDMS substrate and passive layer via air plasma followed by bonding them, and reinforcing the inlet by casting a short PDMS strip over the inlet. (Adapted from C. Murray et al. [30]).
Figure 2.5	Figure 2.5. Scheme showing the reversible shrinking and swelling of a hydrogel based on dominant hydrophilic (left) or hydrophobic (right) interactions, respectively.
Figure 2.6	A microfluidic device demonstrating pH sensitive hydrogels working as a pH flow sorter; (a) flow of pH 4.7 is directed to the right as the p(HEMA-AA) hydrogel is in its contracted state while p(HEMA-DMAEMA) hydrogel is in its expanded state at this pH; (b) the flow is prevented due to the expansion of both hydrogels at pH 6.7; and (c) the flow is directed to the left due to the contraction of the p(HEMA-DMAEMA) hydrogel and p(HEMA-AA) hydrogel expansion at pH 7.8 (Adapted from Beebe D. et al. [13]
Figure 2.7	Schematic illustration and working mechanism of the shut-off valve; a) Diagram of the shut-off valve; b), c) top and side view, respectively, showing

	different illumination conditions.
Figure 3.5	Microscope images (magnification X60) of the hydrogel shrinking and reswelling area of the three V: V ratios ((a) 4:1, (b) 2:1 and (c) 1:1) of the THF: DI water solvent mixture.
Table 3.2	Hydrogel contraction and expansion relative areas (%) during three irradiation cycles (n=3) % area changes calculated relative to the initial area.
Figure 3.6	Photo-actuation cycles of hydrogel samples produced in the presence of different polymerisation solvent mixtures (THF: DI water (a), Dioxane: DI water (b), Acetone: DI water(c)), in real time.
Chapter 4	
Figure 4.1	Side view of in-house made cell for gel polymerisation; insets show the photomask including specific measurements of a single arc-shaped walker.
Figure 4.2	A) Schematic diagram showing the individual components of the ratcheted channel: glass slide, ratcheted channel bottom with side walls in black PMMA and PMMA back layer; Cartoon showing side (B) and front (C) views of the channel after assembly and D) Photo of the real ratcheted channel.
Figure 4.3	Chemical structure of the p(NIPAAm-co-SP-co-AA) hydrogel walkers under different illumination conditions and the physical effect it has on the gel morphology.
Figure 4.4	Series of snapshots showing the effect of light irradiation on the hydrogel walker. A) Light irradiation is initiated; B-D) Gradual reduction of inter-leg distance results in the trailing leg (right) being "dragged" over the bevel of the ratchet step.
Figure 4.5	Series of snapshots showing the walking behaviour of the hydrogel (Video S1). A – B shows contraction of the trailing leg. C – Swelling in the dark results in the forward leg being pushed over the ratchet. D – E The sequence is repeated which results in the gel achieving a unidirectional walking motion (right to left).
Figure 4.6	Photo-curing of hydrogels produced under different light irradiation times (40s, 45s and 50 s, respectively). White light polymerisation was initiated at t=60 s.
Figure 4.7	Three photo-actuation cycles of hydrogel walkers produced after 40s, 45s and 50s of light irradiation, respectively, showing the relative changes in walker area when exposed to different illumination conditions. The measurements have been done in triplicate and the error bars represent standard deviations.
Figure 4.8	Three photo-actuation cycles of hydrogel walkers produced after 40s, 45s and 50s of light irradiation, respectively, showing the relative changes in legs distance when exposed to different illumination conditions.
Figure 4.9	Three photo-actuation cycles of hydrogel walkers produced after 40s, 45s and 50s of light irradiation, respectively, showing the relative changes in legs distance when exposed to different illumination conditions.
Chapter 5	
Figure 5.1	Crystals of the norbornene-spiropyran derivative (SP) exhibiting solid-state photoisomerisation under the following conditions: (a) 1 min UV irradiation, (b) additional 1 min white light irradiation, and (c) additional 2 min white light irradiation. The strong purple colour in (a) is indicative of significant formation of the merocyanine isomer, whereas the lighter purple colour in (b) indicates co-existence of both isomers. The colourless crystals (c) indicate that the system has largely reverted to the spiropyran isomer.
Figure 5.2	Images (a–c) and UV-Vis spectra (d) of the SP solutions in ACN (1.5×10^{-3} M) in the presence of various divalent metal ions (molar ratio SP:M^{2+} 2:1); (a) initial solutions before illumination; (b) after 10 min of UV light illumination; (c) after 10 min of white light illumination; (d) UV-Vis spectra of solutions shown in (b). As it can be observed from the images (a-c) and UV-Vis spectra (d), in the current experimental conditions (M^{2+} concentration in ACN is 0.75×10^{-3} M), no absorbance band due to the presence of M^{2+} salt alone was

	observed in the visible region of the spectrum.
Figure 5.3	Absorbance changes of the SP solutions in ACN (1.5×10^{-3} M) in the presence of increasing concentrations of Co^{2+} (0–1.5 mM) after irradiation with UV light; Inset shows the linear dependence of the ratio of the absorbance at λmax ≈ 500 nm (MC:Co^{2+}) and the absorbance at λmax ≈ 570 nm (MC) as a function of concentration of Co^{2+} for concentration ranges 0–0.15 mM and 0.33–1.5 mM.
Figure 5.4	Absorbance changes of the SP solutions in ACN (1.5×10^{-3} M) in the presence of increasing concentrations of Cu^{2+} (0–1.5 mM) after irradiation with UV light; Inset shows the linear dependence of the absorbance at λmax ≈ 430 nm (MC:Cu^{2+}) as a function of Cu^{2+} concentration (0–0.8 mM).
Figure 5.5	Images (a) and absorption spectra (b) of the coated micro-capillaries when solutions of different metal ions in ACN (10^{-3} M) are passed through the micro-capillary after irradiation for 1 min with UV light.
Figure 5.6	Schematic representation of the metal ion binding, sensing, and release cycle in the SP polymeric brushes coated micro-capillary. (a) polySP coated micro-capillary before irradiation; (b) formation of polyMC upon UV irradiation; (c) binding of M^{2+} to polyMC coating; (d) photo-controlled release of M^{2+} upon white light irradiation and regeneration of polySP coating.
Figure 5.7	Absorbance at 510 nm recorded on a USB400 spectrometer over time, using the set-up depicted in Figure A3.7. Five stages (1–5) are identified as described in the text; The increase of the absorbance band centred at 510 nm indicates the presence of PAR-Co^{2+} complex; Bottom bar indicates the state of the functionalised micro-capillary as per Figure 6: (a) polySP coated micro-capillary before irradiation; (b) formation of polyMC upon UV irradiation; (c) binding of Co^{2+} to polyMC coating; (d) photo-controlled release of Co^{2+} upon white light irradiation and regeneration of polySP coating.
Chapter 6	
Figure 6.1	Schematic of the reaction of 2-(3',3'-dimethyl-6-nitrospiro[chromene-2,2'-indolin]-1'-yl)ethanol (Nitro-SP) and $\alpha \pm lipoic\ acid$ in the presence of DCC and DMAP to produce 2-(3',3'-dimethyl-6-nitrospiro[chromene-2,2'-indolin]-1'yl)-5-(1,2-dithiolan-3-yl) pentanoate (Dithiolane-SP).
Figure 6.2	Functionalisation of gold coated silicon wafer with dithiolane-SP SAMs.
Figure 6.3	Schematic of gold coated substrates functionalized with (a) 100% dithiolane-SP; (b) 1:1 (molar ratio) dithionale-SP: lipoic acid and (c) 1:3 (molar ratio) dithionale-SP: lipoic acid.
Figure 6.4	H^1-NMR spectra of, 2-(3',3'-dimethyl-6-nitrospiro[chromene-2,2'-indolin]-1'-yl)ethanol (Nitro-SP). ^{1}H-NMR ($CDCl_3$): δ 1.21 (s, 3H), 1.31 (s, 3H), 3.38 (m, 2H), 3.75 (m, 2H), 5.90 (d, 1H), 6.69 (d, 1H), 6.92 (d, 1H), 6.94 (m, 2H), 7.11 (d, 1H), 7.20 (m, 1H), 8.01 (m, 2H).
Figure 6.5	H^1-NMR spectra of . $dithiolane,$ ^{1}H-NMR ($CDCl_3$): δ 1.52 (m, 2H), 1.71 (m, 4H), 1.94 (sext, 1H), 2.41 (t, 2H), 2.49 (sext, 1H), 3.16 (m, 2H), 3.60 (sext, 1H), 5.33 (s, 2H).
Figure 6.6	H^1-NMR spectra of 2-(3',3'-dimethyl-6-nitrospiro[chromene-2,2'-indolin]-1'yl)-5-(1,2-dithiolan-3-yl)pentanoate (dithiolane-SP), ^{1}H-NMR ($CDCl_3$): δ 1.18 (d, 3H), 1.21 (m, 4H), 1.34 (m, 3H), 1.53 (m, 5H), 1.80 (sext, 1H), 2.19 (m, 2H), 2.34 (sext, 1H), 3.02 (m, 2H), 3.09 (m, 1H), 3.34 (m, 2H), 4.09 (m, 1H), 4.17 (m, 1H), 5.81 (d, 1H), 6.63 (d, 1H), 6.68 (d, 1H), 6.81 (m, 2H), 7.02 (d, 1H), 7.12 (t, 1H), 7.94 (m, 2H).
Figure 6.7	^{3}Carbon-NMR spectrum of 2-(3',3'-dimethyl-6-nitrospiro[chromene-2,2'-indolin]-1'yl)-5-(1,2-dithiolan-3-yl) pentanoate (dithiolane-SP), ^{13}C-NMR ($CDCl_3$): δ 19.85, 24.54, 25.90, 28.74, 31.00, 33.92, 38.50, 40.24, 42.39, 52.85, 56.31, 62.43, 106.74, 115.57, 118.42, 119.
Figure 6.8	The absorption spectrum of a 10^{-5} M solution of dithiolane-SP in ethanol, under different illumination conditions.
Figure 6.9	Graph depicting the solvatochromic effect of dithiolane-MC isomer that shows

Aishling Dunne

Stimuli-responsive Materials for Microfluidic Applications

Thesis Abstract:

The possibility of using photo-stimulation to perform flow control and sensing in microfluidics is very appealing as light can be applied in a non-invasive and highly precise manner. In the field of stimuli-responsive polymers, hydrogels offer a simple and effective method to fabricate three-dimensional polymeric networks whose water content can be modulated through external stimulation. By incorporating stimuli-responsive units into the gel structure, hydrogels can be actuated by external stimuli such as light, temperature and pH, among others. One of the most popular ways to achieve photo-control is through the use of photo-responsive molecules, such as spiropyrans. This thesis focuses on presenting the synthesis, characterisation and potential applications of stimuli-responsive materials based on spiropyrans, in particular as photo-controlled polymeric actuators, and photo-sensitive coatings.

Chapter 1 offers a brief overview of the field of stimuli-responsive materials and photo-responsive materials in particular, and Chapter 2 discusses possible applications of such materials in microfluidic devices. Chapter 3 describes the synthesis and characterisation of photo-responsive hydrogels based on *N*-isopropylacrylamide-*co*-acrylated spiropyran-*co*-acrylic acid (p(NIPAAm-*co*-SP-*co*-AA)) copolymer, while in chapter 4 this material is used to produce a millimetre-sized bipedal hydrogel walker. When subject to light cycles, the bipedal gel produces a walking motion by taking a series of steps in a given direction. Chapter 5 focuses on spiropyran polymeric brushes as coatings in micro-capillaries and confirms their potential for metal ion binding, sensing and release. Chapters 6 focuses on the synthesis and surface functionalisation of other spiropyran derivatives and describes future work in the area of photo-responsive materials and hydrogels.

List of Publications

Peer-Reviewed Journal Articles

[1] *"***Solvato-Morphologically Controlled, Reversible Photo-Actuated Hydrogels, Operative In Neutral Environments**" Aishling Dunne, Colm Delaney, Larisa Florea, Dermot Diamond. *RSC Adv.,* 2016, 6, 83296-83302.

[2] **"Spiropyran Based Hydrogels Actuators - Walking in the Light"** Wayne Francis, Aishling Dunne, Colm Delaney, Larisa Florea, Dermot Diamond, *Sensors and Actuators B: Chemical*, 2017, 250, 608–616.

[3] *"***Thiol-ene photo-click collagen-PEG hydrogels: impact of water-soluble photoinitiators on cell viability, gelation kinetics and rheological properties***",* Roisin Holmes, Xuebin B Yang, Aishling Dunne, Larisa Florea, David Wood, Giuseppe Tronci, *Polymers* 2017, *9*, 226.

[4] *"***Micro-capillary Coatings Based on Spiropyran Polymeric Brushes for Metal Ion Binding, Detection and Release in Continuous Flow***"* Aishling Dunne, Colm Delaney, Aoife McKeon, Pavel Nesterenko, Brett Paull, Fernando Benito-Lopez, Dermot Diamond, Larisa Florea*, Sensors 2018, 18(4), 1083 – 1095.*

[5] **"Reversible photochromic polynorbornenes bearing spiropyran side groups for layer-by-layer coatings"** Paula Campos, Aishling Dunne, Colm Delaney, Cara Moloney, Simon Moulton, Fernando Benito-Lopez , Marystela Ferreira, Dermot Diamond and Larisa Florea*, Langimur 34 (2018), 4210–4216.*

Book Chapter

[1] *"***Stimuli-controlled fluid control and microvehicle movement in microfluidic channels**" Aishling Dunne, Wayne Francis, Colm Delaney, Larisa Florea, Dermot Diamond, *In Reference Module in Materials Science and Materials Engineering,* Elsevier: 2017, ISBN 978-0-12-803581-8

Peer-Reviewed Conference Proceedings

[1] *"***Biocompatible, reversible photo-actuated hydrogels, operative in neutral environments, for micro-valve applications in microfluidic devices***,"* Aishling Dunne, Larisa Florea, Fernando Benito-Lopez and Dermot Diamond, *15th International Conference on Miniaturized Systems for Chemistry and Life Sciences,* San Antonio, Texas, USA, 26th-30th October 2014.

[2] *"***Solvato-Morphologically Controlled, Reversible Photo-Actuated Hydrogels, Operative in Neutral Environments***,"* Aishling Dunne, Larisa Florea, and Dermot Diamond, *18th International Conference On Solid-State Sensors, Actuators And Microsystems, Transducers,* Anchorage, Alaska, USA, 21st-25th June 2015.

Conference Contributions

(presenting author is underlined)

Oral Presentations

[1] **"Solvato-morphologically controlled photo-actuated hydrogel"** Aishling Dunne, Larisa Florea* and Dermot Diamond*, RACI National Congress,* Adelaide, Australia, 7th-12th December 2014.

[2] **"Photo-responsive hydrogels with enhanced volume changes due to local pH alterations"** Aishling Dunne, Joseph Hennessy, Siobhán Mac Ardle, Larisa Florea and Dermot Diamond, *4th Edition Conference Analytical and Nanoanalytical Methods for Biomedical and environmental Sciences*, Transylvania University of Brasov, Romania, 29th June – 1st July 2016.

Poster Presentations

[1] **"Photo-responsive bipedal hydrogels walking in the light"** Aishling Dunne, Wayne Francis, Colm Delaney, Larisa Florea and Dermot Diamond, *69th Irish Universities Chemistry Research Colloquium,* Dublin City University, Dublin, Ireland, 22nd – 23rd June 2017.

[2] **"Bipedal hydrogels walking in the light"** Aishling Dunne, Wayne Francis, Colm Delaney, Larisa Florea and Dermot Diamond*, School of Chemical Sciences, Chemistry Day*, Dublin City University, Dublin, Ireland, 12th May, 2017.

[3] **"pH and Photo-responsive hydrogel actuators"** Aishling Dunne, Siobhan Mac Ardle, Joseph Hennessy, Siobhán Mac Ardle, Larisa Florea and Dermot Diamond*, The 20th International Conference on Miniaturized Systems for Chemistry and Life Sciences, µTas 2016*, Dublin, Ireland, 9th - 13th October 2016.

[4] *"***Photo-responsive materials functionalised with spiropyran derivatives***"* Aishling Dunne, Wayne Francis, Siobhán Mac Ardle, Joseph Hennessy, Larisa Florea and Dermot Diamond, *68th Irish Universities Research Chemistry Colloquium,* University College Cork, Cork, Ireland, 23rd-24th June 2016.

[5] **"Photo-acid generator comonomer turns pH-responsive into photo-responsive hydrogels***"* Aishling Dunne, Joseph Hennessy, Larisa Florea and Dermot Diamond*, 8th Conference on Analytical Science Ireland (CASi),* Dublin City University, Dublin, Ireland, 14th-15th April 2016.

[6] **"Stimuli-responsive hydrogels based on acrylic acid and acrylamide"** Aishling Dunne, Siobhán Mac Ardle, Larisa Florea and Dermot Diamond*, Insight Student Conference,* Bailey Allen hall, NUI Galway, Galway, Ireland, 30th October 2015.

[7] **"pH-induced shrinking an swelling of hydrogels based on copolymers of acrylic acid and acrylamide"** Aishling Dunne, Siobhán Mac Ardle, Larisa Florea and Dermot Diamond, *Nanonet Conference 2015,* Limerick, Ireland, 21st – 22nd October 2015.

[8] **"Biomimetic microfluidics and stimuli-responsive materials: the key to realising chemical sensing platforms with revolutionary capabilities",** Larisa Florea, Wayne Francis, Aishling Dunne, Alexandru Tudor, and Dermot Diamond, *Royal Society of Chemistry Analytical Research Forum* 2015, London, UK, 3rd July 2015.

[9] **"Solvato-Morphologically Controlled, Reversible Photo-Actuated Hydrogels, Operative In Neutral Environments."** Aishling Dunne, Larisa Florea and Dermot Diamond, *18th International Conference On Solid-State Sensors, Actuators And Microsystems, Transducers,* Anchorage, Alaska, 21st-25th June 2015.

[10] **"The exciting potential of stimuli-responsive materials and biomimetic microfluidics"**, Larisa Florea, Wayne Francis, Simon Coleman, Aishling Dunne and Dermot Diamond, *EuroNanoForum Sensors Workshop*, Riga, Latvia, 10th -12th June 2015.

[11] **"Stimuli-responsive materials and biomimetic fluidics: key building blocks of futuristic autonomous chem/bio-sensing platforms",** Dermot Diamond, Larisa Florea, Wayne Francis, Simon Coleman, and Aishling Dunne, *Invited Seminar, University of Pisa*, 27th May 2015.

[12] "**Biomimetic Microfluidic Systems Incorporating Photoswitchable Building Blocks**" Larisa Florea, Aishling Dunne, Wayne Francis, And Dermot Diamond, *Cost Action Mp 1205 Advances In Optofluidics: Integration Of Optical Control And Photonics With Microfluidics*, Porto, Portugal, 7th-8th May 2015.

[13] "**Solvato-Morphologically Controlled Photo-Responsive Hydrogels For Micro-Valve Applications"**, Aishling Dunne, Larisa Florea and Dermot Diamond, *1st Brazil, Ireland Science Week*, Dublin, Ireland, 23rd-26th February 2015.

[14] **"Biocompatible, reversible photo-actuated hydrogels, operative in neutral environments, for micro-valve applications in microfluidic devices"**, Aishling Dunne, Wayne Francis, Larisa Florea*, Fernando Benito-Lopez and Dermot Diamond, *MicroTAS,* San Antonio, Texas, 26th-30th October 2014.

[15] **"Photo-responsive polymers based on spiropyran as sensors and actuators"**, Larisa Florea, Aishling Dunne, Hillary Straub, Siobhán MacArdle, and Dermot Diamond, *SBPMat Brazil MRS Meeting*, João Pessoa, Paraíba, Brazil, 28th Sept – 2nd Oct 2014.

[16] **"Reversible photo-actuated hydrogels for micro-valve applications"**, Aishling Dunne, Wayne Francis, Larisa Florea*, Dermot Diamond, *Insight Student Conference*, Dublin, Ireland, 12th September 2014.

[17] **"Photo-responsive soft actuators based on spiropyran functionalised hydrogels"**, Aishling Dunne, Larisa Florea*, Dermot Diamond, *CIMTEC, 6th Forum on New Materials*, Montecatini Terme, Italy, 15th-20th June 2014.

[18] **"Stimuli-responsive materials as sensors and actuators in microfluidic devices"**, Larisa Florea, Aishling Dunne and Dermot Diamond, *2014 Ireland-China ISCP Consortium Symposium on Nanoscience*, Dublin, Ireland, 12th-14th May 2014.

[19] **"Using molecular photoswitches to build functionality for microfluidic systems"**, Larisa Florea, Wayne Francis, Aishling Dunne, and Alexandru Tudor and Dermot Diamond, *COST Action MP 1205 Advances in Optofluidics: Integration of Optical Control and Photonics with Microfluidics*, Dublin Institute of Technology, 24th-25th Apr 2014.

[20] **"Stimuli-controlled fluid movement at the microscale"**, Aishling Dunne, Wayne Francis, Larisa Florea, Dermot Diamond, *COST Action MP1205 Meeting - Advances in Optofluidics: integration of optical control and photonics with microfluidics*, Dublin, Ireland, 24th-25th April 2014.

Overall Aim and Thesis Structure

Selected Publications and Author contribution

This thesis includes one literature review chapter, a published review chapter, three original papers published in peer reviewed journals and a future work chapter. The main theme of this thesis is the development of stimuli-responsive materials in particular photo-responsive materials as sensors and actuators for inclusion in microfluidic devices.

In the case of Chapters 2-5, my contribution to the work was as follows:

Thesis Chapter	Publication title	Publication Status	Nature and extent of Candidate's contribution
2	**Stimuli-induced Fluid Control in Microfluidic Channels**	Published *The Reference Module in Materials Science and Materials Engineering, 2017.*	Author, manuscript development and writing up
3	**Solvato-Morphologically Controlled, Reversible NIPAAm Hydrogel Photoactuators**	Published *RSC Advances, 2016, 6, 83296 – 83302.*	Main-author, key ideas, experimental design, data generation and analysis, manuscript development and writing up.
4	**Spiropyran Based Hydrogels Actuators - Walking in the Light**	Published *Sensors and Actuators B. Chemical, 2017, 250, 608–616.*	Shared first author, key ideas, data generation and analysis, manuscript development and writing up.
5	**Micro-capillary Coatings Based on Spiropyran Polymeric Brushes for Metal Ion Binding, Detection and Release in Continuous Flow**	Published *Sensors, 2018, 18(4), 1083 – 1095.*	Main-author, key ideas, experimental design, data generation and analysis, manuscript development and writing up.

Signed: _____ _____

(Candidate) (Principal Supervisor)

Florea

(Principal Supervisor)

Date _____

Chapter Overview

Chapter 1: Literature Survey

This introductory chapter discusses how research into microfluidics has become of great interest, with many researchers attempting to generate and control flow in micro-sized devices through the incorporation of stimuli-responsive materials. Stimuli-responsive materials offer the possibility to externally control fluid flow. Although there are many types of stimuli-responsive materials, the main focus of this chapter is on photo-responsive materials, in particular photo-responsive materials based on spiropyrans switches.

Chapter 2: Stimuli-induced Fluid Control in Microfluidic Channels

This review chapter discusses the use of stimuli-responsive materials incorporated into microfluidic systems, providing a means to locally manipulate flow at the microscale, in a non-invasive manner, while also reducing system complexity. Importantly, there are several modes of stimulation being discussed, including electrical, magnetic, photo and thermal, among others. The chapter describes means of achieving control of flow through stimuli-induced actuation of microfluidic components (valves, pumps, mixers, flow sorters) that are most often fabricated from soft polymeric materials. The focus of this chapter is to identify and compare the similarities and underlying mechanisms employed in the current state of the art research in stimuli-induced fluid control.

Chapter 3: Solvato-Morphologically Controlled, Reversible NIPAAm Hydrogel Photoactuators

In this work, published as an original article, photo-actuator hydrogels were generated using a N-isopropylacrylamide-*co*-acrylated spiropyran-*co*-acrylic acid (p(NIPAAm-*co*-SP-*co*-AA)) copolymer, in 100-1-5 mole ratio. Different ratios of deionised water: organic solvent (tetrahydrofuran, dioxane and acetone) were used as the polymerisation solvent. We successfully demonstrated that the polymerisation solvent had a significant effect on the curing time, the elasticity and morphology of

the resulting hydrogel. To our knowledge, this was the largest reported photo-induced area change for self-protonated spiropyran containing hydrogels to date. The shrinking/reswelling process was completely reversible in DI water with no detectable hysteresis over three repeat irradiation cycles.

Chapter 4: Spiropyran Based Hydrogels Actuators - Walking in the Light

Herein we report on the synthesis of a bipedal hydrogel walker, based on *N*-isopropylacrylamide-*co*-acrylated spiropyran-*co*-acrylic acid p(NIPAAm-*co*-SP-*co*-AA). Due to the presence of the photochromic spiropyran molecule in the polymer structure, these hydrogels reversibly shrink and swell in aqueous environments when exposed to different light conditions. When placed onto a ratcheted surface, the actuation of the bipedal gel produces a walking-like motion by taking a series of steps in a given direction, as determined by the optimised design of the ratchet scaffold. We anticipate that such biomimetic hydrogel walkers could form the basis of light-actuated soft robots capable of more advanced functions such as autonomous migration to specific locations accompanied by triggered release of molecular cargo.

Chapter 5: Micro-capillary Coatings Based on Spiropyran Polymeric Brushes for Metal Ion Binding, Detection and Release in Continuous Flow

Micro-capillaries, capable of light-regulated binding and sensing of divalent metal ions in continuous flow, have been realised through functionalisation with spiropyran photochromic brush-type coatings. Upon irradiation with UV light, the coating switches from the passive non-binding spiropyran form to the active merocyanine form, which binds different divalent metal ions (Zn^{2+}, Co^{2+}, Cu^{2+}, Ni^{2+}, Cd^{2+}), as they pass through the micro-capillary. Furthermore, the merocyanine visible absorbance spectrum changes upon metal ion binding, enabling the ion uptake to be detected optically. Irradiation with white light causes reversion of the merocyanine to the passive spiropyran form, with simultaneous release of the bound metal ion from the micro-capillary coating.

Chapter 6: Future work

This chapter suggests a few potential future pathways of the work presented in this thesis. Several new approaches for the creation of novel materials incorporating spiropyran derivatives for different applications are proposed

Chapter 1

Literature Survey

Chapter 1: Literature Survey

Stimuli-responsive Polymeric Materials as Integrated Photo-Actuators in Micro-Fluidic Devices

1.1 Microfluidics and Lab on a Chip Devices

In general, a microfluidic system deals with the conduct, accurate control and operation of fluids that are forced through micro/nano-litre scale channels [1]. One area that has emerged from microfluidics is the generation of micro-scaled Lab on a Chip (LOC) devices which are also known as micro total analysis systems (μTAS). These devices continue to be developed and produced to execute difficult laboratory tasks on a single device on a small scale [2]. Manufacture of microfluidic devices can be realised by using a variety of technologies and with a large array of materials, such as silicon and glass, together with a wide range of polymers in particular polydimethylsiloxane (PDMS) and poly(methyl methacrylate) (PMMA).

The continued research into microfluidics has enabled several chemical and biological applications that require micro-nano litre scales [3-5]. Unfortunately, to date a disadvantage within microfluidics research in the necessary macro-scaled power supplies, control systems and sensing elements that microfluidic systems depend upon. Consequently, a solution to replace microfluidic sensing elements with stimuli-responsive materials has been in focus in recent years. Using stimuli-responsive materials in this manner has enabled non-invasive externally controlled fluid manipulation with in a LOC device [6-8]. The use of these materials in LOC devices is enabling a tremendous reduction in the complexity of the microfluidic system allowing full processes to occur safely on the developed device. These stimuli-responsive materials have been used as micro-valves [9], mixers [10] and pumps [11] in the channels of a LOC device for fluid manipulation [6]. Furthermore, more recently, stimuli-responsive materials have been successfully applied as coatings for the detection of a specific analytes [12,13]. A variety of stimuli-responsive materials and their applications will be discussed within this thesis.

1.2 Surface Functionalisation

One of the most common approaches for surface functionalization involves the use of self-assembled monolayers (SAMs). As most microfluidic systems are composed of glass, silicon or PDMS, chemical derivatives of trichlorosilanes [14], trimethoxysilanes [15] and triethoxysilanes [16] that have a functional group on one end of the molecule have been largely used for SAM coatings. The creation of a

SAM coating is easily obtained for microfluidic devices as only a flow of gas or a solution passing through the channels of the devices is required to interact with the –OH groups on the walls of the channels [17]. SAMs have been widely researched and have been successfully generated on both flat surfaces and microfluidic devices for a variety of uses.

SAMs can also be used for subsequent attachment of polymer brushes. With the large variety of silanization agents available, it has become easier to conveniently tether the polymer brush to a surface. Polymer brushes are bound at one end to a surface while the other end is free. When a high density of polymer brushes is present in one area, a steric repulsion between the brushes occurs causing the chains to stretch/elongate and give the brush-like conformation.

There are two common methods for chemical grafting of polymer brushes, namely "grafting-to" and "grafting-from". "Grafting-to" can be achieved when the functionalised end of a polymer can interact with a matching functional group found on the surface forming an anchored chain (Figure 1.1(a)). One benefit of this method is that it can be achieved with relative ease on flat surfaces via spin/dip coating in a suitable polymeric solution. However, the disadvantage to this method is that there is a limited number of "binding sites" resulting in low graft densities [18].

In the case of the second method, "grafting-from", the polymerisation starts from the initiating groups previously bound to the surface. The selected monomer then infiltrates through the already grafted polymer layer (much easier compared to the "grafted-to" method) resulting in a high-density layer of polymer brushes (Figure 1.1(b)). This method takes advantage of some of the controlled polymerisation techniques such as; ring-opening-metathesis polymerisation (ROMP) [19,20] or atom-transfer-radical-polymerisation (ATRP) [21], among others.

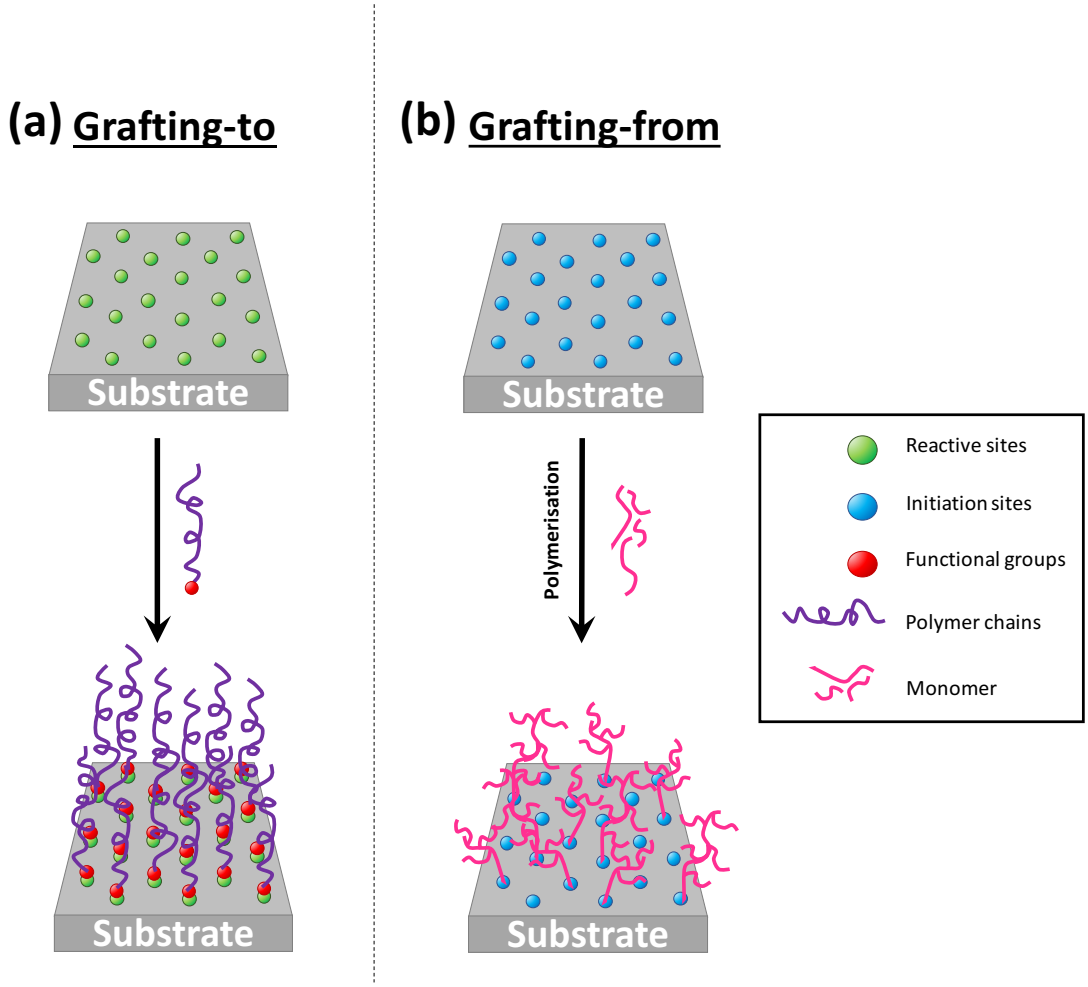

Figure 1.1. Scheme demonstrating two methods of polymer brushes development; (a) Grafting–to and (b) Grafting-from. Adapted from [22-24].

1.3 Hydrogels

Hydrogels are defined as hydrophilic three-dimensional colloidal polymeric materials that are able to uptake and withhold large quantities of aqueous solutions with relation to their physical size [3,25]. This hydrophilic character of hydrogels is a result of the strong interactions between water molecules and the polymer chains hence a high degree of water absorption. However, this ability for a hydrogel to absorb relatively large quantities of water can be altered or controlled by adding a hydrophobic element inside the hydrogel arrangement. Such hydrophobic units will enable polymer-polymer interactions to occur, initiating the expulsion of water molecules and causing the polymer network to collapse. As a result, the ability of the hydrogel to absorb relatively large volumes of water is dependent on the proportion of

hydrophilic (water-polymer) to hydrophobic (polymer-polymer) interactions. It can be said that when the hydrophilic interactions are prevalent, the polymer interacts with the surrounding water molecules through hydrogen bonding causing the hydrogel to swell (Figure 1.2(a)). The opposite can be concluded when the hydrophobic interactions are established, resulting in the expulsion of water and initiating the hydrogel to shrink (Figure 1.2 (b)).

By altering the proportions of the hydrophilic and hydrophobic units inside a hydrogel matrix, the resulting expanding and contracting of the hydrogel can be controlled. For many polymers, the hydrophilic/hydrophobic nature can be switched with the application of one or more types of stimuli, for example thermal, electric, pH (chemical) or photo stimuli among others, enabling the realisation of a vast number of stimuli –responsive hydrogels.

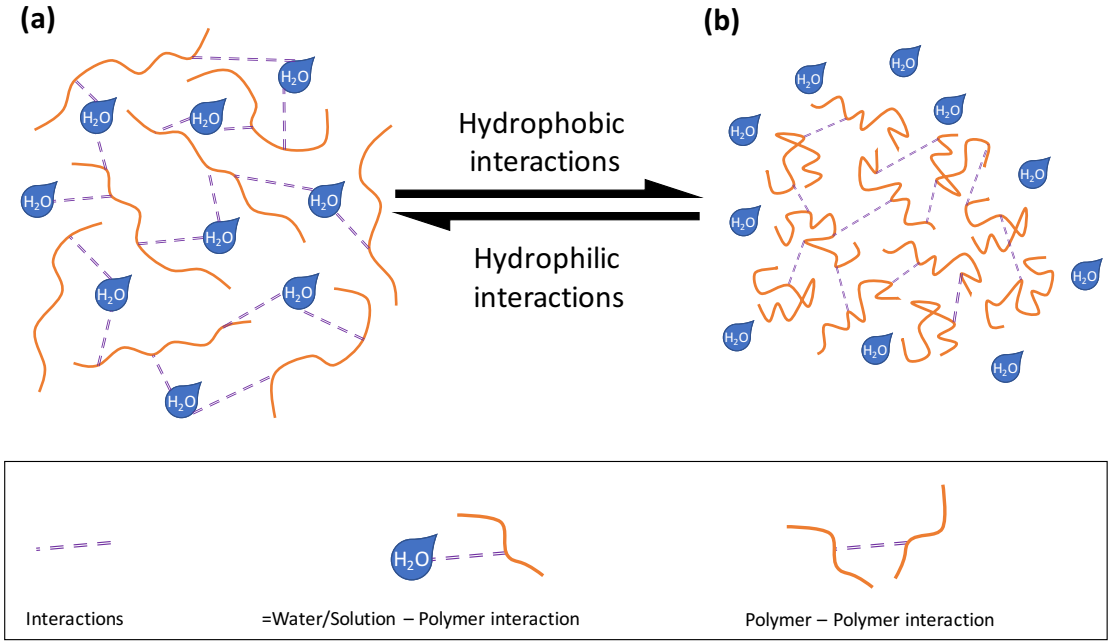

Figure 1.2. Scheme showing the reversible collapse and expansion of a hydrogel system due to dominant (a) hydrophilic water-polymer interactions and (b) hydrophobic polymer-polymer interactions.

Such stimuli-responsive hydrogels have been largely studied, in particular for applications in microfluidics due to the straight-forward fabrications and integrations into such platforms and due to the aptitude of working in aqueous media [7,26,27]. The expansion and contraction of hydrogels is a diffusion-controlled process; when incorporated into a microfluidic platform, this can potentially reduce the diffusion

path-lengths and due to constant flow can improve the time taken for the hydrogels to respond to the relevant stimuli [28,29]. A detailed description of different stimuli-responsive hydrogels, their actuation mechanism and their inclusion in to microfluidic devices is presented in Chapter 2 of this thesis. However, in the interest of this work, the following sections will focus on materials that are responsive to light of different wavelengths.

1.4 Photo-responsive Materials

1.4.1 Overview

Photo-responsive materials have gained a lot of interest in recent years, as photo-stimulus is non-invasive and requires no contact with the responsive material [26].

A photo-responsive material requires the presence of a photochromic molecule within the polymeric material and it is usually integrated by non-covalent doping or through covalent attachment. Photochromic units exhibit an isomeric change between two or more isomers of different properties (*e.g.* polarity, hydrophilic/hydrophobic character, geometry and charge density) when exposed to light of specific wavelengths.

There are many different photochromic units available but three of the most well-known families include spirobenzopyrans [30-32] azobenzenes [33,34], and diarylethenes [35,36]. All three of these molecular families have been widely studied and show reversible photochromic behaviour, transforming from one isomer to another when exposed to alternating wavelengths of light.

In the interest of this discussion, spirobenzopyrans will be the main focus of the following section of this report [37].

1.4.2 Photochromism

Photochromism is defined as a reversible transformation of a chemical species between two isomers due to the absorption of electromagnetic radiation, resulting in a different absorption spectra of each isomeric form [38]. Such chemical species will not only have specific absorption spectra for each isomer form but will also exhibit changes in chemical and physical properties including changes in refractive index, colour and dielectric constant, among others [39].

The isomerisation of many light sensitive compounds in polymer systems offer external results like colour change, shape or size changes, among others, which has allowed these materials to be used in a variety of applications such as sensors [40], medical devices [41], drug delivery systems [42], bio-sensors [43] and for other novel functions [36,44-46].

Among all the different photochromic families, spiropyrans are one of the most studied, due to their clear colour change, relative high photo-sensitivity, potential binding sites for different species including metal ions [47] and the quick switching from one isomer to the other when exposed to alternating light conditions (UV/Vis).

1.4.2.1 Spirobenzopyrans

In 1952 Fischer and Hirshberg were the first to discover the photochromic properties of the spirobenzopyran family [31]. After exposing many spirobenzopyran solutions to light irradiation of different wavelengths, a reversible colour change was observed.

Spiropyrans are generally referred to as a 2H-1-benzopyran (substituted) with a second ring system that is largely heterocyclic but not always. This is attached in a spiro manner to the 2-carbon of the pyran with a common tetrahedral carbon atom [45]. In the spiropyran structure, the two halves of the molecule, the indoline part and the benzopyran part, are present in orthogonal planes bonded at the common tetrahedral sp^3 hybridised carbon atom (Figure 1.3).

The benzopyran section (Figure 1.3 (ii)) is commonplace in the structure of all spiropyrans excluding alternative substituents on the aromatic rings. However, the heterocyclic section (Figure 1.3 (i)) is inconsistent and is often built upon mono or bi-heteroatomic azaheterocycles saturated or benzofused [38].

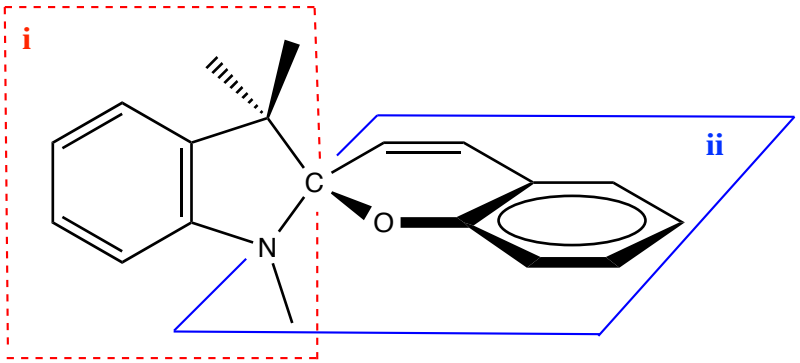

Figure 1.3. Schematic structure of spirobenzopyrans, representing the two orthogonal planes formed by two halves bonded in a spiro manner. The heterocyclic indoline part ***(i)*** *and the benzopyran part* ***(ii)*** *of the spiropyran unit [38].*

In the interest of this report, a certain class of spiropyrans; indolinespirobenzopyran (ISBP) will be the focus of this discussion (Figure 1.4).

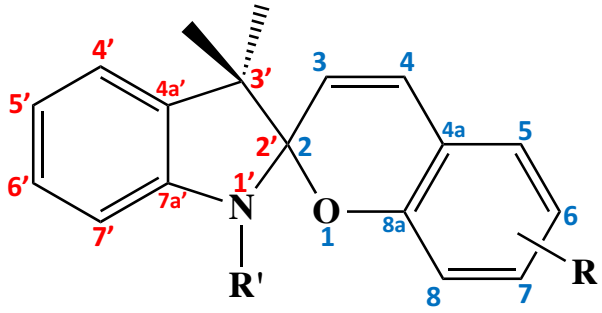

Figure 1.4. Schematic structure of indolinespirobenzopyran (ISBP), showing the position of each atom. R' is typically CH_3, $(CH_2)_2COOH$ or phenyl while R represents a NO_2, OH or Cl group.

In general, spiropyrans can undergo both "positive" and "negative" photochromism [48]. In "positive" photochromism, the thermodynamically less stable state is strongly coloured upon UV illumination and thermally fades back to the original colourless spiropyran form. However, those spiropyrans that contain free hydroxyl, amine or carboxyl groups on either ring can also demonstrate "negative" photochromism which is when the material appears strongly coloured in the dark and reversibly fades when exposed to UV illumination. Photochromism of spiropyrans is observed in solution and solvated polymeric systems (including hydrogels) and very rarely observed in the solid state unless under specific environmental conditions [49].

The isomerisation that occurs in the spirobenzopyran family is the reversible transformation from the spirobenzopyran (SP) isomer to the merocyanine (MC) form.

Spiropyran ('spiro') is a closed ring form that is non-polar, less hydrophilic, colourless and orthogonal in structure. Merocyanine is an open ring form that is polar, more hydrophilic, strongly coloured, conjugated and planar in structure. Upon UV light exposure (~355nm) the colourless closed SP form will transform to the more hydrophilic conjugated pink-purple MC form (zwitterion). This transformation is due to the heterolytic cleavage of the carbon-oxygen (C_{spiro}-O) bond in the spiropyran form. Thus, the sp^3 hybridised spiro carbon becomes sp^2 hybridised, rising in the aromatic groups to swivel making the π–orbitals align changing the structure from orthogonal to planar (Figure 1.5). The newly conjugated bonds enable an ability to absorb photons of visible light causing the MC form to become strongly coloured. When the same material is exposed to visible light (~420nm) or increased temperature, the MC form will transform back to the colourless SP form as the molecules relax back to the ground state and the C-O bond reforms returning to the sp^3 hybridised carbon making the structure orthogonal once more (Figure 1.5) [45].

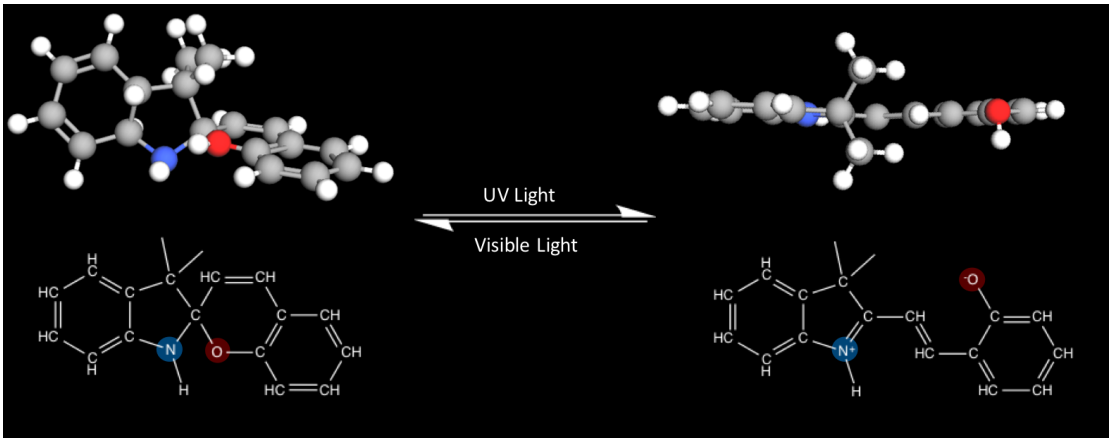

Figure 1.5. 3D structures of the conversion of SP (left) to the MC (right) form upon UV light exposure and reversible switching from the zwitterionic MC form to the SP form upon visible light exposure.

In the presence of available protons, protonation of the negatively charged phenol group in the photochromic MC form will occur, resulting in the more hydrophilic protonated merocyanine form (MC-H^+). When this MC-H^+ is exposed to visible light (~420nm), deprotonation will occur reverting the structure back to the less hydrophilic spiropyran form (Figure 1.6) [50-52]. This property has made spiropyrans the useful in the development of reversible micro-valves [53,54] and sensors [55,56].

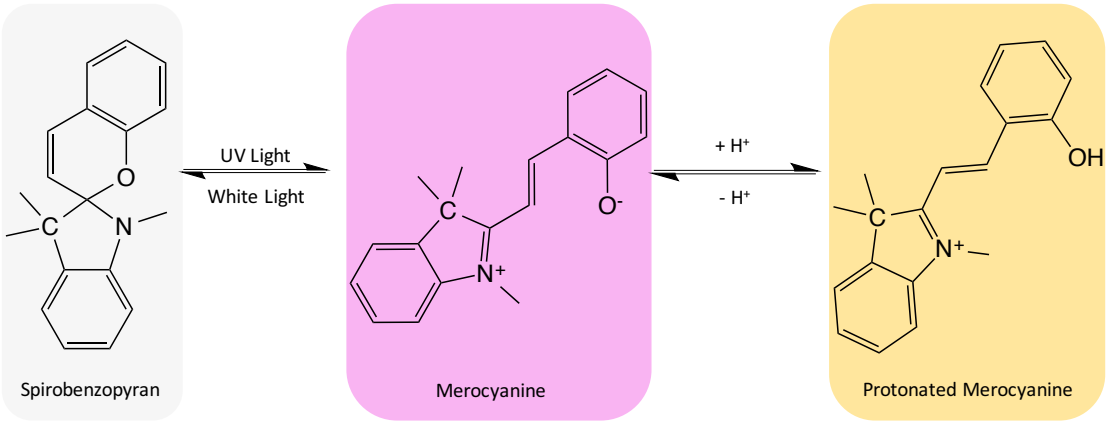

Figure 1.6. Reversible isomerisation of spirobenzopyran (SP) to merocyanine (MC) and protonated merocyanine (MC-H$^+$).

The photochromism of the spiropyran molecule is largely dependent on a few factors; the energy and polarity of the spiro carbon – oxygen (C_{spiro}–O) bond; the charge distribution on the benzopyran ring in particular due to the electron withdrawing/donating substituents in ortho- (C_8) and para- (C_6) positions relative to the oxygen atom; and the extent of the interactions between the indoline and pyran sections of the spirobenzopyran structure [57,58].

All of these affect the spiropyrans properties and are specifically dependant on the spiropyran initial structures. To truly understand the behaviour of photochromic spiropyrans it is important to focus on certain interactions and structural features of the indoline-spirobenzopyrans (ISBP), particularly in their ground state. In doing this an understanding of why spiropyrans exhibit photochromism and unveiling what is importantly influencing this behaviour will be uncovered.

X-ray studies performed on spiropyran structures in their ground states have revealed that within the indoline- spiropyran structure the spiro-carbon (C-$_{spiro}$) is joint covalently to the indoline nitrogen atom and to the benzopyran oxygen atom. These studies have also unveiled how the indoline section is indeed at a right angle to the benzopyran section making the structure orthogonal.

Within the indoline section there is a dihedral angle in the range of 23-30° found at $N_{1'}$-C_{spiro}-C_3 (Figure 1.4). This specific structure of an indoline heterocycle is largely caused by the pyramidal configuration of the nitrogen atom thus reducing the conjugation between the unshared lone pair (UEP) on the nitrogen atom and the π-orbitals of the benzopyran section. The UEP of the nitrogen atom has a sp^3 character,

when the N atom is positioned perpendicularly to the plane formed by the initial carbon of the R' substituent (C_{7a} and $C_{2',2}$ atoms).

However, the oxygen atom UEP's are not equivalent as both π– and σ–orbital characters exist with different configurations; the UEP of the σ–electron density is in the plane of the (Spiro) $C_{2',2} - O_1 - C_{8a}$ atoms but the UEP of the π-electron density transpires perpendicularly to the same plane. By having a SP structure like this, the C_{spiro}-O_1 bond of the heterocyclic pyran occupies a trans-position relative to the UEP of the $N_{1'}$ atom whereas in the indoline heterocycle the C_{spiro}-$N_{1'}$ bond is also in a trans-position but in relation to the π–UEP of the O_1 atom. Due to the nature of this type of structure in SP, specific orbital interactions can happen between the electronegative heteroatoms and the UEP of the $N_{1'}$ and O_1 atoms that are bonded to the chiral sp^3 carbon atom. This type of interaction can also be labelled as an *n* -σ* interaction, which is between the UEP (*n*) of the heteroatom and the antibonding σ* orbital of an adjacent polar bond mainly located on the spiro carbon atom.

As the electronegativity of the oxygen is larger than that of the nitrogen atom, the UEP (*n*) energy of the oxygen atom is lower than that of the UEP (*n*) energy of the nitrogen atom and the antibonding orbital of the C_{spiro}-O (σ^*_{C-O}) bond is lower in energy than the antibonding orbital od the C_{spiro}–N (σ^*_{C-N}) bond. Thus, the interactions between the *n*–electrons of the N atom and the σ*-orbital of the C_{spiro}-O bond are significant in the spiro centre.

As a consequence, the population of the antibonding orbital of the C_{spiro}-O- bond, this interaction ought to result in a strengthening of the C_{spiro}–N bond and weaken the C_{spiro}–O_1 bond, which would appear as a contraction and elongation of these bonds, respectively (Figure 1.6). Studies have should that the 'normal' length of a C (sp^3) - N(sp^3) bond in a five-membered heterocyclic ring are in the range of 1.47-1.48 Å. However, from the work carried out by Aldoshin *et al*. [57,58] the bond length of the C_{spiro}-$N_{1'}$ bond is actually in the range of 1.43-1.45 Å, which is considerably shorter. While the C_{spiro}-O_1 bond was found to be considerably longer (1.45-1.49 Å) than that of the average C-O bond length being in the range of 1.41-1.43 Å. The variation in the C_{spiro}–O_1 bond length is detrimental to the photochromic behaviour of the molecule, as spiropyran structures with C_{spiro}–O_1 bond length higher than 1.42 Å do undergo photochromism while those with a bond length lower than 1.42 Å do not [45].

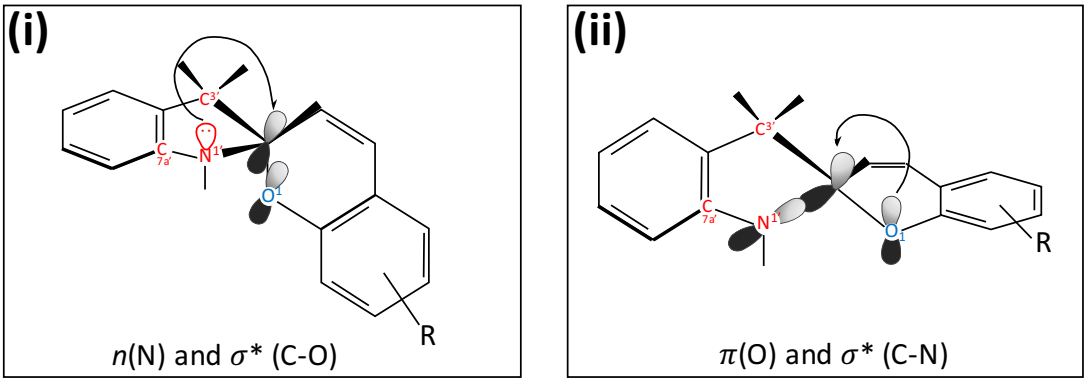

Figure 1.7. Scheme indicating the two spatial interactions that may occur between the lone pairs on $N_{1'}$ and O_1 and antibonding (σ) between C_{spiro}-O and the heteroatoms.* ***(i)*** *($n(N_1)$-$\sigma^*(C_{spiro}$-$O)$) is favoured compared to the oxygen atoms lone pair (n_O) electrons interactions with the antibonding of the $C_{2'2}$-$N_{1'}$ bond ($\sigma^*_{C\text{-}N}$).* ***(ii)*** *($n(O_1)$- $\sigma^*(C_{spiro}$-$N_1)$) determining a weakening of the C_{spiro}-O_1 bond and the strengthening of the C_{spiro}-$N_{1'}$ bond. (reproduced from [57].)*

In these circumstances, UV light photo-excitation of the spiropyran form can cause cleavage of the C_{spiro}-O_1 bond. This is due to the further elongation of the C_{spiro}-O_1 bond similarly to the structural aspects that caused weakening and elongation of the C_{spiro}-O_1 bond in the ground state. Also, the presence of electronegative substituents on the benzene ring of the pyran section could amplify the photochromic properties of the spiropyran molecule.

The cleavage of the C_{spiro}-O_1 bond that is caused by the photo-excitation of the spiropyran molecule leads to the conjugated open merocyanine form (excited state) which intensely absorbs in the visible region due to the delocalisation of the π–electrons [57,59]. Spectroscopic studies on spiropyrans have led to the discovery of many transient isomers of merocyanine [45,60,61]. The different MC forms all differ in the geometrical arrangement at the three conjugated C-C bonds ($C_{2'2}$ –C_3-C_4-C_{4a}). In the MC forms all of these $C_{2'2}$ –C_3-C_4-C_{4a} bonds have a partial double bond aspects with dihedral angles ranging from 0° to 180°, corresponding to cisöid (C) and transöid (T) configurations. Stable MC isomers are known to have a central transöid section as the cisöid configurations are less stable due to the internal steric hindrances [45].

Upon UV light exposure, the ring–opening reaction begins with the C_{spiro}-O_1 cleavage resulting in an internally hindered cisöid intermediate, which quickly transforms to a planar MC isomer. Theoretical modelling calculations have

demonstrated that the TTC and CTC isomeric forms of merocyanine are the most stable due to their highest dipole moments compared to the other MC isomer configurations [45].

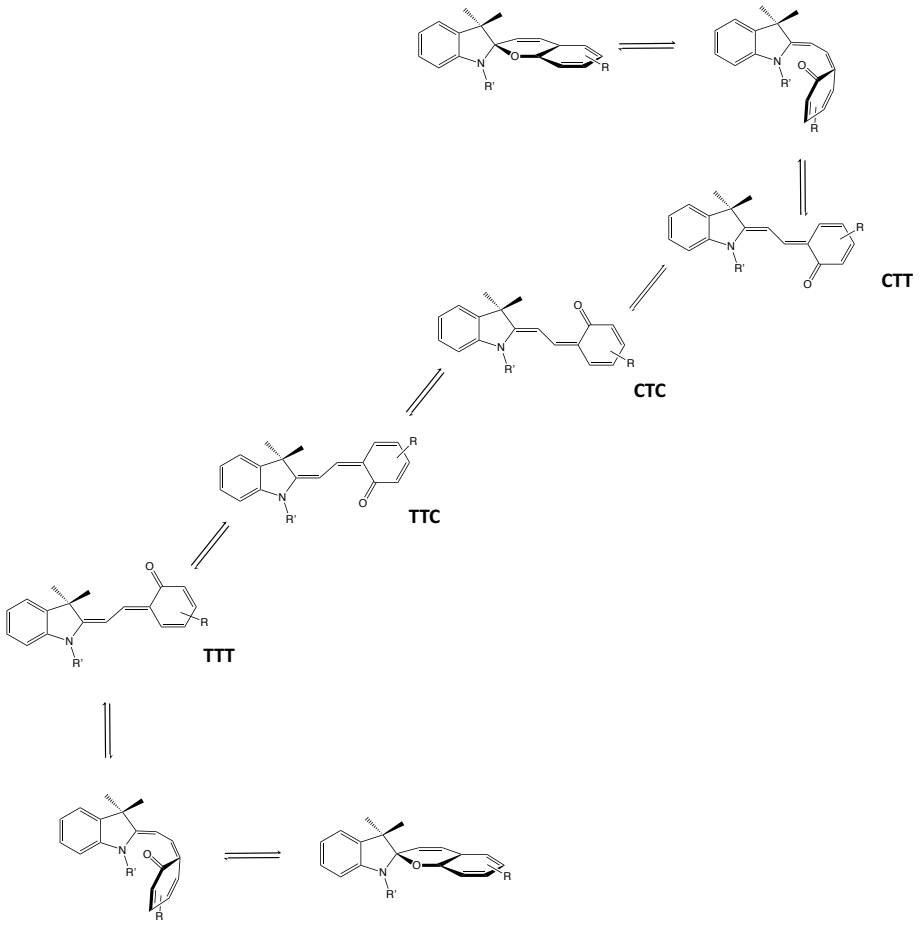

Figure 1.8 Chemical structures of the orthogonal closed ring ISBP form and the probable merocyanine intermediate isomers (represented here by cis (C) or trans (T) configurations around the N-C=C-C, C=C-C=C and C-C=C-CO bonds) upon photo-excitation. (reproduced from [45])

1.4.3 Incorporations in to Polymeric Systems

From the time when the photochromic properties of spiropyrans have been discovered, they have been integrated in a large variety of materials. Such materials include; polymer brushes[21,23,62], polymeric matrices [63-67], colloidal particles [21,68] and initiators for radical polymerisations [69], among many others. There have been a large number of studies carried out that use a photochromic spiropyran derivative as a result of it well known properties like the reversible isomerisation when exposed to specific illumination conditions, conductivity, optical properties[69] and metal ion complexation [40,56,70-74] among others. These properties have been

utilised in a large array of applications to demonstrate the desired effects. Such applications that have employed SP have been used for biological technologies, sensors [17,75], photochromic lenses [76], dye-sensitised solar cells [77], optical recording [78], actuators [79-83] and others [84-88].

1.5 Metal-ion Binding

As previously mentioned, when exposed to UV light, the closed spiropyran form isomerises to the open, more polar, merocyanine form. The merocyanine structure is a zwitterion thus it has a negatively charged phenolate oxygen atom serving as a potential binding site for cations, such as divalent metal ions, allowing for the formation of a (MC-Metal ion) complex (Figure 1.12) [70,89-92]. However when the (MC-Metal ion) complex is exposed to white light illumination conditions, there is a larger population of the closed ring SP form generated, resulting in the release of the metal ion in the process [85]. Knowing this it is possible to develop a metal ion sensing system that can be externally and reversibly controlled with light, in a non-invasive manner.

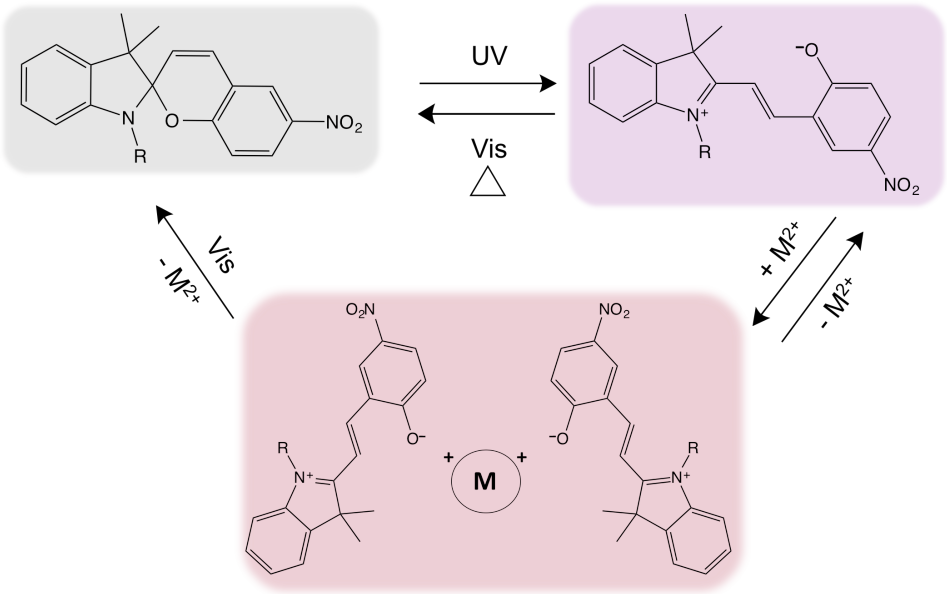

Figure 1.12. General scheme showing the metal ion binding behaviour of spiropyran derivatives. UV irradiation causes the photo-cleavage of the C-O bond and isomerisation of the closed spiropyran form (top left, colourless) to the open merocyanine form (top right, strongly coloured). The reversible process occurs under white light irradiation or temperature. The merocyanine is thought to bind metal ions through the negative phenolate in a 2:1 ratio to metal ion (bottom centre, various colours depending on the metal ion). White light irradiation of the

metal complex causes the return to the original spiropyran form and release of the bound metal ion.

There have been many studies done using spiropyran derivatives as metal ion chelators [93], where the majority of these have proven efficient for divalent metal ion sensing, such as Zn^{2+} [71,92], Co^{2+} [56,71,94], Cu^{2+} [56,71], Ni^{2+} [71,90], and Cd^{2+} [95]. Using divalent metal ions typically involves binding in a 2:1 ratio of MC unit to M^{2+}, as two MC phenolate anions are required to bind to one divalent metal ion [95].

Several research groups have attempted to increase the number of binding sites on the MC unit and achieve a 1:1 binding ratio (MC: M^{2+}) by introducing an additional possible binding site at the C_8 position of the benzopyran ring, including methoxy [56], allyl substituents [56], or by functionalising the indolic nitrogen with carboxylic acid [96], ester [97], or hydroxyl-terminated moieties [56]. However, the metal-ligand interaction is usually weak enough to allow disruption of the complex by the photo-induced ring closing reaction. Therefore, SP derivatives can be used as reversible chelators for metal ions. Further discussion of how different divalent metal ions binding to the merocyanine and the effect on the physical properties observed can be found in Chapter 5.

1.6 Soft Robotics

To date hard robotics has failed to produce a device that could offer the properties largely found in biological systems such as: flexibility, self-repair of adaptability in changing environmental conditions that can be executed by the simplest of living organisms. In a bid to overcome these issues, soft-robotics is a new and interesting field of robotics that is inspired by the movements and function of biological systems by using soft-actuators to execute these movements.

Whitesides *et al.* was among the first to take inspiration from the motion of the earthworm and developed elastomers that can mimic this motion by anisotropic contraction and expansion [98-100].

Since then, there have been many studies that have proposed various materials for soft–robotics development. Among these, hydrogel systems, particularly stimuli-responsive hydrogels are of interest, due to the ability of the hydrogel to undergo

large deformations in size and shape when exposed to the appropriate internal/external stimuli. Techawanitchai *et al.* [101] used two layers of different pH responsive hydrogels bound together via electrolysis; a poly acid (poly(N-isopropylacrylamide-*co*-2-carboxyisopropylacrylamide) (p(NIPAAm-*co*-CIPAAm)) and a poly base layer (poly(N-isopropylacrylamide-*co*-N,N0-dimethylaminopropylacylamide) (p(NIPAAm-*co*-DMAPAAm)). When this bilayer was exposed to UV light, the poly acid contracted and the poly base expanded. As they were bound to each other, this contraction and expansion generated a bending motion. However, the bilayers needed to be immersed in solutions of relevant pH prior to actuation. More recently an electro-driven walker has been created, where the walker's legs were composed of a cationic co-polymer based on acrylamide (AAm)/ quaternized dimethylaminoethyl methacrylate (DMAEMA) and an anionic co-polymer based on acrylamide/ sodium acrylate (NaAc). Upon electro-stimulation each leg moved causing the bipedal gel to "walk" in a unidirectional motion [102]. This field of soft robotics is still in its infancy and shows great potential for the stimuli-responsive materials to mimic biological motions [103].

1.7 Aims of This Work

The aim of this work was to realise a range of stimuli-controlled polymeric systems based on the spiropyran photo-switches. This was achieved by first developing photo-responsive hydrogels based on poly(N-isopropylacrylamide-*co*-acrylated spiropyran-*co*-acrylic acid), p(NIPAAm-*co*-SP-*co*-AA) that could shrink on exposure to white light, and swell in the dark. A comprehensive study demonstrating the critical role of the polymerisation solvent on the morphology of this photo-responsive hydrogel and the kinetics of actuation is presented in Chapter 3 of this thesis.

In Chapter 4, using the same spiropyran-based photo-responsive hydrogel, clever structure and substrate design enabled the realisation of a hydrogel "walker". When bipedal p(NIPAAm-co-SP-co-AA) hydrogel structures were placed onto a ratcheted surface, the actuation of the bipedal gel produced a walking motion by taking a series of steps in a given direction, as determined by the optimised design of the ratchet scaffold.

The next study (Chapter 5) investigates the metal ion binding capabilities of spiropyran polymeric brushes obtained via surface-initiated ring-opening metathesis polymerisation. Coating of glass micro-capillaries with these SP-brushes enabled the realisation of smart fluidic devices that can "sense" the metal ion solution passing through.

The "Future Work" chapter illustrates the progress I have made thus far in the development of additional "Photo-responsive Systems based on Spiropyran" and will hopefully give the reader some insight into the exciting potential of this research.

1.8 References

1. Agarwal, A.; Dong, L.; Beebe, D.; Jiang, H. Autonomously-triggered microfluidic cooling using thermo-responsive hydrogels. *Lab on a chip* **2007**, *7*, 310-315.
2. West, J.; Becker, M.; Tombrink, S.; Manz, A. Micro total analysis systems: Latest achievements. *Analytical Chemistry* **2008**, *80*, 4403-4419.
3. Beebe; Moore; Bauer; Yu; Liu; Devadoss; Jo. Functional hydrogel structures for autonomous flow control inside microfluidic channels. *Nature* **2000**, *404*, 588-590.
4. Lecault, V.; White, A.K.; Singhal, A.; Hansen, C.L. Microfluidic single cell analysis: From promise to practice. *Current opinion in chemical ...* **2012**.
5. Zare, R.N.; Kim, S. Microfluidic platforms for single-cell analysis. *Annual review of biomedical engineering* **2010**.
6. Argentiere, S.; Gigli, G.; Mortato, M.; Gerges, I.; Blasi, L. Smart microfluidics: The role of stimuli-responsive polymers in microfluidic devices. *Chapter* **2014**.
7. Eddington, D.; Beebe, D. Flow control with hydrogels. *Advanced drug delivery reviews* **2004**, *56*, 199-210.
8. Godin, J.; Chen, C.H.; Cho, S.H.; Qiao, W.; Tsai, F. Microfluidics and photonics for bio-system-on-a-chip: A review of advancements in technology towards a microfluidic flow cytometry chip. *Journal of ...* **2008**.
9. ter Schiphorst, J.; Coleman, S.; Stumpel, J.E.; Ben Azouz, A.; Diamond, D.; P.H.J. Shenning, A. Molecular design of light-responsive hydrogels, for in situ generation of fast and reversible valves for microfluidic applications. *Chemistry of materials* **2015**, *27*, 5925-5931.
10. Lee, C.Y.; Chang, C.L.; Wang, Y.N.; Fu, L.M. Microfluidic mixing: A review. *International journal of molecular ...* **2011**.
11. Walker, G.M.; Beebe, D.J. A passive pumping method for microfluidic devices. *Lab on a Chip* **2002**.
12. Florea, L.; McKeon, A.; Diamond, D.; Benito-Lopez, F. Spiropyran polymeric microcapillary coatings for photodetection of solvent polarity. *Langmuir* **2013**, *29*, 2790-2797.

13. Ivashenko, O.; van Herpt, J.T.; Feringa, B.L.; P., R.; Browne, W.R. Uv/vis and nir light-responsive spiropyran self-assembled monolayers, . *Langmuir* **2013**, *29*, 4290 – 4297.
14. Parry, A.V.S.; Lu, K.; Tate, D.J.; Urasinska−Wojcik, B.; Caras−Quintero, D.; Majewski, L.A.; Turner, M.L. Trichlorosilanes as anchoring groups for phenylene−thiophene molecular monolayer field effect transistors. *Advanced Functional Materials* **2014**, *24*, 6677-6683.
15. Kim, I.P.; Martynenko, V.M.; Chernyak, A.V.; Benderskii, V.A. Radical polymerization of tetrafluoroethylene in solutions of trimethoxysilanes: Formation of colloidal solution and gel of oligomers. *High Energy Chemistry* **2017**, *51*, 285-291.
16. Vona, D.; Lo Presti, M.; Cicco, S.; Palumbo, F.; Ragni, R.; Farinola, G. Light emitting silica nanostructures by surface functionalization of diatom algae shells with a triethoxysilane-functionalized π-conjugated fluorophore. *MRS Advances* **2016**, *57*, 3817 - 3823.
17. Florea, L.; Hennart, A.; Diamond, D.; Benito-Lopez, F. Synthesis and characterisation of spiropyran-polymer brushes in micro-capillaries: Towards an integrated optical sensor for continuous flow analysis. *Sensors and Actuators B: Chemical* **2012**, *175*, 92-99.
18. Uhlmann, P.; Ionov, L.; Houbenov, N.; Nitschke, M.; Grundke, K.; Motornov, M.; Minko, S.; Stamm, M. Surface functionalization by smart coatings: Stimuli-responsive binary polymer brushes. *Progress in Organic Coatings* **2006**, *55*, 168 - 174.
19. Miroslav, J.; Bohumil, M.; Ludek, T.; Petr, V.; Petra, L.; Jiri, B.; petr, H. Synthesis of novel types of graft copolymers by a "grafting-from" method using ring-opening polymerisation of lactones and lactides. *Reactive and Functional polymers* **2003**, *57*, 137 -146.
20. Krohm, F.; Kind, J.; Savka, R.; Janßen, A.M.; Herold, D.; Plenio, H.; Thiele, C.M.; Andrieu-Brunsen, A. Photochromic spiropyran- and spirooxazine-homopolymers in mesoporous thin films by surface initiated romp. *Journal of Materials Chemistry C* **2016**, *4*, 4067-4076.
21. Piech, M.; Bell, N., S. Controlled synthesis of photochromic polymer brushes by atom transfer radical polymerisation. *macromolecules* **2006**, *39*.
22. Bogdan, Z.; igor, L. Polymer bruses by the :Grafting to" method. *Macromolecular Rapid Communications* **2011**, *32*, 859 - 869.
23. Zhao, B.; Brittain, W.J. Polymer brushes: Surface-immobilized marcomolecules. *Prog Polym Sci* **2000**, *25*, 677 - 710.
24. Li, D.; Zheng, Q.; Wang, Y.; Chen, H. Combining surface topography with polymer chemistry: Exploring new interfacial biological phenomena. *Polymer Chemistry* **2014**, *5*, 14-24.
25. Geiger, E.J.; Pisano, A.P.; Svec, F. A polymer-based microfluidic platform featuring on-chip actuated hydrogel valves for disposable applications. *Microelectromechanical Systems, Journal of* **2010**, *19*, 944-950.
26. Liang, D.; Hongrui, J. Autonomous microfluidics with stimuli-responsive hydrogels. *Soft Matter* **2007**, *3*, 1223-1230.
27. Xian-Zheng, Z.; Yi-Yan, Y.; Tai-Shung, C. Effect of mixed solvents on characteristics of poly(n -isopropylacrylamide) gels. *Langmuir* **2002**, *18*, 2538-2542.

28. Eichenbaum, G.M.; Kiser, P.F.; Simon, S.A.; Needham, D. Ph and ion-triggered volume response of anionic hydrogel microspheres. *Macromolecules* **1998**, *31*, 5084 - 5093.
29. De, S.K.; Aluru, N.R. Equilibrium swelling and kinetics of ph-responsive hydrogels: Models, experiments and simulations. *journal of MicroElectromechanical Systems* **2002**, *11*, 544 - 555.
30. Berman, E.; Fox, R.E.; Thomson, F.D. Photochromic spiropyrans. I. The effect of substituents on the rate of ring closure. *Journal of the American ...* **1959**.
31. Fischer, E., and Y. Hirshberg. Formation of coloured forms of spirans by low-temperature irradiation. *Journal of the Chemical Society* **1952**, 4522-4524.
32. Kimio, S.; Toshiyuki, T.; Taku, S.; Toshiyuki, K. Photo-induced reversible proton dissociation of spirobenzopyran in aqueous systems. *Journal of Photochemistry and Photobiology A: Chemistry* **2013**, *261*, 46-52.
33. Kumar, S.G.; Neckers, D.C. Photochemistry of azobenzene-containing polymers. *Chemical Reviews* **1989**, *89*, 1915-1925.
34. Wang, Y.; Ma, N.; Wang, Z.; Zhang, X. Photocontrolled reversible supramolecular assemblies of an azobenzene−containing surfactant with α−cyclodextrin. ... *Chemie International Edition* **2007**.
35. Matsuda, K.; Irie, M. Diarylethene as a photoswitching unit. *Journal of Photochemistry and Photobiology C: Photochemistry Reviews* **2004**, *5*, 169-182.
36. Irie, M.; Miyatake, O.; Uchida, K. Photochromic diarylethenes with intralocking arms. *Journal of the American ...* **1994**.
37. Zhang, J.; Peppas, N.A. Synthesis and characterization of ph-and temperature-sensitive poly (methacrylic acid)/poly (n-isopropylacrylamide) interpenetrating polymeric networks. *Macromolecules* **2000**, *33*, 102-107.
38. Heinz Dürr, H.B.-L. Photochromism: Molecules and systems. *Elsevier* **1990**, 315-466.
39. Ichimura, K. Photochromic materials and photoresists. In *Photochromism molecules and stsyems*, Heinz Dürr, H.B.-L., Ed. Elsevier: 1990; pp 903 - 918.
40. Fries, K.; Samanta, S.; Orski, S.; Locklin, J. Reversible colorimetric ion sensors based on surface initiated polymerization of photochromic polymers. *Chem Commun (Camb)* **2008**, 6288-6290.
41. Tabata, Y.; Asahara, T. Hydrogel for medical use. *US Patent App. 11/884* **2006**.
42. Hoare, T.R.; Kohane, D.S. Hydrogels in drug delivery: Progress and challenges. *Polymer* **2008**, *49*, 1993-2007.
43. Hendrickson, G.R.; Lyon, L.A. Bioresponsive hydrogels for sensing applications. *Soft Matter* **2009**.
44. Kimio, S.; Mitsuyoshi, K.; Toshiyuki, K.; Toshio, S. Characteristic phase transition of aqueous solution of poly(n -isopropylacrylamide) functionalized with spirobenzopyran. *Macromolecules* **2004**, *37*, 4949-4955.
45. Minkin, V.I. Photo-, thermo-, solvato-, and electrochromic spiroheterocyclic compounds. *Chemical Reviews* **2004**, *104*, 2751-2776.
46. Bianchia, A.; Delgado-Pinarb, E.; García-Espa˜nab, E.; Giorgia, C.; Pinac, F. Highlights of metal ion-based photochemical switches. *Coordination Chemistry Reviews* **2014**, *260*, 156 - 215.
47. Görner, H.; Chibisov, A.K. *journal of the chemical Society, Faraday Transactions* **1998**, *94*, 2557 - 1564.

48. Barachevsky, V.A. Negative photochromism in organic systems. *Review Journal of Chemistry* **2017**, *7*, 334-371.
49. Harada, J.; Kawazoe, Y.; Ogawa, K. Photochromism of spiropyrans and spirooxazines in the solid state: Low temperature enhances photocoloration. *Chemical Communications* **2010**.
50. Shinji, S.; Kimio, S.; Katsuhide, O.; Kazuaki, H.; Toshiyuki, T.; Toshiyuki, K. Photoresponsive polymer gel microvalves controlled by local light irradiation. *Sensors and Actuators A: Physical* **2007**, *140*.
51. Benito-Lopez, F.; Byrne, R.; Răduţă, A.; Vrana, N.; McGuinness, G.; Diamond, D. Ionogel-based light-actuated valves for controlling liquid flow in micro-fluidic manifolds. *Lab on a chip* **2010**, *10*, 195-201.
52. Czugala, M.; O'Connell, C.; Blin, C.; Fischer, P.; Fraser, K.J.; Benito-Lopez, F.; Diamond, D. Swelling and shrinking behaviour of photoresponsive phosphonium-based ionogel microstructures. *Sensors and Actuators B: Chemical* **2014**, *194*, 105-113.
53. Coleman, S.; ter Schiphorst, J.; Ben Azouz, A.; Bakker, S.; Schenning, A.P.H.J.; Diamond, D. Tuning microfluidic flow by pulsed light oscillating spiropyran-based polymer hydrogel valves. *Sensors and Actuators B: Chemical* **2017**, *245*, 81-86.
54. ter Schiphorst, J.; Saez, J.; Diamond, D.; Benito-Lopez, F.; Schenning, A.P.H.J. Light-responsive polymers for microfluidic applications. *Lab on a Chip* **2018**, *18*, 699-709.
55. Fries, K.H.; Driskell, J.D.; Sheppard, G.R.; Locklin, J. Fabrication of spiropyran-containing thin film sensors used for the simultaneous identification of multiple metal ions. *Langmuir* **2011**, *27*, 12253-12260.
56. Görner, H.; Chibisov, A.K. Complexes of spiropyran-derived merocyannies with metal ions themally activated and light-induced processes. *Journal of Chemistry society, Faraday Trans* **1998**, *94*, 2557-2564.
57. Aldoshin, S.M. Spiropyrans - structural features and photochemical properties *Molecular crystals and liquid crystals science and technology section a-molecular crystals and liquid crystals* **1994**, *246*, 207 - 214.
58. Aldoshin, S.M. Spiropyrans: Structural features and photochemical properties. *Russian chemical reviews* **1990**, *59*, 1144 - 1178.
59. Berkovic, G.; Krongauz, V.; Weiss, V. Spiropyrans and spirooxazines for memories and switches. *Chemical Reviews* **2000**, *100*, 1741-1754.
60. Chibisov, A.K.; Görner, H. Photoprocesses in spirooxazines and their merocyanines. *The Journal of Physical Chemistry A* **1999**, *103*, 5211-5216.
61. Meng, H.; Jinlian, H. A brief review of stimulus-active polymers responsive to thermal, light, magnetic, electric, and water/solvent stimuli. *Journal of Intelligent Material Systems and Structures* **2010**, *21*, 859-885.
62. Samanta, S.; Locklin, J. Formation of photochromic spiropyran polymer brushes via surface-initiated, ring-opening metathesis polymerization: Reversible photocontrol of wetting behavior and solvent dependent morphology changes. *Langmuir* **2008**, *24*, 9558-9565.
63. Park, Y.S.; Ito, Y.; Imanishi, Y. Photocontrolled gating by polymer brushes grafted on porous glass filter. *Macromolecules* **1998**, *31*, 2606-2610.
64. Chung, D.J.; Ito, Y.; Imanishi, Y. Preparation of porous membranes grafted with poly(spiropyran−containing methacrylate) and photocontrol of permeability. *J. Appl. Polym. Sci.* **1994**, *51*, 2027-2033.

65. Adelmann, R.; Mela, P.; Gallyamov, M.O.; Keul, H.; Möller, M. Synthesis of high−molecular−weight linear methacrylate copolymers with spiropyran side groups: Conformational changes of single molecules in solution and on surfaces. *Journal of Polymer Science Part A: Polymer Chemistry* **2009**, *47*, 1274-1283.
66. Ivanov, A.E.; Eremeev, N.L.; Wahlund, P.O.; Galaev, I.Y.; Mattiasson, B. Photosensitive copolymer of n-isopropylacrylamide and methacryloyl derivative of spyrobenzopyran. *Polymer* **2002**, *43*, 3819-3823.
67. Sharifian, M.; Mahdavian, A.; Salehi-Mobarakeh, H. Effects of chain parameters on kinetics of photochromism in acrylic-spiropyran copolymer nanoparticles and their reversible optical data storage. *Langmuir* **2017**, *32*, 8023 - 8031.
68. Sakai, K.; Imaizumi, Y.; Oguchi, T.; Sakai, H.; Abe, M. Adsorption characteristics of spiropyran-modified cationic surfactants at the silica/aqueous solution interface. *Langmuir* **2010**, *26*, 9283-9288.
69. Such, G.K.; Evans, R.A.; Davis, T.P. Rapid photochromic switching in a rigid polymer matrix using living radical polymerization. *Macromolecules* **2006**, *39*, 1391-1396.
70. Phillips, J.P.; Mueller, A.; Przytal, F. Photochromic chelating agents. *Journal of the American Chemical Society* **1965**, *87*, 4020 - 4021.
71. Natali, M.; Giordani, S. Interation studies between photochromic spiropyrans and transition metal cations: The curious case of copper. *Organic & Biomolecular Chemistry* **2012**, *10*, 1162-1171.
72. Natali, M.; Aakeröy, C.; Desper, J.; Giordani, S. The role of metal ions and counterions in the switching behavior of a carboxylic acid functionalized spiropyran. *Dalton Transactions* **2010**.
73. Fries, K.H.; Driskell, J.D.; Samanta, S.; Locklin, J. Spectroscopic analysis of metal ion binding in spiropyran containing copolymer thin films. *Analytical Chemistry* **2010**, *82*, 3306-3314.
74. Chhatwal, M.; Kumar, A.; Singh, V.; Gupta, R.D.; Awasthi, S.K. Addressing of multiple-metal ions on a single platform. *Coordination Chemistry Reviews* **2015**, *292*, 30-55.
75. Florea, L.; McKeon, A.; Diamond, D.; Benito-Lopez, F. Spiropyran polymeric microcapillary coatings for photodetection of solvent polarity. *Langmuir* **2013**, *29*, 2790-2797.
76. Kadowaki, S. Photochromic lens for eye glasses. Google Patents: 2016.
77. Johnson, N.M.; Smolin, Y.Y.; Shindler, C.; Hagaman, D.; Soroush, M.; Lau, K.K.; Ji, H.-F. Photochromic dye-sensitized solar cells. **2015**.
78. Berkovic, G.; Krongauz, V.; Weiss, V. Spiropyrans and spirooxazines for memories and switches. *Chemical reviews* **2000**.
79. Stumpel, J.E.; Ziółkowski, B.; Florea, L.; Diamond, D.; Broer, D.J.; Schenning, A.P. Photoswitchable ratchet surface topographies based on self-protonating spiropyran–nipaam hydrogels. *ACS applied materials & interfaces* **2014**, *6*, 7268-7274.
80. Williamson, A.; Ferro, M.; Leleux, P.; Ismailova, E.; Kaszas, A.; Doublet, T.; Quilichini, P.; Rivnay, J.; Rózsa, B.; Katona, G. Localized neuron stimulation with organic electrochemical transistors on delaminating depth probes. *Advanced Materials* **2015**, *27*, 4405-4410.

81. Francis, W.; Dunne, A.; Delaney, C.; Florea, L.; Diamond, D. Spiropyran based hydrogels actuators—walking in the light. *Sensors and Actuators B: Chemical* **2017**, *250*, 608-616.
82. Dunne, A.; Delaney, C.; Florea, L.; Diamond, D. Solvato-morphologically controlled, reversible nipaam hydrogel photoactuators. *RSC Advances* **2016**, *6*, 83296-83302.
83. Ziółkowski, B.; Florea, L.; Theobald, J.; Benito-Lopez, F.; Diamond, D. Self-protonating spiropyran-co-nipam-co-acrylic acid hydrogel photoactuators. *Soft Matter* **2013**, *9*, 8754-8760.
84. Klajn, R. Spiropyran-based dynamic materials. *Chemical Society Reviews* **2014**, *43*, 148-184.
85. Benito-Lopez, F.; Scarmagnani, S.; Walsh, Z.; Paull, B.; Macka, M.; Diamond, D. Spiropyran modified micro-fluidic chip channels as photonically controlled self-indicating system for metal ion accumulation and release. *Sensors and Actuators B: Chemical* **2009**, *140*, 295-303.
86. Fries, K.H.; Driskell, J.D.; Samanta, S.; Locklin, J. Spectroscopic analysis of metal ion binding in spiropyran containing copolymer thin films. *Anal. Chem.* **2010**, *82*, 3306-3314.
87. Florea, L.; Diamond, D.; Benito−Lopez, F. Photo−responsive polymeric structures based on spiropyran. *Macromolecular Materials and Engineering* **2012**, *297*, 1148-1159.
88. Florea, L.; Diamond, D.; Benito-Lopez, F. Opto-smart systems in microfluidics. *Research Perspectives on Functional Micro-and Nanoscale Coatings* **2016**, 265.
89. Chernyshev, A.V.; Voloshin, N.A.; Metelitsa, A.V.; Tkachev, V.V.; Aldoshin, S.M.; Solov'eva, E.; Rostovtseva, I.A.; Minkin, V.I. Metal complexes of new photochromic chelator: Structure, stability and photodissociation. *Journal of Photochemistry and Photobiology A: Chemistry* **2013**, *265*, 1 - 9.
90. Taylor, L.D.; Nichoslon, J.; Davis, R.B. Photochromic chelating agents. *Tetrahedron Letters* **1967**, *8*, 1585 - 1588.
91. Shao, N.; Jin, J.Y.; Wang, H.; Zhang, Y.; Yang, R.H.; Chan, W.H. Tunable photochromism of spirobenzopyran via selective metal ion coordination: An efficient visual and ratioing fluorescent probe for divalent copper ion. *Analytical chemistry* **2008**, *80*, 3466-3475.
92. Wojtyk, J.C.; Kazmaier, P. Effects of metal ion complexation on the spiropyran–merocyanine interconversion: Development of a thermally stable photo-switch. *Chemical Communications* **1998**, 1703-1704.
93. Wojtyk, J.T.C.; Communications, K.-P.M. Effects of metal ion complexation on the spiropyran–merocyanine interconversion: Development of a thermally stable photo-switch. *Chemical Communications* **1998**.
94. Florea, L.; McKeon, A.; Diamond, D.; Benito-Lopez, F. Spiropyran polymeric microcapillary coatings for photodetection of solvent polarity. *Langmuir* **2013**, *29*, 2790-2797.
95. Fries, K.; Samanta, S.; Orski, S.; Locklin, J. Reversible colorimetric ion sensors based on surface initiated polymerization of photochromic polymers. *Chemical Communications* **2008**, 6288-6290.
96. Natali, M.; Aakeröy, C.; Desper, J.; Giordani, S. The role of metal ions and counterions in the switching behavior of a carboxylic acid functionalized spiropyran. *Dalton Transactions* **2010**, *39*, 8269-8277.

97. Fries, K.H.; Sheppard, G.R.; Bilbrey, J.A.; Locklin, J. Tuning chelating groups and comonomers in spiropyran-containing copolymer thin films for color-specific metal ion binding. *Polymer Chemistry* **2014**, *5*, 2094 - 2102.
98. Whitesides, G.M. The orgins and the future of microfludics. *Nature* **2006**, *442*, 368 - 378.
99. Quillin, K. Ontogenetic scaling of hydrostatic skeletons: Geometric, static stress and dynamic stress scaling of the earthworm lumbricus terrestris. *journal of Exerimental Biology* **1998**, *201*, 1871 - 1883.
100. Menciassi, A.; Gorini, S.; Pernorio, P.; Dario, P. In *In sma actuated artificail earthworm, robotics and automation*, IEEE internaitional conference, 2004; pp 3282 - 3287.
101. Techawanitchai, P.; Mitsuhiro, E.; Naokazu, I.; Taka-Aki, A.; Akihiko, K.; Takao, A. Photo-switchable control of ph-responsive actuators via ph jump reaction. *Soft Matter* **2012**, *8*.
102. Morales, D.; Palleau, E.; Dickey, M.D.; Velev, O.D. Electro-actuated hydrogel walkers with dual responsive legs. *Soft Matter* **2014**, *10*, 1337 – 1348
103. Rus, D.; Tolley, M.T. Design, fabrication and control of soft robots. *Nature* **2015**, *521*, 467 - 475.

Chapter 2

Stimuli-induced fluid control in microfluidic channels*

*Stimuli-controlled fluid control and microvehicle movement in microfluidic channels**, Aishling Dunne, Wayne Francis, Colm Delaney, Larisa Florea*, Dermot Diamond, *The Reference Module in Materials Science and Materials Engineering*, Elsevier, 2017.

Chapter 2:

2.1 Abstract

Integration of stimuli-responsive materials into microfluidic systems provides a means to locally manipulate flow at the microscale, in a non-invasive manner, while also reducing system complexity. In recent years, several modes of stimulation have been applied, including electrical, magnetic, light and temperature, among others. To achieve remote control of flow in microfluidics using external stimulation, different approaches have emerged in the recent years. In the interest of this work, the control of flow through stimuli-induced actuation of microfluidic components (valves, pumps, mixers, flow sorters), most often fabricated from soft polymeric materials will be discussed.

The focus of this chapter will be to identify and compare the similarities and underlying mechanisms employed in the current state of the art in stimuli-induced actuation for fluid control, offering an up-to-date view of this exciting research area.

2.2 Introduction

Since the onset of research into microfluidics during the 1990s, there has been much progress made in the generation and control of flow in micrometre-sized devices [1,2]. The aim of these tiny devices is to perform complex biological and chemical tasks on a single chip [3]. Advantages of this approach include a significant reduction in reactant volume (down to microlitres or even picolitres), parallel processing of multiple analytes, portability [4], multistage automation [5], single cell sampling[6] and manipulation [7]. Therefore, the potential for microfluidic devices is tremendous. Nevertheless, the microfluidics field is still very much in its infancy and a number of areas are constantly under heavy investigation, including micro-fabrication, component integration, device generalisation and fluid flow and control [8]. Despite considerable advances in recent years, fluid handling on microfluidic chips still relies, in many cases, on macroscopic external control boxes containing power supplies, high power sources, sensing elements and complicated control systems based on external computers and/or electronics [9]. While there are still many challenges facing this

field, there have been a number of revolutionary approaches, one of the most exciting of which is the incorporation of stimuli-responsive actuators within the fluidics, to achieve integrated fluid handling on-chip. This approach can result in flow control,[10,11] mixing,[12] flow sorting,[13] pumping[14] and even sensing components fully integrated into the microfluidics chip [15]. Recent exciting developments in stimuli-responsive materials, and particularly stimuli responsive polymers and surfaces make microfluidics a great platform for demonstrating the capabilities and highlighting the functionality of these materials [16,17]. Indeed, the microfluidic platform generally enhances the functionality of smart materials by offering faster kinetics and shorter reaction times due to increased surface to volume ratios; improved interfacial and chemical interactions; dominant surface tension and capillary effects and efficient absorption of electro-magnetic radiation.

To-date, one of the main approaches to achieve flow control in microfluidic devices using stimuli-responsive materials is an indirect approach, where flow control is realized through stimuli-induced actuation of microfluidic components (valves, pumps, mixers, flow sorters), most often fabricated from soft polymeric materials or polymer thin films. Several examples in this space will be reviewed and discussed in this current chapter.

2.3 Control of flow through stimuli-induced actuation of microfluidic components

The most commonly used stimuli-responsive actuators in microfluidic devices are based on multilayer polymer films or soft polymer hydrogels. Although the actuation mechanism of these two classes is considerably different, they offer similar functionality to microfluidic devices through the generation of valves, pumps, flow sorters, filters and mixers[18].

2.3.1 Multilayer Polymer Films

Thin film actuators are based on a bilayer principle, in which two materials respond differently to a chosen stimulus[19]. Such bilayers are commonly comprised of a metal and conducting polymer, such as a gold/polypyrrole couple, where metal

cations are inserted into the polymer upon reduction and removed when the polymer is oxidised [20,21]. Depending on the doping regime in the conducting polymer, a positive bias usually generates the oxidised state, leading to an increase in volume. Application of a negative bias can then result in actuation of the material. The oxidation rate of the polymer can be controlled by variation of the applied voltage. These properties result in a wide variety of applications for conductive polymer actuators, such as artificial muscles[22], biomedical devices[23], microfluidics[24] and novel actuators[25-27]. A pertinent example by Smela *et al*.[21] demonstrates an electrochemically driven conducting polymer bilayer, based on a doped gold/polypyrrole bilayer fabricated *via* reactive ion etching (RIE) (shown in Figure 2.1), which can be used as a hinge to move silicon plates.

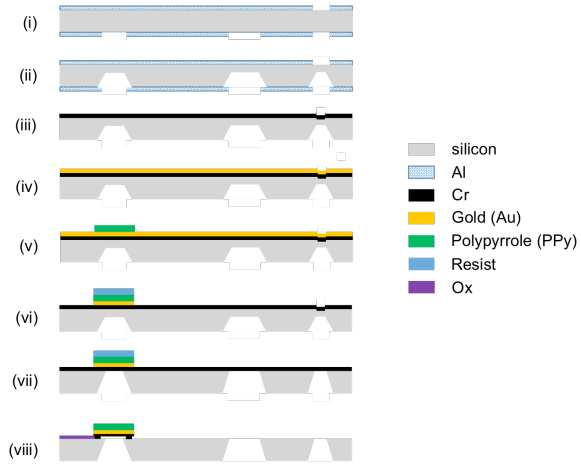

Figure 2.1. Manufacture schematic: (i) patterned etch mask applied for RIE, (ii) RIE etch to define SI plates, (iii) deposit of SiO_2, (iv) deposit of Cr and Au, (v) deposit and pattern of PPy, (vi) pattern of Cr and Au, (vii) finished etching, (viii) free plates and hinge by etching SiO_2 (Adapted from Smela et al. [21]).

The actuation speeds and lifetime of these Au/PPy-DBS electroactive bilayer hinges, which operate in a voltage range of 0 to -1 V, are extremely reliant on the thickness of the bilayer, and hindered by the possibility of delamination. These disadvantages were significantly outweighed by the high strength, low required voltage and the control of actuation observed (Figure 2.2). Such actuator hinges are

envisioned for lab-on-a-chip applications where they can be used to control sealable lids over silicon etched cavities to capture cells.

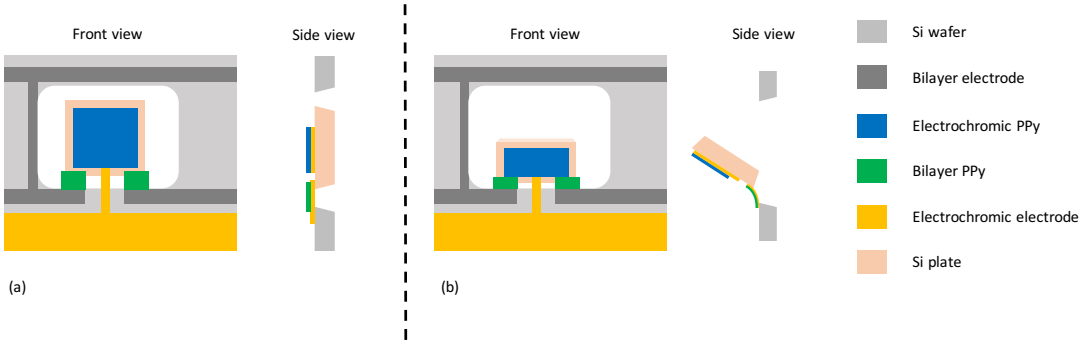

Figure 2.2. Schematic image of Si plate rotating on PPy/gold hinges; a) Bilayer PPy is reduced, plate lies flat. B) Bilayer PPy is partly oxidized, plate rotates out of the plane. (the electrochromic PPy is oxidised in both) (Adapted from E. Smela [28]).

The scope of this research has been further developed with alternative materials to broaden potential applications in microfluidic devices, in the work undertaken by *Tanaka et al.*[29]. They report an electroactive polymer-based micro-stop valve occupying a small space on a microchip. This valve was achieved by taking advantage of the controlled deformation of the electroactive polymer by an applied voltage. The valve, created by positioning the electroactive polymer film membrane between two 5 µm thick soft electrode sheets, were placed on top of a 500 µm glass microchannel using a silicon rubber diaphragm (Figure 2.3). The flow in the microchannel produced by constant pressure from a microfluidic controller (under 4.0 kPa) was completely stopped within 1s by applying an electric field of 60 V/µm.

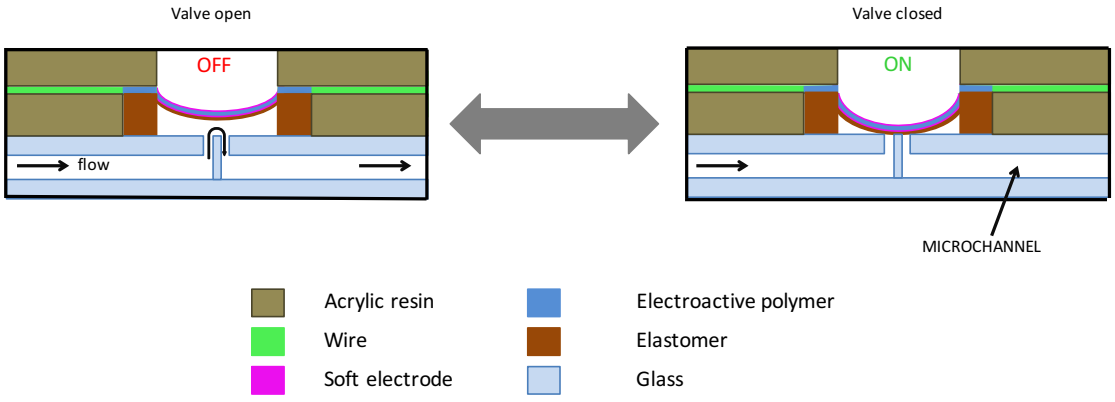

Figure 2.3. Design and working principles of the stop valve incorporated into the microfluidic chip. (Adapted from Y. Tanaka et al.[29]).

An alternative microfluidic actuator has been developed using a hybrid device consisting of an electroactive polymer within an electro-adaptive microfluidic (EAM) system. Recent investigations resulted in an EAM device which consisted of a five layer acrylic dielectric elastomer (VHBTM tape), single walled carbon nanotubes (SWCNT) and a 60 μm casting layer of PDMS to protect the electroactive polymer. A microfluidic channel made of PDMS, as seen in Figure 2.4, was attached to the electroactive polymer by oxygen plasma bonding. This multi-layered actuator allowed for modulation of the shape and dimensions of a microfluidic channel with the applied bias voltage, and a consequence permitted fluidic resistance alteration. This type of hybrid device can combat clogging issues in microfluidic systems, used for self-clearing channels, or provide design flexibility via tunable channel geometries [30].

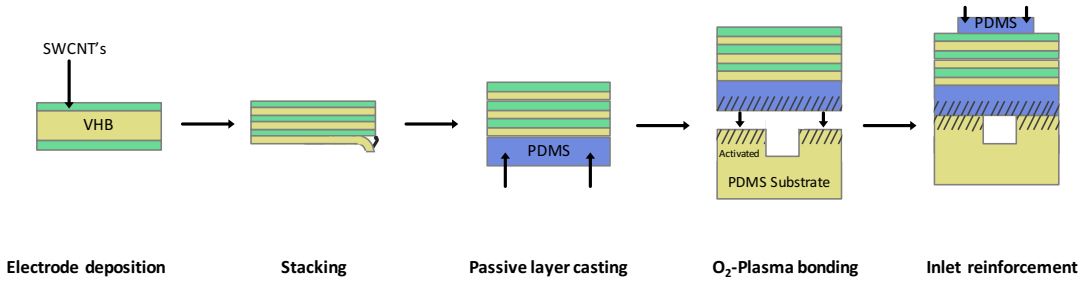

Figure 2.4. Overview of the fabrication steps involved for the electro-adaptive microfluidic system, including electrode deposition onto the VHB acrylic elastomer, stacking of these actuators, casting of the PDMS passive layer, activating the PDMS substrate and passive layer via air plasma followed by bonding them, and reinforcing the inlet by casting a short PDMS strip over the inlet. (Adapted from C. Murray et al. [30]).

2.3.2 Soft actuators – Hydrogels

Hydrogels are an alternative to thin films, considerably more exploited in microfluidics, mainly due to their ease of fabrication and integration and also to their compatibility with aqueous media[13,18,31,32]. Due to the hydrophilic character of hydrogels, strong associative interactions between polymer chains and water

molecules occur, resulting in a high degree of water absorption (up to 95% of total mass)[13,33]. As the swelling of the hydrogel is a diffusion-controlled process, the microfluidic systems provide an ideal platform to demonstrate hydrogel functionality, as the micro/nanoscale dimensions considerably reduce water and the diffusion pathlengths, thereby improving actuation kinetics that in some cases can reduce hydrogel response time from hours to seconds [34,35].

The capability of a hydrogel to absorb water can be altered through the introduction of competitive hydrophobic segments inside the hydrophilic network. These hydrophobic segments facilitate polymer-polymer interactions, causing the polymer to collapse and expel water molecules. Thus, the capacity of a hydrogel to absorb water relies on competing polymer-polymer and polymer-water interactions which are strongly dependent on the ratio of hydrophilic to hydrophobic segments present in the macromolecular network. When the hydrophilic interactions dominate, the polymer interacts with the surrounding water molecules through hydrogen bonds and the hydrogel swells due to water ingress (Figure 2.5(a)). Conversely, when hydrophobic interactions dominate, the polymer-polymer interactions are increased, causing the hydrogel to shrink (Figure 2.5(b)). Therefore, by varying the ratio between the hydrophobic/hydrophilic segments inside the macromolecular network, the shrinking/swelling behaviour of the hydrogel can be easily controlled (Figure 5).

Conveniently, the hydrophilic/hydrophobic character of many polymers and chemical groups can be altered by applying different stimuli, such as temperature, pH, electric fields or light, among others [36,37].

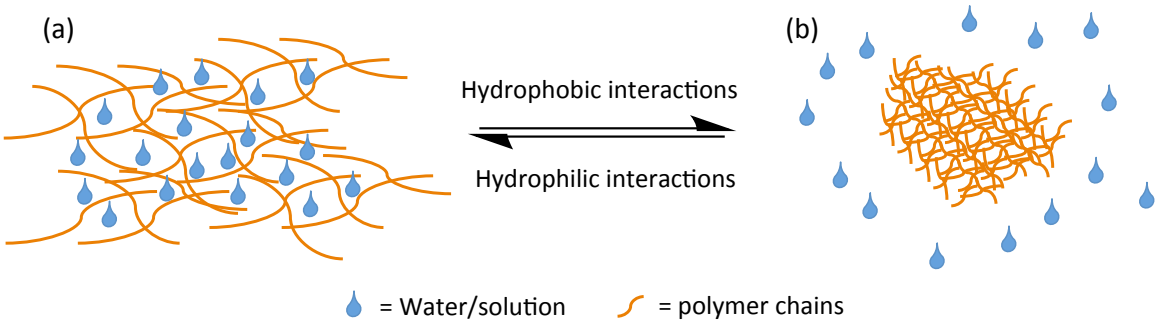

Figure 2.5. Scheme showing the reversible shrinking and swelling of a hydrogel based on dominant hydrophilic (left) or hydrophobic (right) interactions, respectively.

2.3.3 pH-induced Actuation

pH responsive hydrogel systems have multiple potential applications in the biomedical[38], environmental[39] and drug delivery fields[40,41]. pH responsive hydrogels change volume when exposed solutions of differing pH. Such polymeric materials are generally composed of monomeric units which carry an acidic or basic group in their structure; such as carboxyl or amine groups. The effective pH is determined by the pK_a of the pH responsive sensing material within the hydrogel. Around this pH, the responsive material will ionize through protonation/deprotonation, resulting in an alteration of charge on the polymer chain and thus causing a change in the balance of polymer/water – polymer/polymer interactions thereby modulating the physical size of the hydrogel. A variety of pH responsive hydrogels have been developed to date, based on maleic anhydride (MA), methacrylic acid (MAA), N,N-dimethylaminoethyl methacrylate (DMAEMA) or acrylic acid (AA), among others [42,43].

Beebe *et al.* [13] found that by clever design, a dual hydrogel system can simultaneously sense a chemical environment change and control the direction of flow. In this work, the hydrogels were composed of poly(2-hydroxyethyl methacrylate–*co*–acrylic acid) (p(HEMA-AA)) and poly(2-hydroxyethyl methacrylate-*co*-(dimethylamino)ethyl methacrylate) (p(HEMA-DMAEMA)) and were used to control the direction of the flow based on the pH of the fluid passing inside the channel (Figure 2.6). The acrylic acid based hydrogel (p(HEMA-AA)) expands at pH values above the pk_a of AA (pH=6.7 and pH=7.8 cases, Figure 2.6) due to the presence of charged COO^- moieties. Conversely, at pH values below the pk_a of AA (pH=4.7 case, Figure 2.6) the p(HEMA-AA) hydrogel is in its contracted state. Simultaneously, the p(HEMA-DMAEMA) hydrogel, which contains pendant tertiary amine groups (DMAEMA, pk_a=7) will be in its contracted state above pH 7, due to the presence of nonionised DMAEMA moieties (pH=7.8 case, Figure 2.6), and in the expanded state below pH 7 (pH=4.7 and pH=6.7 cases, Figure 2.6) due to the presence of protonated, hydrophylic amine groups. Therefore, at pH 4.7 (Figure 2.6a), the flow is directed down the right branch as the p(HEMA-DMAEMA) hydrogel on the left is in its expanded state while the p(HEMA-AA) hydrogel is in its contracted state. Oppositely, at pH 7.8 (Figure 2.6c), the p(HEMA-AA) hydrogel on the right expands to the walls of the channel constricting fluid flow while the p(HEMA-AA)

hydrogel on the left is contracted resulting in the flow being directed down the left channel. When the pH of the solution is ~6.7 (Figure 2.6b), both hydrogels expand blocking the channels and preventing any fluid flow. This work resulted in the successful demonstration of a "self-regulated flow sorter".

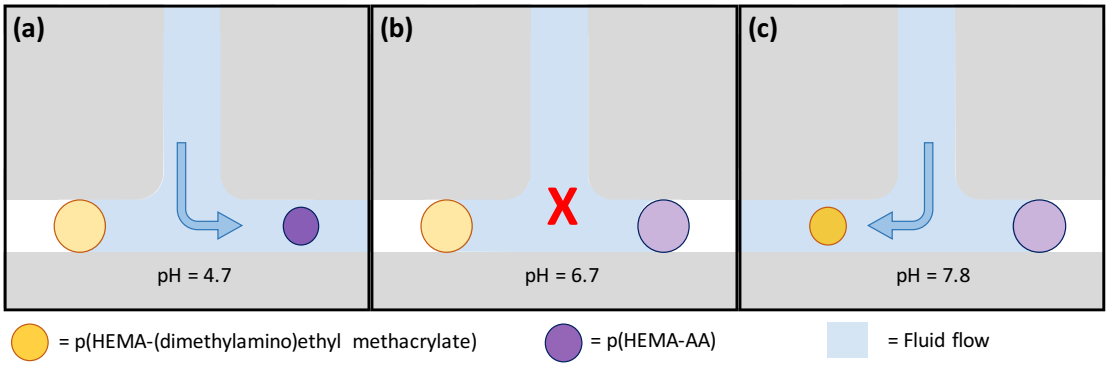

Figure 2.6. A microfluidic device demonstrating pH sensitive hydrogels working as a pH flow sorter; (a) flow of pH 4.7 is directed to the right as the p(HEMA-AA) hydrogel is in its contracted state while p(HEMA-DMAEMA) hydrogel is in its expanded state at this pH; (b) the flow is prevented due to the expansion of both hydrogels at pH 6.7; and (c) the flow is directed to the left due to the contraction of the p(HEMA-DMAEMA) hydrogel and p(HEMA-AA) hydrogel expansion at pH 7.8 (Adapted from Beebe D. et al. [13]).

In the same study a second microfluidic system was created, using the same pH-responsive materials (acrylic acid, 2-hydroxyethyl methacrylate and ethylene glycol dimethacrylate) to work as a shut off valve to control flow. The shut off valve design was composed of an upper and lower section, separated by a conformable membrane, with the hydrogel occupying the upper area and an aqueous solution occupying the lower area. When the hydrogel was exposed to solutions of varied pH, expansion or contraction was observed. The hydrogel expansion resulted in the application of sufficient pressure being placed on the deformable membrane to cause it to close the channel below, thus blocking the flow (Figure 2.7).

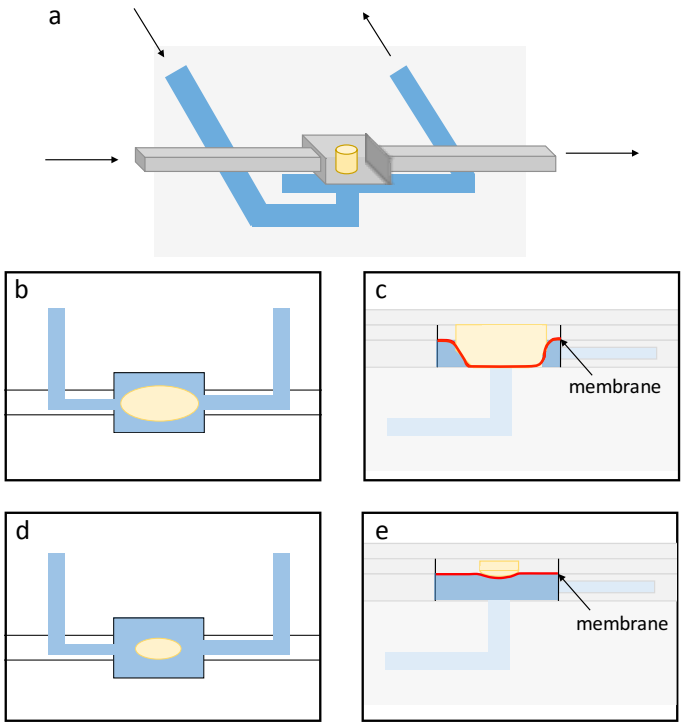

Figure 2.7. Schematic illustration and working mechanism of the shut-off valve; a) Diagram of the shut-off valve; b), c) top and side view, respectively, showing hydrogel expansion, deforming the membrane and blocking flow in the adjacent channel; d), e) top and side view, respectively, showing hydrogel contraction, causing the membrane to return to the initial position and allowing fluid to flow. (Adapted from Beebe D. et al. [13]).

2.3.4 Thermo-induced Actuation

Thermo-responsive materials have greatly impacted research into actuating materials with many possible applications such as drug delivery[40,43,44], chromatography techniques [45], biomedicine [46-48] being explored.

The thermo-response arises from a shift in the hydration forces which occur between the polymer chains and the aqueous medium, at temperatures close to the lower critical solution temperature (LCST) of a polymer [49]. At temperatures below the LCST the dominant interactions taking place are hydrogen bonding between the hydrophilic sections of the polymer chain and water. This results in water uptake and the polymer chains are elongated with negligible internal stresses. When the polymer is in a temperature environment above the LCST, hydrophobic polymer-polymer interactions become dominant and hydrogen bonding and hydrophilic interactions

weaken, resulting in aggregation of the linear chains into a globular form, due to expulsion of water with a concomitant decrease in the physical size of the hydrogel [50]. An important consideration for a thermo-response is the presence of both hydrophilic (*i.e.* amide, carboxyl etc.) and hydrophobic (*i.e.* alkyl, aryl etc.) groups in the polymer structure. Some of the most studied thermo-responsive materials include poly(*N*-isopropylacrylamide) (p(NIPAAm))[43,48,50], and copolymers such as poly(2-(2-methoxyethoxy)ethyl methacrylate-*co*-oligo(ethylene glycol)methacrylate) [51].

pNIPAAm hydrogels exhibit a negative volume change in response to increase in temperature, *i.e.*, the pNIPAAm hydrogels shrink as the temperature increases above the LCST associated with the volume phase transition. Below the LCST (32 °C), the pNIPAAm polymer chains are soluble in water. Above the LCST, they become increasingly hydrophobic and insoluble, leading to precipitation. The thermal transition of pNIPAAm hydrogels is generally considered to be a competitive result of the hydrophobic interaction of pendant isopropyl groups and polymer segments (polymer-polymer interactions) and the hydrogen bonding association between amide groups and water molecules (polymer-water interactions).

pNIPAAm gels are being increasingly used in microfluidic systems as microscale valves. Two possible valve systems containing pNIPAAm gels have been produced by Wang *et al.* [52] which require no mechanical parts and exhibit minimal dead volume. The first example shows gel actuators which were fabricated outside the channel and compressed into a 1.2 mm diameter Teflon^{tm} tube (Figure 2.8a).

Following this, the Teflon^{tm} tube was placed on a heater (58 °C), causing valve contraction, thereby opening the tube and allowing for the flow of fluid. The closing time of the hydrogel valve was about 4.5 s, and it was found to be independent of the plug's length as it relies on the local swelling of the upstream end of the gel plug. Average opening times were 5 s and 12 s, when the hydrogel length was 300 μm and 1500 μm, respectively. This size dependency is due to the fact that the entire length of the gel plug must de-swell, and the excess water must be expelled through the gel's length, before the fluid can flow through the tube. A second design was fabricated (Figure 2.8b), in order to improve valve performance and tolerance.

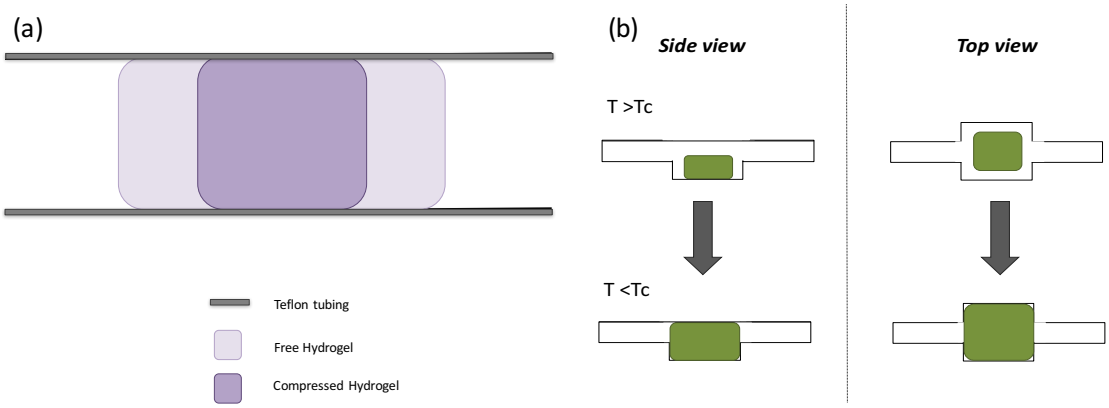

Figure 2.8. Schematic illustration of the pNIPAAm thermo-responsive hydrogel valve; (a) shows the hydrogel plug confined in the Teflon tube under free conditions and when compressed by two stainless steel rods that fit into the Teflon tube; (b) shows the side and top views of the valve when incorporated into a polycarbonate microfluidic devices at temperatures above (valve open) and below (valve closed) the critical temperature (Tc). Adapted from J. Wang et al. [52]

One important advance in this field is the *in-situ* polymerisation of hydrogels within microfluidic devices. In the work by Giger *et al.* [33], a p(NIPAAm) based polymer matrix was photo-polymerised using UV-light within an injection-molded channel. The thermal response was investigated for both on and off-chip actuation. Off-chip actuation involved the manual movement of the device on/off an aluminium hot plate set at 45 °C. On-chip actuation was made possible through the use of "on-chip" micro-heaters. In both cases, when the heat supplied to the systems reached a temperature at or above the LCST of p(NIPAAm), the polymer matrix contracted in volume, and the off-chip and on-chip opening times were ~3 s. Off-chip reclosing of the channel took ~20 s compared to ~5 s for on-chip reclosing. The results demonstrate that incorporation of micro-heaters into the microfluidic device can enable fast actuation and successful repeatability when compared to the manual off-chip method [33]. Recently this ability to use thermo-responsive hydrogels in autonomous microfluidic systems with little or no human intervention has been further improved through the work of Agarwal *et al.,* [53] through their work on "*autonomously-triggered on-chip microfluidic cooling devices*". They integrated a thermally-responsive polymer material at the axle of a nickel impeller with the purpose of controlling the impeller rotation autonomously. This study employed p(NIPAAm) as the thermally-sensitive actuation material in a microfluidic system

which comprised micro-channels, an on-chip cooling reservoir, an external heater and an external magnetic stirrer (Figure 2.9). At temperatures above the LCST, the polymer material contracted, enabling the rotation of the impeller and allowing fluid flow from the reservoir to cool the system. The opposite phenomenon was observed below the LCST, when expansion of the hydrogel prevented the Ni impeller from rotating. Integration of this thermo-responsive hydrogel into the aforementioned system as an actuator therefore provides the basis of autonomously-triggered on-chip microfluidic cooling device that could have applicability in a number of scenarios where on-chip temperature control and regulation is necessary.

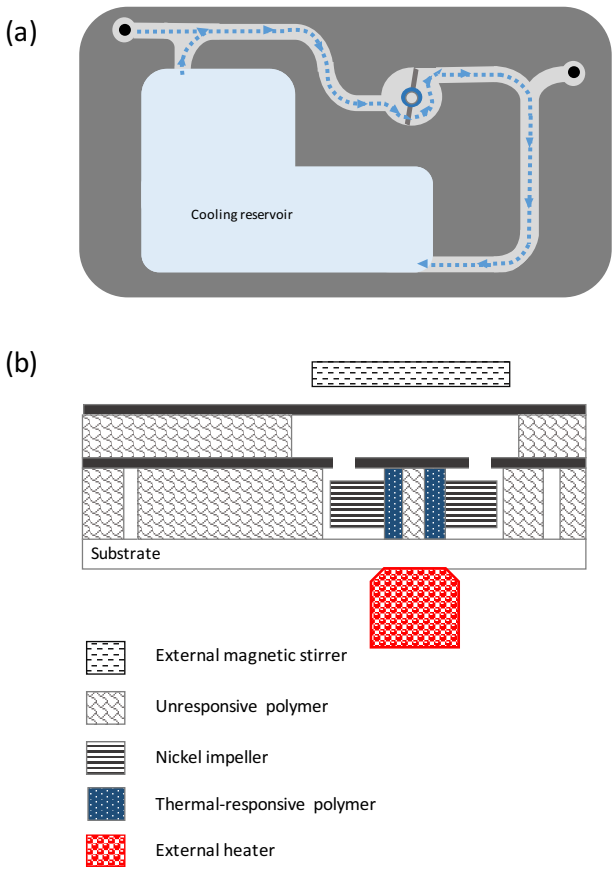

Figure 2.9. (a) Schematic illustration of the autonomously-triggered on-chip microfluidic cooling device. The dashed blue line and arrows show the pathway of the fluid as it is pumped and recirculated through the microchannels; (b) Cross-section of the device showing the device components; when the temperature of the heater is 32 °C, the hydrogel contracts and the Ni impeller rotates, pumping and recirculating cool water. Oppositely, when local temperatures drop below 32 °C, the hydrogel expands stopping the Ni impeller from rotating. (Adapted from Agarwal A. K. [53]).

2.3.5 Photo-induced Actuation

Light-driven responsiveness in polymers is normally achieved through the inclusion of a photochromic molecule, either by non-covalent doping or covalent attachment. When the photochromic unit is exposed to light of specific wavelengths[54-58] it exhibits an isomerisation change between two or more isomers that can have dramatically different properties (*e.g.* polarity, hydrophilic/hydrophobic character, geometry and charge density), that in turn can affect the properties of the surrounding polymeric matrix. Many photochromic molecules have been studied, but three of the best-known are spirobenzopyrans (SP) [54-56,59,60], azobenzenes[61,62], and diarylethenes[63], all of which show reversible photochromic behaviour, transforming from one isomer to another when exposed to different wavelengths of light. Much research has been carried out into optimising the photo-response of these materials when incorporated into hydrogel matrices, for exploitation in microfluidic systems as valves, pumps, mixers and alternating the topography of surfaces[64-67]. In addition to the development of the materials themselves (*e.g.* for optimisation of the photo-response kinetics), various polymerisation strategies have been investigated to enable the generation of precise micro-structures. Amongst them, the use of micropatterened light irradiation[68] enables specific hydrogels of different shapes and sizes to be polymerised using pre-designed photo-masks.

Sugiura *et al.* [69] first reported the use of photo-responsive hydrogels based on pNIPAAm as microfluidic integrated valves in acidic environments. The microfluidic platform presented was made of PDMS composed of three adjacent micro-channels, each with a micro-pillar around which the photo-responsive hydrogel was polymerized (Figure 2.10). Using three micro-channels in parallel, enabled individual valve actuation without the interference of adjacent channels to be demonstrated. The polymer material was p(NIPAAm) functionalised with a spirobenzopyran (SP) chromophore, photo-polymerised *in situ* around the micro-pillars to form micro-valves (Figure 2.10). In the dark, when SP-functionalised p(NIPAAm) is exposed to acidic conditions (*e.g.* pH 2-3), the following interactions occur: (1) the less hydrophilic colourless SP will transform to the more hydrophilic protonated, yellow coloured merocyanine ($MC\text{-}H^{+}$); (2) this triggers a conversion of the gel to a more hydrophilic configuration in which polymer-water interactions dominate; (3) the

pNIPAAm-*co*-SP hydrogel expands as more water is drawn in through diffusion. When exposed to visible light, the hydrogel material contracts, as the MC-H^+ isomer reverts to the SP form, triggering precipitation of the pNIPAAm chains and expulsion of water from the gel.

To enable reversible actuation of this material, the hydrogel required an acidic environment (0.05 mM HCl). Each valve was tested separately and a reduction of 52% in diameter was obtained within 18-32 s of light irradiation. After a total of 120 s, the gel had contracted by 68% of the initial diameter due to photo-induced dehydration of the polymer chain. Although the shrinking response was fast, the reswelling of the gel needed more than one hour, in the 0.05 mM HCl solution [60,68-72].

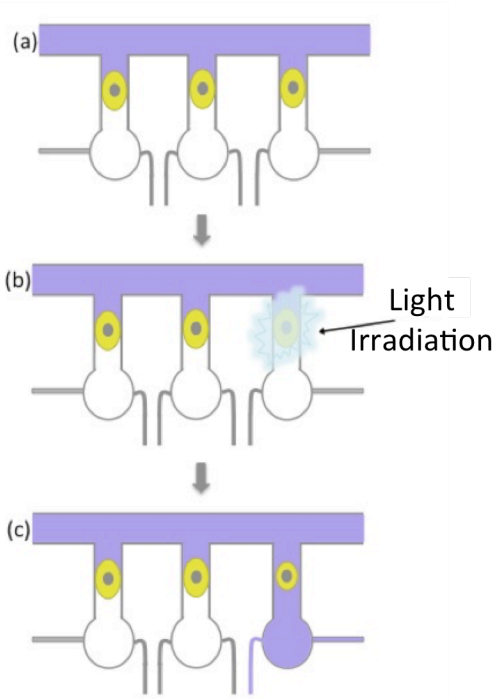

Figure 2.10. Illustration showing three parallel micro-channels each containing a photo-polymerised hydrogel valve; individual valve actuation can be achieved without interference with adjacent valves. (a) channels before valve photo-actuation, (b) during photo-actuation and (c) represents the channel after photo-actuation (Adapted from Sugiura et al. [69]).

In order to improve the response time of p(NIPAAm-*co*-SP) hydrogels, ionic liquids (ILs) were introduced as plasticizers. Four different novel ionogels were used as

photo-actuated valves in microfluidic manifolds. The spiropyran-functionalised ionogels were composed of pNIPAAm and phosphonium-based ionic liquids. The ionogels were photo-polymerized *in situ*, in micro-channels of a poly(methyl methacrylate) (PMMA) microfluidic device. Varying the ionogel composition meant that only one source of light was required for actuation (Figure 2.11). The response and visible contraction observed was very fast (seconds), while the re-expansion remained relatively slow (minutes). As each gel opened the channel at different times, such device allowed independent control of multiple micro-valves. In this work, it was found that the anion present in the ionic liquids directly affected the photo-responsiveness of the ionogel and thus the actuation behaviour; *i.e.* the actuation kinetics could be controlled to an extent by varying the anion of the phosphonium IL, with the $[NTf_2]^-$ exhibiting the fastest reponse. Although it was possible to reuse these valves, their long reswelling times and requirement for an acidic environment (0.1 mM HCl) made them a more appropriate candidate for single use devices [73].

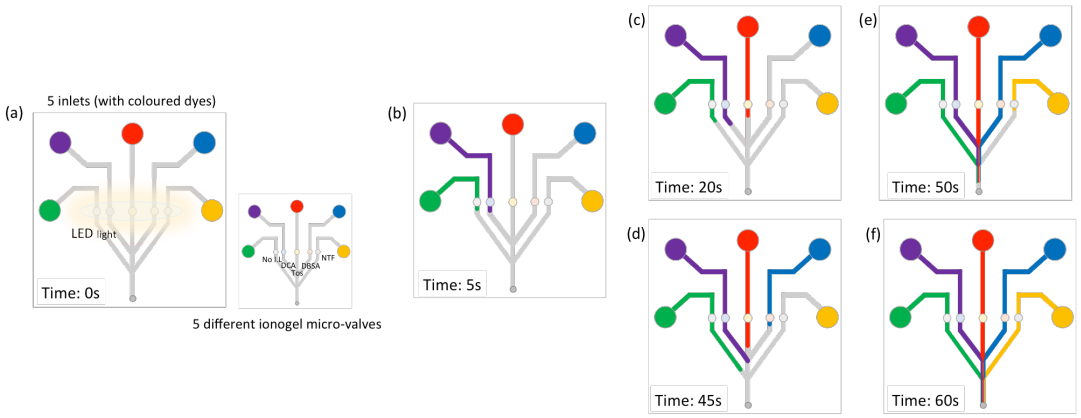

Figure 2.11. Illustration showing the performance of the ionogel micro-fluidic valves; a) micro-valves composed of the different ionogels are expanded and the valves are closed before light irradiation. b)-d) depending on the anion incorporated inside the ionogel, each valves opens after different times of light irradiation. (Adapted from Benito-lopez et al [73]).

Ziółkowski *et al*.[66] demonstrated an acrylic acid (AA) moiety incorporated into the backbone of p(NIPAAm-*co*-SP) could provide an internal source of protons, enabling photo-responsive hydrogel behavior at neutral pH (Figure 2.12). This is because in the dark, at neutral pH, acrylic acid (pK_a ~ 4.2) dissociates and the H^+ is used to spontaneously protonate MC (pk_a~6-7) to MC-H^+. Hence, in the absence of

light, the gel will become populated with MC-H^+ and $–COO^-$ groups, considerably increasing the gel hydrophilicity, and triggering gel swelling due to water ingress. Conversely, when MC-H^+ is converted to the SP form under white light irradiation (Figure 2.12), it is believed that the localised pH decrease, causes the protons released from MC-H^+ to migrate back to the acrylate anions in the polymer, as they are now the strongest base present (–COOH pK_a ~ 4.2 compared to SP pk_a ~ 2.3). Protonation of the acrylate $–COO^-$ anions and simultaneous formation of uncharged SP induces a much more hydrophobic gel character, causing the pNIPAAm based polymer to collapse and water is expelled. Therefore, during swelling and contraction cycles, protons migrate between these sites, as shown in Figure 2.12. This study also investigated optimal acrylic acid: monomer ratio in the polymer, for improved light-induced volume changes. The study showed that these acrylic acid/spiropyrans modified gels (p(NIPAAm-*co*-SP-*co*-AA) could be used to make photo-controlled valves in a microfluidic system without the need for an acidic environment for reswelling [66].

In a related development, Dunne A. *et al*. [54] showed that the polymerisation solvent used can have a dramatic impact on the gel morphology, which also affects the light-induced actuation behavior of the resulting hydrogel.

Building on this research, Schiphorst J. *et al.* [67] further improved the actuation kinetics by varying the side chain on the spiropyran derivative. The improved formulation was then polymerised *in-situ* in a microfluidic channel to create a valve structure and exposed to blue light. Upon photo-exposure for 1 min the hydrogel valves contracted, opening the micro-channel and allowing fluid to flow. When the light was removed, the hydrogel expanded, once again blocking the channel (Figure 2.13). This process was seen to be successfully repeatable for several actuation cycles. This type of photo-actuation offers a scalable, reversible and non-invasive form of control in microfluidic devices, which requires no direct contact with the material.

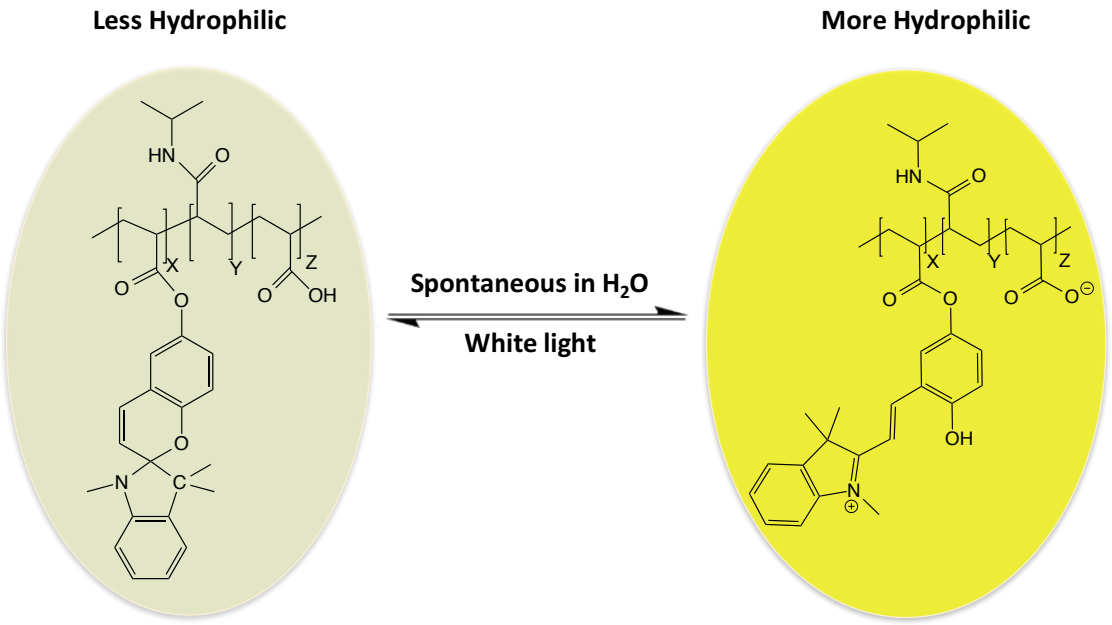

Figure 2.12. Representation of the proton exchange in the p(NIPAAm-co-SP-co-AA) hydrogels, between the acrylic acid and the spiropyran moieties together with the effect of white light irradiation; (right) more hydrophilic chains containing the protonated, yellow coloured merocyanine (MC-H^+); left: less hydrophilic chains obtained after white light irradiation due to the conversion of MC-H^+ to the hydrophobic SP form;

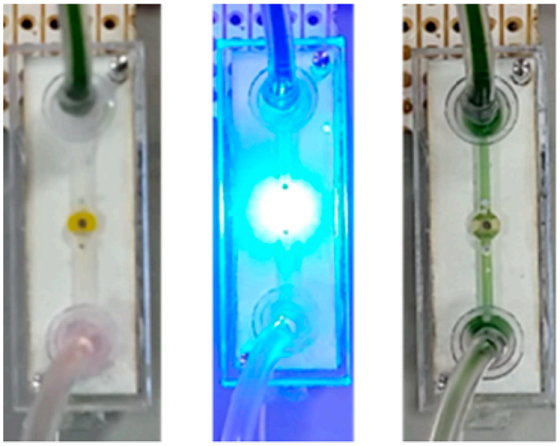

Figure 2.13. Photo-induced hydrogel valve actuation showing fluid flow modulation in a micro-channel; (left) p(NIPAAm-co-SP-co-AA) hydrogel is expanded and valve is closed; (middle) application of blue light; (right) hydrogel contracts upon light irradiation and valve opens allowing fluid to flow. (Reproduced from [67]).

2.3.6 Magneto-induced Actuation

Another mode of stimulation used to control stimuli-responsive hydrogels in microfluidics is the application of a magnetic field. Hydrogels responsive to magnetic stimuli can be created by replacing the polymerisation solvent with a colloidal solution that contains nanometer to micrometer scale magnetic particles. Examples include magnetorheological fluids or Ferro fluids [74]. When a magnetorheological fluid is exposed to a magnetic field, its viscosity will increase, directly affecting the mobility of the polymer chains and the shape of the hydrogel. Magnetic stimulation has shown to work best when coupled with a thermally responsive polymer, such as p(NIPAAm) based hydrogels. After incorporation into a pNIPAAm hydrogel, the magnetic particles adhere directly to the polymeric network. When these hydrogels are exposed to an Alternating Magnetic field (AMF), the magnetic particles begin to heat up, directly affecting the pNIPAAm polymer. When the temperature increases to above the pNIPAAm LCST , the hydrogel transitions to the less hydrophilic state, resulting in water expulsion and hydrogel volume contraction [75]. (Figure 2.14)

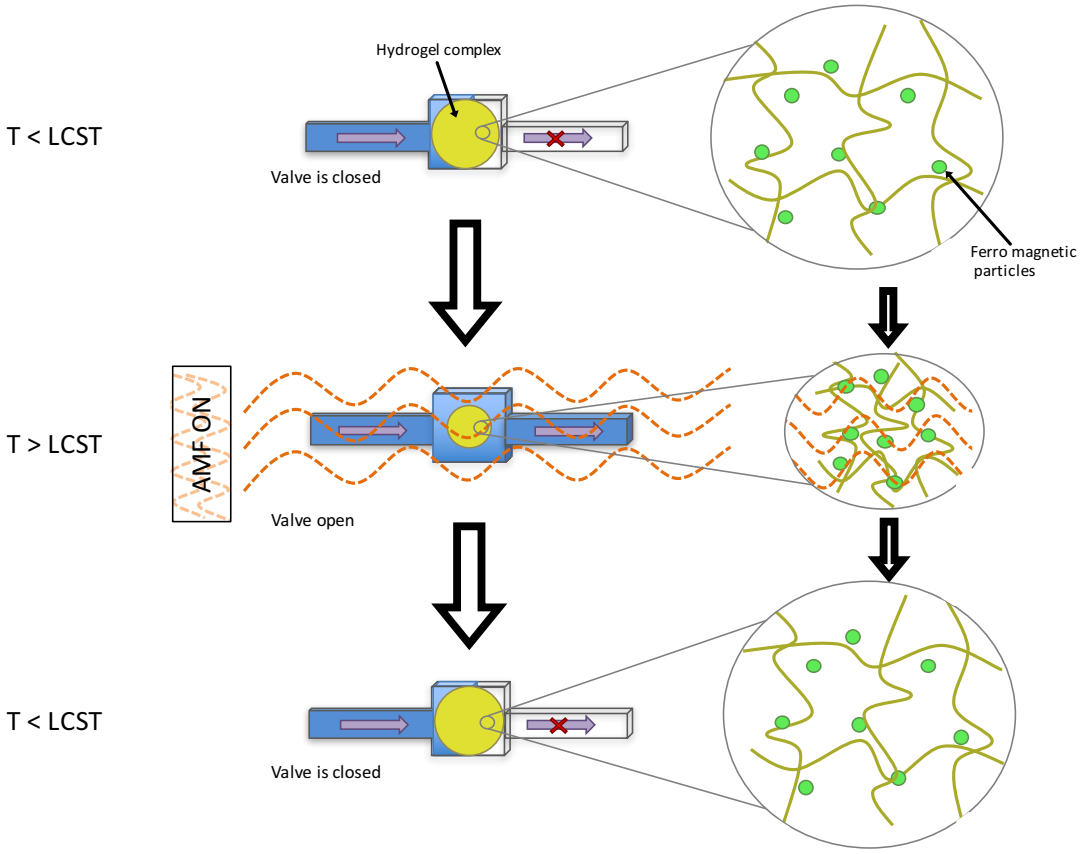

Figure 2.14. Schematic showing collapse of the hydrogel with the application of AMF, opening the valve. Adapted from N.S. Satarkar et al. [75].

Similarly, Ghosh *et al.* [76] has successfully demonstrated a magnetic-responsive ON/OFF system to control flow. The polymer material was composed of a p(NIPAAm) based hydrogel incorporating ferromagnetic nanoparticles (Fe_3O_4). Using oscillating magnetic fields a hydrogel contraction of ~80% was seen within 3 s of the magnetic field being applied. This study is consistent with the general rule that smaller scale hydrogel structures improve the kinetics of the actuation response. Most recently Hohlbein *et al.* have also presented a concept for on-demand self-healing elastomeric composites. Here, the magnetic nano-particles of different size, shape and composition were employed to act as nano-heaters, driven by a high-frequency AMF. This on-demand effect required very short times in order to 'self-heal' the elastomer, restoring its original shape [77].

Among the stimuli-responsive materials proposed for microfluidic applications described above, several advantages and disadvantages can be mentioned for each. For example, one great advantage of pH-responsive materials is their internal response to the pH of the solution flowing inside the microchannel, without external intervention. Therefore, there is no need for the addition of external specialised equipment to control the actuation of such materials, as their response relies on localised pH changes. A disadvantage of pH-responsive materials however, is the specific working pH range (typically 3-5 pH units), meaning that they are non-universal and have to be designed towards a specific application.

Thermo-responsive materials on the other hand, commonly exhibit fast response times and are generally independent of the working solution. However, they require external heating elements, which represents a significant hurdle for integration. Moreover, the increase in temperature can affect the surrounding solution and this can become problematic for biomedical applications, for example.

It could be then proposed that photo-responsive materials are possibly the most applicable for integration in microfluidic devices, primarily due to the nature of their autonomous (non-contact, external) actuation and the ease of integration of LED light

sources in the microfluidic device, if desired. This permits selective actuation of individual photo-actuators with minimal energy consumption.

2.4 Conclusions and Outlook

We believe that the use of stimuli-responsive materials in microfluidics forms the core of autonomous microfluidic-based analytical devices, which are of considerably lower cost compared to their etched silicon (glass) counterparts, more biomimetic in nature and offer increased adaptability. Although this chapter is focused on the use of stimuli-responsive materials for fluid movement at the microscale, it gives an insight into how the incorporation of such materials into microfluidics can allow for additional tasks *beyond the transport of reagents or samples.*

In living organisms, the fluidics system (*e.g.* cardiovascular system) performs multiple complex functions (*e.g.* sensing, detection, repair, waste removal; pH and temperature stabilization) in addition to the transport of fluids. Such characteristics of biological systems could be transferred into microfluidics through the creative use of adaptive materials and chemistries, to enable fundamental breakthroughs in chem/bio-sensing device performance. However, the future of biomimetic microfluidics relies on convincing demonstrators and their application in real scenarios where advanced functions such as autonomous fluid handling, sensing, detection and repair of damage, self-management and healing, could be demonstrated.

2.5 References

1. Stone, H.A.; Stroock, A.D.; Ajdari, A. Engineering flows in small devices. *Annual Review of Fluid Mechanics* **2004**, *36*, 381-411.
2. Gravesen, P.; Branebjerg, J.; Sonderga; rd Jensen, O. Microfluidics-a review. *J. Micromech. Microeng. J. Mioromech. Microeng* **1993**, *3*, 16-82.
3. Issadore, D.; Franke, T.; Brown, K.A.; Westervelt, R.M. A microfluidic microprocessor: Controlling biomimetic containers and cells using hybrid integrated circuit/microfluidic chips. *Lab on a chip* **2010**, *10*, 2937-2943.
4. Beebe, D.J.; Mensing, G.A.; Walker, G.M. Physics and applications of microfluidics in biology. *Annu. Rev. Biomed. Eng* **2002**, *4*, 261-286.
5. He, M.; Herr, A.E. Automated microfluidic protein immunoblotting. *Nat. Protocols* **2010**, *5*, 1844-1856.

6. Plessy, C.; Desbois, L.; Fujii, T.; Carninci, P. Population transcriptomics with single-cell resolution: A new field made possible by microfluidics. *BioEssays* **2013**, *35*, 131-140.
7. Argentiere, S.; Gigli, G.; Irini Gerges, M.M.; Blasi, L. Smart microfluidics: The role of stimuli- responsive polymers in microfluidic devices. In *Advances in Microfluidics*, InTech: 2012.
8. Tang, S.K.Y.; Whitesides, G.M. Basic microfluidic and soft lithographic techniques 2-1 introduction 2-3 materials for fabricating microfluidic devices.
9. Zhang, D.; Zhang, D.; Men, L.; Chen, Q. Review microfabrication and applications of opto-microfluidic sensors. **2011**.
10. Benito-Lopez, F.; Antoñana-Díez, M.; Curto, V.F.; Diamond, D. Modular microfluidic valve structures based on reversible thermoresponsive ionogel actuators. *Lab on a Chip* **2014**, *14*, 3530.
11. Ter Schiphorst, J.; Coleman, S.; Stumpel, J.E.; Ben Azouz, A.; Diamond, D.; Schenning, A.P.H.J. Molecular design of light-responsive hydrogels, for in situ generation of fast and reversible valves for microfluidic applications. *Chemistry of Materials* **2015**, *27*, 5925-5931.
12. Prettyman, J.B.; Eddington, D.T. Leveraging stimuli responsive hydrogels for on/off control of mixing. *Sensors & Actuators: B. Chemical* **2011**, *157*, 722-726.
13. Beebe, D.J.; Moore, J.S.; Bauer, J.M.; Yu, Q.; Liu, R.H.; Devadoss, C.; Jo, B.-H. Functional hydrogel structures for autonomous flow control inside microfluidic channels. *Nature* **2000**, *404*, 588-590.
14. Richter, A.; Klatt, S.; Paschew, G.; Klenke, C. Micropumps operated by swelling and shrinking of temperature-sensitive hydrogels. *Lab on a chip* **2009**, *9*, 613-618.
15. Florea, L.; Martin-Mayor, A.; Bou-Ali, M.M.; Meagher, K.; Diamond, D.; Tutar, M.; Benito-Lopez, F. Adaptive coatings based on polyaniline for direct 2d observation of diffusion processes in microfluidic systems. *Sensors and Actuators B: Chemical* **2016**, *231*, 744-751.
16. Riahi, R.; Tamayol, A.; Shaegh, S.A.M.; Ghaemmaghami, A.M.; Dokmeci, M.R.; Khademhosseini, A. Microfluidics for advanced drug delivery systems. *Current Opinion in Chemical Engineering* **2015**, *7*, 101-112.
17. Pfeiffer, S.A.; Nagl, S. Microfluidic platforms employing integrated fluorescent or luminescent chemical sensors: A review of methods, scope and applications. *Methods and Applications in Fluorescence* **2015**, *3*, 034003.
18. Eddington, D.T.; Beebe, D.J. Flow control with hydrogels. *Advanced drug delivery reviews* **2004**, *56*, 199-210.
19. Poelman, D.; Smet, P.F. Methods for the determination of the optical constants of thin films from single transmission measurements: A critical review. *Journal of Physics D: Applied Physics* **2003**, *36*, 1850.
20. Smela, E.; Gadegaard, N. Surprising volume change in ppy (dbs): An atomic force microscopy study. *Advanced Materials* **1999**, *11*, 953-957.

21. Smela, E.; Kallenbach, M.; Holdenried, J. Electrochemically driven polypyrrole bilayers for moving and positioning bulk micromachined silicon plates. *Journal of microelectromechanical systems* **1999**, *8*, 373-383.
22. Baughman, R. Conducting polymer artificial muscles. *Synthetic metals* **1996**, *78*, 339-353.
23. Smela, E. Conjugated polymer actuators for biomedical applications. *Advanced materials* **2003**, *15*, 481-494.
24. i Solvas, X.C.; Lambert, R.A.; Kulinsky, L.; Rangel, R.H.; Madou, M.J. Micromixing and flow manipulation with polymer microactuators. *Microfluidics and nanofluidics* **2011**, *11*, 405-416.
25. Madden, J.D.; Cush, R.A.; Kanigan, T.S.; Hunter, I.W. Fast contracting polypyrrole actuators. *Synthetic Metals* **2000**, *113*, 185-192.
26. Jager, E.W.; Smela, E.; Inganäs, O. On-chip microelectrodes for electrochemistry with moveable ppy bilayer actuators as working electrodes. *Sensors and Actuators B: Chemical* **1999**, *56*, 73-78.
27. Smela, E. Microfabrication of ppy microactuators and other conjugated polymer devices. *Journal of micromechanics and microengineering* **1999**, *9*, 1.
28. Smela, E. A microfabricated movable electrochromic "pixel" based on polypyrrole. *Advanced Materials* **1999**, *11*, 1343-1345.
29. Tanaka, Y.; Fujikawa, T.; Kazoe, Y.; Kitamori, T. An active valve incorporated into a microchip using a high strain electroactive polymer. *Sensors and Actuators B: Chemical* **2013**, *184*, 163-169.
30. Murray, C.; McCoul, D.; Sollier, E.; Ruggiero, T.; Niu, X.; Pei, Q.; Di Carlo, D. Electro-adaptive microfluidics for active tuning of channel geometry using polymer actuators. *Microfluidics and nanofluidics* **2013**, *14*, 345-358.
31. Dong, L.; Jiang, H. Autonomous microfluidics with stimuli-responsive hydrogels. *Soft matter* **2007**, *3*, 1223-1230.
32. Moorthy, J. Hydrogels in microfluidics. *SMART POLYMERS: Application in biotechnology and biomedicine, Taylor & Francis* **2007**, 437-457.
33. Geiger, E.J.; Pisano, A.P.; Svec, F. A polymer-based microfluidic platform featuring on-chip actuated hydrogel valves for disposable applications. *Journal of Microelectromechanical Systems* **2010**, *19*, 944-950.
34. Eichenbaum, G.M.; Kiser, P.F.; Simon, S.A.; Needham, D. Ph and ion-triggered volume response of anionic hydrogel microspheres. *Macromolecules* **1998**, *31*, 5084-5093.
35. De, S.K.; Aluru, N.; Johnson, B.; Crone, W.; Beebe, D.J.; Moore, J. Equilibrium swelling and kinetics of ph-responsive hydrogels: Models, experiments, and simulations. *Journal of Microelectromechanical Systems* **2002**, *11*, 544-555.
36. Kumar, A.; Srivastava, A.; Galaev, I.Y.; Mattiasson, B. Smart polymers: Physical forms and bioengineering applications. *Progress in Polymer Science* **2007**, *32*, 1205-1237.

37. Chaterji, S.; Kwon, I.K.; Park, K. Smart polymeric gels: Redefining the limits of biomedical devices. *Progress in polymer science* **2007**, *32*, 1083-1122.
38. Miyata, T.; Uragami, T.; Nakamae, K. Biomolecule-sensitive hydrogels. *Advanced drug delivery reviews* **2002**, *54*, 79-98.
39. Rodriguez, E.D.; Luo, X.; Mather, P.T. Linear/network poly (ε-caprolactone) blends exhibiting shape memory assisted self-healing (smash). *ACS applied materials & interfaces* **2011**, *3*, 152-161.
40. Hoare, T.R.; Kohane, D.S. Hydrogels in drug delivery: Progress and challenges. *Polymer* **2008**, *49*, 1993-2007.
41. Gupta, P.; Vermani, K.; Garg, S. Hydrogels: From controlled release to ph-responsive drug delivery. *Drug discovery today* **2002**, *7*, 569-579.
42. Turan, E.; Caykara, T. Swelling and network parameters of ph-sensitive poly (acrylamide-co-acrylic acid) hydrogels. *Journal of applied polymer science* **2007**, *106*, 2000-2007.
43. Schmaljohann, D. Thermo-and ph-responsive polymers in drug delivery. *Advanced drug delivery reviews* **2006**, *58*, 1655-1670.
44. Chung, J.; Yokoyama, M.; Yamato, M.; Aoyagi, T.; Sakurai, Y.; Okano, T. Thermo-responsive drug delivery from polymeric micelles constructed using block copolymers of poly (n-isopropylacrylamide) and poly (butylmethacrylate). *Journal of Controlled Release* **1999**, *62*, 115-127.
45. Kanazawa, H.; Yamamoto, K.; Matsushima, Y.; Takai, N.; Kikuchi, A.; Sakurai, Y.; Okano, T. Temperature-responsive chromatography using poly (n-isopropylacrylamide)-modified silica. *Analytical Chemistry* **1996**, *68*, 100-105.
46. Cirillo, G.; Spataro, T.; Curcio, M.; Spizzirri, U.G.; Nicoletta, F.P.; Picci, N.; Iemma, F. Tunable thermo-responsive hydrogels: Synthesis, structural analysis and drug release studies. *Materials Science and Engineering: C* **2015**, *48*, 499-510.
47. Prabaharan, M.; Mano, J.F. Stimuli-responsive hydrogels based on polysaccharides incorporated with thermo-responsive polymers as novel biomaterials. *Macromolecular bioscience* **2006**, *6*, 991-1008.
48. Okano, T.; Kikuchi, A.; Sakurai, Y.; Takei, Y.; Ogata, N. Temperature-responsive poly (n-isopropylacrylamide) as a modulator for alteration of hydrophilic/hydrophobic surface properties to control activation/inactivation of platelets. *Journal of controlled release* **1995**, *36*, 125-133.
49. Heskins, M.; Guillet, J.E. Solution properties of poly (n-isopropylacrylamide). *Journal of Macromolecular Science—Chemistry* **1968**, *2*, 1441-1455.
50. Wang, X.; Qiu, X.; Wu, C. Comparison of the coil-to-globule and the globule-to-coil transitions of a single poly (n-isopropylacrylamide) homopolymer chain in water. *Macromolecules* **1998**, *31*, 2972-2976.
51. Lutz, J.-F.; Hoth, A. Preparation of ideal peg analogues with a tunable thermosensitivity by controlled radical copolymerization of 2-(2-

methoxyethoxy) ethyl methacrylate and oligo (ethylene glycol) methacrylate. *Macromolecules* **2006**, *39*, 893-896.
52. Wang, J.; Chen, Z.; Mauk, M.; Hong, K.-S.; Li, M.; Yang, S.; Bau, H.H. Self-actuated, thermo-responsive hydrogel valves for lab on a chip. *Biomedical Microdevices* **2005**, *7*, 313-322.
53. Agarwal, A.K.; Dong, L.; Beebe, D.J.; Jiang, H. Autonomously-triggered microfluidic cooling using thermo-responsive hydrogels. *Lab on a Chip* **2007**, *7*, 310-315.
54. Dunne, A.; Delaney, C.; Florea, L.; Diamond, D. Solvato-morphologically controlled, reversible nipaam hydrogel photoactuators. *RSC Advances* **2016**, *6*, 83296-83302.
55. Florea, L.; Diamond, D.; Benito-Lopez, F. Photo-responsive polymeric structures based on spiropyran. *Macromolecular Materials and Engineering* **2012**, *297*, 1148-1159.
56. Florea, L.; Hennart, A.; Diamond, D.; Benito-Lopez, F. Synthesis and characterisation of spiropyran-polymer brushes in micro-capillaries: Towards an integrated optical sensor for continuous flow analysis. *Sensors and Actuators B: Chemical* **2012**, *175*, 92-99.
57. Tudor, A.; Florea, L.; Diamond, D. Multi-responsive semi-interpenetrating network hydrogels. **2015**.
58. Rosales, A.M.; Mabry, K.M.; Nehls, E.M.; Anseth, K.S. Photoresponsive elastic properties of azobenzene-containing poly (ethylene-glycol)-based hydrogels. *Biomacromolecules* **2015**, *16*, 798-806.
59. Fischer, E.; Hirshberg, Y. Formation of coloured forms of spirans by low-temperature irradiation. ROYAL SOC CHEMISTRY THOMAS GRAHAM HOUSE, SCIENCE PARK, MILTON RD, CAMBRIDGE CB4 0WF, CAMBS, ENGLAND: 1952; pp 4522-4524.
60. Sumaru, K.; Takagi, T.; Satoh, T.; Kanamori, T. Photo-induced reversible proton dissociation of spirobenzopyran in aqueous systems. *Journal of Photochemistry and Photobiology A: Chemistry* **2013**, *261*, 46 - 52.
61. Wang, Y.; Ma, N.; Wang, Z.; Zhang, X. Photocontrolled reversible supramolecular assemblies of an azobenzene-containing surfactant with α-cyclodextrin. *Angewandte Chemie International Edition* **2007**, *46*, 2823-2826.
62. Kumar, G.S.; Neckers, D. Photochemistry of azobenzene-containing polymers. *Chemical Reviews* **1989**, *89*, 1915-1925.
63. Matsuda, K.; Irie, M. Diarylethene as a photoswitching unit. *Journal of Photochemistry and Photobiology C: Photochemistry Reviews* **2004**, *5*, 169-182.
64. Stumpel, J.E.; Ziółkowski, B.; Florea, L.; Diamond, D.; Broer, D.J.; Schenning, A.P. Photoswitchable ratchet surface topographies based on self-protonating spiropyran–nipaam hydrogels. *ACS applied materials & interfaces* **2014**, *6*, 7268-7274.

65. Florea, L.; Diamond, D.; Benito-Lopez, F. Opto-smart systems in microfluidics. *Research Perspectives on Functional Micro-and Nanoscale Coatings* **2016**, 265.
66. Ziółkowski, B.; Florea, L.; Theobald, J.; Benito-Lopez, F.; Diamond, D. Self-protonating spiropyran-co-nipam-co-acrylic acid hydrogel photoactuators. *Soft Matter* **2013**, *9*, 8754-8760.
67. ter Schiphorst, J.; Coleman, S.; Stumpel, J.E.; Ben Azouz, A.; Diamond, D.; Schenning, A.P. Molecular design of light-responsive hydrogels, for in situ generation of fast and reversible valves for microfluidic applications. *Chemistry of Materials* **2015**, *27*, 5925-5931.
68. Sugiura, S.; Szilágyi, A.; Sumaru, K.; Hattori, K.; Takagi, T.; Filipcsei, G.; Zrínyi, M.; Kanamori, T. On-demand microfluidic control by micropatterned light irradiation of a photoresponsive hydrogel sheet. *Lab on a Chip* **2009**, *9*, 196-198.
69. Sugiura, S.; Sumaru, K.; Ohi, K.; Hiroki, K.; Takagi, T.; Kanamori, T. Photoresponsive polymer gel microvalves controlled by local light irradiation. *Sensors and Actuators A: Physical* **2007**, *140*, 176-184.
70. Sumaru, K.; Takagi, T.; Sugiura, S.; Kanamori, T. Spiropyran-functionalized hydrogels. In *Soft actuators*, Springer: 2014; pp 219-229.
71. Szilágyi, A.; Sumaru, K.; Sugiura, S.; Takagi, T.; Shinbo, T.; Zrínyi, M.; Kanamori, T. Rewritable microrelief formation on photoresponsive hydrogel layers. *Chemistry of materials* **2007**, *19*, 2730-2732.
72. Sumaru, K.; Ohi, K.; Takagi, T.; Kanamori, T.; Shinbo, T. Photoresponsive properties of poly (n-isopropylacrylamide) hydrogel partly modified with spirobenzopyran. *Langmuir* **2006**, *22*, 4353-4356.
73. Benito-Lopez, F.; Byrne, R.; Răduţă, A.M.; Vrana, N.E.; McGuinness, G.; Diamond, D. Ionogel-based light-actuated valves for controlling liquid flow in micro-fluidic manifolds. *Lab on a Chip* **2010**, *10*, 195-201.
74. Zrinyi, M. Intelligent polymer gels controlled by magnetic fields. *Colloid and Polymer Science* **2000**, *278*, 98-103.
75. Satarkar, N.S.; Zhang, W.; Eitel, R.E.; Hilt, J.Z. Magnetic hydrogel nanocomposites as remote controlled microfluidic valves. *Lab on a Chip* **2009**, *9*, 1773-1779.
76. Ghosh, S.; Yang, C.; Cai, T.; Hu, Z.; Neogi, A. Oscillating magnetic field-actuated microvalves for micro-and nanofluidics. *Journal of Physics D: Applied Physics* **2009**, *42*, 135501.
77. Hohlbein, N.; Shaaban, A.; Schmidt, A. Remote-controlled activation of self-healing behavior in magneto-responsive ionomeric composites. *Polymer* **2015**, *69*, 301-309.

Chapter 3

Solvato-Morphologically Controlled, Reversible NIPAAm Hydrogel Photoactuators*

***Solvato-Morphologically Controlled, Reversible Photo-Actuated Hydrogels, Operative in Neutral Environments**, Aishling Dunne, Colm Delaney, Larisa Florea*, Dermot Diamond, *RSC Advances,* 6 (2016) 83296-83302.

Chapter 3:

Solvato-Morphologically Controlled, Reversible NIPAAm Hydrogel Photoactuators

3.1 Abstract

Photo-actuator hydrogels were generated using a *N*-isopropylacrylamide-*co*-acrylated spiropyran-*co*-acrylic acid (p(NIPAAm-*co*-SP-*co*-AA)) copolymer, in 100-1-5 mole ratio. Different ratios of deionised water: organic solvent (tetrahydrofuran, dioxane and acetone) were used as the polymerisation solvent. By changing the polymerisation solvent, the pore size and density of the hydrogels were altered, which in turn had an impact on the diffusion path-length of water molecules, thus influencing the swelling and photo-induced shrinking kinetics of the hydrogel. We successfully demonstrated that the polymerisation solvent has a significant effect on the curing time, the elasticity and morphology of the resulting hydrogel. The highest shrinking ratio was obtained in the case where 4:1 acetone: deionised water was used as the polymerisation solvent, with the hydrogel reaching 39.56% (±2.37% (n=3)) of its hydrated area after 4 min of white light irradiation followed by reswelling in the dark to 61.95% (±5.76% (n=3)) after 11 min. Conversely, the best reswelling capabilities were obtained for the hydrogels polymerised in the presence of 1:1 tetrahydrofuran: deionised water, when the shrunk hydrogel (61.73±0.26% (n=3)) regained 91.31% (±0.22% (n=3)) of its original size after 11 min in the dark. To our knowledge, this is the largest reported photo-induced area change for self-protonated spiropyran containing hydrogels. The shrinking/reswelling process was completely reversible in DI water with no detectable hysteresis over three repeat irradiation cycles.

3.2 Introduction

Hydrogels can be defined as three dimensional polymer matrices which are able to hold large quantities of water in relation to their size[1]. In recent years hydrogels have been used in a number of different applications such as diagnostics and therapeutics [2,3] tissue engineering [4], wound dressings [5] and drug delivery [6-8], microfluidics[9], among others[10,11]. Stimuli-responsive hydrogels in particular have gained increasing attention over the last decade due to their responsive nature towards internal or external stimuli, with little or no human intervention [9,12]. By incorporating stimuli-responsive units in their structure, hydrogel actuators can be

developed, that respond to a variety of stimuli such as light [10,11,13,14], pH [10,15,16], electric [10,11] or magnetic fields [10,11,17] and temperature [10,11,16,18]. Amongst these, photo-responsive materials are particularly attractive as they can be actuated externally, in a non-invasive, non-contact manner.

In recent years, photo-responsive hydrogels reported in the literature have been overwhelmingly focused on crosslinked copolymers of *N*-isopropylacrylamide (NIPAAm) with spiropyran photochromic derivatives. One disadvantage of this approach was the need for an external acidic environment (typically 10 mM HCl) to ensure protonation of the spiropyran (SP) to the protonated merocyanine (MC-H^+) form. The MC-H^+ form is more hydrophilic compared to the SP form, and its formation triggers swelling of the gel. When irradiated with white/blue light (λ_{max} MC-H^+= 422 nm)[19,20], the MC-H^+ form is converted back to the more hydrophobic SP form and the free protons diffuse into the external environment. Simultaneously, the polymer network collapses into the compact globular form, the water is expelled, and the hydrogel contracts. In order to induce re-swelling, the hydrogel had to be immersed again in acidic environments to drive formation of the protonated merocyanine [14,20,21]. Additionally, the re-swelling times were long, typically up to several hours[14,19,20]. These disadvantages restricted p(NIPAAm-*co*-SP) photo-actuated hydrogels to single-use applications.

Recently, we reported that the addition of acrylic acid (AA), which, when copolymerised within the hydrogel, provides an internal source of protons for reversible hydrogel photo-actuation in neutral pH environments[22,23]. The addition of the AA comonomer successfully removed the requirement for external acidic conditions and expanded the working range of the photo-actuator to between pH 2 - pH 7, making it suitable for a wide variety of biological applications. However, the prolonged shrinking and reswelling times (20 min of white light irradiation to reach ~82% of its fully hydrated size followed by 60 min in the dark to achieve reswelling up to 98%) [22], constituted significant limitations for application of these photo-actuators.

In order to improve the shrinking/swelling kinetics of hydrogels, several approaches have been undertaken including 1) the introduction of novel materials such as ionic liquids to tune the overall hydrophilicity/hydrophobicity of the gel network [24-26] or

2) the use of pore-forming agents to create highly porous gels with shorter average pathlengths for water diffusion [27,28].

Alternatively, hydrogel actuation can be controlled through variation of the photochromic unit itself, through the use of electron withdrawing or electron-donating substituents [20,21].

The polymerisation solvent has also been shown to directly influence the morphology of hydrogels, by producing hydrogels with differing degrees of porosity [29-32].

In this study, photo-actuator hydrogels were generated using a *N*-isopropylacrylamide-*co*-acrylated spiropyran-*co*-acrylic acid (p(NIPAAm-*co*-SP-*co*-AA)) copolymer, in a 100-1-5-mole ratio. In order to allow for control of the photo-induced shrinking and reswelling times of the hydrogels, different ratios of DI water: organic solvent (tetrahydrofran (THF), dioxane and acetone) were used as the polymerisation solvent. Varying the organic solvent, and the volume ratio of the solvent mixtures resulted in hydrogels with varying porosity, which in turn has affected the physical and mechanical properties, swelling/shrinking degree and photo-actuation kinetics of the hydrogel system.

3.3 Experimental

3.3.1 Materials and Methods

N-isopropylacrylamide 98% (NIPAAm), N,N'-methylenebisacrylamide 99% (MBIS), phenylbis(2,4,6 trimethyl benzoyl) phosphine oxide 97% (PBPO), acrylic acid (180-200ppm MEHQ as inhibitor) 99% (AA), were acquired from Sigma Aldrich, Ireland and used as received. 1',3',3'-Trimethyl-6-acryloylspiro(2H-1-benzopyran-2,2-indoline) (SP-A) was synthesised as described elsewhere[22].

3.3.2 Single-Crystal X-ray Diffraction

Crystals of SP-A, suitable for Single-Crystal X-ray Diffraction, were grown by slow diffusion from hexane: ethyl acetate (8:1). The structure was solved and refined using the Bruker SHELXTL Software Package, with a P21/c space group, for Z = 4.

The final anisotropic full-matrix least-squares refinement on F^2 with 238 variables converged at R1 = 6.29%, for the observed data and wR2 = 17.36% for all data. The goodness-of-fit was 1.029. The molecules were observed to pack in a head-to-tail manner, as shown in Fig. A1, with strong π-π interactions between adjacent benzopyran and indoline portions of neighbouring molecules.

3.3.3 Gel Preparation

For hydrogel synthesis, the monomeric cocktail consisted of 200 mg NIPAAm, 8.17 mg MBIS (3 mol% relative to NIPAAm), 6.09 mg SP-A (1 mol% relative to NIPAAm), 7.34 mg PBPO (1 mol% relative to NIPAM) and 6.03 µL AA (5 mol% relative to NIPAAm) dissolved in 500 µL of the polymerisation solvent (4:1, 2:1 and 1:1, respectively, vol: vol, organic solvent: DI water). Circular hydrogels were prepared in a home-made cell consisting of a 1H,1H,2H,2H-perfluorodecyltriethoxy saline functionalised glass slide and a glass cover slide separated by a 250 µm high spacer made out of poly(methyl methacrylate)/pressure sensitive adhesive (PMMA/PSA)(Fig. A1.2). The cell was filled by capillary action with the monomer solution and subsequently exposed to white light through a photo-mask consisting of 1 mm diameter transparent disks. The polymerization time was 20-30s, depending on the polymerization solvent mixture employed. The white light source used was a Dolan-Jenner-Industries Fiber-Lite LMI LED lamp having two gooseneck waveguides placed at a distance range of 1 to 2 cm from the platform. The light intensity measured with a Multicomp LX-1309 light meter was 320–337 kLux. After polymerisation, the obtained circular hydrogels were washed gently with ethanol and DI water to remove any unpolymerised materials and allowed to swell in deionised water for 4-6 hours to ensure full hydration.

3.3.4 Rheology

Rheology curing measurements were performed on the unpolymerised cocktail. The measurements were carried out on an Anton Paar MCR 301 rheometer using a CP50-2 tool with a diameter of 49.97 mm and a cone angle of 1.996°. White light curing was initiated after 60 s with a light intensity of 200-225 kLux at 25°C. Rheology

studies of the hydrated gels were done using the PP15 parallel plate tool of 15 mm diameter. For this, amplitude sweep tests were carried out at a 100 rad/s angular frequency and a normal force of 1 N.

3.3.5 Scanning Electron Microscopy

The hydrogel samples were first swollen in DI water, and then frozen with liquid nitrogen and subsequently freeze-dried using a Labconco freeze-drier, model 7750060. The samples were kept overnight at 0.035 mBar pressure and a temperature of -40 ˚C. The freeze-dried hydrogels were imaged using Scanning Electron Microscopy (SEM) performed on a Carl Zeiss EVOLS 15 system at an accelerating voltage of 14.64 kV. Samples were placed onto silicon wafers and coated with a 10 nm gold layer prior to imaging.

3.3.6 Photo-actuation Measurements

For white light irradiation shrinking and reswelling measurements, the hydrogels were placed in a custom-made cell, comprising 2 cover glass slides separated by 500 μm high spacers made out of PMMA/PSA. The imaging was carried out with an Aigo GE-5 microscope using a 60x objective lens with the accompanying software. The light was provided by a Dolan-Jenner-Industrie Fiber-Lite LMI with a light intensity of ~210 kLux through two waveguide goosenecks placed 2-3 cm away from the sample. Each sample was exposed to white light irradiation for 4 min then placed in the dark for a further 11 min. The area measurements of the freestanding hydrogel discs were performed using Image J (1.47v) software. Three different hydrogels were measured for each point and the relative area % was calculated using the following equation (n=3):

$$Relative\ area\ (\%) = \frac{A_t}{A_o} \times 100$$

A_t = Measured area at time t

A_o = Area of a fully hydrated gel

3.4 Results and Discussion

3.4.1 Photo-induced Curing

Rheology was used to study the effects of the polymerisation solvent on the curing times and properties of the hydrogels obtained. The photo-induced curing measurements were carried out for each monomeric cocktail using different polymerisation solvent mixtures, as described in the experimental section. All samples were exposed to white light and the storage modulus recorded. The storage modulus increased with time and reached a plateau, indicating that full polymerisation had occurred. It was observed that the plateau region of the storage modulus was dependent on the polymerisation solvent used (Fig. 3.1, Fig. A1.4-A1.6). The storage moduli in the 4:1 organic solvent: DI water series remain relatively unchanged after ~190s of white light irradiation, confirming that full polymerisation had been achieved (Fig. 3.1). The hydrogels which were polymerised in the presence of dioxane: DI water showed the highest storage modulus plateau (Fig. A1.3), suggesting that when dioxane was used in the polymerisation mixture, hydrogels with greater elastic properties were produced (Table 3.1)[33].

During the curing process the storage modulus quickly surpassed the loss modulus. This is known as the "gel point" and is where the material exhibits more elastic than viscous behaviour. For all the samples examined, the gel point was achieved within the first ~70 s after the start of the experiment, meaning that it was reached within ~10 s after the photo-polymerisation was initiated (white light is turned on after 60s).

Tanδ is a representation of the ratio of the elastic (storage modulus) and viscous (loss modulus) moduli, (G″/G′). This parameter helps to identify how tacky/sticky the hydrogel is (Table 3.1). It was observed that hydrogels which were polymerised in the presence of 1:1 organic solvent: DI water had the highest Tanδ values in their respective series (Table 3.1). These results suggest that using lower organic solvent content in the polymerisation mixture produced hydrogels which were tackier/stickier and more delicate to handle.

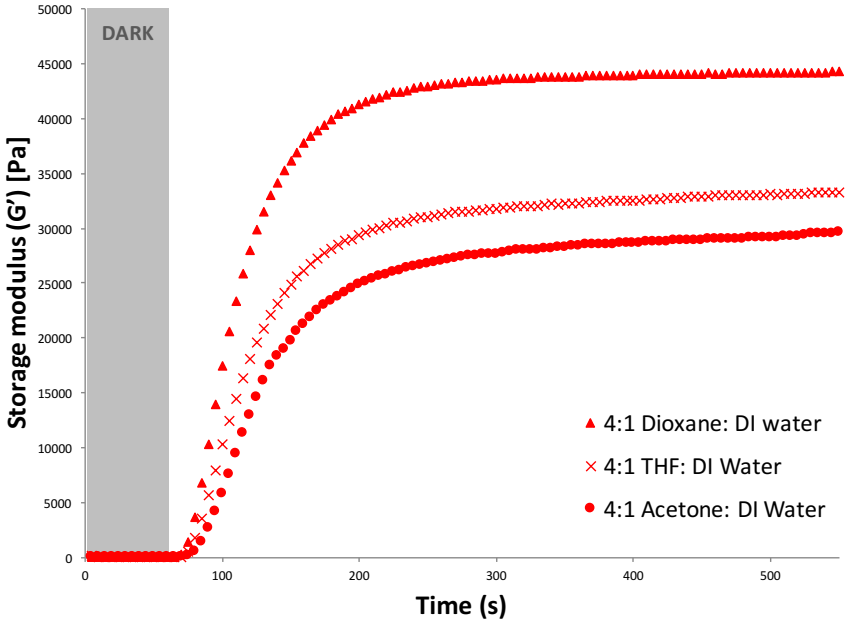

Figure 3.1: Photo-curing of hydrogels produced when the polymerisation solvent was 4:1 (V:V) organic solvent (THF, dioxane and acetone, respectively) : deionised water. White light polymerisation was initiated after 60 s.

Table 3.1. Rheological properties of monomeric cocktails during photo-induced curing in the presence of different polymerisation solvent mixtures. The storage (G') and loss moduli (G") measurements were recorded after 360s of white light irradiation. (G'-storage modulus, G" - loss modulus).

Gel ID	***G' [Pa]***	***G" [Pa]***	***Tan δ (G"/G')***	***Gel point [s]***
4:1 THF: DI water	32600	168	5.15×10^{-3}	70
2:1 THF: DI water	30700	110	3.58×10^{-3}	70
1:1 THF: DI water	12000	184	1.53×10^{-2}	70
4:1 Dioxane: DI water	44000	74.9	1.70×10^{-3}	70
2:1 Dioxane: DI water	44400	49.8	1.12×10^{-3}	70
1:1 Dioxane: DI water	47700	202	4.23×10^{-3}	75
4:1 Acetone: DI water	28700	30.2	1.05×10^{-3}	70
2:1 Acetone: DI water	35900	93.8	2.61×10^{-3}	70
1:1 Acetone: DI water	13000	80.5	6.19×10^{-3}	75

3.4.2 Hydrogel Morphology

A Scanning Electron Microscopy (SEM) study was carried out as described in the experimental section, to investigate the effect of different polymerisation solvents on the morphology of the resulting hydrogels. Varying solvent ratios was seen to produce hydrogels of different pore sizes. For example, when THF: DI water was employed as the polymerisation solvent (Fig. 3.2), it was revealed that as the organic solvent content was decreased, the pore size also decreased. This is possibly due to the well-known co-nonsolvency of pNIPAAm in different solvent mixtures, including THF:water, where depending on the solvent ratio, pNIPAAm shows drastic conformation changes from fully swollen coil to a globular state [32,34-36]. For example, in the case of MeOH:water mixtures, it was shown that pNIPAAm becomes insoluble at a molar ratio of MeOH (X_{MeOH}) between 0.13-0.4, while for $X_{MeOH} < 0.13$ and $X_{MeOH} > 0.4$ PNIPAAm is soluble[34]. Similar observations have been made in the case of other binary solvent systems such as THF:water and DMSO:water, where the solubility of pNIPAAm depends on the ratio of the two solvents[32,36,37]. It is therefore believed that as the polymeric chains are growing they will either precipitate in a globular conformation or adopt an extended coil conformation due to their solvency. This in turn determines the pore size and density of the resulting hydrogel. From the representative SEM images of the THF: DI water series, it is revealed that the pore size range of the hydrogels polymerised in the presence of 1:1 v:v THF: DI water was 1.11-1.66 μm (Fig. 3.2c), considerably smaller when compared to 4:1 volume ratio, which resulted in hydrogels having pore sizes ranging from 5.61-6.47 μm (Fig. 3.2a). This shows the direct effect of the solvent ratio on the pore size development. The hydrogels which were polymerised in the presence of Dioxane: DI water did not follow the pore development pattern seen for THF: DI water, but produced gels with a much broader pore size distribution in the range of 4.75 μm to 8.15 μm (Fig. A1.6-A1.8).

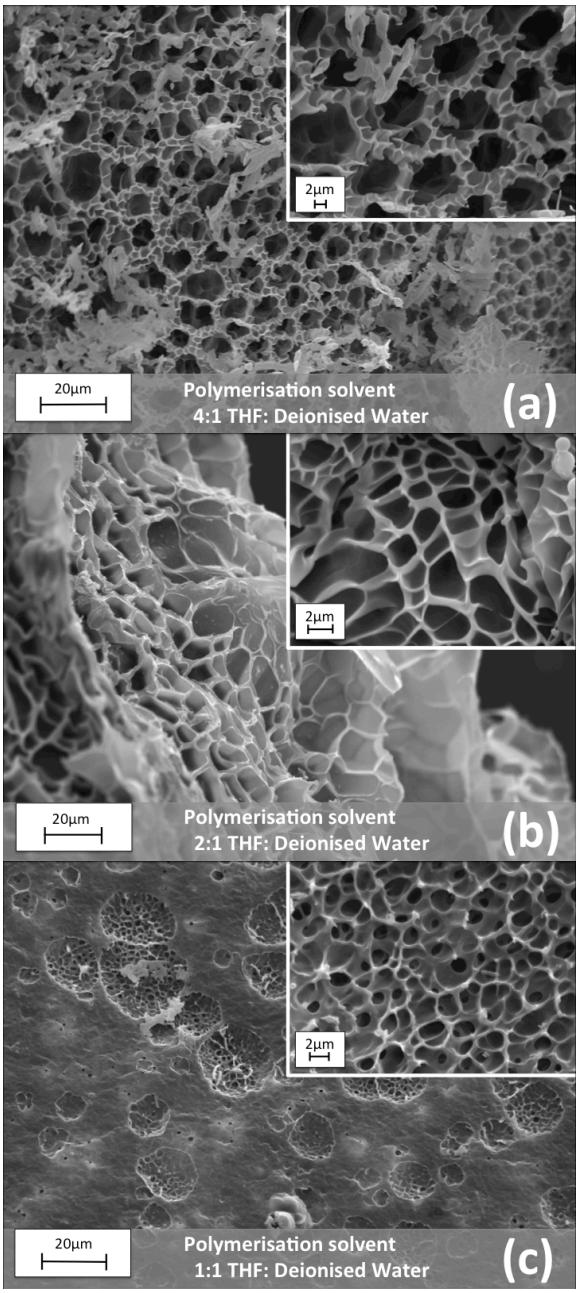

Figure 3.2: SEM images of hydrogels synthesised using different (V: V) ratios of THF: DI water as the polymerisation solvent.

3.4.3 Oscillation Analysis

Amplitude sweep measurements (Fig. 3.3 and ESI Fig. A12 and A13) were performed on the fully hydrated gels in order to determine their mechanical properties and relate these with the porosity of the hydrogels. It would be expected that the hydrogels with larger pore sizes would show weaker mechanical properties due to less polymer being present. This correlation was evident when comparing the results from

the oscillation study of the hydrated gels with the SEM data. In the case when THF: DI water mixture was used as the polymerisation solvent, amplitude sweep measurements (Fig. 3.3) show that the 1:1 THF: DI water and 2:1 THF: DI water gels have a higher (visco)elastic modulus (10–13 kPa) compared to the 4:1 THF: DI water gel (~5 kPa). Intuitively, one would expect that highly porous gels are more flexible, less stiff and cannot withstand high stress, causing them to reach the linear viscoelastic range (LVE) quicker than less porous polymers. In this study we have selected 10% as tolerance threshold and all G' values below 90% of the plateau value are considered to be outside the LVE range. In this context, the 1:1 THF: DI water gel can withstand higher shear stress before it reaches the linear viscoelastic range (LVE) of ~1 kPa. The 4:1 and 2:1 THF: DI Water hydrogels reached the LVE limit quicker and with less shear stress of ~300 Pa.

The amplitude sweep results for the hydrogels with Acetone: DI water and dioxane: DI water as the polymerisation solvents (ESI Fig. A12 and Fig. A13, respectively) have provided results that complement the pore sizes obtained from the SEM study (ESI Table A2). The LVE limits for the dioxane: DI water gels show similar values of ~800 Pa for all the solvent ratios in agreement with the porosity data obtained from the SEM. Similar comparisons can be made in the case of the hydrogels polymerised in the presence of Acetone: DI water (LVE range 1 - 2.2 kPa).

Overall the increase in hydrogel porosity decreases the stiffness and mechanical strength of the hydrogels. Nevertheless, all the hydrogels obtained in this study are still strong enough to be handled for actuation and measuring purposes, and possess storage modulus values of about 5-20 kPa [38].

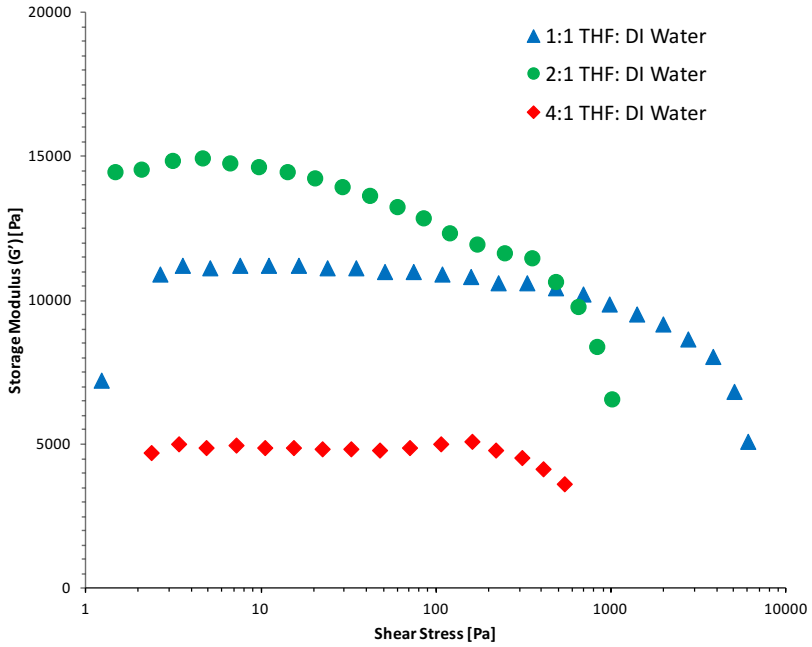

Figure 3.3: Storage moduli versus shear stress of the hydrated hydrogels polymerised in the presence of THF: DI water solvent mixtures during a strain amplitude sweep using a normal force of 1N.

3.4.4 Photo-actuation Study

The main objective of this study was the correlation of the photo-induced shrinking and subsequent swelling of the p(NIPAAm-*co*-SP-*co*-AA) hydrogels in relation to their solvato-induced porosity and mechanical properties. In this context, a photo-actuation study was carried out on the nine hydrogel variations polymerised in the presence of different solvent mixtures. The expansion and contraction of each hydrogel sample were measured in a series of three actuation cycles in DI water in order to investigate the reversibility of photo-actuation. When the p(NIPAAm-*co*-SP-*co*-AA) hydrogels were immersed in DI water, in the dark, they expanded due to the protonation of the SP unit to the more hydrophilic MC-H^+ by the AA comonomer (pK_a ~4.5) which serves as an internal acid source (Fig. 3.4). Under these conditions the hydrogel has a yellow colour due to the absorption spectrum of MC-H^+ (λ_{max} = 422nm) [19]. When the same hydrogel was irradiated with white light, a rapid colour change was observed due to the deprotonation of MC-H^+ and its reversion back to the colourless SP form. The SP form is more hydrophobic causing the polymer chains to collapse, thereby expelling water and triggering hydrogel contraction.

During this study, the fully hydrated gels were exposed to white light for 4 min and returned to the dark for a further 11 min to allow reswelling and this process was repeated three times (Fig. 3.5, Fig. 3.6 and Fig. A14-A20). These times were sufficient to reach a close steady state (Fig. A21-A23). The area contraction and expansion of the hydrogels polymerised in the presence of THF: DI water are shown in Figure 3.5. Comparing the three volume ratios 4:1, 2:1 and 1:1, respectively, of the THF: DI water solvent mixture, a difference in the degree of hydrogel contraction was observed. The hydrogel samples polymerised using 4:1 THF: DI water as the polymerisation solvent have contracted the most in this series (to 51.43% of their initial size), when compared to the hydrogels 2:1 (58.94%) and 1:1 (61.78%) of the same solvent mixture (Table 3.2). The results are in agreement with the pore sizes obtained, where the 4:1 THF: DI water hydrogels showed the largest pores of the series, enhancing the degree of shrinking of this sample by improving the water diffusion out of the hydrogel. However, the expansion in relative area for the 2:1 hydrogel is much lower (75.17%) than the 4:1 and 1:1 ratios (82.99% and 91.31% respectively). This may be attributed to the increased storage modulus of the 2:1 (Figure 3.3) which can contribute to the poor reswelling of the gel and thus the decreased relative area change.

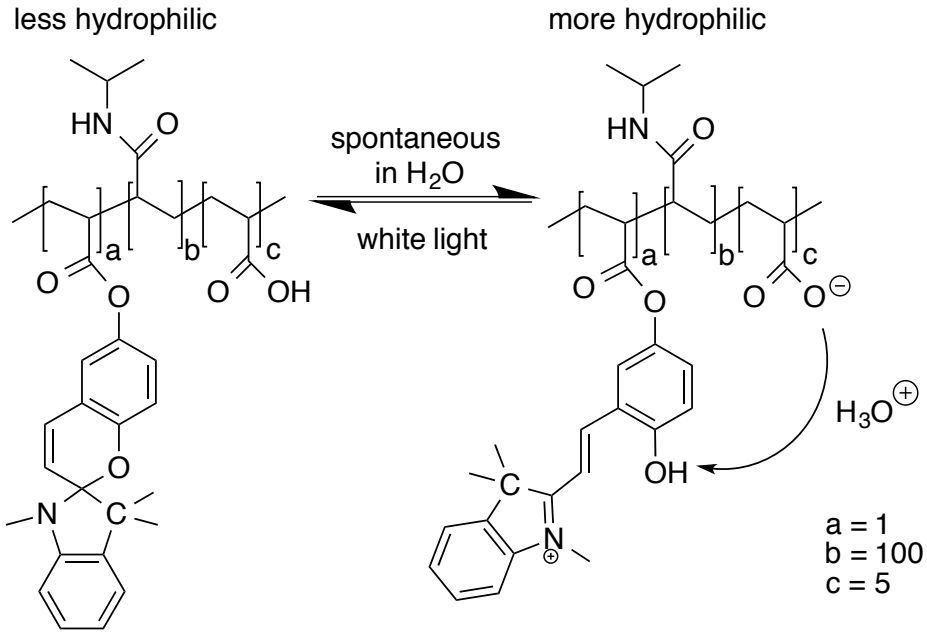

Figure 3.4: Chemical structure of p(NIPAAm-co-SP-co-AA) polymer chains under different illumination conditions.

In the case of dioxane: DI water as the polymerisation solvent mixture (Fig. A1.14 (4:1), A1.15 (2:1) and A1.16 (1:1)), there is not a clear difference between the contraction values (47.23%, 49.51%, and 51.83% respectively) or the expansion values (73.36%, 74.65%, and 81.57% respectively) (Table 3.3).

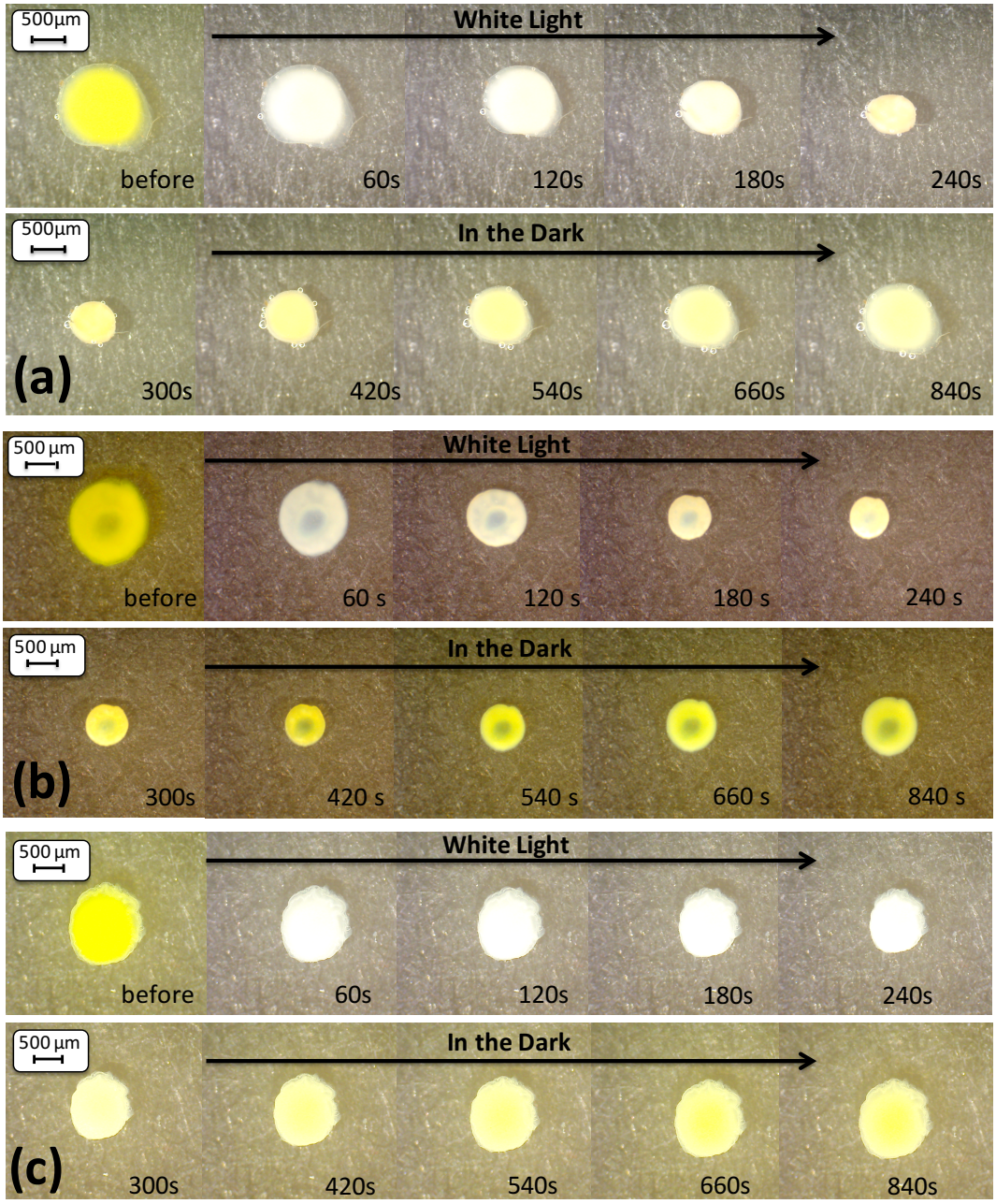

Figure 3.5: Microscope images (magnification X60) of the hydrogel shrinking and reswelling area of the three V: V ratios ((a) 4:1, (b) 2:1 and (c) 1:1) of the THF: DI water solvent mixture.

Table 3.2. Hydrogel contraction and expansion relative areas (%) during three irradiation cycles (n=3) % area changes calculated relative to the initial area.

Gel ID	Relative area [%] after Contraction	Error [%] (n=3) after Contraction	Relative area [%] after Expansion	Error [%] (n=3) after Expansion	Relative area Change [%]
4:1 THF: DI water	51.43	0.95	82.99	0.87	31.64
2:1 THF: DI water	58.94	6.04	75.17	3.39	16.23
1:1 THF: DI water	61.78	0.26	91.31	0.22	29.53
4:1 Dioxane: DI water	47.23	2.62	73.36	3.44	26.13
2:1 Dioxane: DI water	49.51	1.08	74.65	1.37	25.14
1:1 Dioxane: DI water	51.83	1.01	81.57	1.36	29.74
4:1 Acetone: DI water	39.56	2.37	61.95	5.76	22.39
2:1 Acetone: DI water	50.34	2.35	71.63	3.26	21.29
1:1 Acetone: DI water	46.07	1.30	86.95	0.92	40.88

These results would be expected, taking into account their similar pore sizes (Fig. A1.6-A1.8) and mechanical properties (G' = 44 - 47kPa, Fig. A4).

In the acetone: DI water series, the 4:1 ratio shows the highest relative shrinking (hydrogels shrink to 39.56% of their hydrated size) but on reswelling it only reaches 61.95% of its initial size. In contrary, the 1:1 acetone: DI water shows a smaller relative shrinking to 46.07% (Table 3.3), but over all shows the highest relative area change upon repeating actuation cycles (40.88%). This could be attributed to its high pore density of various sizes (Fig. A1.11) compared to the other ratios, which in turn has been shown to improve water diffusion in the hydrogel. For each of the polymerisation solvent mixtures, the photo-induced contraction and expansion of the hydrogels were shown to be successfully reproducible over at least three illumination cycles with minimal hysteresis (Figure 3.6).

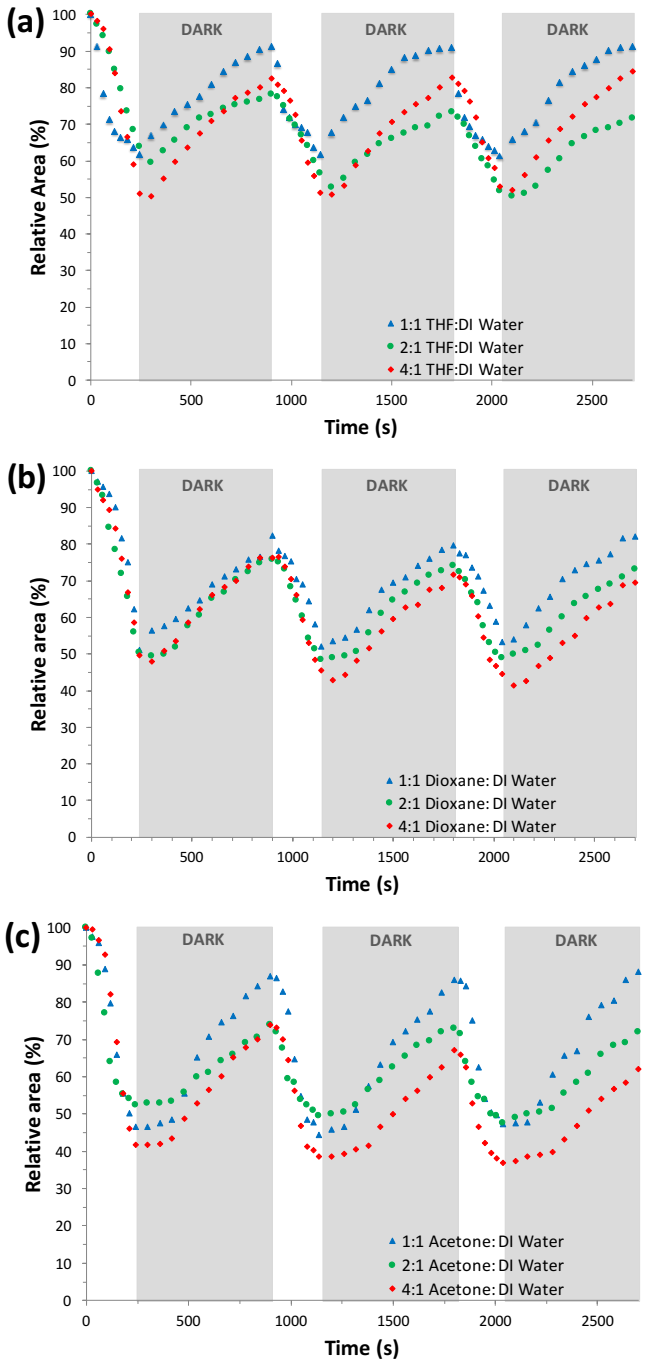

Figure 3.6: Photo-actuation cycles of hydrogel samples produced in the presence of different polymerisation solvent mixtures (THF: DI water (a), Dioxane: DI water (b), Acetone: DI water(c)), in real time.

During this study, the polymerisation solvent mixture and volume ratio were shown to play a crucial role in the resulting morphology and mechanical properties of the hydrogels. The THF: DI water mixture best highlighted the importance of the polymerisation solvent. During the curing study the 4:1 hydrogel had the highest storage modulus value of 32600 Pa, which resulted in hydrogels that were robust and

easy to handle. Upon swelling, however, the mechanical properties of the gel drastically changed, showing the smallest storage modulus of the series, at 5000 Pa. This is the first indication that the 4:1 hydrogel absorbed the highest amount of water of the series, as indicated also by its high porosity. In comparison, the 1:1 volume ratio produced a hydrogel with the highest tanδ value of the series, of 1.55×10^{-2}, resulting in a tacky hydrogel with smaller pores (1.66 - 1.11 μm), that upon water absorption had a much higher storage modulus of ~12 kPa, indicating a hydrogel with higher mechanical strength compared to 4:1 THF: DI water. Furthermore, the higher storage modulus of the hydrated 2:1 hydrogel (~15 kPa) implies an even more rigid material, making it less susceptible to photo-induced actuation (Table 3.2). This demonstrates that using polymerisation solvents with different ratios of organic solvents can dramatically affect the mechanical properties of the polymerised hydrogel due to the relative solvency of the growing polymeric chains (mainly composed of pNIPAAm) in the solvent mixture. As described above, there is a direct correlation between the solvent used during polymerisation, the morphology of the resulted hydrogels and the photo-actuation degree. Impressive variations in the overall photo-induced area change of p(NIPAAm-*co*-SP-*co*-AA) hydrogels from ~15% to 40% can be observed (Table 3.2) just by changing the polymerisation solvent mixture. This study provides essential information on the importance of the polymerisation environment in allowing the synthesis of pNIPAAm-based hydrogels with desired actuation responses.

3.5 Conclusions

In this study, nine different variations of organic solvent: DI water mixtures were used as polymerisation solvents to produce photo-actuating p(NIPAAm-*co*-SPA-*co*-AA) hydrogels, with the aim to control their morphology and therefore their actuation capabilities. The work has successfully demonstrated how the polymerisation solvent affects the morphology of the resulting hydrogel, directly influencing the curing properties, pore sizes, physical properties and degree of photo-actuation. This development has allowed for greater degrees of photo-actuation than previously reported and provides critical information for the development of micro-valves and photo-regulated flow controllers of optimal response times, in microfluidic devices.

3.6 References

1. Peppas, N.A.; Khare, A.R. Preparation, structure and diffusional behavior of hydrogels in controlled release. *Advanced Drug Delivery Reviews* **1993**, *11*, 1-35.
2. Rosiak, J.M.; Yoshii, F. Hydrogels and their medical applications. *Nuclear Instruments and Methods in Physics ...* **1999**, *151*, 56-64.
3. Tabata, Y.; Asahara, T. Hydrogel for medical use. *US Patent App. 11/884* **2006**.
4. Lee, K.; Mooney, D.J. Hydrogels for tissue engineering. *Chemical reviews* **2001**, *101*, 1869-1880.
5. Balakrishnan, B.; Mohanty, M.; Umashankar, P.R. Evaluation of an in situ forming hydrogel wound dressing based on oxidized alginate and gelatin. *Biomaterials* **2005**, *26*, 6335-6342.
6. Hoare, T.R.; Kohane, D.S. Hydrogels in drug delivery: Progress and challenges. *Polymer* **2008**, *49*, 1993-2007.
7. Kim, B.; Shin, Y. Ph-sensitive swelling and release behaviors of anionic hydrogels for intelligent drug delivery system. *Journal of Applied Polymer Science* **2007**, *105*, 3656 - 3661.
8. Peppas, N.A. Hydrogels and drug delivery. *Current opinion in colloid & interface science* **1997**, *2*, 531-537.
9. Liang, D.; Hongrui, J. Autonomous microfluidics with stimuli-responsive hydrogels. *Soft Matter* **2007**, *3*, 1223-1230.
10. Suk-kyun, A.; Rajeswari, M.K.; Seong-Cheol, K.; Nitin, S.; Yuxiang, Z. Stimuli-responsive polymer gels. *Soft Matter* **2008**, *4*, 1151-1157.
11. Meng, H.; Jinlian, H. A brief review of stimulus-active polymers responsive to thermal, light, magnetic, electric, and water/solvent stimuli. *Journal of Intelligent Material Systems and Structures* **2010**, *21*, 859-885.
12. Shinji, S.; Kimio, S.; Katsuhide, O.; Kazuaki, H.; Toshiyuki, T.; Toshiyuki, K. Photoresponsive polymer gel microvalves controlled by local light irradiation. *Sensors and Actuators A: Physical* **2007**, *140*, 176-184.
13. Kimio, S.; Toshiyuki, T.; Taku, S.; Toshiyuki, K. Photo-induced reversible proton dissociation of spirobenzopyran in aqueous systems. *Journal of Photochemistry and Photobiology A: Chemistry* **2013**, *261*, 46-52.
14. Sumaru, K.; Ohi, K.; Takagi, T.; Kanamori, T.; Shinbo, T. Photoresponsive properties of poly(n-isopropylacrylamide) hydrogel partly modified with spirobenzopyran. *Langmuir : the ACS journal of surfaces and colloids* **2006**, *22*, 4353-4356.
15. Sina, N.; Joselito, M.R.; Philip, G.W.; Gordon, G.W.; Geoffrey, M.S. A ph-sensitive, strong double-network hydrogel: Poly(ethylene glycol) methyl ether methacrylates-poly(acrylic acid). *Journal of Polymer Science Part B: Polymer Physics* **2012**, *50*, 423-430.

16. Gao, X.; Cao, Y.; Song, X.; Zhang, Z.; Xiao, C.; He, C.; Chen, X. Ph- and thermo-responsive poly(n-isopropylacrylamide-co-acrylic acid derivative) copolymers and hydrogels with lcst dependent on ph and alkyl side groups. *Journal of Materials Chemistry B* **2013**, *1*, 5578.
17. Zrínyi, M. Intelligent polymer gels controlled by magnetic fields. *Colloid & Polymer Science* **2000**, *278*, 98-103.
18. Ziółkowski, B.; Diamond, D. Thermoresponsive poly(ionic liquid) hydrogels. *Chemical communications (Cambridge, England)* **2013**, *49*, 10308-10310.
19. Kimio, S.; Mitsuyoshi, K.; Toshiyuki, K.; Toshio, S. Characteristic phase transition of aqueous solution of poly(n -isopropylacrylamide) functionalized with spirobenzopyran. *Macromolecules* **2004**, *37*, 4949-4955.
20. Satoh, T.; Sumaru, K.; Takagi, T.; Takai, K.; Kanamori, T. Isomerization of spirobenzopyrans bearing electron-donating and electron-withdrawing groups in acidic aqueous solutions. *Physical chemistry chemical physics : PCCP* **2011**, *13*, 7322-7329.
21. Taku, S.; Kimio, S.; Toshiyuki, T.; Toshiyuki, K. Fast-reversible light-driven hydrogels consisting of spirobenzopyran-functionalized poly(n-isopropylacrylamide). *Soft Matter* **2011**, *7*, 8030-8034.
22. Ziółkowski, B.; Florea, L.; Theobald, J.; Benito-Lopez, F.; Diamond, D. Self-protonating spiropyran-co-nipam-co-acrylic acid hydrogel photoactuators. *Soft Matter* **2013**, *9*, 8754-8760.
23. Stumpel, J.E.; kowski, B.; Florea, L.; Diamond, D.; Broer, D.J.; Schenning, A. Photoswitchable ratchet surface topographies based on self-protonating spiropyran□nipaam hydrogels. *ACS applied materials & interfaces* **2014**, *6*, 7268-7274.
24. Benito-Lopez, F.; Byrne, R.; Răduţă, A.; Vrana, N.; McGuinness, G.; Diamond, D. Ionogel-based light-actuated valves for controlling liquid flow in micro-fluidic manifolds. *Lab on a chip* **2010**, *10*, 195-201.
25. Gallagher, S.; Kavanagh, A.; Zíołkowski, B.; Florea, L.; MacFarlane, D.R.; Fraser, K.; Diamond, D. Ionic liquid modulation of swelling and lcst behavior of n-isopropylacrylamide polymer gels. *Physical chemistry chemical physics : PCCP* **2014**, *16*, 3610-3616.
26. Le Bideau, J.; Viau, L.; Vioux, A. Ionogels, ionic liquid based hybrid materials. *Chemical Society Reviews* **2011**, *40*, 907-925.
27. Singh, T.; Garland, M.J.; Migalska, K.; Salvador, E.; Shaikh, R.; McCarthy, H.O.; Woolfson, D.A.; Donnelly, R.F. Influence of a pore forming agent on swelling, network parameters, and permeability of poly (ethylene glycol) crosslinked poly (methyl vinyl ether co maleic acid) hydrogels: Application in transdermal delivery systems. *Journal of Applied Polymer Science* **2012**, *125*, 2680-2694.
28. Ziołkowski, B.; Florea, L.; Theobald, J.; Benito-Lopez, F.; Diamond, D. Porous self-protonating spiropyran-based nipaam gels with improved reswelling kinetics. *J. Mater. Sci* **2016**, *51*, 1392 - 1399.

29. Zhang, X.; Zhuo, R.; Yang, Y. Using mixed solvent to synthesize temperature sensitive poly (n-isopropylacrylamide) gel with rapid dynamics properties. *Biomaterials* **2002**, *23*, 1313-1318.
30. Genoveva, F.; Kimio, S.; Toshiyuki, T.; Toshiyuki, K.; Miklós, Z. Swelling degree and shape change of photo- and thermo-response of spirobenzopyran-functionalized porous pnipaam hydrogels. *Journal of Molecular Liquids* **2014**, *189*.
31. Crowther, H.M.; Vincent, B. Swelling behavior of poly- n - isopropylacrylamide microgel particles in alcoholic solutions. *Colloid & Polymer Science* **1998**, *276*, 46-51.
32. Francoise, M.W.; Ringsdorf, H.; Venzmer, J. Methanol-water as a co-nonsolvent system for poly(n-isopropylacrylamide). *Macromolecules* **1990**, *23*, 2415-2416.
33. Mezger, T.G. *The reology handbook*.
34. Bischofberger, I.; Calzolari, D.C.E.; Trappe, V. Co-nonsolvency ofpnipam at the transition between solvation mechanisms. *Soft Matter* **2014**, *00*, 1 - 8.
35. Hao, J.; Cheng, H.; Butler, P.; Zhang, L.; Han, C.C. Origin of cononsolvency, based on the structure of tetrahydrofuran-water mixture. *J. Chem. Phys.* **2010**, *132*.
36. Schild, H.G.; Muthukumar, M.; Tirrell, D.A. Cononsolvency in mixed aqueous solutions. *Macromol. J. Chem. Phys* **1991**, *24*, 948 - 952.
37. Costa, R.O.R.; Freitas, R.F.S. Phase behaviour of poly (n-isopropylacrylamide) in binary aqueous solutions. **2002**, *43*, 5879 - 5885.
38. Anseth, K.S.; Bowman, C.N.; Brannon-peppas, L. Mechanical properties of hydrogels and thier experimental determination. **1996**, *17*, 1647 - 1657.

Chapter 4

Spiropyran Based Hydrogel Actuators – Walking in the Light*

***Spiropyran Based Hydrogels Actuators − Walking in the Light**, Wayne Francis, Aishling Dunne, Colm Delaney, Larisa Florea*, Dermot Diamond, *Sensors and Actuators B: Chem.* 250 (2017): 608-616 .

Chapter 4:

Spiropyran Based Hydrogel Actuators - Walking in the Light

4.1 Abstract

Herein we report the synthesis of a bipedal hydrogel walker, based on *N*-isopropylacrylamide-*co*-acrylated spiropyran-*co*-acrylic acid p(NIPAAm-*co*-SP-*co*-AA). Due to the presence of the photochromic spiropyran molecule in the polymer structure, these hydrogels reversibly shrink and swell in aqueous environments when exposed to different light conditions. When placed onto a ratcheted surface, the actuation of the bipedal gel produces a walking motion by taking a series of steps in a given direction, as determined by the optimised design of the ratchet scaffold. We anticipate that such biomimetic hydrogel walkers could form the basis of light-actuated soft robots capable of more advanced functions such as autonomous migration to specific locations accompanied by triggered release of molecular cargo.

4.2 Introduction

The motile behaviour of life forms, from the most primitive to the more complex, has long fascinated scientists who remain captivated by their ability to navigate through challenging environments in response to external stimuli. The simple earthworm, for example, has been the focus of attention for scientific groups who attempt to achieve synthetic mimicry of its means of movement [1-3]. The earthworm's body is composed of cylinder-shaped segments which are filled with a fixed volume of incompressible fluid and its movement is attributed to the contraction of the circular and longitudinal muscle layers which run through the body of the worm. When the longitudinal muscles contract, the worm is made shorter and the liquid is forced into the sides of the cavity, causing the body to widen. Conversely, contraction of the circular muscles serves to elongate the worm's body. Sequential fine control over the length of individual segments allows the worm to move in one direction [4]. More advanced means of locomotion, as exhibited by humans and other large mammals, is controlled through interaction of both soft and hard materials. Many groups, studying soft and hard robotics, have looked to the human body for inspiration [5-7]. To date however, the hard robotics field has failed to produce devices that can match the functionalities offered by biology, such as flexibility, adaptability and self-repair observed in even the simplest living organisms (e.g. cells, bacteria, jellyfish and worms). These types of functionality cannot be offered by present robotics technologies, mainly because of the lack of mechanical compliance between the

conventional robotics and the biological systems. For implantable devices this hard-soft material mismatch can lead to tissue damage and foreign body response, resulting in hypoxia, acidosis, thrombosis and implant rejection [8]. Great recent progress has been made at the macro-scale towards soft-fluidics by using soft elastomers with embedded pneumatic networks [9,10]. These actuators contain inflatable channels fabricated in elastomeric materials which are configured to create specific movement when pressure is applied. Dielectric elastomers have also been proposed for the realisation of soft electro-actuators, however their main disadvantage remains the typically large actuation voltage needed [11,12]. Currently, soft-robotics may offer actuators of modest complexity, which exhibit increased compliance with biological matrices. Biological inspiration has also led to the realisation of stimuli-responsive soft actuators through the use of hydrogels as a primitive mimic of biological tissue. Hydrogels comprise a broad range of polymeric materials which are capable of holding large volumes of water, due to their hydrophilic nature. Incorporation of stimuli-responsive compounds into the gel structure can be used to control the gel's overall hydrophilic character. This offers a means to modulate the volume and shape of the hydrogel structure through the expulsion or absorption of water from the surrounding environment. A large number of stimuli-responsive mechanisms for these gels have been reported, including thermal [13,14], pH [15], magnetic [16], glucose [17], antigen [18], electro [19], photo [20], and even multi-responsive hydrogels [21,22]. Of particular interest is the development of hydrogels with biomimetic properties [23,24], such as the ability to walk [25]. Yang et al [26] developed an arc shaped hydrogel based on poly(2-acrylamido-2-methylpropanesulfonic acid-co-acrylamide) (poly(AMPS-co-AAm), which was able to walk across a ratcheted surface upon electrical stimulation. The hydrogel contained cross-linked networks bearing bound negatively-charged sulfonic groups. In sodium chloride (NaCl) solutions, upon the application of an electric potential, the free ions of the NaCl electrolyte move towards their respective counter electrodes. Inside the hydrogel however, only the cations of the bound negatively-charged sulfonic groups are mobile and can move towards the cathode. This ion motion creates an ionic concentration gradient within the hydrogel and in turn an osmotic pressure difference within the hydrogel walker. This translates into a bending motion towards the cathode upon application of an electric field. Depending on the position of the electrodes, one side of the gel experiences a greater osmotic pressure difference, resulting in bending/deformation of the hydrogel. The bending behaviour is reversible and repeatable through successive "on/off " application of an electric field. When placed on a ratcheted

surface and by repeatedly applying an electric field, a hydrogel arc can be made to "walk". When the electric field is switched "on" the gel will shrink, resulting in the legs of the gel to come closer. Because of the shape of the ratchet, only one leg can move and the trailing leg will be "dragged" across the ratchet steps. When the electric field is removed the gel will expand, but as the trailing leg cannot expand back against the ratchet, the leading leg will be pushed forward.

Development of other forms of hydrogel stimulation offer more promising means of fine-tuning actuation. The use of photo-responsive hydrogels offers the possibility of accurately controlling irradiance, time, distance, position and wavelength of the light while offering non-contact stimulus that can be applied in a non-invasive manner. The incorporation of photo-responsive compounds in the modulation of hydrogels has been widely documented, most notably through the use of spiropyrans (SP), which also offer added sensitivity to pH, solvent polarity and metal ions [27-29]. Our group has been one of the pioneers in demonstrating that incorporation of spiropyrans into gel structures (hydrogels [30] and ionogels [31,32]) can be used for the fabrication of photo-controlled liquid flow micro-fluidic manifolds [33], reversible microfluidic valves [34] and photo-programmable surface topographies [35]. The photo-responsive hydrogels used in these studies were typically composed of copolymers of *N*-isopropylacrylamide-*co*-acrylated spiropyran-*co*-acrylic acid (p(NIPAAm-*co*-SP-*co*-AA), in a molar ratio of 100:1:5. In an acidic environment SP is protonated, generating the more hydrophilic (MC-H^+) form. Absorption of water from the external environment thereby results in expansion of the hydrogel. Upon irradiation with white light (λ_{max} = 422 nm) MC-H^+ releases a proton causing it to isomerize back to the more hydrophobic SP form. This increase in hydrophobicity results in the expulsion of water and the contraction of the gel. The addition of acrylic acid into the hydrogel backbone provides an internal source of protons for reversible switching [20] removing the need for an external acidic environment and enabling the switching of SP to MC-H^+ to occur in neutral conditions. This allows for reversible photo-actuation to be performed in deionised water.

Expanding on this work, herein we present photo-responsive hydrogel walkers based on p(NIPAAm-*co*-SP-*co*-AA). These walkers can reversibly shrink and expand via on/off white light irradiation. When submerged in water and placed onto a ratcheted surface the walkers can achieve a unidirectional walking motion when exposed to different light conditions. These hydrogels offer a promising route for the development of directed locomotion in soft light robotics.

4.3 Experimental

4.3.1 Materials

N-isopropylacrylamide 98% (NIPAAm), N,N'-methylenebisacrylamide 99% (MBIS), Phenylbis(2,4,6 trimethyl benzoyl) phosphine oxide 97% (PBPO), acrylic acid (180-200ppm MEHQ as inhibitor) 99% (AA), tetrahydrofuran 99% (THF), anhydrous dichloromethane (50-150 ppm amylene as stabilizer) 99% (DCM), ethyl acetate 99%, n-hexane 95%, were acquired from Sigma Aldrich, Ireland and used as received. 1',3',3'-Trimethyl-6-acryloylspiro(2H-1-benzopyran-2,2-indoline) (SP-A) was synthesised as described elsewhere [20].

4.3.2 Gel Preparation

The hydrogel walkers were synthesised using a monomeric cocktail which consisted of 200 mg NIPAAm, 8 mg MBIS (3 mol% relative to NIPAAm), 6 mg SP-A (1 mol% relative to NIPAAm), 7 mg PBPO (1 mol% relative to NIPAAM) and 6 μL AA (5 mol% relative to NIPAAm) dissolved in 500 μL of the polymerisation solvent (4:1 vol: vol, THF: DI water). The arc-shaped hydrogel walkers were prepared by using a home-made cell consisting of a PMMA mask (Figure 4.1), a glass slide and a glass cover slide separated by a 500 μm high spacer made out of poly(methyl methacrylate)/pressure sensitive adhesive (PMMA/PSA). The cell was filled by capillary action with the monomer solution and subsequently exposed to white light through the mask (Figure 8). The polymerisation time was varied from 40 to 50 s, in order to compare polymerisation times with walker functionality. The white light source used was a Dolan-Jenner-Industries Fiber-Lite LMI LED lamp with two gooseneck waveguides placed at a distance range of 1 to 2 cm from the platform. The light intensity measured with a Multicomp LX-1309 light meter was 310 - 320 kLux. After polymerisation, the hydrogel walkers were washed gently with ethanol and DI water to remove any unpolymerised material and allowed to swell in deionised water for 4-6 hours to ensure full hydration.

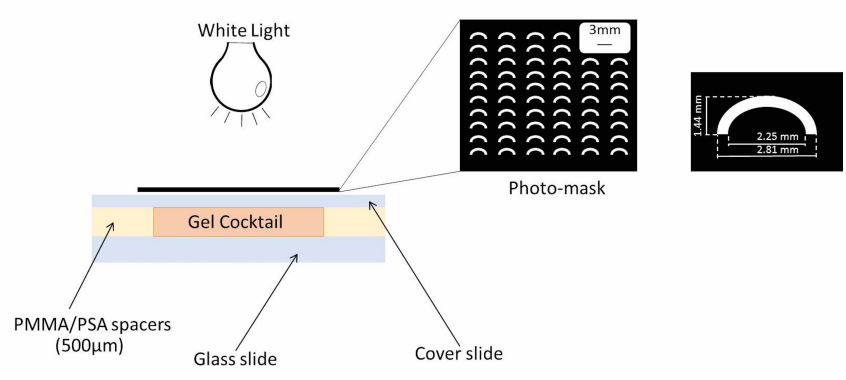

Figure 4.1. Side view of in-house made cell for gel polymerisation; insets show the photomask including specific measurements of a single arc-shaped walker.

4.3.3 Photo-Mask Fabrication

The photo-mask used for gel polymerisation was firstly designed using AutoCAD 2014 and cut from a 1 mm thick sheet of black PMMA using a CO_2 laser ablation system (Epilog Zing Laser Series). The mask contained a 7 x 5 array of walkers of 1.44 mm height, 2.81 mm (outer) distance between the legs, and a width of 0.56 mm.

4.3.4 Ratcheted Channel Fabrication

The ratcheted systems in this study were first designed using AutoCAD 2014 and a CO_2 laser ablation system (Epilog Zing Laser Series) was used to cut the required pieces out of black PMMA sheets. To assemble the ratcheted channel, a back PMMA layer, the ratchet layer and a glass slide were attached (Figure 4.2). The back layer and the main ratchet section were cut from 1 mm black PMMA. To avoid melting of the ratchet during laser cutting, 50 µm PSA was hand cut and applied to both sides after cutting. The back layer was joined with the main section first, then the glass slide was attached. Using clamps, the three sections were placed under pressure overnight. The ratcheted channel had a length of 45 mm, a 1 mm width and a height of 12 mm, while the ratchets had a height of 0.5 mm and a 7 mm distance between two consecutive ratchets.

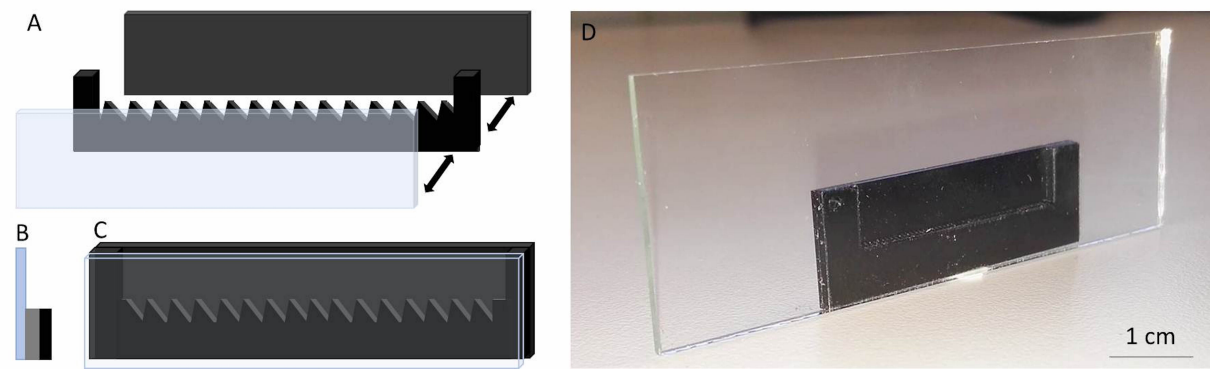

Figure 4.2. A) Schematic diagram showing the individual components of the ratcheted channel: glass slide, ratcheted channel bottom with side walls in black PMMA and PMMA back layer; Cartoon showing side (B) and front (C) views of the channel after assembly and D) Photo of the real ratcheted channel.

4.3.5 Hydrogel Walker Relative Area and Relative Leg Distance Analysis

The distance between the walker's legs and the area measurements of the freestanding hydrogel walkers were performed using Image J (1.47v) software. For each polymerisation time, three hydrogel samples were measured. The relative area % (Eq. 4.1) and relative Legs distance% (Eq. 4.2) were calculated using the following equations (n=3):

$$Relative\ area\ (\%) = \frac{A_t}{A_o}\ x\ 100 \qquad \text{(Eq. 4.1)}$$

Where A_t = Measured area at time t and A_o = Area of a fully hydrated gel.

$$Relative\ leg\ distance\ (\%) = \frac{L_t}{L_0}\ x\ 100 \qquad \text{(Eq. 4.2)}$$

Where L_t = Measured inner leg distance at time t and L_0 A_o= Initial inner leg distance of the fully hydrated walker.

4.3.6 Rheology

Rheology curing measurements were performed on the unpolymerised cocktail. The measurements were carried out using an Anton-Paar MCR301 rheometer with a CP50-2 measuring tool with a diameter of 49.97 mm and a cone angle of 1.996° to measure the mechanical properties during polymerisation. The rheometer had a glass plate to which 900 µl of monomer mixture was placed and pressed with the CP50-2 tool with a space of 208 µm. A

Dolan-Jenner-Industrie Fiber-Lite LMI white light was placed under the glass plate having a light intensity of 320 kLux, measured on top of the glass plate using a LX-1309: light meter. The curing and mechanical properties of the p(NIPAAm-*co*-SPA-*co*-AA) cocktail were measured over 15 minutes with data collected every second. White light curing was initiated after 60s and after the allotted time (40 s, 45 s and 50 s, respectively) the light was turned off. The loss and storage moduli were analysed at 0.1% strain and 1Hz oscillation frequency against time.

Polymer films of 500 μm thickness were polymerised for the specific times (40 s, 45 s and 50 s) in the same manner as the walkers in the absence of the photomask with a light intensity of 318 kLux. After the polymer films were hydrated, circular disks of 15 mm diameter were cut using a manual puncher and used for further rheology analysis. The polymer discs from the various polymerisation times were placed under the PP15 rheometer tool (15 mm diameter) of the Anton Paar MCR 301 rheometer. Amplitude sweeps were carried out at 100 rad s^{-1} angular frequency, a normal force of 1 N with a gradual strain from 0.01 – 100%. The storage modulus was monitored with data being collected every 20 seconds.

4.3.7 Hydrogel Walker Actuation

To achieve the "walking" behaviour of the hydrogels, a single walker was placed on to one of the ratcheted channels. The channel was then carefully filled with deionised water. An Aigo GE-5 microscope (using a 60x objective lens and accompanying software) was placed facing the glass side of the ratcheted channels. Finally, the white light source was adjusted so both goosenecks were pointed at the walker and had an intensity of ~305 kLux. Once recording began the white light source was switched on. The walker was then monitored in real time and once the trailing leg had moved across at least one of the ratchet steps the light was removed. The gel was then monitored in the dark and once the leading leg had been pushed at least one ratchet step, the white light source was turned back on. This was continued until the hydrogel had walked a number of steps.

4.4 Results and Discussion

4.4.1 Hydrogel Walker

The (p(NIPAAm-*co*-SP-co-AA) hydrogels in this study were able to achieve reversible swelling and contraction through repeatable white light irradiation. In the absence of white light, the SP component of the gels underwent protonation to the more hydrophilic MC-H^+ form, due to protonation from the AA substituent (pKa ~ 4.5). Under these conditions, the gels expanded to the maximum capacity and had a yellow colour. When the hydrogels were illuminated with white light, the MC-H^+ was deprotonated back to the SP form (Figure 4.3). This resulted in a rapid colour change towards white/colourless as the gel began to contract. This is due to the hydrophobic nature of SP which causes the polymer chains within the gel to collapse and water from the gel to be expelled to the external environment (Figure 4.3).

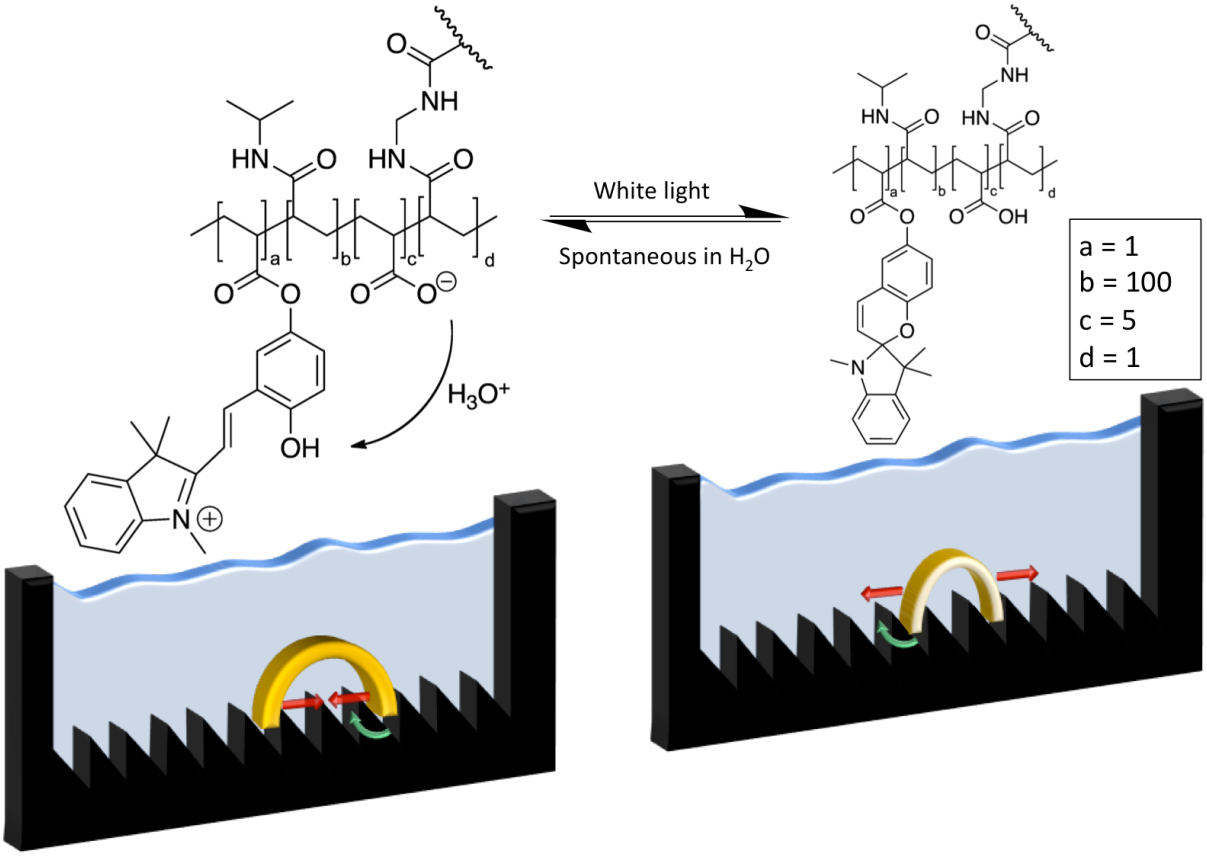

Figure 4.3. Chemical structure of the p(NIPAAm-co-SP-co-AA) hydrogel walkers under different illumination conditions and the physical effect it has on the gel morphology.

To achieve the walking motion this process was performed on a ratcheted polymethyl methacrylate (PMMA) surface, from right to left, as depicted in Figure 4.4. After a period of white light irradiation (5 min at ~305 kLux intensity), the gel began to contract, thereby causing deformation of the gel's structure. When the leading leg comes in contact with the vertical section of the ratchet step (Figure 4.4 (A)), a gradual photo-induced reduction of the distance between the legs causes the trailing leg to be "dragged" over the bevel of the ratchet step (Figure 4.4 (B-D)).

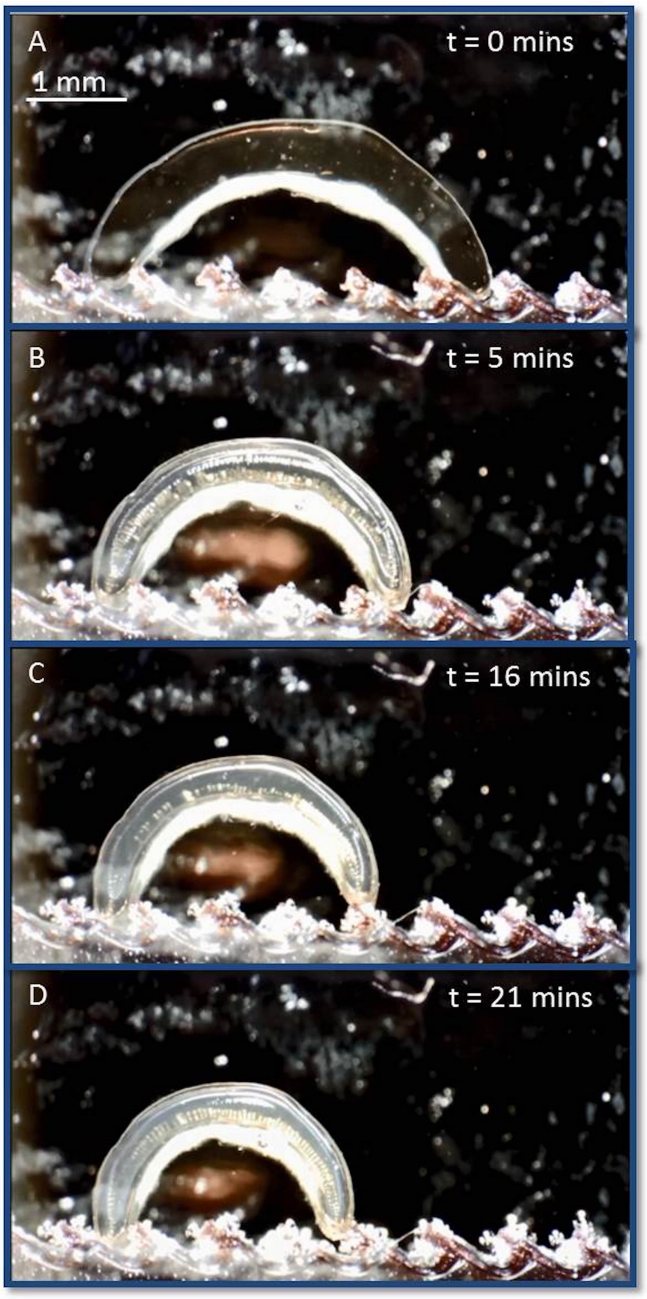

Figure 4.4. Series of snapshots showing the effect of light irradiation on the hydrogel walker. A) Light irradiation is initiated; B-D) Gradual reduction of inter-leg distance results in the trailing leg (right) being "dragged" over the bevel of the ratchet step.

When the light was removed, the gel would gradually begin to re-swell and regain its original colour. Swelling continued until the trailing leg became lodged on a vertical section of a ratchet step, thus causing the leading leg to be pushed over the bevel of the corresponding ratchet step. By repeating this process, the p(NIPAAm-co-SP-co-AA) walkers could be made walk in a single direction, determined by the direction of the ratchet (see **Figure 4.5**, **Figure A2.1**, **Video A2.1** and **Video A2.2**).

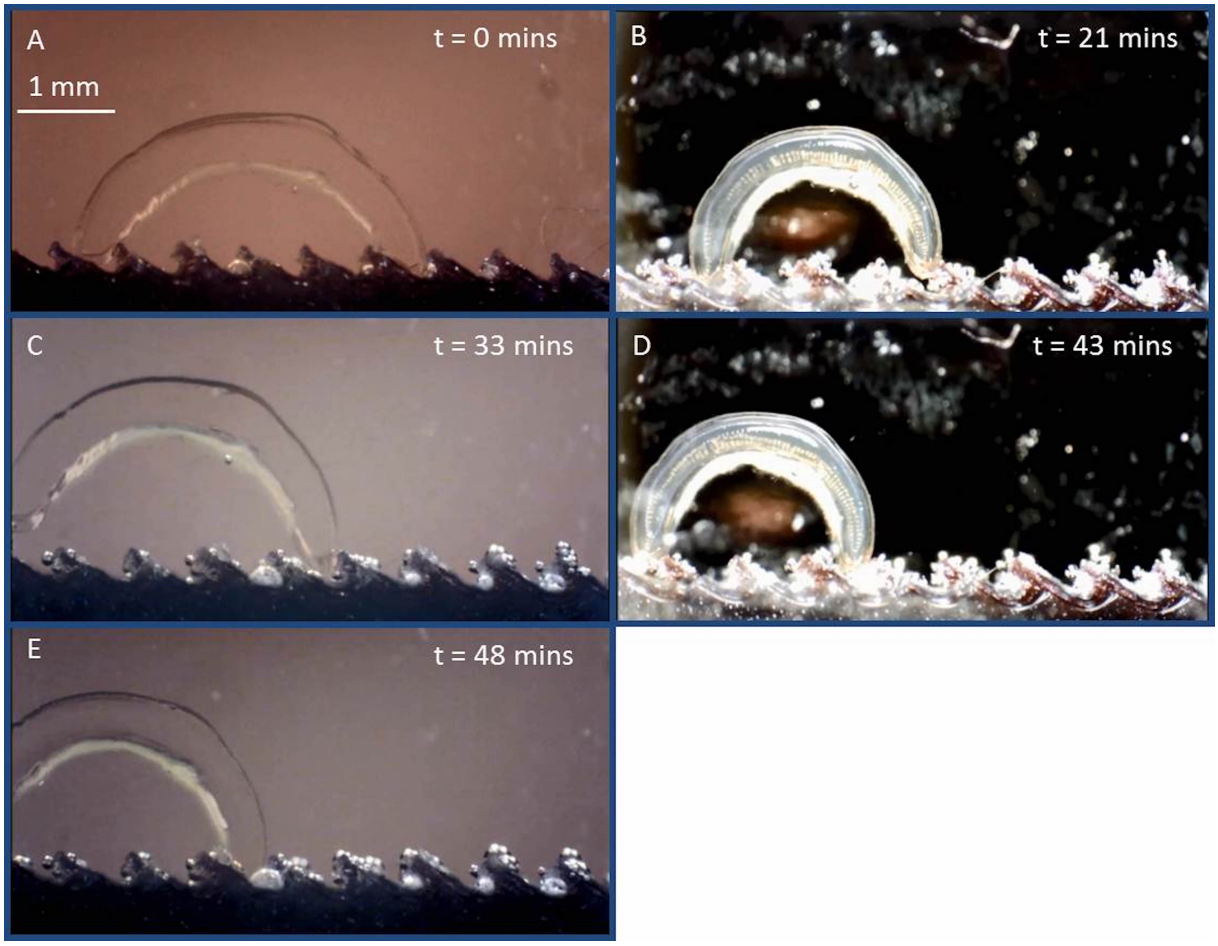

Figure 4.5. Series of snapshots showing the walking behaviour of the hydrogel (Video S1). A – B shows contraction of the trailing leg. C – Swelling in the dark results in the forward leg being pushed over the ratchet. D – E The sequence is repeated which results in the gel achieving a unidirectional walking motion (right to left).

4.4.2 Mechanical Properties

To design a hydrogel walker which can actuate over a series of predefined distances, it is necessary to have a comprehensive knowledge of the mechanical properties of the hydrogel walker. The elastic nature of a hydrogel can have a dramatic influence on its ability to actuate

under a given stimulus. To best understand the effect of varied degrees of cross-linking, a rheology study was used to ascertain the most appropriate curing time. Three different polymerisation times were chosen (40 s, 45 s and 50 s, respectively), during which the monomeric cocktail was exposed to white light irradiation and the storage modulus recorded (Figure 4.6). The storage modulus increases abruptly when the light is turned on (time = 60 s) owing to significant growth of elastic structures due to the crosslinking. When the light is turned off (after 40 s, 45 s and 50 s, respectively) no new radicals are formed by initiation, and therefore the increase in storage modulus is significantly slowed, as only the free radicals that are present when the light is turned off continue to propagate and terminate [36]. The hydrogels polymerised under 50s of light irradiation showed the highest storage modulus plateau at around 3700 Pa, and therefore exhibit the greatest elastic properties of the hydrogels studied (Figure 4.6). Polymerisation times longer than 60s were not suitable as polymerisation-induced diffusion, beyond the exposed areas of the photo mask, resulted in peripheral polymerisation.

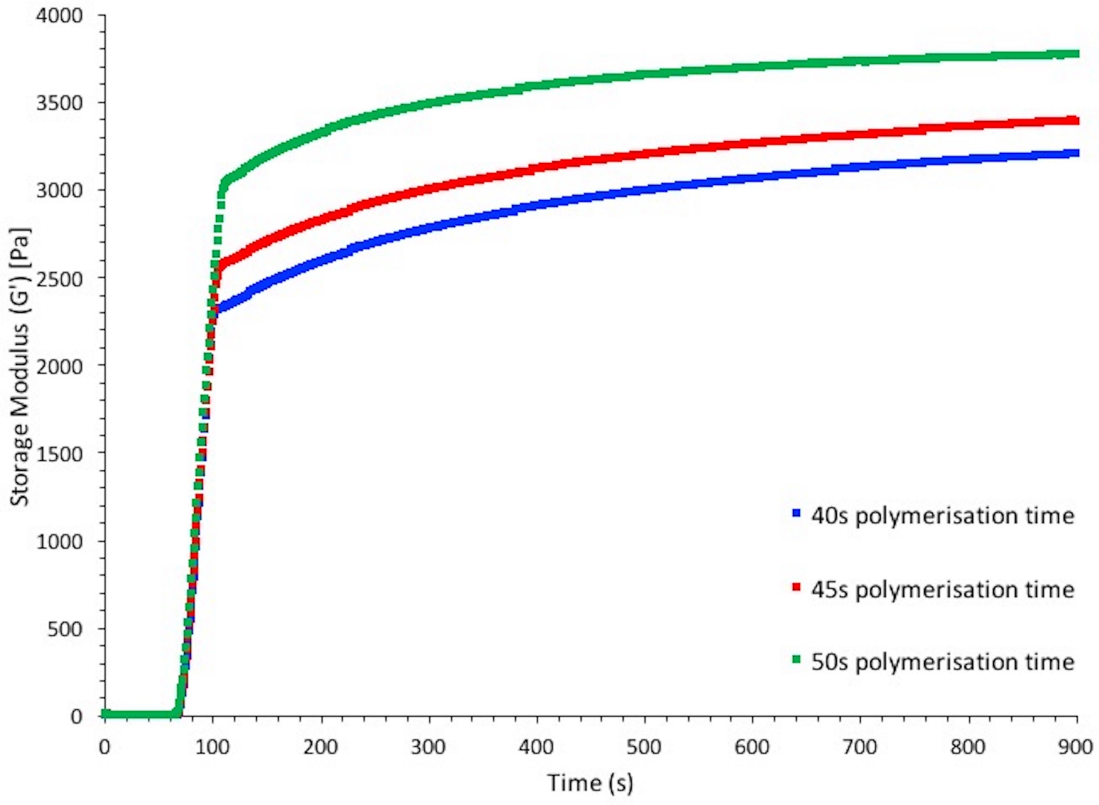

Figure 4.6. Photo-curing of hydrogels produced under different light irradiation times (40 s, 45 s and 50 s, respectively). White light polymerisation was initiated at t=60 s.

Mechanical studies of the hydrogels were also performed after hydration, as detailed in the experimental section. It was revealed that upon hydration, the storage modulus of the hydrogels polymerised under different polymerisation times (40 s, 45 s, and 50 s, respectively), although increasing with the polymerisation time, does not vary significantly (Figure A2.1). However, amplitude sweeps reveal that the linear viscoelastic range (LVE) is significantly different and decreases with increased polymerisation time. This could be due to the crosslinking density increasing with the polymerisation time, also causing an increase in chain entanglement. Therefore, when an increase shear stress is applied, physical interactions and entanglements will be destroyed prior to covalent bonds. As a result, the sudden decrease in G' (indicating the end of the LVE) occurs at lower shear stress for the hydrogels polymerised under a longer polymerisation time, which implies that there are more physical crosslinks and chain entanglements in these sample networks [37].

4.4.3 Relative Area and Relative Leg Distance Analysis

Extending our knowledge of these materials to fabricate a simple hydrogel walker required not only an insight into the mechanical properties but also greater understanding of the volume change of the material during actuation cycles. On a stepped surface, it is important to fully understand both the swelling of the respective legs and maximum bipedal distance, during actuation. To determine the actuation properties of the hydrogel walkers polymerised under different polymerisation times, a study was performed to examine the effect on both the relative area of the entire gel and the distance between the legs upon irradiation with white light. Polymerisation time is an important parameter when synthesising hydrogels as it affects the crosslinking density of the hydrogel, thus its mechanical properties (Figure 4.6) and its ability to absorb and expel water and the material's shape memory [38-41].

Figure 4.7 shows the relative area of each of the gels when exposed to three cycles of white light irradiation. It confirms, as expected, that polymerisation times plays only a minor role in the extent of swelling or contraction exhibited by the resulted hydrogel, in these particular conditions (polymerisation times of 40 s, 45 s and 50 s, respectively). The 50 second polymerised gels showed the greatest repeatability and were better able to swell close to their original size when compared to the shorter polymerization times. Relative area change is Area. change = 24.14 ± 7.43% (n=3) for the hydrogels polymerised under 40 s of light irradiation, Area. change = 23.11 ± 9.24% (n=3) for 45 s polymerisation time and Area.

change = 25.87 ± 2.35% (n=3) for 50 s polymerisation time, respectively. For the hydrogel polymerised under 40 s of white light irradiation, there is a clear gradual decrease in the size of the hydrogel both under light and dark conditions (40 s: 2nd cycle 62.28 ±5.41% (contracted); 78.98 ±6.04% (expanded) and 3rd cycle 56.94 ±6.41% (contracted) 75.17 ±7.75% (expanded). This is most likely due to the decreased crosslinking density and physical entanglements present in these hydrogels, which may impede the hydrogels from returning to their original size.

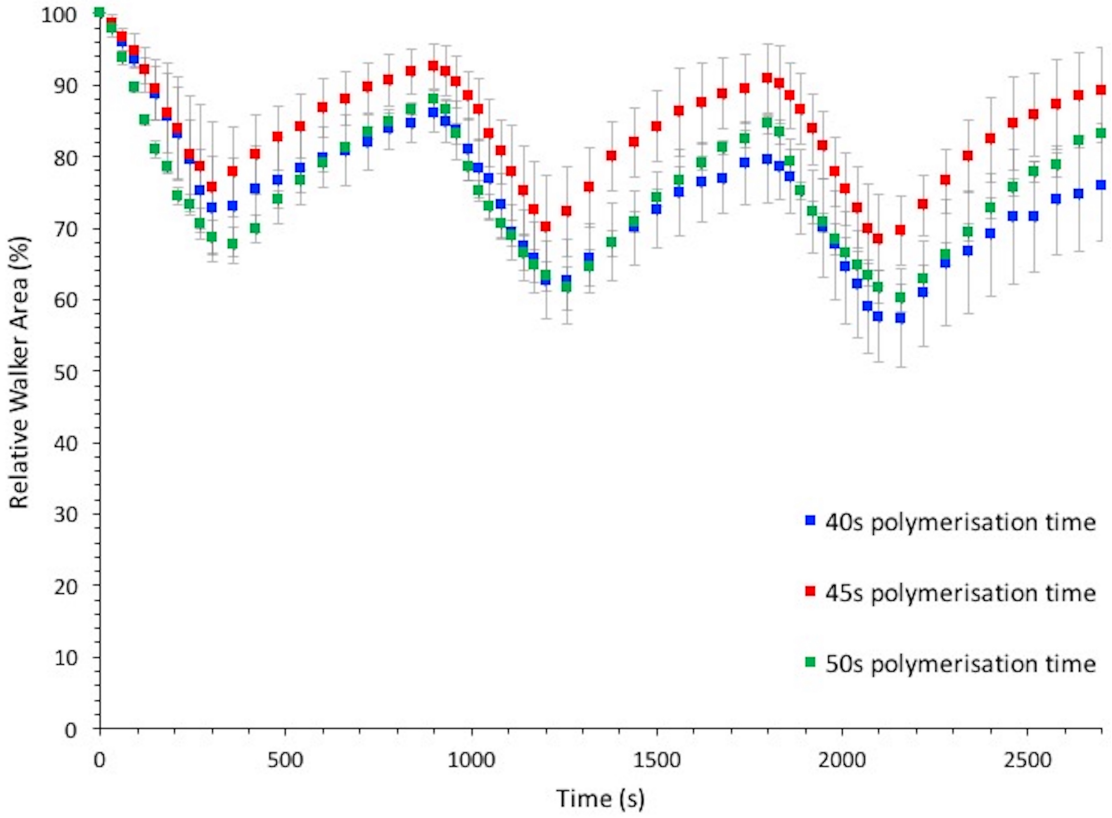

Figure 4.7. Three photo-actuation cycles of hydrogel walkers produced after 40 s, 45 s and 50 s of light irradiation, respectively, showing the relative changes in walker area when exposed to different illumination conditions. The measurements have been done in triplicate and the error bars represent standard deviations.

An analysis of the relative inter-leg distance for a set of walkers of varied polymerisation time was also performed. Figure 4.9 shows the effect polymerisation times had on the actuation of the hydrogel structures, and in particular the relative changes in leg distance when the gels were exposed to different illumination conditions. As seen from Figure 4.6, polymerization times of 40 s and 45 s, respectively, resulted in gels with a lower storage modulus. Upon actuation, this failed to show an appreciable change on the centre angle of the

arc-shaped walker. When exposed to white light all of the hydrogel walkers were able to expand and contract (Figure 4.8), however the ones polymerised for 40 s and 45 s (Figure 4.8 (a) +(b)), respectively, couldn't maintain their shape and became flat when irradiated on a ratcheted surface.

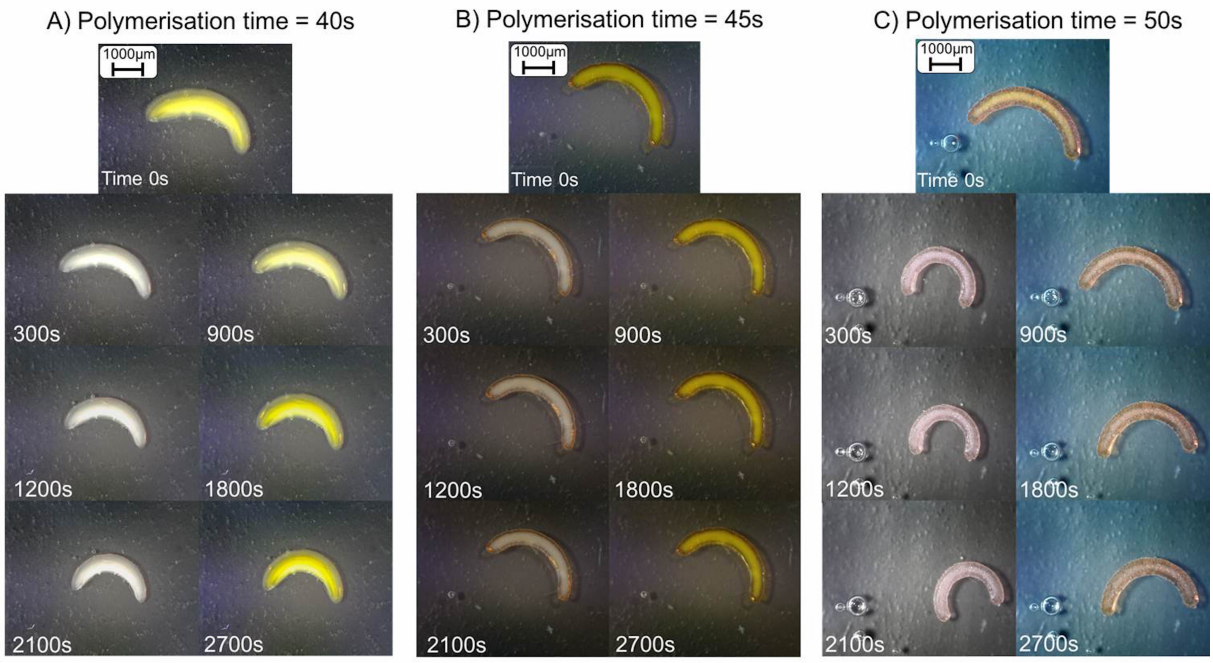

Figure 4.8. Three photo-actuation cycles of hydrogel walkers produced after 40 s, 45 s and 50 s of light irradiation, respectively, showing the relative changes in legs distance when exposed to different illumination conditions.

The results of this assessment of actuation behaviour, in particular inter-leg distance, are summarised in the plots shown in Figure 4.9. This clearly demonstrates that the gels synthesised using a 50 second polymerisation time had the greatest reduction in distance between the legs when exposed to white light. The 40 and 45 second gels showed minor and irreproducible inter-leg distance changes and therefore limited movement. Knowledge of the extent of change in the centre angle of the arc-shaped walker/ inter-leg distance is integral to the design of the ratcheted surface on which the walker moves. By assessing the distance between the legs before and after actuation it is possible to design ratchets of optimal dimensions to maximise the potential for unidirectional movement. These results had a direct influence on the width of ratchets used for further studies, as outlined in the experimental section.

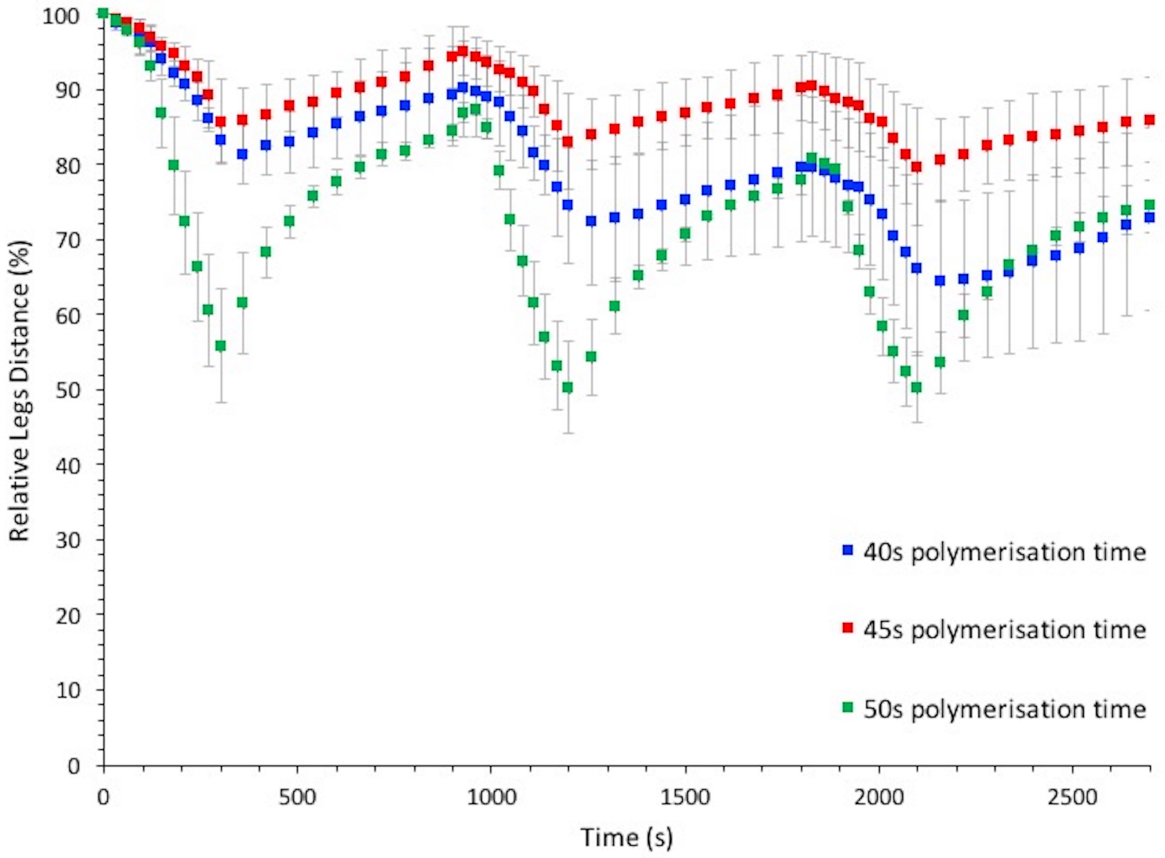

Figure 4.9. Three photo-actuation cycles of hydrogel walkers produced after 40 s, 45 s and 50 s of light irradiation, respectively, showing the relative changes in legs distance when exposed to different illumination conditions.

As the actuation behaviour (swelling, contraction) in hydrogels is essentially diffusion controlled, the reduction of the scale of these structures can dramatically increase the rate at which these effects occur [42]. Improved kinetics of the actuation could also be realised by increasing the pore density of the hydrogel structure [43] as this can substantially reduce the overall diffusion pathlength for water uptake and release. Furthermore, modification of substituents on the photoswitch molecule produces dramatic improvements in the switching kinetics, which also contributes to the overall effectiveness of the gel actuation effect [44,45]. This in turn will allow for the realisation of soft micro-robots, capable of various forms of locomotion on a significantly reduced timescale. In addition, photo-switchable dynamic ratchet structures that emerge /disappear can be created, and linking this behaviour with the 'walkers' offers the intriguing possibility of externally switching between 'on' (ratchet

features present, directed movement turned on) and 'off' (smooth surface restored, directed movement turned off)[35].

4.5 Conclusion

In conclusion, we have synthesised a hydrogel walker based on p(NIPAAm-*co*-SP-*co*-AA) which can reversibly swell and contract when submerged in water and subjected to cycles of white light irradiation. The hydrogel is able to achieve unidirectional walking when placed onto a ratcheted surface. These results show that photo-responsive hydrogels make promising candidates for the development of biomimetic soft robots which could exploit their reversible and repeatable actuation. This study opens the possibility for development of more advanced biomimetic walking soft robots which can perform tasks such as cargo transport, sensing and targeted drug delivery. The ability to control on-demand uptake and release, with porous materials of this nature, offers the possibility of localised triggered reactions upon secondary stimulation at desired destinations [46,47]. The combination of these processes could be used to achieve targeted transport, delivery and release within fluidic systems.

4.6 References

1. Quillin, K. Ontogenetic scaling of hydrostatic skeletons: Geometric, static stress and dynamic stress scaling of the earthworm lumbricus terrestris. *J. Exp. Biol.* **1998**, *201*, 1871-1883.
2. Menciassi, A.; Gorini, S.; Pernorio, G.; Dario, P. In *A sma actuated artificial earthworm*, Robotics and Automation, 2004. Proceedings. ICRA'04. 2004 IEEE International Conference on, 2004; IEEE: pp 3282-3287.
3. Murakami, Y.; Uchiyama, H.; Kurata, J.; Maeda, M. In *Dynamical locomotion analysis and a model for the peristaltic motion of earthworms*, 2006 SICE-ICASE International Joint Conference, 2006; IEEE: pp 4224-4229.
4. Quillin, K.J. Kinematic scaling of locomotion by hydrostatic animals: Ontogeny of peristaltic crawling by the earthworm lumbricus terrestris. *J. Exp. Biol.* **1999**, *202*, 661-674.
5. Kim, S.; Laschi, C.; Trimmer, B. Soft robotics: A bioinspired evolution in robotics. *Trends Biotechnol.* **2013**, *31*, 287-294.
6. Hirose, S.; Umetani, Y. The development of soft gripper for the versatile robot hand. *Mechanism and machine theory* **1978**, *13*, 351-359.
7. Godage, I.S.; Branson, D.T.; Guglielmino, E.; Medrano-Cerda, G.A.; Caldwell, D.G. In *Shape function-based kinematics and dynamics for variable length continuum robotic arms*, Robotics and Automation (ICRA), 2011 IEEE International Conference on, 2011; IEEE: pp 452-457.

8. Scholten, K.; Meng, E. Materials for microfabricated implantable devices: A review. *Lab on a Chip* **2015**, *15*, 4256-4272.
9. Shen, H. Meet the soft, cuddly robots of the future. *Nature* **2016**, *530*, 24-26.
10. Mosadegh, B.; Polygerinos, P.; Keplinger, C.; Wennstedt, S.; Shepherd, R.F.; Gupta, U.; Shim, J.; Bertoldi, K.; Walsh, C.J.; Whitesides, G.M. Pneumatic networks for soft robotics that actuate rapidly. *Advanced Functional Materials* **2014**, *24*, 2163-2170.
11. Yuan, X.; Changgeng, S.; Yan, G.; Zhenghong, Z. In *Application review of dielectric electroactive polymers (deaps) and piezoelectric materials for vibration energy harvesting*, Journal of Physics: Conference Series, 2016; IOP Publishing: p 012077.
12. Rossiter, J.; Walters, P.; Stoimenov, B. In *Printing 3d dielectric elastomer actuators for soft robotics*, SPIE Smart Structures and Materials+ Nondestructive Evaluation and Health Monitoring, 2009; International Society for Optics and Photonics: pp 72870H-72870H-72810.
13. Kim, J.H.; Randall Lee, T. Discrete thermally responsive hydrogel‐coated gold nanoparticles for use as drug‐delivery vehicles. *Drug Dev. Res.* **2006**, *67*, 61-69.
14. Weng, H.; Zhou, J.; Tang, L.; Hu, Z. Tissue responses to thermally-responsive hydrogel nanoparticles. *J. Biomater. Sci. Polym. Ed.* **2004**, *15*, 1167-1180.
15. Kim, J.-H.; Lee, T.R. Thermo-and ph-responsive hydrogel-coated gold nanoparticles. *Chem. Mater.* **2004**, *16*, 3647-3651.
16. Ozay, O.; Ekici, S.; Baran, Y.; Aktas, N.; Sahiner, N. Removal of toxic metal ions with magnetic hydrogels. *Water Res.* **2009**, *43*, 4403-4411.
17. Peppas, N.A.; Bures, C.D. Glucose-responsive hydrogels. *Encyclopedia of Biomaterials and Biomedical Engineering", DOI* **2006**, *10*.
18. Miyata, T.; Asami, N.; Uragami, T. A reversibly antigen-responsive hydrogel. *Nature* **1999**, *399*, 766-769.
19. Murdan, S. Electro-responsive drug delivery from hydrogels. *J. Controlled Release* **2003**, *92*, 1-17.
20. Ziółkowski, B.; Florea, L.; Theobald, J.; Benito-Lopez, F.; Diamond, D. Self-protonating spiropyran-co-nipam-co-acrylic acid hydrogel photoactuators. *Soft Matter* **2013**, *9*, 8754-8760.
21. Dumitriu, R.P.; Mitchell, G.R.; Vasile, C. Multi‐responsive hydrogels based on n‐isopropylacrylamide and sodium alginate. *Polym. Int.* **2011**, *60*, 222-233.
22. Tudor, A.; Florea, L.; Gallagher, S.; Burns, J.; Diamond, D. Poly (ionic liquid) semi-interpenetrating network multi-responsive hydrogels. *Sensors* **2016**, *16*, 219.
23. Moon, J.J.; Saik, J.E.; Poche, R.A.; Leslie-Barbick, J.E.; Lee, S.-H.; Smith, A.A.; Dickinson, M.E.; West, J.L. Biomimetic hydrogels with pro-angiogenic properties. *Biomaterials* **2010**, *31*, 3840-3847.
24. Venkatesh, S.; Sizemore, S.P.; Byrne, M.E. Biomimetic hydrogels for enhanced loading and extended release of ocular therapeutics. *Biomaterials* **2007**, *28*, 717-724.
25. Morales, D.; Palleau, E.; Dickey, M.D.; Velev, O.D. Electro-actuated hydrogel walkers with dual responsive legs. *Soft Matter* **2014**, *10*, 1337-1348.
26. Chao Yang; Wei Wang; Chen Yao; Rui Xie; Xiao-Jie Ju; Zhuang Liu; Chu, L.-Y. Hydrogel walkers with electro-driven motility for cargo transport. *Scientific Reports* **2015**, *5*, 13622.
27. Florea, L.; Diamond, D.; Benito‐Lopez, F. Photo‐responsive polymeric structures based on spiropyran. *Macromolecular Materials and Engineering* **2012**, *297*, 1148-1159.

28. Rosario, R.; Gust, D.; Hayes, M.; Jahnke, F.; Springer, J.; Garcia, A.A. Photon-modulated wettability changes on spiropyran-coated surfaces. *Langmuir* **2002**, *18*, 8062-8069.
29. Shao, N.; Jin, J.; Wang, H.; Zheng, J.; Yang, R.; Chan, W.; Abliz, Z. Design of bis-spiropyran ligands as dipolar molecule receptors and application to in vivo glutathione fluorescent probes. *J. Am. Chem. Soc.* **2009**, *132*, 725-736.
30. Dunne, A.; Delaney, C.; Florea, L.; Diamond, D. Solvato-morphologically controlled, reversible nipaam hydrogel photoactuators. *RSC Advances* **2016**, *6*, 83296-83302.
31. Benito-Lopez, F.; Antoñana-Díez, M.; Curto, V.F.; Diamond, D.; Castro-López, V. Modular microfluidic valve structures based on reversible thermoresponsive ionogel actuators. *Lab on a Chip* **2014**, *14*, 3530-3538.
32. Czugala, M.; O'Connell, C.; Blin, C.; Fischer, P.; Fraser, K.J.; Benito-Lopez, F.; Diamond, D. Swelling and shrinking behaviour of photoresponsive phosphonium-based ionogel microstructures. *Sensors Actuators B: Chem.* **2014**, *194*, 105-113.
33. Benito-Lopez, F.; Byrne, R.; Răduţă, A.M.; Vrana, N.E.; McGuinness, G.; Diamond, D. Ionogel-based light-actuated valves for controlling liquid flow in micro-fluidic manifolds. *Lab on a Chip* **2010**, *10*, 195-201.
34. ter Schiphorst, J.; Coleman, S.; Stumpel, J.E.; Ben Azouz, A.; Diamond, D.; Schenning, A.P. Molecular design of light-responsive hydrogels, for in situ generation of fast and reversible valves for microfluidic applications. *Chem. Mater.* **2015**, *27*, 5925-5931.
35. Stumpel, J.E.; Ziółkowski, B.; Florea, L.; Diamond, D.; Broer, D.J.; Schenning, A.P. Photoswitchable ratchet surface topographies based on self-protonating spiropyran–nipaam hydrogels. *ACS applied materials & interfaces* **2014**, *6*, 7268-7274.
36. Ye, Q.; Spencer, P.; Wang, Y.; Misra, A. Relationship of solvent to the photopolymerization process, properties, and structure in model dentin adhesives. *Journal of Biomedical Materials Research Part A* **2007**, *80*, 342-350.
37. Shangguan, Y.; Yang, J.; Zheng, Q. Rheology of nitrile rubber with hybrid crosslinked network composed of covalent bonding and hydrogen bonding. *RSC Advances* **2017**, *7*, 15978-15985.
38. Stumpel, J.E.; Liu, D.; Broer, D.J.; Schenning, A.P. Photoswitchable hydrogel surface topographies by polymerisation‐induced diffusion. *Chemistry‐A European Journal* **2013**, *19*, 10922-10927.
39. Huang, C.; Lv, J.-a.; Tian, X.; Wang, Y.; Yu, Y.; Liu, J. Miniaturized swimming soft robot with complex movement actuated and controlled by remote light signals. *Sci. Rep.* **2015**, *5*.
40. Maeda, S.; Hara, Y.; Sakai, T.; Yoshida, R.; Hashimoto, S. Self‐walking gel. *Adv. Mater.* **2007**, *19*, 3480-3484.
41. Wang, L.; Liu, Y.; Cheng, Y.; Cui, X.; Lian, H.; Liang, Y.; Chen, F.; Wang, H.; Guo, W.; Li, H. A bioinspired swimming and walking hydrogel driven by light‐controlled local density. *Advanced Science* **2015**, *2*.
42. Shibayama, M.; Tanaka, T. Volume phase transition and related phenomena of polymer gels. In *Responsive gels: Volume transitions i*, Springer: 1993; pp 1-62.
43. Ziółkowski, B.; Florea, L.; Theobald, J.; Benito-Lopez, F.; Diamond, D. Porous self-protonating spiropyran-based nipaam gels with improved reswelling kinetics. *Journal of materials science* **2016**, *51*, 1392-1399.
44. Satoh, T.; Sumaru, K.; Takagi, T.; Takai, K.; Kanamori, T. Isomerization of spirobenzopyrans bearing electron-donating and electron-withdrawing groups in acidic aqueous solutions. *PCCP* **2011**, *13*, 7322-7329.

45. Coleman, S.; ter Schiphorst, J.; Stumpel, J.E.; Ben Azouz, A.; Diamond, D.; Schenning, A.P. Molecular design of light-responsive hydrogels, for in-situ generation of fast and reversible valves for microfluidic applications. *Chem. Mater.* **2015**, *27*, 5925-5931.
46. Jiang, H.; Kobayashi, T. Ultrasound stimulated release of gallic acid from chitin hydrogel matrix. *Materials Science and Engineering: C* **2017**, *75*, 478-486.
47. Huynh, C.T.; Nguyen, M.K.; Tonga, G.Y.; Longé, L.; Rotello, V.M.; Alsberg, E. Photocleavable hydrogels for light‐triggered sirna release. *Advanced healthcare materials* **2016**, *5*, 305-310.

Chapter 5

Micro-capillary Coatings Based on Spiropyran Polymeric Brushes for Metal Ion Binding, Detection and Release in Continuous Flow*

Micro-Capillary Coatings Based on Spiropyran Polymeric Brushes for Metal Ion Binding, Detection, and Release in Continuous Flow,** Aishling Dunne, Colm Delaney, Aoife McKeon, Pavel Nesterenko, Brett Paull, Fernando Benito-Lopez, Dermot Diamond, Larisa Florea,** *Sensors,* 2018, 18(4), 1083 – 1095.

Chapter 5:

Micro-capillary Coatings Based on Spiropyran Polymeric Brushes for Metal Ion Binding, Detection and Release in Continuous Flow

5.1 Abstract

Micro-capillaries, capable of light-regulated binding and qualitative detection of divalent metal ions in continuous flow, have been realised through functionalisation with spiropyran photochromic brush-type coatings. Upon irradiation with UV light, the coating switches from the passive non-binding spiropyran form to the active merocyanine form, which binds different divalent metal ions (Zn^{2+}, Co^{2+}, Cu^{2+}, Ni^{2+}, Cd^{2+}), as they pass through the micro-capillary. Furthermore, the merocyanine visible absorbance spectrum changes upon metal ion binding, enabling the ion uptake to be detected optically. Irradiation with white light causes reversion of the merocyanine to the passive spiropyran form, with simultaneous release of the bound metal ion from the micro-capillary coating.

5.2 Introduction

The photochromic properties of spirobenzopyrans were first discovered by Fischer and Hirshberg in 1952 [1]. Since then, spiropyrans have been studied for a wide range of applications including optical recording [2,3], photochromic lenses [4], dye-sensitised solar cells[5], light harvesting artificial membranes [6,7], sensors [8-10], and actuators [11-15], among others [16-20]. Upon irradiation with UV light, spiropyrans isomerise to the more polar, open merocyanine form. Metal ions can complex with the open merocyanine form, thereby influencing this isomerisation process. Conversely, irradiation with visible light results in a high concentration of the closed form, thereby releasing the metal ion. It is therefore possible to trigger metal ion binding by irradiation with UV light and to reverse this process through white light irradiation of the coloured complex. This regenerates the inactive spiropyran form and results in the release of metal ions [17].

The use of light to trigger the chelator offers unique opportunities, as the binding/releasing process is reversible and can be controlled externally in a non-invasive manner. We are particularly interested in this type of ‘switchable’ behaviour, as it enables a ‘4D’ character to be developed in which materials can respond to local stimuli (changes in local molecular environment, heat, light etc.) and switch between dramatically different modes of behaviour over time (the 4th dimension). Many of these behaviours, which are bio-inspired, have been previously used to generate micro-vehicles that can follow sources of chemical attractants by mimicking the movement of chemotactic organisms [21], or adaptive surfaces that can

dramatically alter their physical and chemical properties in response to external stimuli [22,23].

In this paper, we present the metal ion binding capabilities of a norbornene-functionalised spiropyran monomer (SP) in solution, in addition to its photochromic behaviour in the crystal state and when polymerised to form 3D polymeric brushes on substrates. Moreover, through the integration of the beneficial characteristics of both miniaturised platforms and spiropyran photochromic dyes, a simple and innovative micro-capillary capable of switchable metal ion uptake and release has been realised that can simultaneously communicate its state (i.e., passive (non-binding); active (binding) and free; and active and populated). The functionalised micro-capillary model we have developed can therefore act as a photonically controlled self-indicating system for controlled metal ion uptake and release, operating in a continuous flow regime.

5.3 Experimental

5.3.1 Materials

7-Octenyltrichlorosilane (Gelest, Morrisville, PA, USA), 5-norbornene-2-carboxylic acid, exo- (Sigma-Aldrich, St. Louis, MO, USA), 1-(2-Hydroxyethyl)-3,3-dimethylindolino-6′-nitrobenzopyrylospiran (SP1) (TCI Europe, Zwijndrecht, Belgium), *N*,*N*′-dicyclohexylcarbodiimide (DCC) (Sigma-Aldrich), 4-(dimethylamino)pyridine (DMAP) (Sigma-Aldrich), and Grubbs Generation-II catalyst (Sigma-Aldrich) were used as received. For the SP and poly(SP) synthesis, dry tetrahydrofuran and dry dichloromethane solvents were purchased from Sigma-Aldrich and used as received. Fused-silica micro-capillaries (100 μm ID, 375 μm OD) were purchased from Polymicro Technologies (Phoenix, AZ, USA). Acetonitrile (ACN) solvent used for solution and capillary studies was Sigma-Aldrich HPLC grade and was used without further purification.

5.3.2 Synthesis of Spiropyran Norbornene Monomer (SP)

The spiropyran monomer (SP) was prepared from the reaction of exo-5-norbornyl carboxylic acid with SP1 in the presence of DCC and DMAP as described elsewhere [9]. After synthesis, the resulting red wax was purified using silica gel column chromatography

and a solvent mixture of hexane: ethyl acetate (10:1). Crystals of SP, used to study the solid-state photochromism, were grown by slow evaporation from hexane: ethyl acetate (10:1).

5.3.3 Synthesis of Spiropyran Polymeric Brushes (polySP)

Si-ROMP was performed using a previously described method [9]. Prior to functionalisation, the micro-capillaries (internal diameter of 100 μm and 15 cm length) were washed with acetone and water. Following this, the fused silica surface was activated by passing a solution of 0.2 M NaOH for 30 min at a flow rate of 0.25 μL min^{-1} through the micro-capillary using a syringe pump, followed by a 0.2 M HCl solution for 30 min at the same flowrate. The micro-capillary was rinsed profusely with deionised water and dried under N_2 stream after both the acid and base treatments. Next, the micro-capillary was flushed with a 0.1 M solution of 7-octenyl trichlorosilane in dry toluene for 90 min at a flow rate of 0.25 μL min^{-1}. The micro-capillary was then washed with acetone, dried under a N_2 stream, and left at room temperature for 24 h. Later, the micro-capillary was filled, in an inert atmosphere, with a 0.02 M solution of Grubbs Catalyst Second Generation in degassed CH_2Cl_2, sealed by rubber septa at both ends, and put in a water bath for 1 h at 45 °C. Following this, the catalyst-functionalised micro-capillary was thoroughly washed with degassed CH_2Cl_2 under inert atmosphere. Next, the micro-capillary was filed with SP monomer solution (0.5 M in degassed CH_2Cl_2), sealed at both ends using rubber septa, and put in a water bath at 50 °C for 1 h. The polymerisation was quenched by rinsing the micro-capillary with ethyl vinyl ether. Finally, the polySP polymeric-brushes functionalised micro-capillary was thoroughly washed with acetone to remove any physisorbed materials and dried under a N_2 stream.

5.3.4 Light Source

Photo-conversion of the monomer solutions from SP to MC was achieved in a UVP CL-1000 Ultraviolet chamber using a wavelength of 365 nm at a power level of 3.5 mW cm^{-2} for 10 min (solutions) and 1–2 min (capillaries and crystals), respectively, to ensure full switching to the MC form. The white light irradiation was provided via a LMI-6000 LED Fiber Optic Illuminator obtained from Dolan-Jenner Industries and was used to switch the MC solutions and the polyMC coatings back to the closed SP and polySP forms, respectively.

The vials/capillaries were placed at 2 cm from the light source and were irradiated for 2–3 min (solutions, crystals) and 10 min (capillaries), to ensure equilibrium interconversion. The maximum light output of the lamp was 780 Lumens, and the intensity control of the light output was fixed at 50%.

5.3.5 Methods

UV-Vis spectroscopy of the SP solutions in the presence of different metal ions was performed using a Cary 50 spectrophotometer (Varian, Palo Alto, CA, USA). Microscopy images of the micro-capillaries and microscopy images and videos of the SP crystals were captured on an Aigo digital microscope (The Dolomite Centre Ltd., Royston, UK) equipped with auxiliary objectives to allow a magnification of 60×, 180× and 540×, respectively. UV-Vis spectroscopy was used to study the photo-binding and sensing of divalent metal ions to the poly(SP/MC) coatings while in different illumination conditions. The absorbance spectra were recorded using two fiber-optic light guides connected to a Miniature Fiber Optic Spectrometer (USB4000, Ocean Optics, Dunedin, FL, USA) and aligned using a cross-shaped cell (Supplementary Materials, Figure A3.1). The light source used was a DH-2000-92 BAL UV-NIR deuterium tungsten halogen source (Ocean Optics). The six metal ion solutions (in ACN) were passed through the micro-capillary at a constant flow rate of 0.5 μL min^{-1} using a syringe pump (PHD 2000 Syringe, Harvard Apparatus, Cambridge, MA, USA) and a glass Hamilton micro-syringe of 100 μL. The data from the spectrometer were processed using Spectrasuite software provided by Ocean Optics Inc. For clarity, each recorded absorbance spectrum was smoothed using Origin software with a Savitzky-Golay algorithm. The set-up used for metal ion detection after being photo-released from the micro-capillary is described in detail in Appendix 3.

The SP crystals were grown by slow evaporation from hexane: ethyl acetate (10:1 *v*/*v*) over several days to produce clear crystals.

5.4 Results and Discussion

5.4.1 Photochromism of Spiropyrans

Photochromism of spiropyran derivatives is reliant on the interconversion between the closed spiropyran (orthogonal) form and the open merocyanine (planar) form. For the most part, photochromism of spiropyran-derivatives has been largely studied in solution, but few derivatives are known to show photochromism in the crystalline state [24-26]. The common belief is that SP derivatives do not show solid state photochromism in crystals, though this has been disputed by Harada et al. [27] who demonstrated solid state photochromism in crystals for a range of spiropyrans and spirooxazines at low temperatures (−195 °C to −70 °C).

However, the SP monomer synthesised in this research exhibits rapid and reversible room temperature photochromism in the crystal state upon UV/white light irradiation (Video A3.1). Upon UV light (365 nm) exposure, the colour of the crystals rapidly changes towards purple (Figure 5.1(a); 1 min UV irradiation).

Progressive reversal of this process is indicated by decolouration produced by illumination with white light (Figure 5.1(b), 1 min, and Figure 5.1(c), additional 2 min). This effect is observed at room temperature (20 °C). Although the determination of the crystal structure in the two forms was attempted, as in previously reported cases [27], this was unfruitful, most likely because of the disorder arising from the co-existence of both SP and MC forms in the crystal lattice. Further investigation will be carried out to ascertain if photo-conversion takes place at crystal sites under lattice control or is restricted to crystal defects.

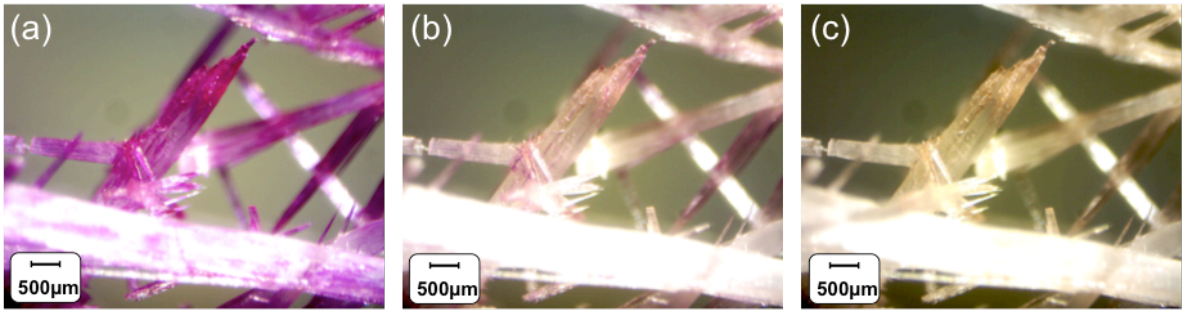

Figure 5.1. Crystals of the norbornene-spiropyran derivative (SP) exhibiting solid-state photoisomerisation under the following conditions: (a) 1 min UV irradiation, (b) additional 1 min white light irradiation, and (c) additional 2 min white light irradiation. The strong purple colour in (a) is indicative of significant formation of the merocyanine isomer, whereas the lighter purple colour in (b) indicates co-existence of both isomers. The colourless crystals (c) indicate that the system has largely reverted to the spiropyran isomer.

5.4.2 Metal Ion Binding – Solution Studies

Solution studies have shown that the open MC form of the spiropyran norbornene functionalised monomer can bind certain metal ions in solution. An integral characteristic of spiropyran is the photo-cleavage of the C_{spiro}-O bond, which occurs during UV illumination, to generate the merocyanine form. The merocyanine possesses a negatively charged phenolate oxygen which serves as a potential site for cation binding [28-32]. In this context, there have been several research studies on SP-derivatives for metal ion binding, predominantly for divalent metal ions such as Zn^{2+} [32,33], Co^{2+} [10,33,34], Cu^{2+} [33,34], Ni^{2+} [30,33], and Cd^{2+} [35], in which binding generally happens in a 2:1 ratio of merocyanine to M^{2+}, due to the coordination of the divalent metal ion by two MC phenolate anions [35]. Several research groups have attempted to increase the number of binding sites and achieve a 1:1 binding ratio (merocyanine: M^{2+}) through variation of the R group in the eighth position of the benzopyran ring to include methoxy [34] or allyl substituents [34], or by functionalising the indolic nitrogen with carboxylic acid [36], ester [37], or hydroxyl-terminated moieties [34]. These groups can promote complex formation by offering additional sites to the merocyanine phenolate anion for stabilisation of the metal centre, resulting in a thermodynamically stable MC:M^{2+} complex [32]. However, the metal-ligand interaction is usually weak enough to allow disruption of the complex by the photo-induced ring closing reaction. Therefore, SP derivatives can be used as reversible chelators for metal ions.

The SP norbornene functionalised spiropyran ester, used in this study, has two potential binding sites for the metal ion; the phenolic oxygen of the MC form, and carbonyl oxygen of the ester side chain, and could potentially allow for both 1:1 and 2:1 (MC:M^{2+}) binding ratios. The MC−M^{2+} complexes have been successfully characterised in solution using UV-Vis spectroscopy. In the presence of the MC form, certain metal ions exhibit a unique colorimetric response, due to formation of the metal ion complexes (Figure 5.2(a–c)). The colourless, ring-closed spiropyran (SP) shows no absorption in the visible region. After irradiation of the solution with UV light (2 min), the ring-opened merocyanine (MC) form is clearly visible, characterised by an intense absorption at ~570 nm, specific to the zwitterionic MC form. Upon complexation with Ni^{2+}, Cd^{2+}, Co^{2+}, Zn^{2+}, and Cu^{2+} ions, there is a decrease in the long wavelength absorbance at 570 nm, along with a significant hypsochromic shift in absorbance band, which is dependent on the metal ion contained in the solution. This blue shift of the absorbance band is due to a disruption in planarity of the trans-MC that occurs upon complexation. The MC:Ni^{2+} complex yields a small hypsochromic shift of 40 nm ($\lambda max \approx 530$ nm. The MC:Co^{2+} and MC:Zn^{2+} complexes exhibit blue shifts of 70 nm ($\lambda max \approx 500$ nm) and 90 nm ($\lambda max \approx 460$ nm), respectively. Shifts in the λmax can be attributed to the disruption of planarity in trans-MC [18]. In the case of some of the metal ions (Ni^{2+}, Co^{2+}, Cd^{2+}), as seen in Figure 5.2 (d), the characteristic MC absorbance band still remains. This suggests that under the same experimental conditions (1.5×10^{-3} M SP in ACN, 2:1 molar ratio SP:M^{2+}, and identical illumination conditions), the MC presents different binding affinities for different metal ions. The co-existence of both absorbance features characteristic of the free MC and the MC:M^{2+} complex is evidence of an equilibrium between the two forms. Irradiation of the solutions with white light caused the disappearance of the band characteristic to MC and MC:M^{2+}, indicating reversible binding for all cases except Cu^{2+} (Figure 5.2(c)). While this result is somewhat surprising, it has been previously demonstrated by Natali et al. [33] that the merocyanine:Cu^{2+} interaction is rather “curious”, as it can lead to the formation of stable SP dimers mediated by Cu^{2+}. We believe a similar symmetric dimer is obtained in the case of this SP in the presence of Cu^{2+} analogous to that suggested by Natali et al. [33].

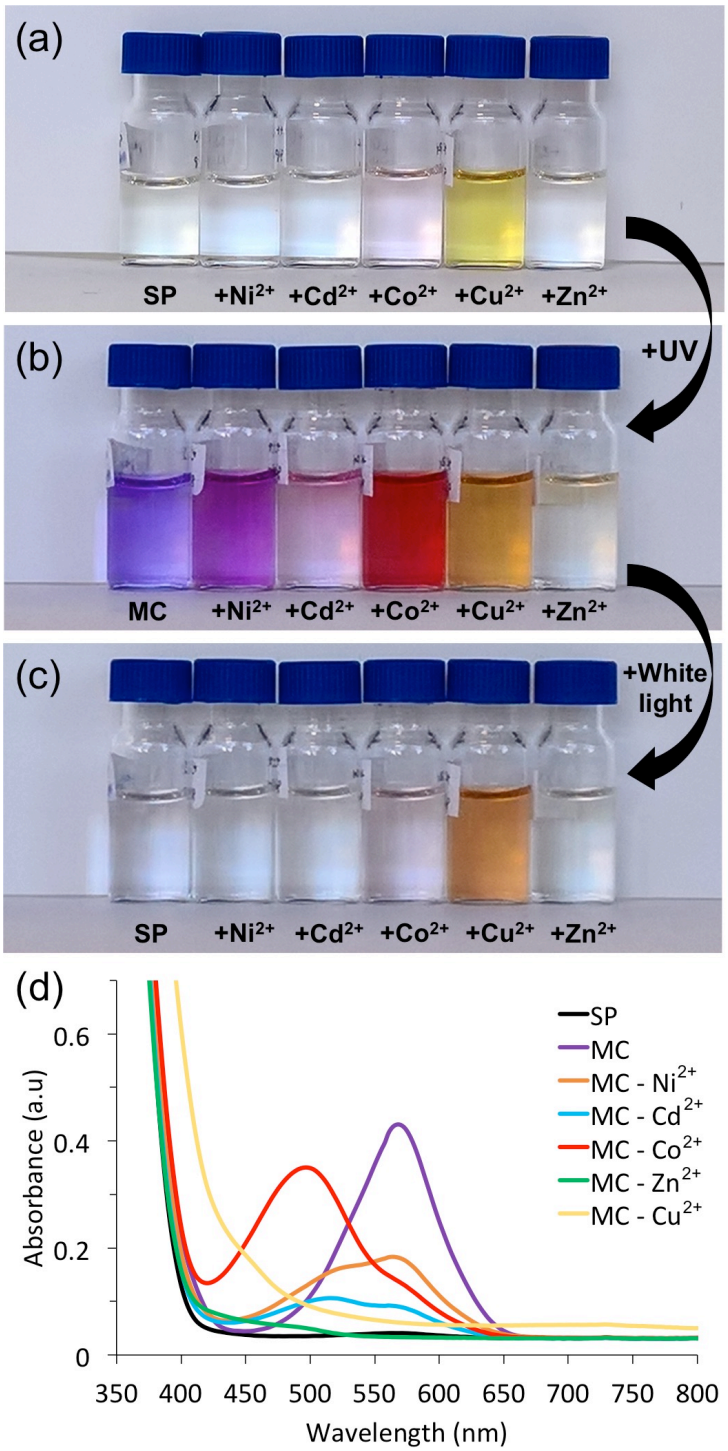

Figure 5.2. Images (a–c) and UV-Vis spectra (d) of the SP solutions in ACN (1.5×10^{-3} M) in the presence of various divalent metal ions (molar ratio SP:M^{2+} 2:1); (a) initial solutions before illumination; (b) after 10 min of UV light illumination; (c) after 10 min of white light illumination; (d) UV-Vis spectra of solutions shown in (b). As it can be observed from the images (a,c) and UV-Vis spectra (d), in the current experimental conditions (M^{2+} concentration in ACN is 0.75×10^{-3} M), no absorbance band due to the presence of M^{2+} salt alone was observed in the visible region of the spectrum.

To evaluate the potential of the MC form of the SP norbornene functionalised spiropyran ester as a quantitative probe for divalent metal ions, MC was subjected to UV-Vis titrations with increasing concentrations of Co^{2+} and Cu^{2+}, respectively. Figure 5.3 shows the absorbance spectra of MC (1.5×10^{-3} M SP in ACN) in the presence of increasing concentrations of Co^{2+}. As observed, the absorbance band specific to the MC form is seen to decrease with increasing Co^{2+} (0–0.15 mM), with the simultaneous appearance of a new shoulder at ~500 nm. Increasing the concentration of Co^{2+} even further (0.15 mM–1.5 mM) causes the appearance of the MC:Co^{2+} band centred at $\lambda_{max} \approx 500$ nm, which induced a colour change from purple (MC) to red (MC:Co^{2+}). A linear dependence of the ratio of the absorbance at $\lambda_{max} \approx 500$ nm (MC:Co^{2+}) and the absorbance at $\lambda_{max} \approx 570$ nm (MC) as a function of concentration of Co^{2+} for concentration ranges 0–0.15 mM and 0.33–1.5 mM (Figure 5.3, inset) was observed.

Similarly, the spectrophotometric titration of MC (1.5×10^{-3} M SP in ACN) with Cu^{2+} (0–1.5 mM) was also investigated under the same conditions (2 min of UV irradiation). In this case, the absorbance band specific to MC ($\lambda_{max} \approx 570$ nm) disappeared completely once the concentration of Cu^{2+} was increased upon 0.03 mM and a new absorbance band specific to MC:Cu^{2+} was observed, centred at 430 nm. A linear dependence of this absorbance band ($\lambda_{max} \approx 430$ nm) as a function of Cu^{2+} concentration was observed (Figure 5.4, inset). No noticeable difference in the MC binding behaviour was observed when the Co^{2+} or Cu^{2+} solutions containing 10^{-3} M Na^{+}. This result is expected, as MC dyes are not known to bind monovalent metal ions.

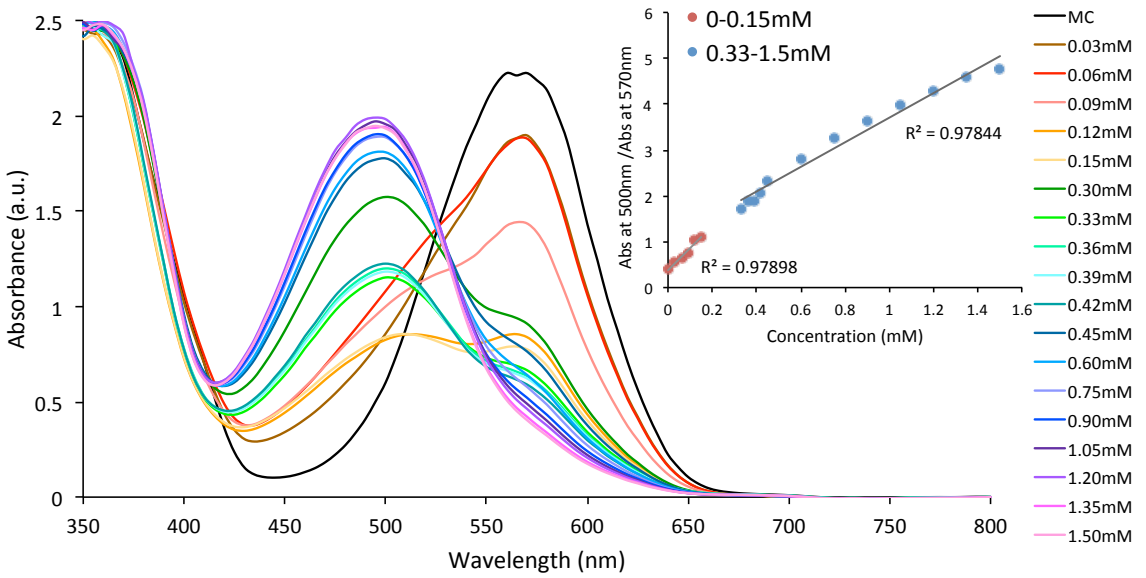

Figure 5.3. Absorbance changes of the SP solutions in ACN (1.5×10^{-3} M) in the presence of increasing concentrations of Co^{2+} (0–1.5 mM) after irradiation with UV light; Inset shows the linear dependence of the ratio of the absorbance at λmax ≈ 500 nm ($MC:Co^{2+}$) and the absorbance at λmax ≈ 570 nm (MC) as a function of concentration of Co^{2+} for concentration ranges 0–0.15 mM and 0.33–1.5 mM.

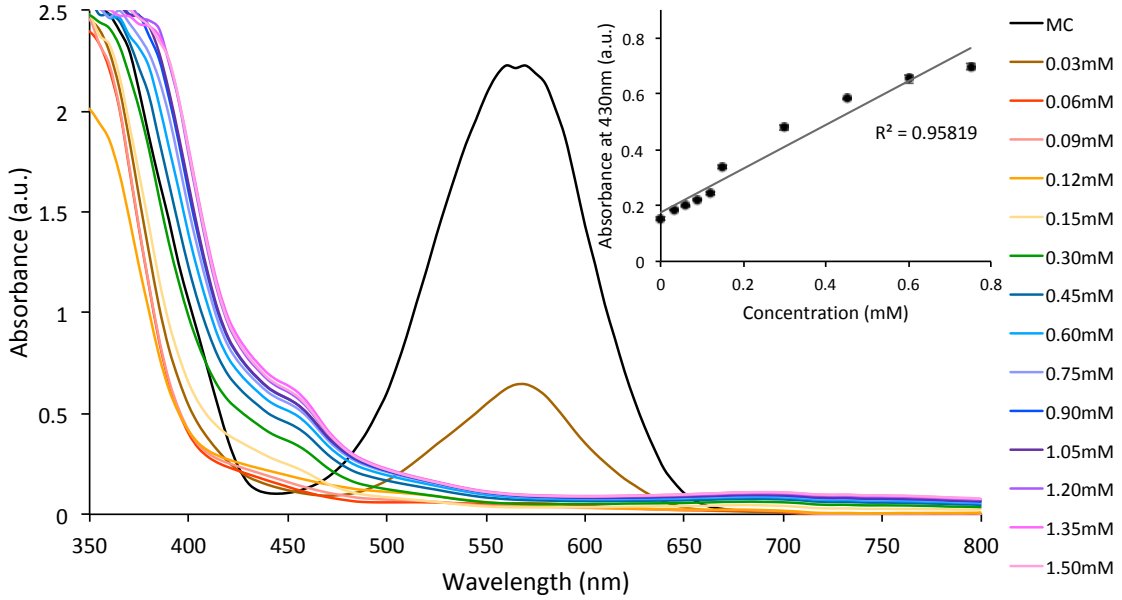

Figure 5.4. Absorbance changes of the SP solutions in ACN (1.5×10^{-3} M) in the presence of increasing concentrations of Cu^{2+} (0–1.5 mM) after irradiation with UV light; Inset shows the linear dependence of the absorbance at λmax ≈ 430 nm ($MC:Cu^{2+}$) as a function of Cu^{2+} concentration (0–0.8 mM).

5.4.3 Metal Ion Binding – Micro-capillary Studies

Coating of the glass micro-capillaries was performed using ring-opening metathesis polymerisation, as described in the experimental section, to produce a 2–3 μm homogenous coating (Figure A3.2) comprised of colourless spiropyran (SP) homopolymeric brushes. We have previously characterised such polymeric brushes [9], in addition to their UV-induced photochromism [9] and solvatochromic properties [10]. Figure 5.5 shows the colour of the micro-capillary post UV light irradiation in the presence of divalent metal ions and the corresponding UV-vis spectra. Upon irradiation with UV light, the SP form (non-binding) (Figure 5.6(a)) is converted to the polar MC form that exhibits metal ion chelation capabilities (Figure 5.6(b)). When certain divalent metal ion solutions (e.g., Cu^{2+}, Co^{2+}, Cd^{2+}, Ni^{2+}, Zn^{2+}) are passed through the coated micro-capillary in a continuous flow, metal ions are bound by free MC sites (Figure 5.6(c)) in the capillary coating through the spontaneous formation of polyMC:M^{2+}, signalled by clearly visible changes in the colour of the micro-capillary (Figure 5.5). Subsequent irradiation of the micro-capillary with white light causes the MC:M^{2+} to revert to the SP form and the bound metal ion is released (Figure 5.6(d)). Simultaneously, the micro-capillary reverts to colourless and the passive SP-coating is regenerated (Figure 5.6(a)). The change in colour of the micro-capillary upon UV irradiation in the absence or presence of the different metal ion solutions under continuous flow (0.5 μL min−1) was recorded using the set-up described in Figure A3.3. The corresponding spectra are presented in Figure 6(b). UV-Vis spectroscopy studies of the SP polymer (polySP) brush films on the micro-capillary revealed that UV irradiation leads to a strong absorbance in the visible region centred at approximately 565 nm, corresponding to conversion of the SP-functionalised norbornene polymer to the MC form (polyMC). As in the case of the monomer in solution, this absorbance λmax is shifted to lower wavelengths in the presence of the metal ions in the order: MC (λmax ≈ 565 nm) > MC:Ni^{2+}(λmax ≈ 534 nm) > MC:Cd^{2+}(λmax ≈ 522 nm) > MC:Co^{2+}(λmax ≈ 508 nm) > MC:Zn^{2+}(λmax ≈ 489 nm) > MC:Cu^{2+}(λmax ≈ 430 nm). The fact that the absorption characteristic of the MC unbound form does not appear in any of the polyMC:M^{2+} spectra, indicates that polyMC is extensively involved in the complex formation. A broadening of the absorption bands is also observed compared to the solution studies (Figure 5.2(d)). The coated micro-capillary represents a self-indicating, photo-controlled system that can report its status—passive, active (free), bound with metal ion through changes in colour/absorbance; and to some extent, it is possible to distinguish which metal ion is bound from differences in the visible absorbance spectrum. As in the case of

solution studies, it was observed that the binding process was reversible for each of the metal ions (Figure A3.4) except for Cu^{2+}.

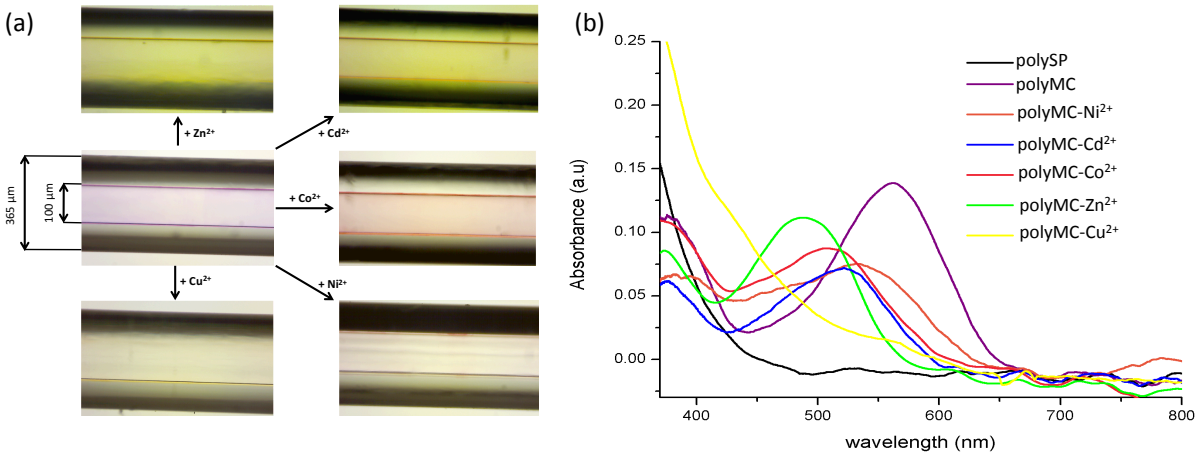

Figure 5.5. Images (a) and absorption spectra (b) of the coated micro-capillaries when solutions of different metal ions in ACN (10^{-3} M) are passed through the micro-capillary after irradiation for 1 min with UV light.

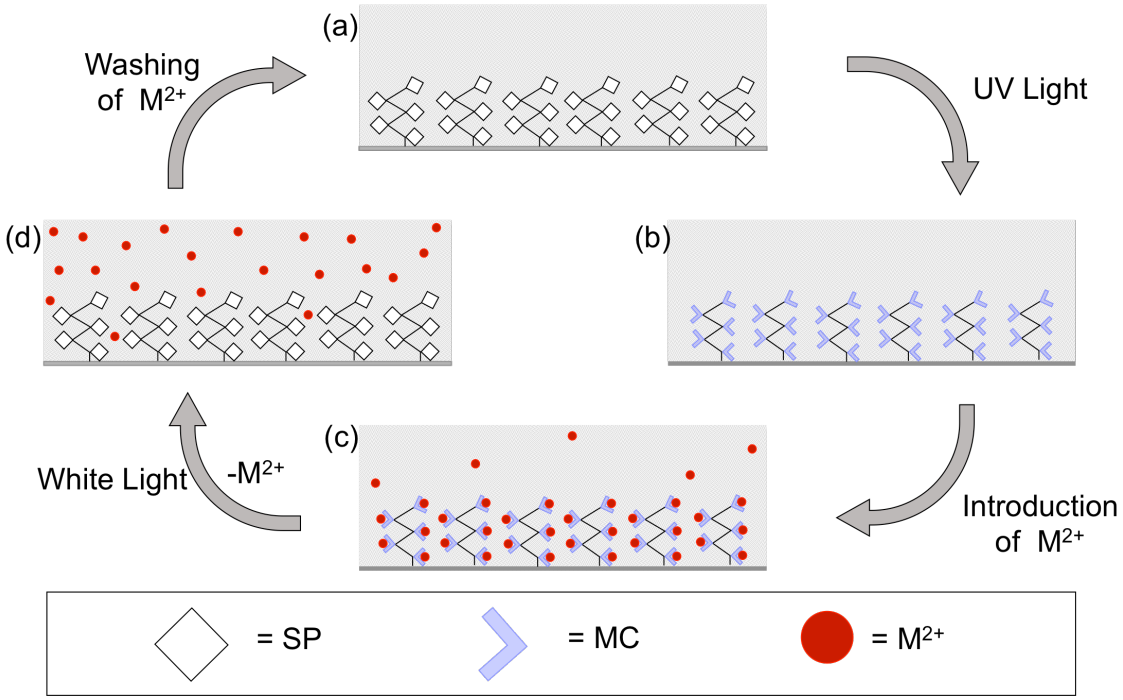

Figure 5.6. Schematic representation of the metal ion binding, sensing, and release cycle in the SP polymeric brushes coated micro-capillary. (a) polySP coated micro-capillary before irradiation; (b) formation of polyMC upon UV irradiation; (c) binding of M^{2+} to polyMC coating; (d) photo-controlled release of M^{2+} upon white light irradiation and regeneration of polySP coating.

Co^{2+} was selected for further study on the basis of its very clear spectral shift from free MC to MC:M^{2+}. In addition to the spectral changes inherent to the ion binding and release observable from the coating in the capillary, detection of free Co^{2+} released from the poly(SP) functionalised micro-capillary upon white light irradiation was evaluated using a post column reaction with 4-(2-pyridylazo)resorcinol (PAR). PAR is a well-known chelating reagent, offering multiple coordination possibilities for metal ions [38,39] through a pyridyl nitrogen, azo group and o-hydroxyl group, as shown in Figure A3.5. This results in an easily identifiable PAR:Co^{2+} coloured complex with a λ_{max} at ~510 nm, as shown in the UV-Vis spectra in Figure A3.6. The set-up used for recording the absorbance at 510 nm before and after irradiation of the poly(MC) functionalised micro-capillary with white light (release) is shown in Figure A3.7. Figure 5.7 shows the monitoring of the absorbance at 510 nm (characteristic for the PAR:Co^{2+} coloured complex) as a function of time. Several stages (1–5) are identified (Figure 5.7), in relation to the state of the functionalised micro-capillary (Figure 5.6), as described below:

Passive form (polySP) in the presence of solvent; capillary is colourless, no Co^{2+} present; low baseline signal at 510 nm (Figure5. 6a).

UV source ON; passive polySP converted to active binding polyMC form; capillary has a purple colour (Figure 5.2(b)); no Co^{2+} present; low baseline signal at 510 nm (Figure 5.7(b)).

Co^{2+} is injected in the mobile phase; capillary indicates binding by colour change to a reddish colour (Figures 5.2(c) and 5.7(c)); large peak at 510 nm is due to the detection of unbound Co^{2+} passing through the micro-capillary.

Switch back to solvent without Co^{2+}; signal returns to baseline indicating unbound Co^{2+} has been removed. Capillary still has a reddish colour suggesting bound Co^{2+} is present in the coating (Figure 5.7(c)).

White light source is turned ON; coating reverts to colourless (polySP) passive form; bound Co^{2+} is simultaneously released (Figure 5.7(d)) and detected as the peak at ca. 30 min.

This experiment confirms the release of Co^{2+} from the micro-capillary upon white light irradiation. In the case of Cu^{2+}, the micro-capillary maintained its yellow colour after the binding event, despite white light irradiation. This suggests that the dimer formation mentioned previously is also occurring in the polymeric brushes.

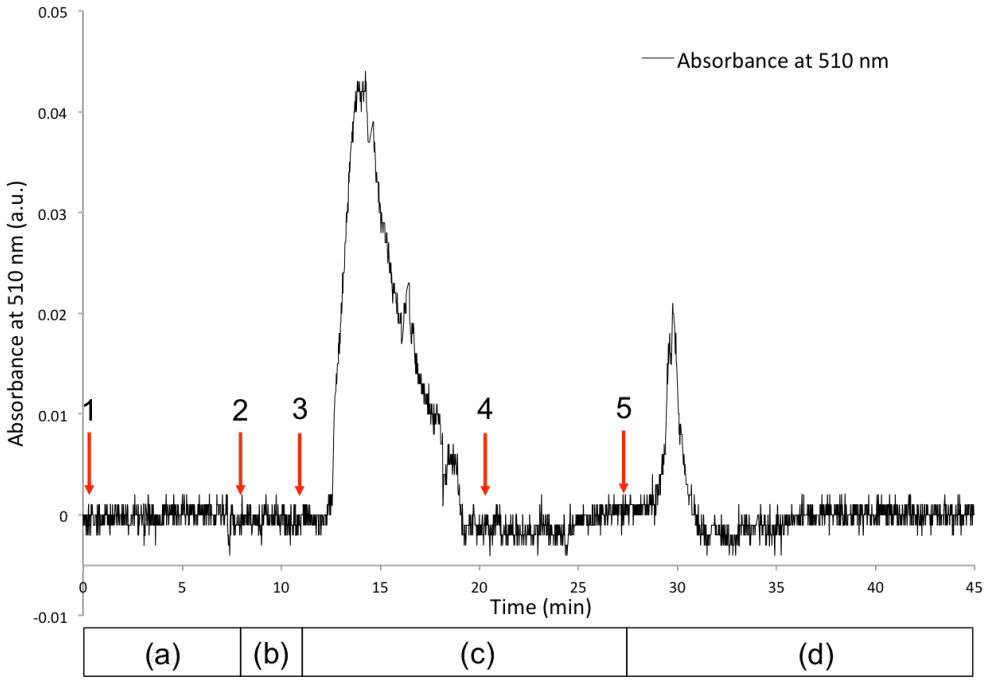

Figure 5.7. Absorbance at 510 nm recorded on a USB400 spectrometer over time, using the set-up depicted in Figure A3.7. Five stages (1–5) are identified as described in the text; The increase of the absorbance band centred at 510 nm indicates the presence of PAR-Co^{2+} complex; Bottom bar indicates the state of the functionalised micro-capillary as per Figure 6: (a) polySP coated micro-capillary before irradiation; (b) formation of polyMC upon UV irradiation; (c) binding of Co^{2+} to polyMC coating; (d) photo-controlled release of Co^{2+} upon white light irradiation and regeneration of polySP coating.

5.5 Conclusions

Herein, we have demonstrated the photochromism of a norbornene-functionalised spiropyran derivative and its ability to reversibly bind divalent metal ions present in solution, accompanied by significant variations in the visible absorbance spectrum. Micro-capillaries were coated with spiropyran polymer brushes using ROMP chemistry, and the resulting flow system was found to exhibit self-indication of status (passive, active, metal-ion bound) through a colorimetric response. In addition, this metal ion uptake and release behaviour is photo-controlled using external light sources. Although photo-controlled metal ion detection using spiropyran derivatives has been previously demonstrated by us [17] and others [33-37], this represents the first example in which photo-controlled uptake and release has been demonstrated within a micro-capillary system using polymeric brushes, in a continuous flow regime. Although, without doubt, there are many specific sensor molecules for quantitative

metal ion detection, the ability to achieve a self-indicating flow-system, capable of photo-controlled binding and release, may prove to be of particular importance for the integration of advanced bioinspired functionalities in microfluidic systems. The use of light to trigger the chelator offers unique opportunities that minimise waste generation and power requirements. In addition, advances in the integration of LED (light emitting diode) sources in the system hold promise for the production of low cost miniaturised systems.

5.6 References

1. Fischer, E., and Y. Hirshberg. Formation of coloured forms of spirans by low-temperature irradiation. *Journal of the Chemical Society* **1952**, 4522-4524.
2. Triolo, C.; Patanè, S.; Mazzeo, M.; Gambino, S.; Gigli, G.; Allegrini, M. Pure optical nano-writing on light-switchable spiropyrans/merocyanine thin film. *Optics express* **2014**, *22*, 283-288.
3. Berkovic, G.; Krongauz, V.; Weiss, V. Spiropyrans and spirooxazines for memories and switches. *Chemical Reviews* **2000**, *100*, 1741-1754.
4. Kadowaki, S. Photochromic lens for eye glasses. Google Patents: 2016.
5. Johnson, N.M.; Smolin, Y.Y.; Schinler, C.; Hagaman, D.; Soroush, M.; Lau, K.K.S.; Ji, H.-F. Photochromic dye-senitized solar cells. *AIMS Material Science* **2015**, *2*, 503 - 509.
6. Xie, X.; Crespo, G.A.; Mistlberger, G.; Bakker, E. Photocurrent generation based on a light-driven proton pump in an artificial liquid membrane. *Nature chemistry* **2014**, *6*, 202-207.
7. Xie, X.; Bakker, E. Creating electrochemical gradients by light: From bio-inspired concepts to photoelectric conversion. *Physical Chemistry Chemical Physics* **2014**, *16*, 19781-19789.
8. Xie, X.; Mistlberger, G.n.; Bakker, E. Reversible photodynamic chloride-selective sensor based on photochromic spiropyran. *Journal of the American Chemical Society* **2012**, *134*, 16929-16932.
9. Florea, L.; Hennart, A.; Diamond, D.; Benito-Lopez, F. Synthesis and characterisation of spiropyran-polymer brushes in micro-capillaries: Towards an integrated optical sensor for continuous flow analysis. *Sensors and Actuators B: Chemical* **2012**, *175*, 92-99.
10. Florea, L.; McKeon, A.; Diamond, D.; Benito-Lopez, F. Spiropyran polymeric microcapillary coatings for photodetection of solvent polarity. *Langmuir* **2013**, *29*, 2790-2797.
11. Stumpel, J.E.; Ziółkowski, B.; Florea, L.; Diamond, D.; Broer, D.J.; Schenning, A.P. Photoswitchable ratchet surface topographies based on self-protonating spiropyran–nipaam hydrogels. *ACS applied materials & interfaces* **2014**, *6*, 7268-7274.
12. Williamson, A.; Ferro, M.; Leleux, P.; Ismailova, E.; Kaszas, A.; Doublet, T.; Quilichini, P.; Rivnay, J.; Rózsa, B.; Katona, G. Localized neuron stimulation with organic electrochemical transistors on delaminating depth probes. *Advanced Materials* **2015**, *27*, 4405-4410.
13. Francis, W.; Dunne, A.; Delaney, C.; Florea, L.; Diamond, D. Spiropyran based hydrogels actuators—walking in the light. *Sensors and Actuators B: Chemical* **2017**, *250*, 608-616.

14. Dunne, A.; Delaney, C.; Florea, L.; Diamond, D. Solvato-morphologically controlled, reversible nipaam hydrogel photoactuators. *RSC Advances* **2016**, *6*, 83296-83302.
15. Ziółkowski, B.; Florea, L.; Theobald, J.; Benito-Lopez, F.; Diamond, D. Self-protonating spiropyran-co-nipam-co-acrylic acid hydrogel photoactuators. *Soft Matter* **2013**, *9*, 8754-8760.
16. Klajn, R. Spiropyran-based dynamic materials. *Chemical Society Reviews* **2014**, *43*, 148-184.
17. Benito-Lopez, F.; Scarmagnani, S.; Walsh, Z.; Paull, B.; Macka, M.; Diamond, D. Spiropyran modified micro-fluidic chip channels as photonically controlled self-indicating system for metal ion accumulation and release. *Sensors and Actuators B: Chemical* **2009**, *140*, 295-303.
18. Fries, K.H.; Driskell, J.D.; Samanta, S.; Locklin, J. Spectroscopic analysis of metal ion binding in spiropyran containing copolymer thin films. *Anal. Chem.* **2010**, *82*, 3306-3314.
19. Florea, L.; Diamond, D.; Benito-Lopez, F. Photo-responsive polymeric structures based on spiropyran. *Macromolecular Materials and Engineering* **2012**, *297*, 1148-1159.
20. Florea, L.; Diamond, D.; Benito-Lopez, F. Opto-smart systems in microfluidics. *Research Perspectives on Functional Micro-and Nanoscale Coatings* **2016**, 265.
21. Francis, W.; Fay, C.; Florea, L.; Diamond, D. Self-propelled chemotactic ionic liquid droplets. *Chemical Communications* **2015**, *51*, 2342-2344.
22. Sun, T.; Qing, G.; Su, B.; Jiang, L. Functional biointerface materials inspired from nature. *Chemical Society Reviews* **2011**, *40*, 2909-2921.
23. Sanchez, C.; Arribart, H.; Giraud Guille, M.M. Biomimetism and bioinspiration as tools for the design of innovative materials and systems. *Nature Materials* **2005**, *4*, 277.
24. Kobatake, S.; Yamada, T.; Uchida, K.; Kato, N.; Irie, M. Photochromism of 1, 2-bis (2, 5-dimethyl-3-thienyl) perfluoro-cyclopentene in a single crystalline phase. *Journal of the American Chemical Society* **1999**, *121*, 2380-2386.
25. Hadjoudis, E.; Durr, H.; Bouas-Laurent, H. Elsevier: Photochromism molecules and systems, 1990; p 685 - 712.
26. Bénard, S.; Yu, P. New spiropyrans showing crystalline-state photochromism. *Advanced Materials* **2000**, *12*, 48-50.
27. Harada, J.; Kawazoe, Y.; Ogawa, K. Photochromism of spiropyrans and spirooxazines in the solid state: Low temperature enhances photocoloration. *Chemical Communications* **2010**, *46*, 2593-2595.
28. Chernyshev, A.V.; Voloshin, N.A.; Metelitsa, A.V.; Tkachev, V.V.; Aldoshin, S.M.; Solov'eva, E.; Rostovtseva, I.A.; Minkin, V.I. Metal complexes of new photochromic chelator: Structure, stability and photodissociation. *Journal of Photochemistry and Photobiology A: Chemistry* **2013**, *265*, 1 - 9.
29. Phillips, J.P.; Mueller, A.; Przytal, F. Photochromic chelating agents. *Journal of the American Chemical Society* **1965**, *87*, 4020 - 4021.
30. Taylor, L.D.; Nichoslon, J.; Davis, R.B. Photochromic chelating agents. *Tetrahedron Letters* **1967**, *8*, 1585 - 1588.
31. Shao, N.; Jin, J.Y.; Wang, H.; Zhang, Y.; Yang, R.H.; Chan, W.H. Tunable photochromism of spirobenzopyran via selective metal ion coordination: An efficient visual and ratioing fluorescent probe for divalent copper ion. *Analytical chemistry* **2008**, *80*, 3466-3475.

32. Wojtyk, J.C.; Kazmaier, P. Effects of metal ion complexation on the spiropyran–merocyanine interconversion: Development of a thermally stable photo-switch. *Chemical Communications* **1998**, 1703-1704.
33. Natali, M.; Giordani, S. Interation studies between photochromic spiropyrans and transition metal cations: The curious case of copper. *Organic & Biomolecular Chemistry* **2012**, *10*, 1162-1171.
34. Görner, H.; Chibisov, A.K. Complexes of spiropyran-derived merocyannies with metal ions themally activated and light-induced processes. *Journal of Chemistry society, Faraday Trans* **1998**, *94*, 2557-2564.
35. Fries, K.; Samanta, S.; Orski, S.; Locklin, J. Reversible colorimetric ion sensors based on surface initiated polymerization of photochromic polymers. *Chemical Communications* **2008**, 6288-6290.
36. Natali, M.; Aakeröy, C.; Desper, J.; Giordani, S. The role of metal ions and counterions in the switching behavior of a carboxylic acid functionalized spiropyran. *Dalton Transactions* **2010**, *39*, 8269-8277.
37. Fries, K.H.; Sheppard, G.R.; Bilbrey, J.A.; Locklin, J. Tuning chelating groups and comonomers in spiropyran-containing copolymer thin films for color-specific metal ion binding. *Polymer Chemistry* **2014**, *5*, 2094 - 2102.
38. Ghasemi, J.; Niazi, A.; Maeder, M. Spectrophotometric studies on the protonation and nickel complexation equilibria of 4-(2-pyridylazo) resorcinol using global analysis in aqueous solution. *Journal of the Brazilian Chemical Society* **2007**, *18*, 267-272.
39. Ghasemi, J.; Peyman, H.; Meloun, M. Study of complex formation between 4-(2-pyridylazo) resorcinol and al3+, fe3+, zn2+, and cd2+ ions in an aqueous solution at 0.1 m ionic strength. *Journal of Chemical and Engineering Data* **2007**, *52*, 1171-1178.

Chapter 6

Future Work and Perspectives

Chapter 6

Future Work and Perspectives

6.1 Photo-induced Actuation of Micro-cantilevers Coated with Spiropyran Monolayers

6.1.1 Introduction

As previously mentioned, spiropyrans represent one of the most popular families of photochromic molecules. Upon irradiation with UV light, the spiropyran molecule converts to the more polar merocyanine (MC) form due to the photo-cleavage of the C_{spiro}-O bond. When the MC form is exposed to visible light, the structure returns to the less polar spiropyran (SP) form. In this work, a dithiolane -spiropyran derivative was produced, namely 2-(3',3'-dimethyl-6-nitrospiro[chromene-2,2'-indolin]-1'yl)-5-(1,2-dithiolan-3-yl) pentanoate (Dithiolane-SP). Further, the Dithiolane-SP was used to functionalise gold coated-silicon substrates with self-assemble monolayers (SAMs), including flat silicon wafers and micro-cantilevers. Cantilever deflection was studied under different illumination conditions (UV and white light), in order to investigate the effect of SP-MC photo-conversion on surface stress and therefore cantilever deflection.

6.1.2 Materials

N,N'-dicyclohexylcarbodiimide (purity ≥99.0%) (DCC), 4-N,N-dimethylamino-pyridine (purity ≥99.0%) (DMAP), α ± lipoic acid (purity ≥98.0%), dichloromethane (DCM), and ethyl acetate were purchased from Sigma Aldrich (Germany), and were used as received. 2-(3',3'-dimethyl-6-nitrosoiro[chromene-2,2'-indolin]-1'-yl)ethanol (purity >93.0%) was purchased from TCI (United Kingdom), and was used as received.

Silicon wafers were purchased from University-Wafer, USA (Mech Grade 100mm N Type).

6.1.3 Synthesis of 2-(3',3'-dimethyl-6-nitrospiro[chromene-2,2'-indolin]-1'yl)-5-(1,2-dithiolan-3-yl)pentanoate Monomer (Dithiolane-SP)

The synthesis of Dithiolane-SP was produced from the reaction of 2-(3',3'-dimethyl-6-nitrosoiro[chromene-2,2'-indolin]-1'-yl)ethanol (Nitro-SP) and α ±

lipotic acid in the presence of DCC and DMAP using DCM as the solvent, as described by Ivashenko et al.[1]. After 24h, the by-product, dicyclohexylurea, was filtrated and the solvent was evaporated by vacuum filtration using a rotary evaporator. The obtained red solid was purified by column chromatography using 1:5:1 (V:V:V) hexane: DCM : ethyl acetate as the mobile phase. The reaction scheme of this synthesis is shown in Figure 6.1

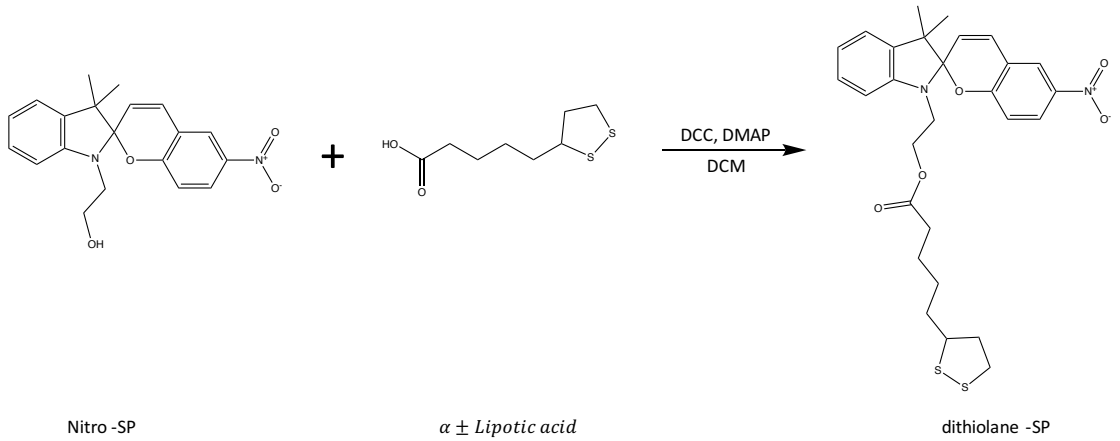

Figure 6.1. Schematic of the reaction of 2-(3',3'-dimethyl-6-nitrospiro[chromene-2,2'-indolin]-1'-yl)ethanol (Nitro-SP) and $\alpha \pm$ lipoic acid in the presence of DCC and DMAP to produce 2-(3',3'-dimethyl-6-nitrospiro[chromene-2,2'-indolin]-1'yl)-5-(1,2-dithiolan-3-yl) pentanoate (Dithiolane-SP).

6.1.4 Methods

H^1-NMR and ^{13}C-NMR spectra were obtained on a Bruker Avance 400MHz NMR using $CDCl_3$ used as the solvent.

UV-Vis spectra of Dithiolane-SP were recorded in DCM (10^{-4}M) and Ethanol (10^{-5}M), respectively. For the MC spectra, the solutions were irradiated prior to analysis for one minute with UV light in a CL-1000 Ultra Violet chamber. The UV-Vis spectra were recorded on a Varian Carey 50 probe spectrophotometer.

The repeated switching of the MC-SP isomerisation were recorded in EtOH (10^{-5}M) in real-time by measuring the absorbance at λ_{max}=545 nm, under cycles of UV and white light irradiation. Measurements were taken in 1 s intervals for 1 h. The samples were exposed to UV light, until the absorbance value began to stabilise. Once the

values stabilised, the samples were exposed to white light, until the absorbance value stabilised. This process was repeated four times.

The flat substrates used were silicon wafers which were cleaned and coated with gold, using a Quorum Q150T S gold sputter coater (gold sputtering conditions: current 20 mA, time 60 s (thin layer) and 180 s (thick layer), respectively)

These substrates then underwent functionalization with dithionale-SP SAMs (Figure 6.2).

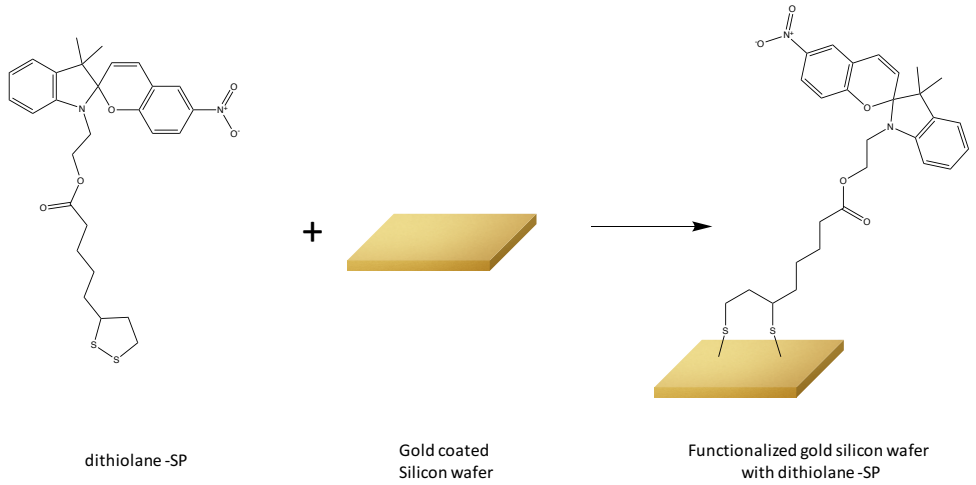

Figure 6.2. Functionalisation of gold coated silicon wafer with dithiolane-SP SAMs.

For this purpose, three dithionale-SP solutions in DCM were used (total concentration 10^{-4} M), as follows: dithionale-SP (Figure 6.3A); dithionale-SP: lipoic acid 1:1 molar ratio (Figure 6.3B); and dithionale-SP: lipoic acid 1:3 molar ratio (Figure 6.3C). The substrates were immersed in their respective solutions overnight, and then gently washed with DCM and dried under a gentle stream of nitrogen gas.

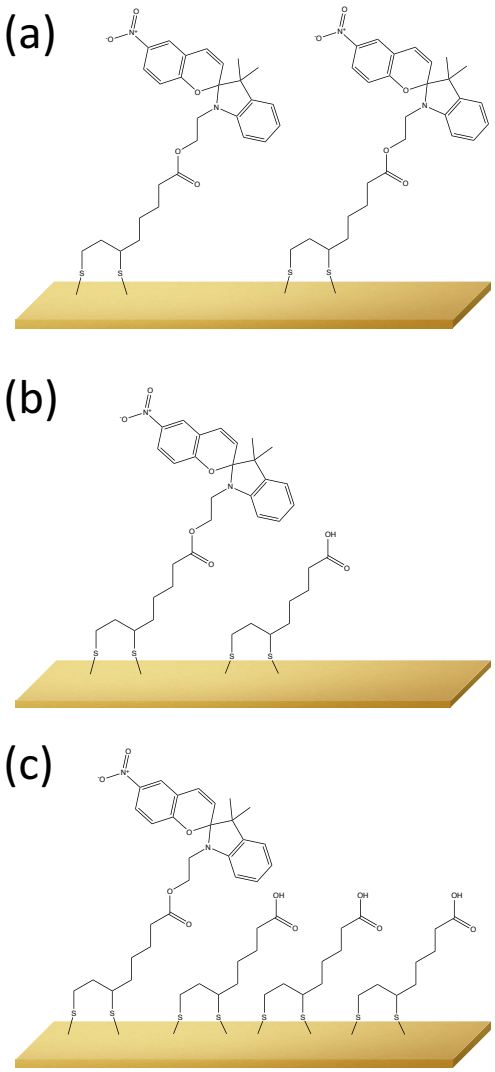

Figure 6.3: Schematic of gold coated substrates functionalised with (a) 100% dithiolane-SP; (b) 1:1 (molar ratio) dithionale-SP: lipoic acid and (c) 1:3 (molar ratio) dithionale-SP: lipoic acid.

The contact angle of the functionalized flat substrates was measured using an FTÅ200. Measurements were taken for each substrate after UV and white light irradiation, respectively, in the dry state. Measurements were also taken after UV and white light irradiation in ethanol, followed by drying the substrate under nitrogen gas prior to measurement, in order to investigate the influence of photo-induced switching in the wet state.

Prior to functionalization, the gold-coated micro-cantilevers were imaged by scanning electron microscopy (SEM), using a Carl Zeiss EVOLS 15. The system was kept at an accelerating voltage of 14.64 kV.

As in the contact angle study, different ratios of dithiolane-SP: lipoic acid solutions were used for the functionalisation of the micro-cantilevers.

Cantilever deflection measurements were carried out by Catherine Grogan (Focas Institute, D.I.T.), using a Veriscan 3000 by Protiveris Inc system. Once a baseline was established, individual cantilevers were exposed to UV light for 10 minutes. After 10 minutes, the UV light was removed, and the cantilevers were left for 10 minutes to re-establish a new baseline. Once this baseline was established, white light was introduced to the cantilevers for 10 minutes, and then they were left for 10 minutes to establish a new baseline. This process was repeated several times.

6.1.5 Results and Discussion

6.1.5.1 Analysis of dithiolane-SP

To ensure accurate peak assignment of the product (dithiolane-SP), ^{1}H-NMR in $CDCL_3$ was carried of both starting materials, Nitro-SP and α ± lipoic acid (Figure 6.4 and 6.5 respectively).

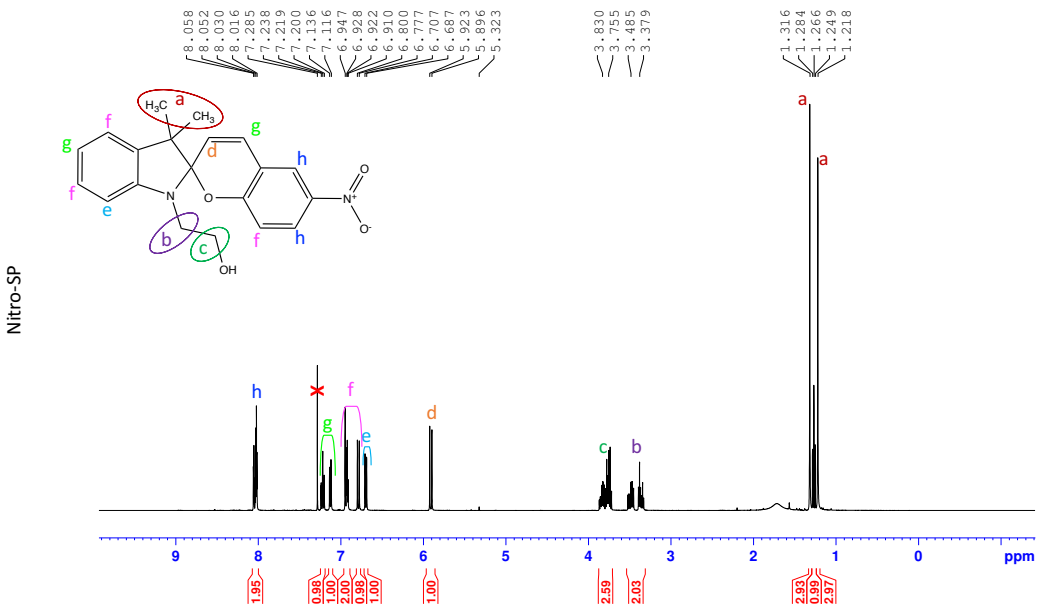

Figure 6.4. H[1]-NMR spectra of, 2-(3',3'-dimethyl-6-nitrospiro[chromene-2,2'-indolin]-1'-yl)ethanol (Nitro-SP). ^{1}H-NMR ($CDCl_3$): δ 1.21 (s, 3H), 1.31 (s, 3H), 3.38 (m, 2H), 3.75 (m, 2H), 5.90 (d, 1H), 6.69 (d, 1H), 6.92 (d, 1H), 6.94 (m, 2H), 7.11 (d, 1H), 7.20 (m, 1H), 8.01 (m, 2H).

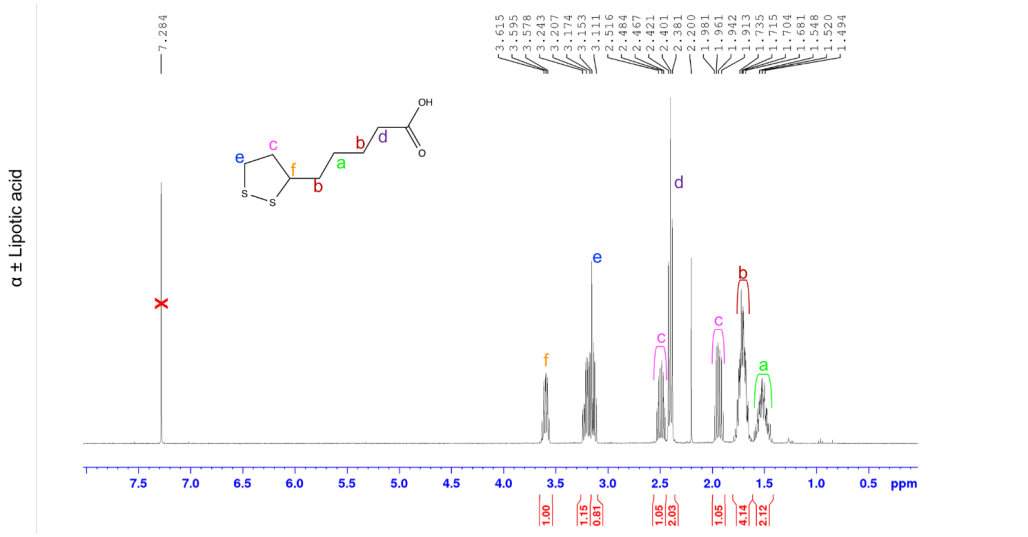

Figure 6.5. H[1]-NMR spectra of . dithiolane, [1]H-NMR ($CDCl_3$): δ 1.52 (m, 2H), 1.71 (m, 4H), 1.94 (sext, 1H), 2.41 (t, 2H), 2.49 (sext, 1H), 3.16 (m, 2H), 3.60 (sext, 1H), 5.33 (s, 2H).

The identification and assignments of the peaks in the [1]H-NMR of product are shown below (Figure 6.6). These assignments were further confirmed from prior literature [1].

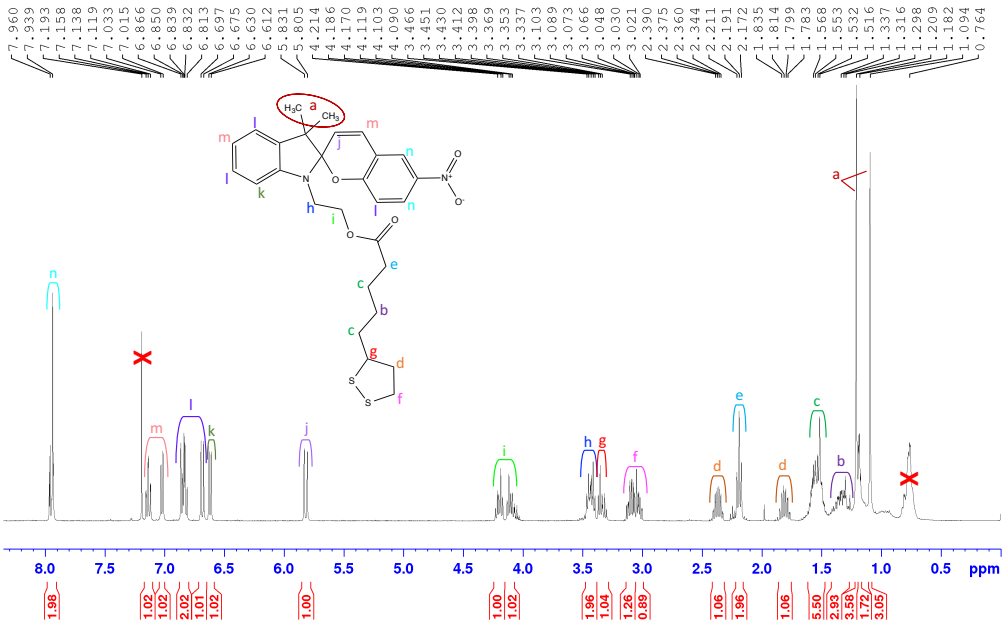

Figure 6.6. H[1]-NMR spectra of 2-(3',3'-dimethyl-6-nitrospiro[chromene-2,2'-indolin]-1'yl)-5-(1,2-dithiolan-3-yl)pentanoate (dithiolane-SP), [1]H-NMR ($CDCl_3$): δ 1.18 (d, 3H), 1.21 (m, 4H), 1.34 (m, 3H), 1.53 (m, 5H), 1.80 (sext, 1H), 2.19 (m, 2H), 2.34 (sext, 1H), 3.02 (m, 2H), 3.09 (m, 1H), 3.34 (m, 2H), 4.09 (m, 1H), 4.17 (m, 1H), 5.81 (d, 1H), 6.63 (d, 1H), 6.68 (d, 1H), 6.81 (m, 2H), 7.02 (d, 1H), 7.12 (t, 1H), 7.94 (m, 2H).

The ^{13}C-NMR further confirms the production of dithiolane-SP (Figure 6.7).

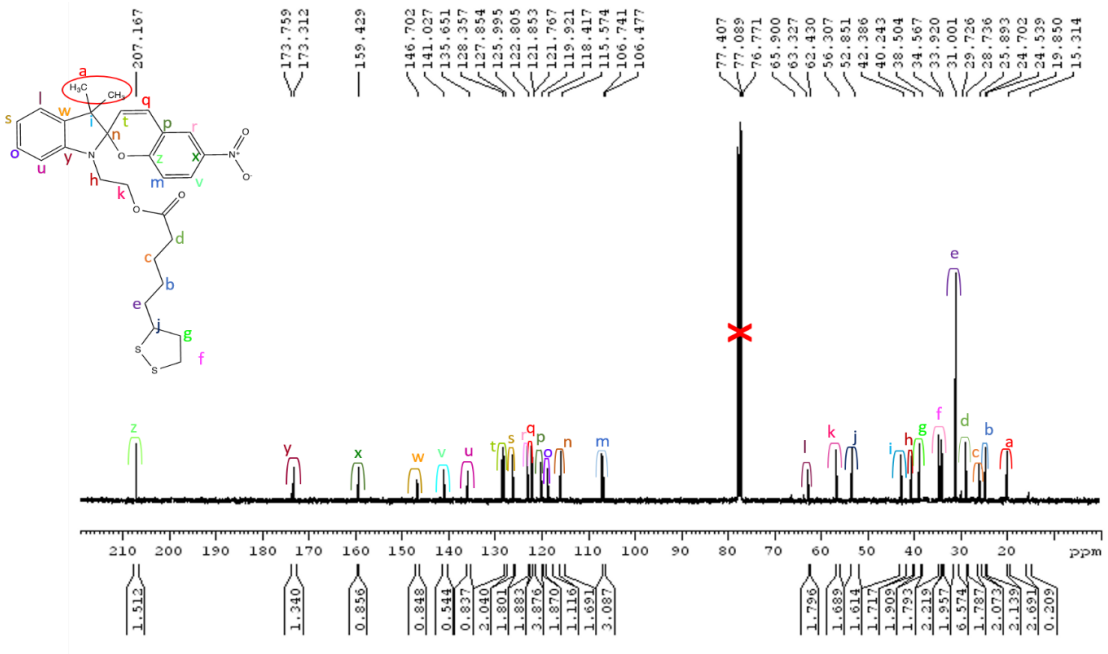

Figure 6.7. ^{13}Carbon-NMR spectrum of 2-(3',3'-dimethyl-6-nitrospiro[chromene-2,2'-indolin]-1'yl)-5-(1,2-dithiolan-3-yl) pentanoate (dithiolane-SP), ^{13}C-NMR ($CDCl_3$): δ 19.85, 24.54, 25.90, 28.74, 31.00, 33.92, 38.50, 40.24, 42.39, 52.85, 56.31, 62.43, 106.74, 115.57, 118.42, 119.92, 121.77, 121.85, 125.99, 127.85, 135.61, 141.03, 146.70, 159.43, 173.31, 207.17.

6.1.5.2 Spectroscopic Analysis

The UV/Vis analysis was carried out as described above. The absorbance spectra of the dithiolane-SP solutions (10^{-4} M in DCM and 10^{-5} M in ethanol) were recorded after UV and white light exposure, respectively (Figure 6.8 and 6.9).

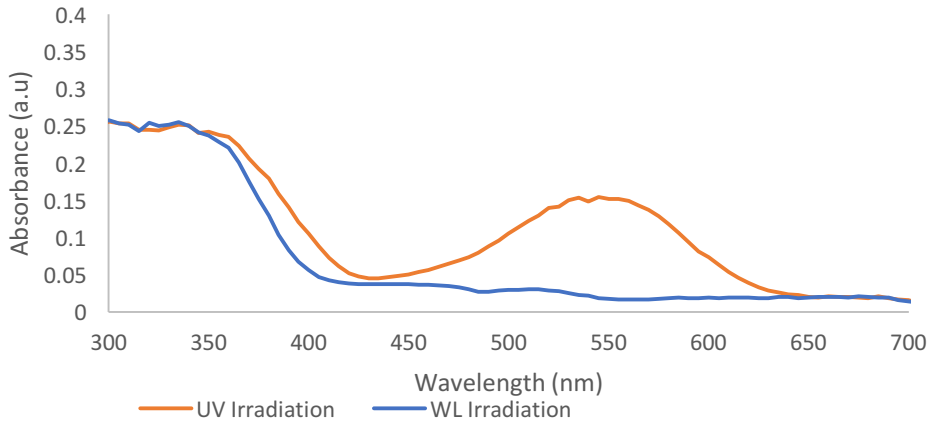

Figure 6.8. The absorption spectrum of a 10^{-5} M solution of dithiolane-SP in ethanol, under different illumination conditions.

The absorption spectrum in Figure 6.8 shows the difference in absorption of dithiolane-SP after UV light and white light exposure. The UV irradiation data represents the MC isomer which has a λ_{max} of ~550 nm. When the same analysis is carried out for a 10^{-4} M solution of dithiolane-SP in DCM, the MC peak shifts to a higher wavelength of ~590 nm (Figure 6.9). The difference in the MC λ_{max} values is due to the solvatochromic properties of MC isomers.

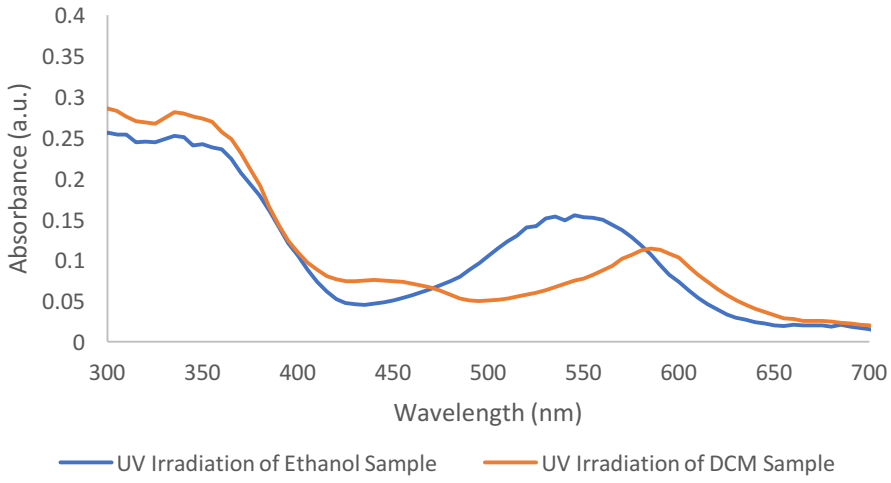

Figure 6.9. Graph depicting the solvatochromic effect of dithiolane-MC isomer that shows a different absorption λ_{max} in solvents of different polarity (DCM and Ethanol).

The reversible switching process between SP/MC was repeated several times as described in the experimental section. Under UV irradiation, the dithiolane-SP (10^{-4} M solution in ethanol) isomerized to the MC form, causing an increase in the

absorbance at λ_{max} 550 nm. Once the absorbance stabilized, white light was introduced. This led to a dramatic drop in the absorbance at λ_{max} 550 nm, indicating that the MC form had reversibly switched back to the SP form. This process was repeated four times. The graph shows that the photo-induced isomerization happens rapidly, and that the isomers stabilize relatively fast. Both ring opening and ring closing switching was measured in triplicate.

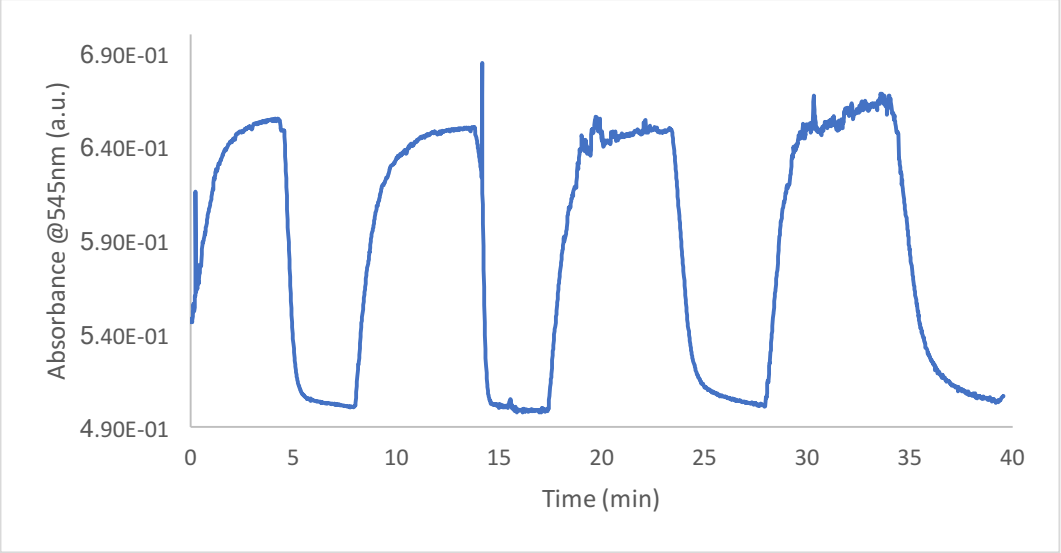

Figure 6.10. The UV/Vis cycles following SP and MC isomerisation. UV irradiation causes the switching of the SP to the MC form, resulting in an increase in the absorbance at λ_{max} 550 nm, until equilibrium is reached. Following this, the UV light is removed and replaced with white light, causing the switching back to the SP form. This process is monitored through the decrease in the absorbance at λ_{max} 550 nm. The cycle is repeated four times.

6.1.5.3 Contact Angle

The contact angle analysis was carried out with the purpose of investigating if there is a change in the hydrophilicity of the functionalised substrate after different illumination conditions. After UV illumination it would be expected that the contact angle would be smaller due to the more hydrophilic MC isomer being present. Similarly, after WL illumination the contact angle would be expected to be larger due to the more hydrophobic spiropyran form being present (Figure 6.11).

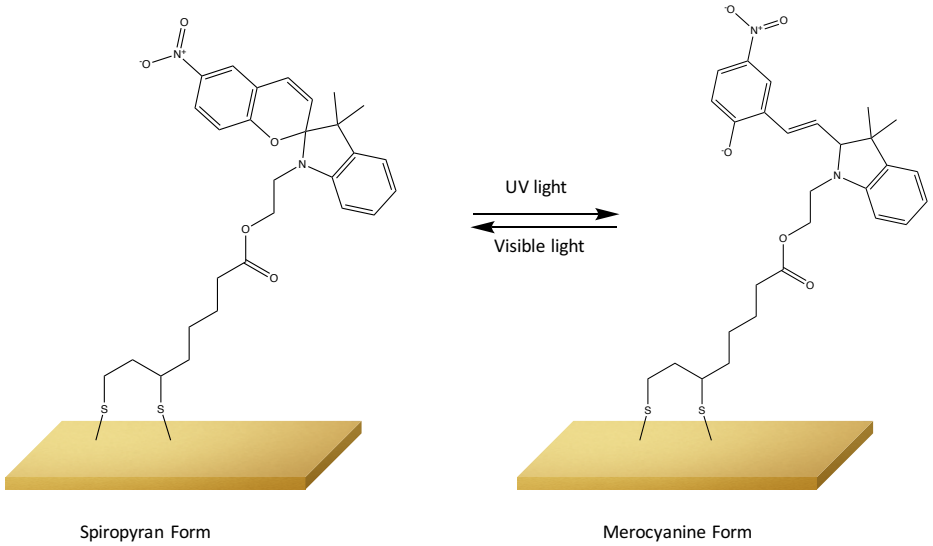

Figure 6.11. Isomerisation of dithiolane-SP SAMs, between the SP and the MC form after specific illumination conditions.

With a purpose of finding the optimal conditions for functionalisation, two different thicknesses of gold were used, and different ratios of dithiolane-SP to lipoic acid were used during the functionalisation process. For the "thin gold layer", gold was sputtered for 60 s at 20mA, while for the "thick gold layer", gold was sputtered for 180 s at 20mA. For both types of gold thicknesses three different dithiolane-SP ratios were used; 100% dithiolane-SP, 1:1 (molar ratio) dithiolane-SP: lipoic acid and 1:3 (molar ratio) dithiolane-SP: lipoic acid. A bare silicon wafer was also used as a control (Figure 6.12).

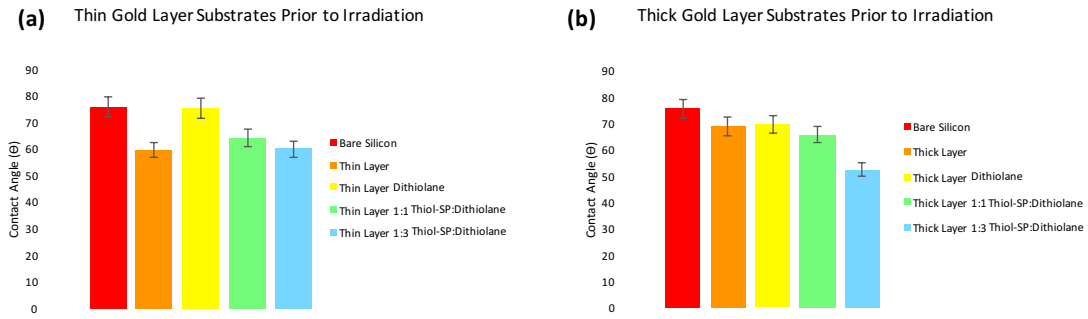

Figure 6.12. Contact angle graphed data of functionalised gold slides with different ratios of Dithoilane-SP: Dithoilane prior to illumination. (a)thin gold layer (b) thick gold layer

Of all the substrates analysed it was found that the 1:3 dithiolane-SP: α ± lipoic acid functionalisation was found to be the most consistent in both thin and

think gold layers. Using the 1:3 dithiolane-SP: α ± lipoic acid coated substrates, the contact angle was measured during successive UV/WL irradiation cycles in the dry (Figure 6.13a) and wet states (Figure 6.13b).

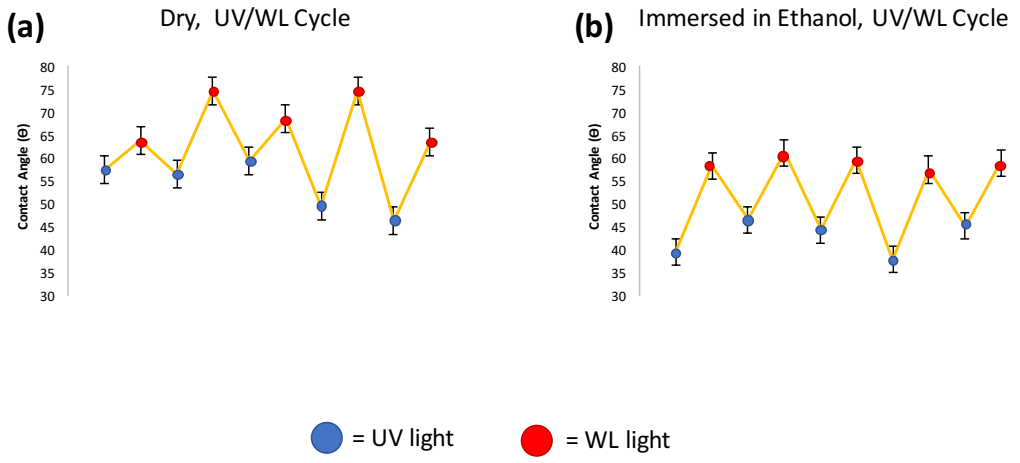

Figure 6.13. Contact angles obtained for the thin gold layer functionalised with SAMs using 1:3 dithiolane-SP: α ± lipoic acid solution; (a) UV and WL illumination cycles were carried out in dry conditions; (b) UV and WL illumination cycles were carried out in ethanol.

Figure (6.13) shows that the SP-MC isomerisation process is repeatable in both dry and wet states. When in the SP state, the SAM-coated substrate shows a higher contact angle due to the more hydrophobic nature of the SP, whereas the MC form produces a lower contact angle. However, when the illumination cycles are carried out in dry conditions (Figure 6.13 (a)) there are inaccuracies in the degree of reproducibility of the contact angle. The SP form in (a) gives a contact angle range of 63-74° and the MC form gives a contact angle range of 46-59°. These ranges are relatively large when compared to the data obtained from the UV/WL cycles during immersion in ethanol (Figure 6.13 (b)). This method produced a more consistent and reproducible SP contact angle range (58-61°) and a MC contact angle range (37-46°). This difference between the two methods could be partially due to the improved isomerisation in the wet state.

6.1.5.4 Scanning Electron Microscopy

The images obtained from SEM analysis (Figure 6.14) illustrate the type of cantilevers used in this study, which were gold-coated silicon cantilevers. The top left image is a schematic of the cantilever showing the cantilever numbering in each well. Well 1 was kept as a reference and only the remaining wells (2-4) were functionalised as previously described.

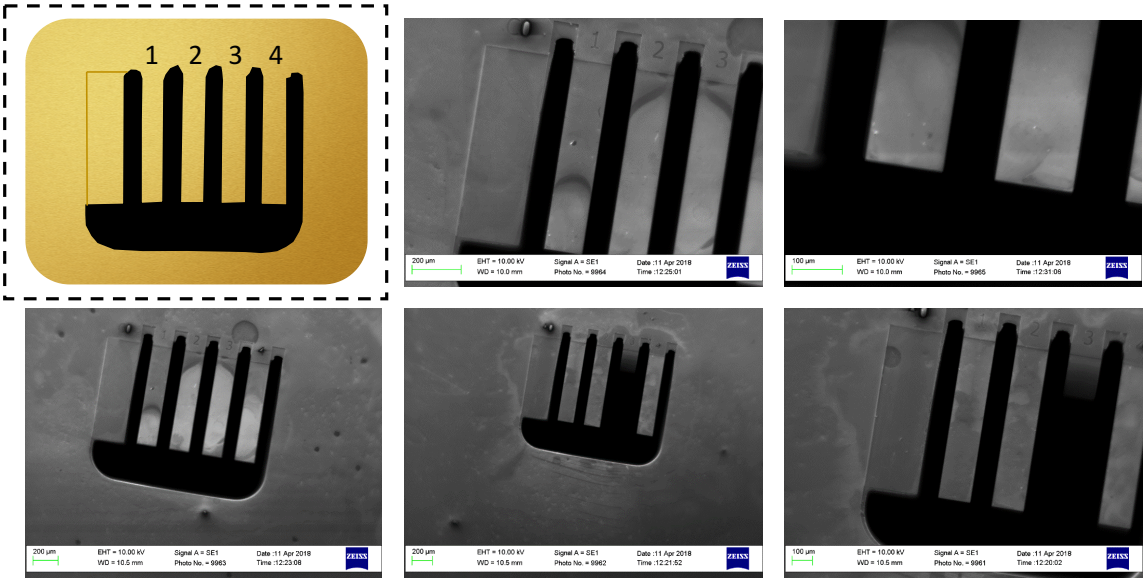

Figure 6.14. Schematic of cantilevers with cantilevers numbering in each well (top left) along with SEM images of the cantilevers at different magnifications.

6.1.5.5 Cantilever Deflection

Figure 6.15 (a,b) shows the downward deflection of the dithiolane-SP coated micro-cantilevers, which occurs as a result of UV irradiation. When UV light was introduced to the cantilever (t ~ 1200 s), there was a downward deflection, which appeared more significant in the case of the functionalized cantilevers. The difference in deflection between the reference cantilever (represented by A_0 in Figure 6.15 (a)) and the two functionalized cantilevers (represented by B_3 and C_3 in Figure 6.15 (a)) is ~6 nm. Although this is a relatively low change in deflection, it still confirmed that the cantilevers can measure small changes within the nm region, occurring due to structural changes of SP to MC. Although there is a small drift observed around 1400 s, but there is no major change in deflection after this time. Similarly, Figure 6.15 (c) and (d) show the deflection experienced by the cantilevers upon white light exposure. To establish a baseline between UV and WL exposure, a 10-minute waiting period is executed. It is feasible that, during the waiting period the MC switches back to SP, however it is not possible to determine if this occurred from the data obtained. WL was introduced to the system at 1200 s, and there was a very small upward deflection experienced by the cantilever. The deflection appears to stop around 1300 s, and then a drift occurs. This would suggest that the MC → SP process occurs rapidly (within 100 s) and that there is little impact of the SP on the surface stress (the difference in deflection is very small ~ 1 nm).

More investigations will be required in order to test the reproducibility of the deflection caused by SP-MC switching. Further investigations will also be carried out in order to investigate the effect of dithiolane-SP: lipoic acid molar ratio on the cantilever deflection. Only the 100% dithiolane-SP functionalised cantilevers were investigated during the duration of this investigation. The effect of the dithiolane-SP: lipoic acid ratio on cantilever deflection will be examined to determine the optimum coating.

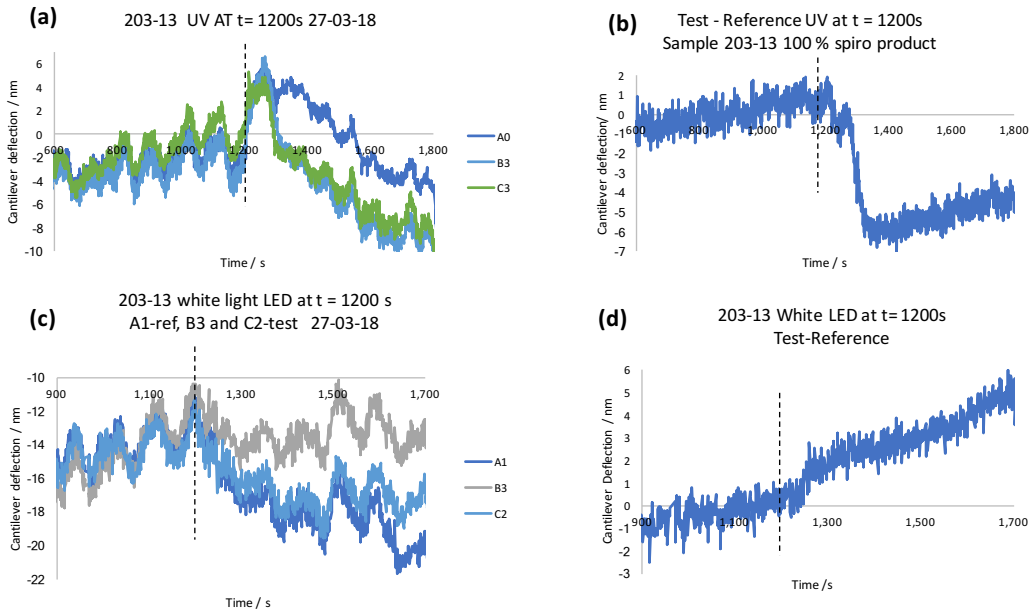

Figure 6.15. (a) Reference and cantilever response to UV irradiation for cantilever functionalised with 100% dithiolane-SP solution; A0 is the reference cantilever. (b) Difference in deflection between the reference cantilever and the functionalised cantilevers. There was a relatively small difference in deflection, which was in a downward direction. (c) Reference and cantilever response to white light irradiation for cantilever functionalised with 100% dithiolane-SP solution; A1 is the reference cantilever. (d) Difference in deflection between the reference cantilever and the functionalised cantilevers. There was a relatively small difference in deflection, which was upwards, back to the original position prior to UV light irradiation.

6.2 Photo-responsive Free Moving 'Origami' Materials

Biological systems in nature have demonstrated great functions responsive to external stimuli. Some examples include the motion of the earthworm, the camouflage attained by the octopus, the rapid closure of the Venus flytrap upon insect touch or the opening of the pine cone in humid environments [2]. Stimuli-responsive materials have become an increasing area of research in recent years, and in particular soft stimuli-responsive materials have shown great potential due to their flexibility, size and shape changes observed in response to external stimuli.

A subclass of stimuli-responsive materials that has become popular is self-folding/bending origami systems. The term origami comes from Japanese and signifies the art of folding paper. Although originating as an art form, origami has

become an intriguing new research prospect in the materials science community [3]. Some of the possible applications for scientific origami are; foldable solar panels, origami stents for medical use [4], self-folding polymer sheets [5] and self-moving polymer materials. Self-folding or self-moving polymer materials are becoming an interesting research field as they can be used in a wide variety of applications such as drug delivery systems [6], DNA-polymer tubes [7,8] and electronics [9,10]. So far, the production of 'origami' soft polymeric materials has been proposed in a few ways;

1. polymerising a polymeric hydrogel sheet and actuate specific regions to promote bending [11,12];
2. polymerisation using photo-masks [13];
3. 3D printing[14];
4. Two- photon photolithography [14]

In Chapter 4 'walkers' were successfully developed by creating an arc shaped hydrogel composed of poly(NIPAAm-co-SPA-co-AA) that "walked" across a pre-designed ratchet system. Going forward, one method we propose is an origami styled folding "hinge type" polymeric material (Figure 6.17) containing desired bending points with pre-programmable actuation. In this case, the two non-active substrates or inactive polymer films would be joined by a photo-responsive hydrogel like the one used in Chapters 3 and 4. This photo-active layer would be put in place using a photo-mask system or by 3D printing on to the substrates. Possible future applications for such actuators include valves, pumps or mixers in microfluidic devices.

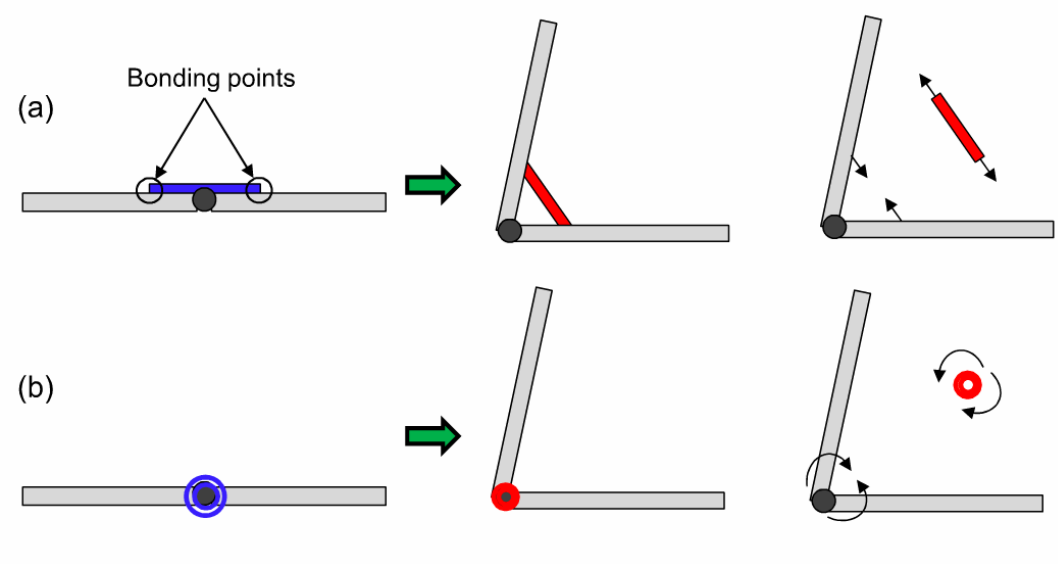

Figure 6.16. Proposed hydrogel self-moving origami style hinges.

A second design that we propose is a self-folding cube or tetrahedron using poly(NIPAAm-co-SPA-co-AA) material that would be "closed" when exposed to white light and "open" in the dark. If this proves to be successful it could subsequently used for chemical delivery, releasing the specific species upon white light irradiation.

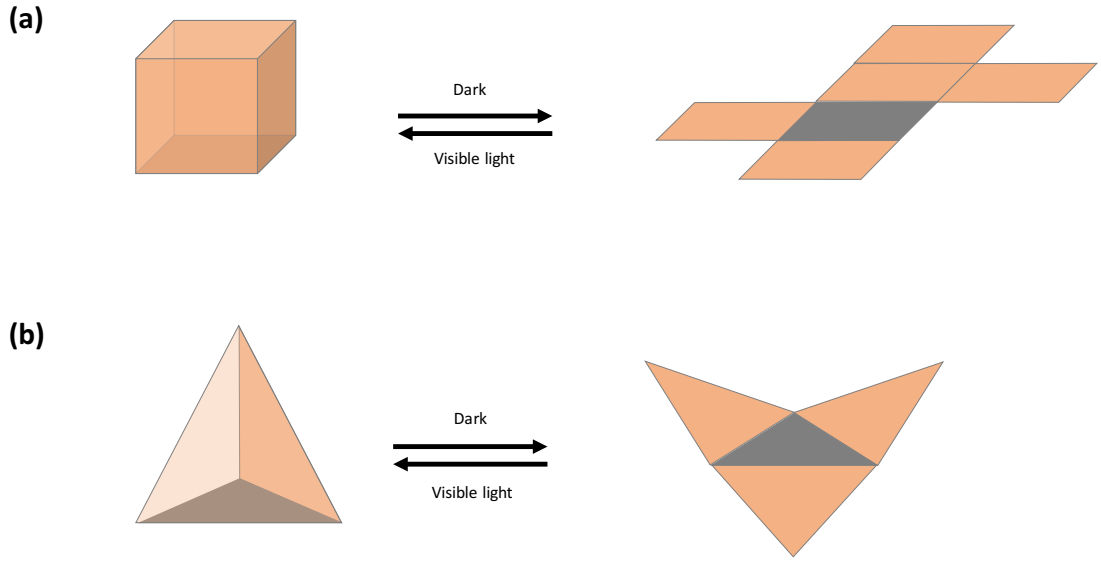

Figure 6.17. Proposed hydrogel self-folding 3D shapes: (a) cube (b) tetrahedron.

6.3 Further studies

The ideas summarised in this chapter are only a few potential concepts of further research for the spiropyran derivatives discussed. However, the realisation of these approaches is still to be established. In my opinion, the incorporation of stimuli-responsive materials remains vital in the advancement of the microfluidics and soft robotics fields.

6.4 References

1. Ivashenko, O.; van Herpt, J.T.; Feringa, B.L.; P., R.; Browne, W.R. Uv/vis and nir light-responsive spiropyran self-assembled monolayers, . *Langmuir* **2013**, *29*, 4290 – 4297.
2. Ko, H.; Javey, A. Smart actuators and adhesives for reconfigurable matter. *Acc. Chem. Res.* **2017**, *50*.
3. Fei, L.J.; Sujan, D. Origami theory and its applications: A literature review. *World Academy of Science, Engineering and Technology International Journal of Humanities and Social Sciences* **2013**, *7*, 229 - 233.

4. You, Z.; Kuribayashi, K. A novel origami stent. In *Summer Bioengineering Conference* Sonesta Beach Resort in Key Biscayne, Florida, 2003; pp 257 - 258.
5. Overvelde, J.T.; de Jong, T.A.; Shevchenko, Y.; Becerra, S.A.; Whitesides, G.M.; Weaver, J.C.; Hoberman, C.; Bertoldi, K. A three-dimensional actuated origami-inspired transformable metamaterial with multiple degrees of freedom. *Nature communications* **2016**, *7*, 10929.
6. Sun, J.; Xianyu, Y.; Li, M.; Liu, W.; Zhang, L.; Liu, D.; Liu, C.; Hu, G.; Jiang, X. A microfluidic origami chip for synthesis of functionalized polymeric nanoparticles. *Nanoscale* **2013**, *5*, 5262-5265.
7. Tokura, Y.; Harvey, S.; Xu, X.; Chen, C.; Morsbach, S.; Wunderlich, K.; Fytas, G.; Wu, Y.; Ng, D.Y.W.Y.W.; Weil, T. Polymer tube nanoreactors via DNA-origami templated synthesis. *Chemical communications (Cambridge, England)* **2018**, *54*, 2808-2811.
8. Kiviaho, J.K.; Linko, V.; Ora, A.; Tiainen, T.; Järvihaavisto, E.; Mikkilä, J.; Tenhu, H.; Nonappa; Kostiainen, M.A. Cationic polymers for DNA origami coating - examining their binding efficiency and tuning the enzymatic reaction rates. *Nanoscale* **2016**, *8*, 11674-11680.
9. Peraza Hernandez, E.A.; Hartl, D.J.; Lagoudas, D.C. Design and simulation of origami structures with smooth folds. *Proceedings of the Royal Society A: Mathematical, Physical and Engineering Science* **2017**, *473*.
10. Peraza-Hernandez, E.; Hartl, D.J.; Malak Jr, R.J.; Lagoudas, D.C. Origami-inspired active structures: A synthesis and review. *Smart Mater. Struct.* **2014**, *23*, 1 - 50.
11. Ionov, L.; Zakharchenko, S.; Stoychev, G.; Sperling, E. Soft microorigami : Self-folding polymer films. *Soft Matter* **2012**, *7*, 6786 – 6791
12. Morales, D.; Palleau, E.; Dickey, M.D.; Velev, O.D. Electro-actuated hydrogel walkers with dual responsive legs. *Soft Matter* **2014**, *10*, 1337 – 1348
13. Mu, X.; Sowan, N.; Tumbic, J.A.; Bowman, C.N.; Mather, P.T.; Qi, H.J. Photo-induced bending in a light-activated polymer laminated composite. *Soft matter* **2015**, *11*, 2673-2682.
14. Ahn, B.Y.; Shoji, D.; Hansen, C.J.; Hong, E.; Dunand, D.C.; Lewis, J.A. Printed origami structures. *Adv. Mater.* **2010**, *22*, 2251-2254.

Appendix 1

Supporting Information for

Solvato-Morphologically Controlled, Reversible NIPAAm Hydrogel Photoactuators*

***Solvato-Morphologically Controlled, Reversible Photo-Actuated Hydrogels, Operative in Neutral Environments**, Aishling Dunne, Colm Delaney, Larisa Florea*, Dermot Diamond, *RSC Advances,* 6 (2016) 83296-83302.

Single-Crystal X-ray Diffraction:

The structure of SP-A was solved and refined using the Bruker SHELXTL Software Package, with a P21/c space group, for Z = 4. Representation of the Single-Crystal X-ray Diffraction structure of SP-A is shown in Figure A1.1. Full crystal data and structure refinement are presented in Table A1.1.

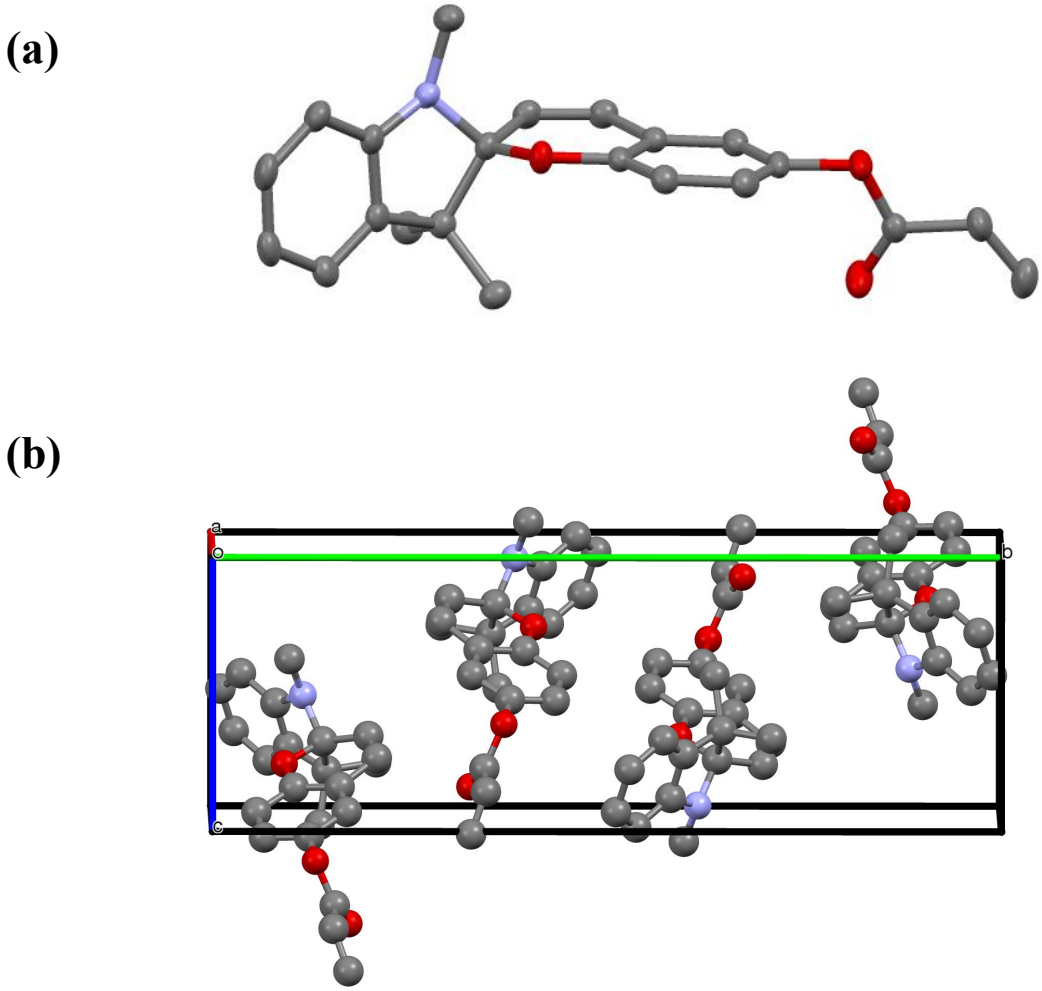

Figure A1.1. Representation of the Single-Crystal X-ray Diffraction structure of SP-A. (a) Single molecule structure with thermal ellipsoids at 50%; (b) shows the packing in the crystal lattice, offset along the a-axis. Hydrogen atoms are removed for clarity. Red: Oxygen; Blue: Nitrogen.

Table A1.1: Crystal data and structure refinement for SP-A

Empirical formula	$C_{22}H_{21}NO_3$	
CCDC	1475017	
Formula weight	347.40	
Temperature	297.78 K	
Wavelength	0.71073 Å	
Crystal system	Monoclinic	
Space group	$P2_1/c$	
Unit cell dimensions	a = 11.520(3) Å	α= 90°.
	b = 21.866(6) Å	β= 100.443(9)°.
	c = 7.630(2) Å	γ = 90°.
Volume	1890.1(9) $Å^3$	
Z	4	
Density (calculated)	1.221 Mg/m^3	
Absorption coefficient	0.081 mm^{-1}	
F(000)	736	
Crystal size	0.27 x 0.23 x 0.14 mm^3	
Theta range for data collection	2.589 to 28.394°.	
Index ranges	-15≤h≤15, -29≤k≤29, -9≤l≤10	
Reflections collected	43348	
Independent reflections	4690 [R(int) = 0.0520]	
Completeness to theta = 25.242°	99.9 %	
Absorption correction	Semi-empirical from equivalents	
Max. and min. transmission	0.7457 and 0.6810	
Refinement method	Full-matrix least-squares on F^2	
Data / restraints / parameters	4690 / 0 / 238	
Goodness-of-fit on F^2	1.029	
Final R indices [I>2σ(I)]	R1 = 0.0629, wR2 = 0.1492	
R indices (all data)	R1 = 0.1055, wR2 = 0.1736	
Largest diff. peak and hole	0.293 and -0.223 $e.Å^{-3}$	

Hydrogel fabrication:

Hydrogel discs were photo-polymerised using a photo-mask that had a 1mm diameter circle pattern. An "in-house cell" was fabricated to make the hydrogels discs, consisting of a bottom glass slide and a glass cover slide separated by a 250 µm high spacer made out of Poly(methyl methacrylate)/pressure sensitive adhesive (PMMA/PSA) and the photo mask placed on top of the cover slide.

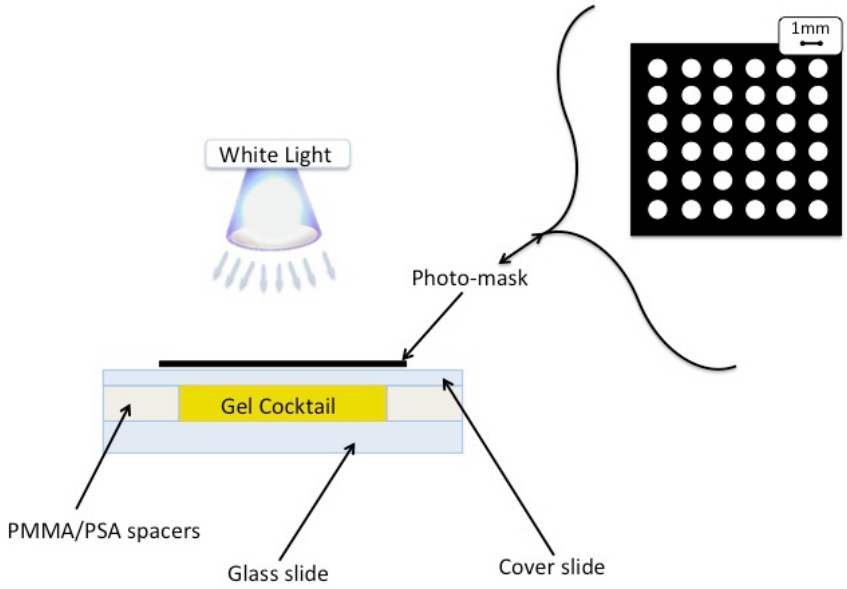

Figure A1.2. Schematic of "in-house" cell used for hydrogel fabrication.

The chosen monomeric cocktail was used to fill in the cell by capillary forces. Once the cell was filled with the specific cocktail, it was exposed to white light through the photo-mask for a predetermined time (20-30 s) depending on the polymerisation solvent used. Following polymerisation, the hydrogel discs were washed gently with ethanol to remove any unpolymerised cocktail and finally washed with deionised water. The washed hydrogels were then placed in deionised water for 4-6 hrs to ensure full hydration. All of the hydrogels in this study were fabricated in this fashion.

Rheology:

The rheology curing study was carried out to investigate the effect different polymerization solvents have on the curing times and mechanical properties of the

resulting hydrogels. Each sample cocktail was made up to 1 ml and this quantity was placed under the CP50-2 Anton Paar rheometer tool having an angle of 1.996°. Once the tool was lowered on to the cocktail sample the experiment was initiated, after 60 s the white light was switched on and remained this way for a further 8 mins.

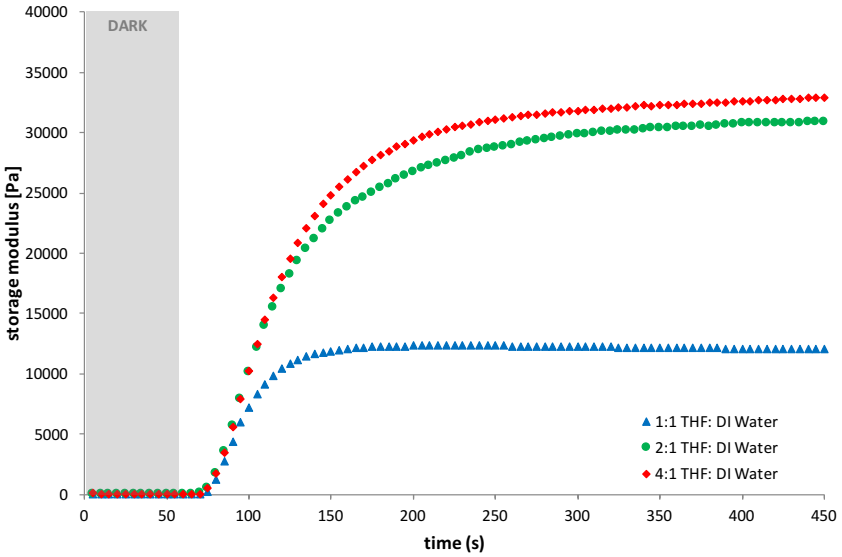

Figure A1.3. Photo curing of hydrogels produced when the polymerisation solvent was THF: deionised water ((V:V) 4:1, 2:1 and 1:1). White light polymerisation was initiated after 60 s.

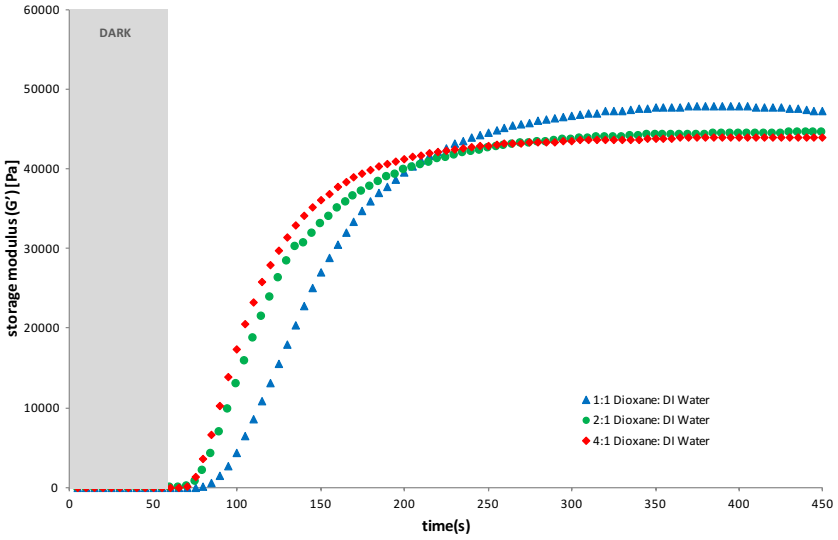

Figure A1.4. Photo curing of hydrogels produced when the polymerisation solvent was Dioxane: deionised water ((V:V) 4:1, 2:1 and 1:1). White light polymerisation was initiated after 60 s.

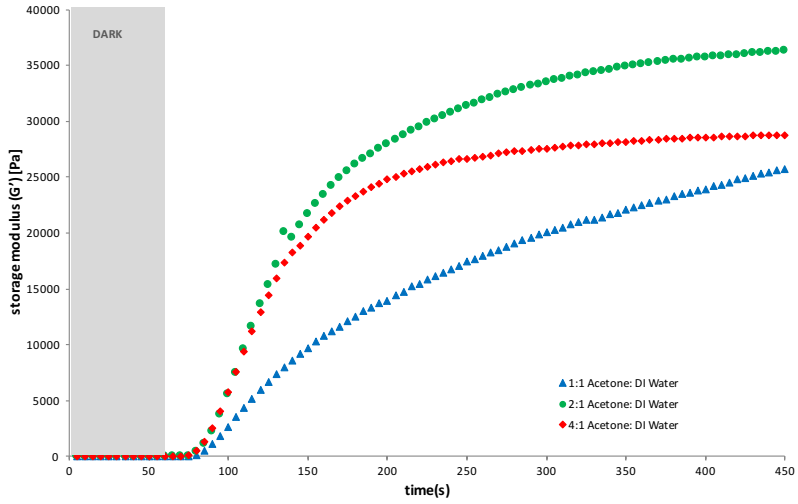

Figure A1.5. Photo curing of hydrogels produced when the polymerisation solvent was Acetone: deionised water ((V:V) 4:1, 2:1 and 1:1). White light polymerisation was initiated after 60 s.

SEM study:

The hydrogel samples were first swollen in DI water, and then frozen with liquid nitrogen and subsequently freeze-dried. The samples were kept overnight at 0.035 mBar pressure and temperature of -40 °C. Samples were attached onto silicon wafers and coated with 10 nm gold layer prior to imaging. The freeze-dried hydrogels were imaged using Scanning Electron Microscopy (SEM).

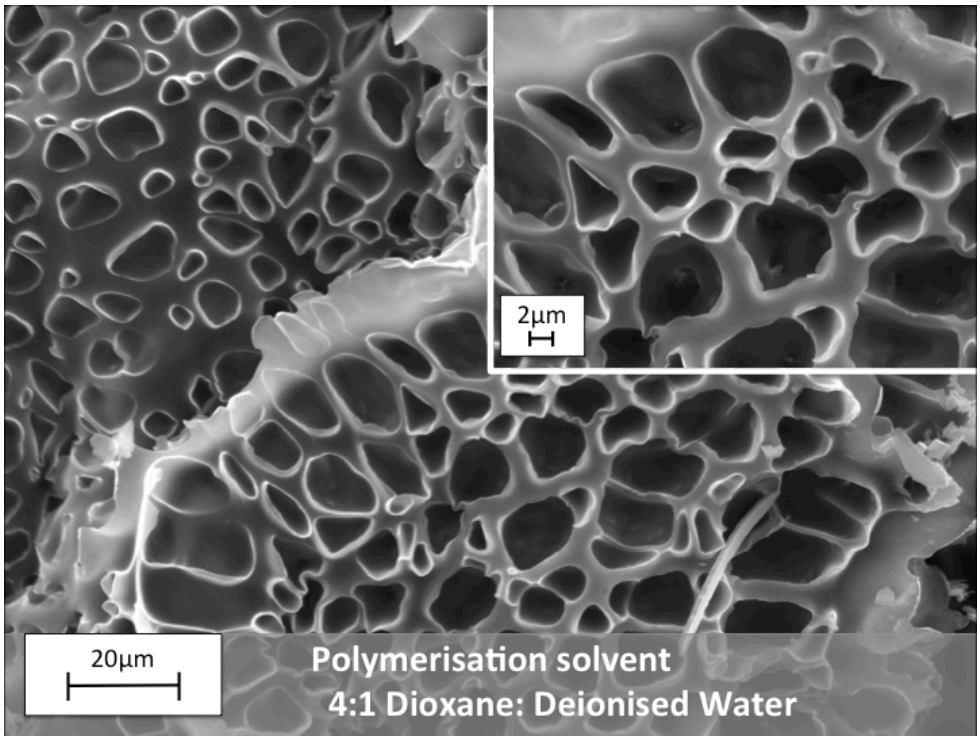

Figure A1.6. SEM image of hydrogel synthesised using 4:1 (v: v) ratio of Dioxane: DI water as the polymerisation solvent.

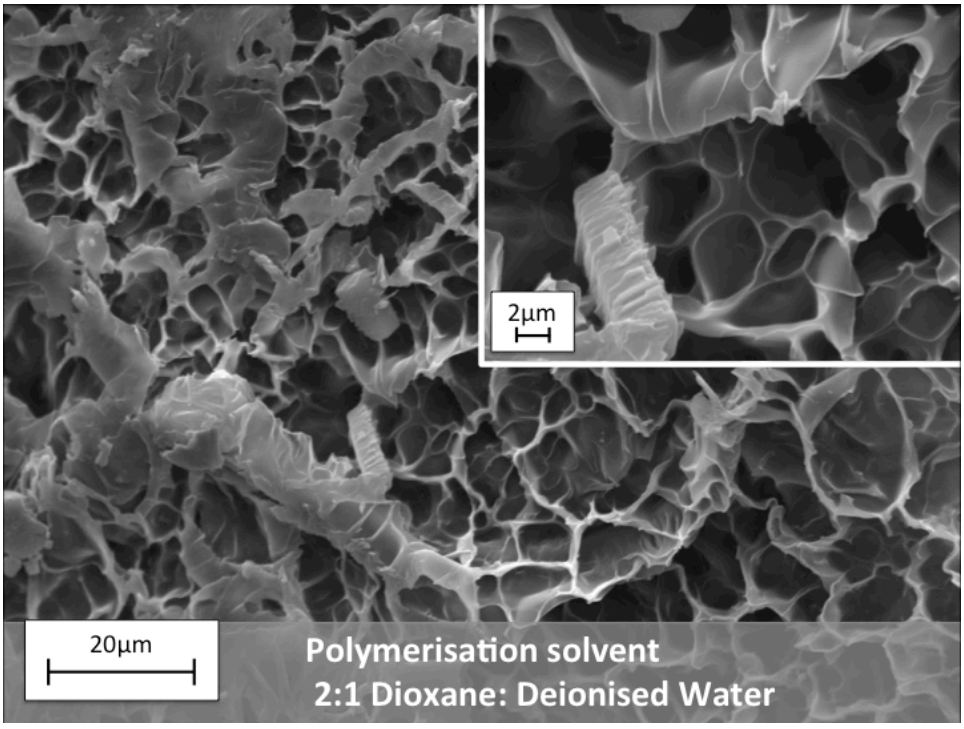

Figure A1.7. SEM image of hydrogel synthesised using 2:1 (V: V) ratio of Dioxane: DI water as the polymerisation solvent.

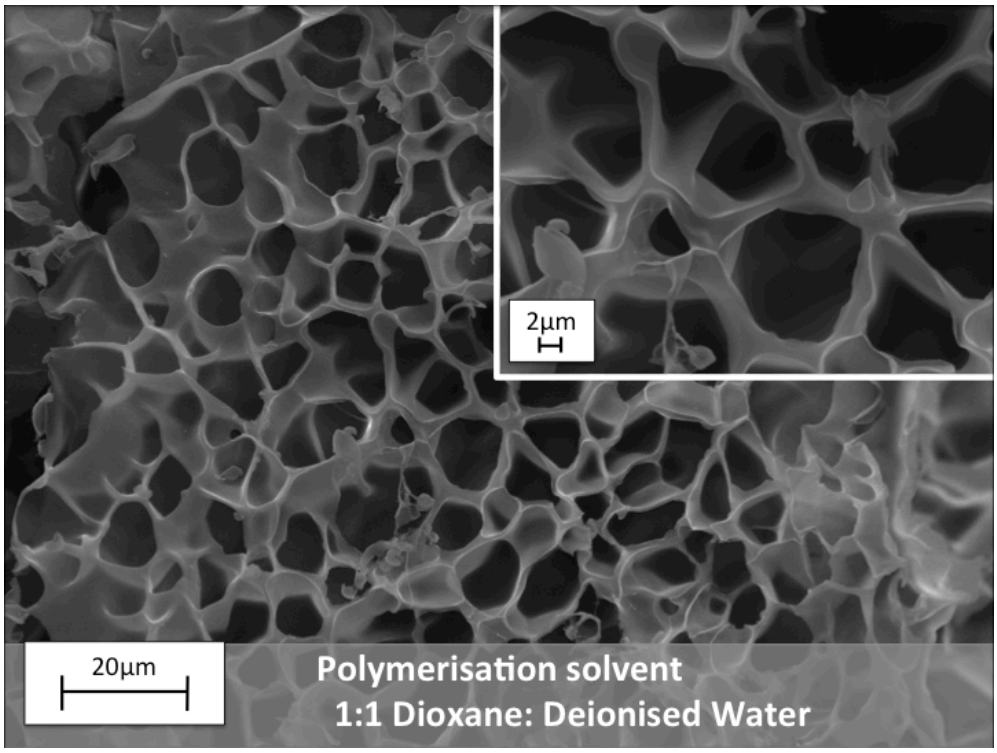

Figure A1.8. SEM image of hydrogel synthesised using 1:1 (V: V) ratio of Dioxane: DI water as the polymerisation solvent.

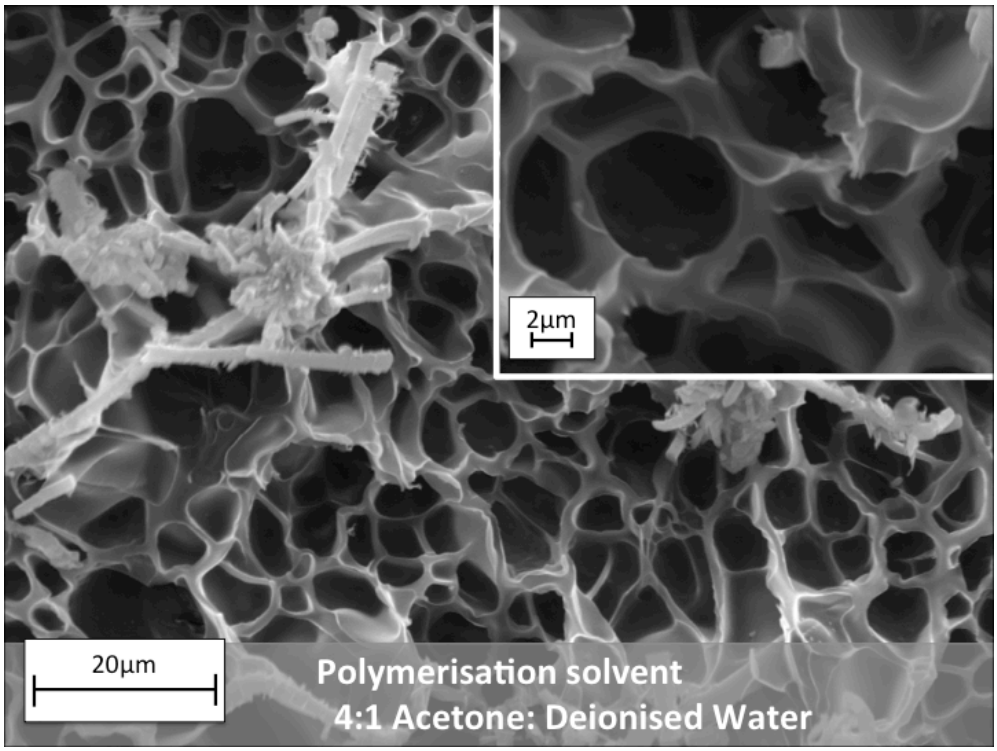

Figure A1.9. SEM image of hydrogel synthesised using 4:1 (V: V) ratio of Acetone: DI water as the polymerisation solvent.

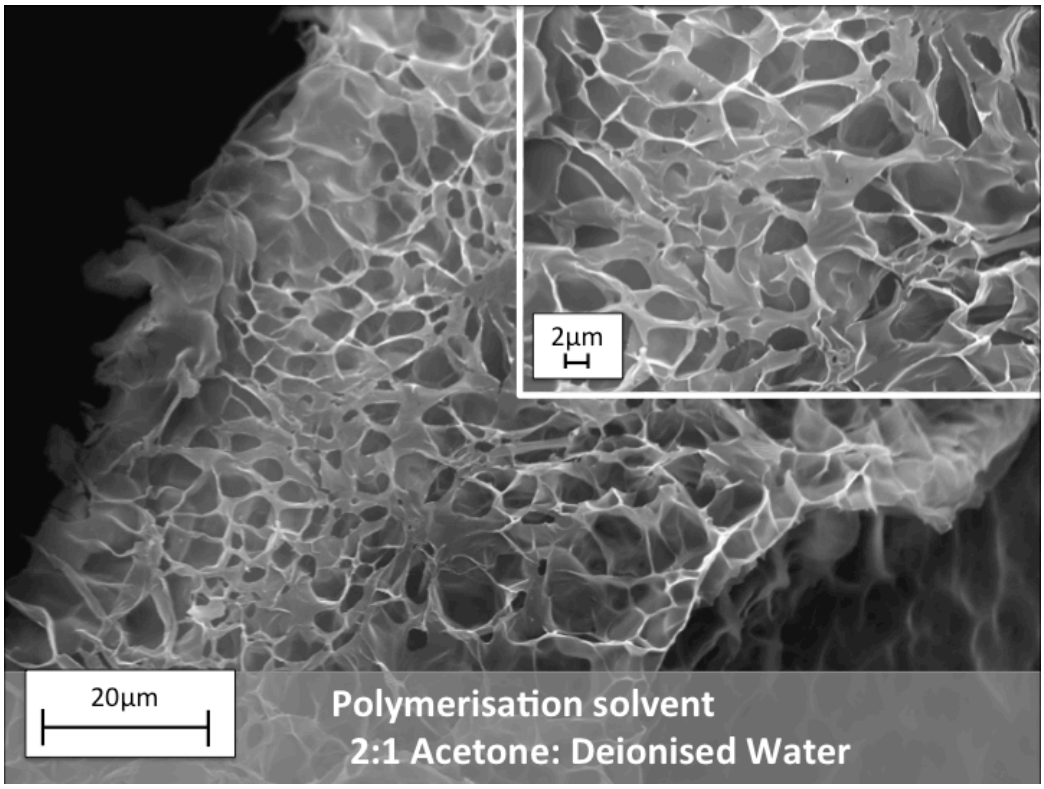

Figure A1.10. SEM image of hydrogel synthesised using 2:1 (V: V) ratio of Acetone: DI water as the polymerisation solvent.

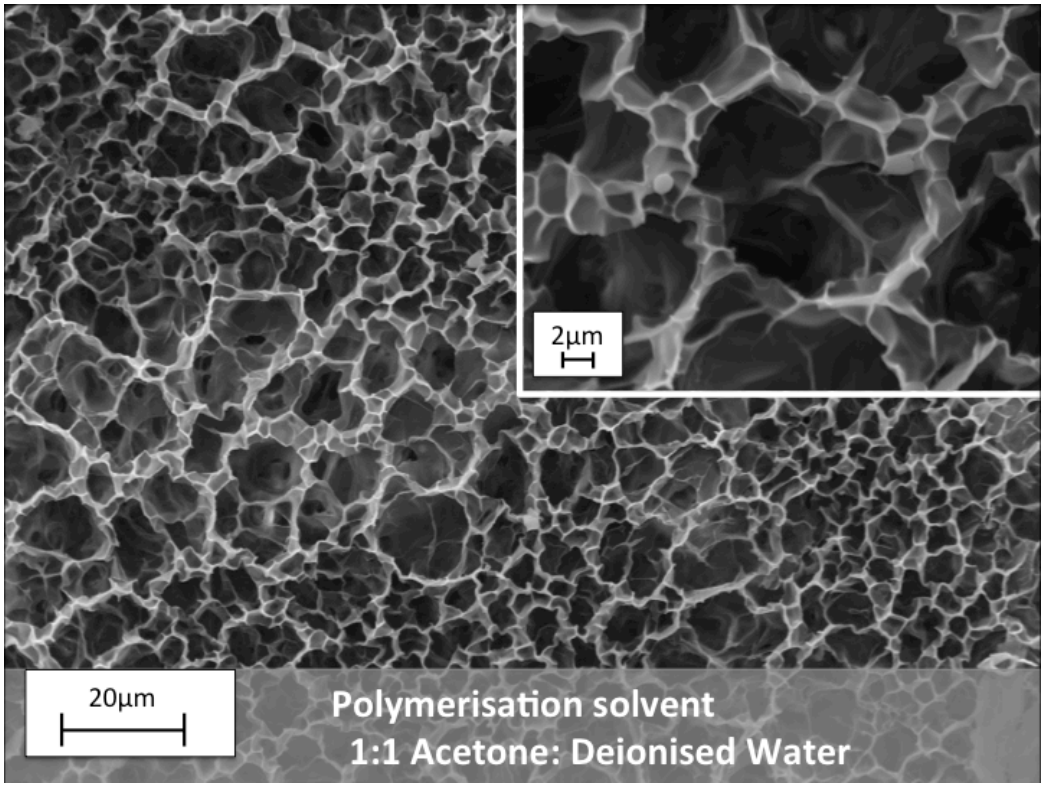

Figure A1.11. SEM image of hydrogel synthesised using 1:1 (V: V) ratio of Acetone: DI water as the polymerisation solvent.

Oscillation study:

The oscillation study was carried out on hydrated hydrogel samples. The results are presented as *Storage modulus versus Shear Stress. During the experiment, the shear stress was increased from 0.01 to 100%, while the Angular Frequency was kept at 100 rad/s at a normal force of 1N.*

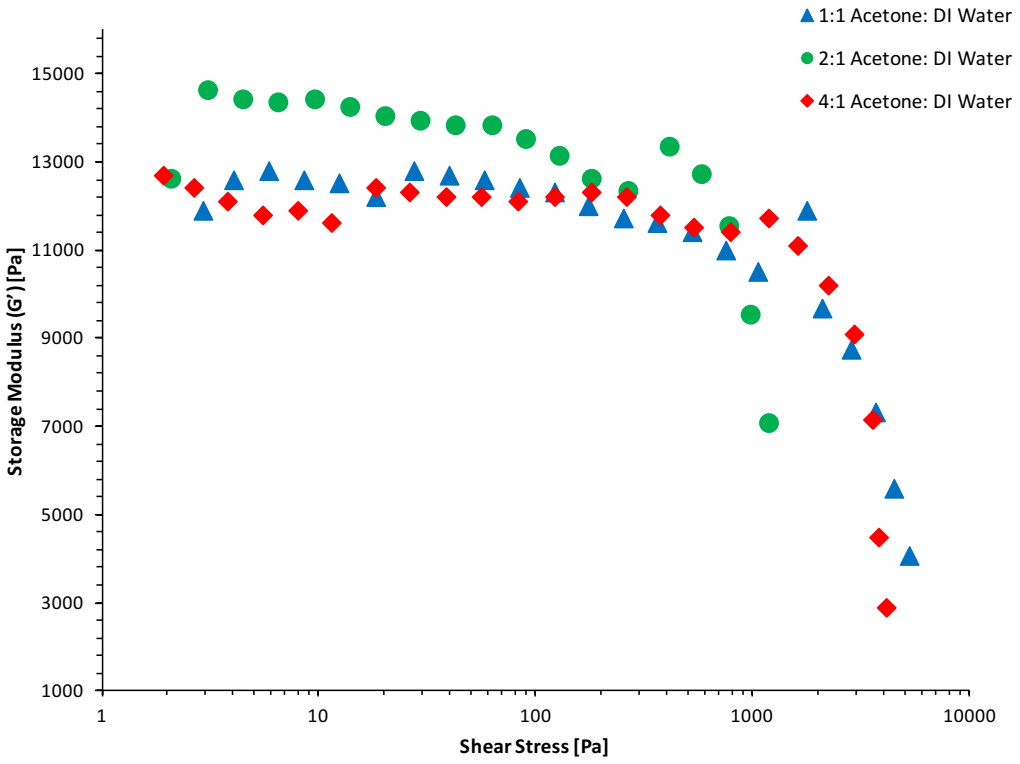

Figure A1.12. Storage modulus versus Shear Stress of the hydrated hydrogels polymerised in the presence of Acetone: DI water mixtures during a strain amplitude sweep (Frequency was 1N).

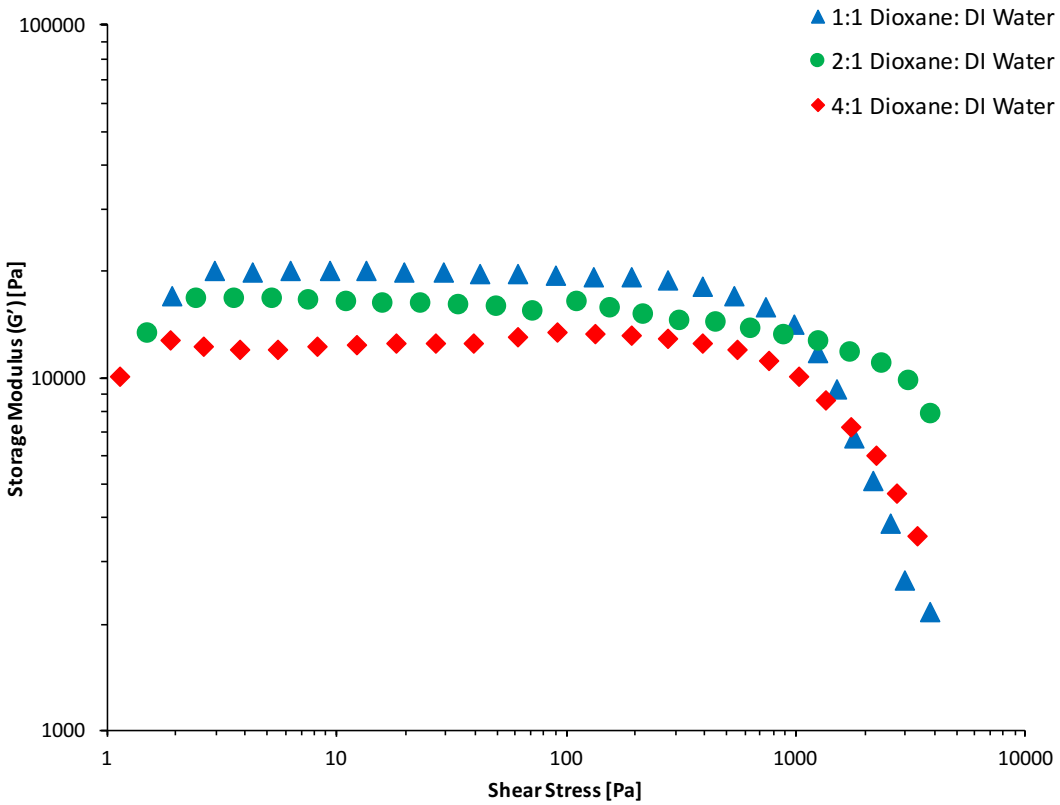

Figure A1.13. Storage moduli Versus Shear Stress of the hydrated hydrogels polymerised in the presence of Dioxane: DI water mixtures during a strain amplitude sweep (Frequency was 1N)

Photo-actuation:

For white light irradiation shrinking and reswelling measurements, the hydrogels were placed in a "in house" cell, comprised of 2 cover glass slides separated by 500 μm high spacers made out of PMMA/PSA arranged in a square fashion on the bottom glass slide. The hydrogel sample was placed in this "in house" cell and filled with deionised water. The cell was placed on a black background to aid the area measurements in the image J software. The hydrogel was measured under an Aigo digital-microscope –GE5 with a lens of X60 magnification during and after light actuation.

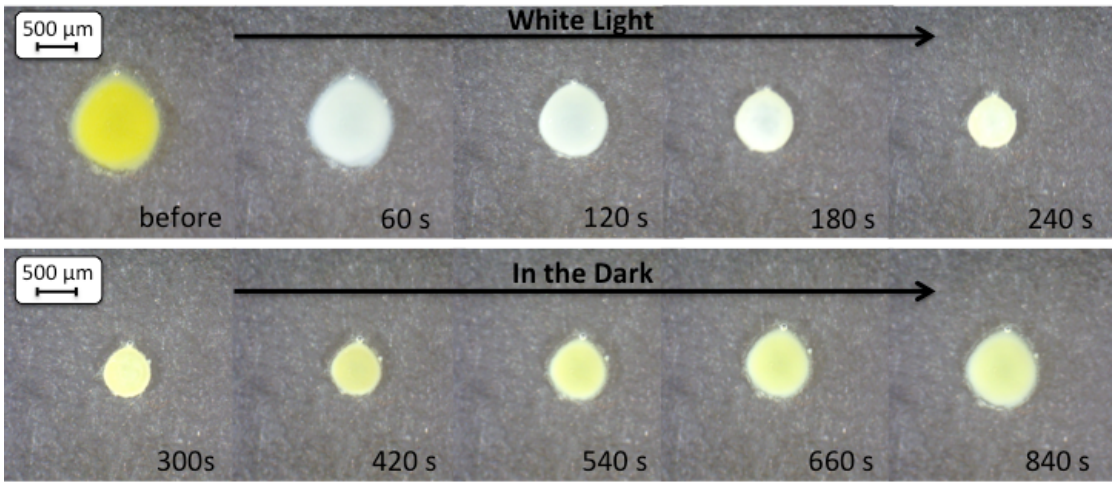

Figure A1.14. Microscope images (magnification X60) of the 4:1 Dioxane: DI water hydrogel during a shrinking and reswelling cycle.

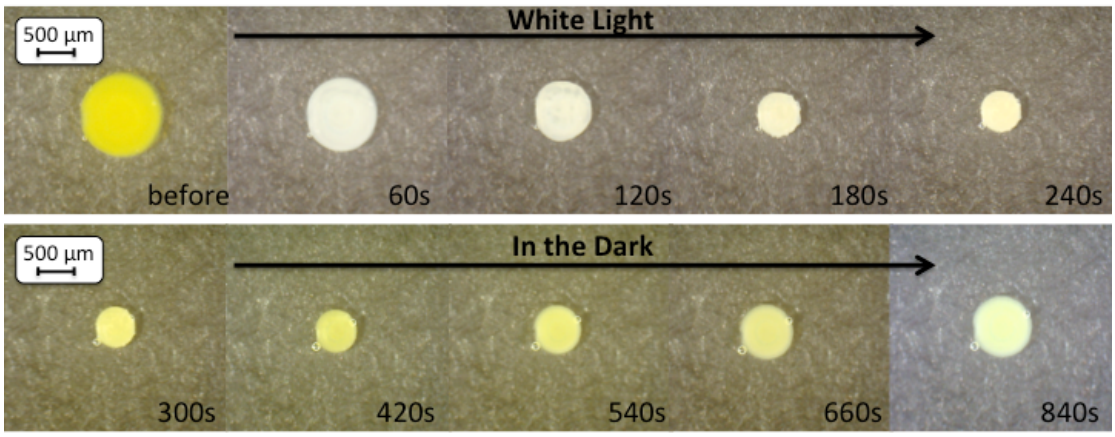

Figure A1.15. Microscope images (magnification X60) of the 2:1 Dioxane: DI water hydrogel during a shrinking and reswelling cycle.

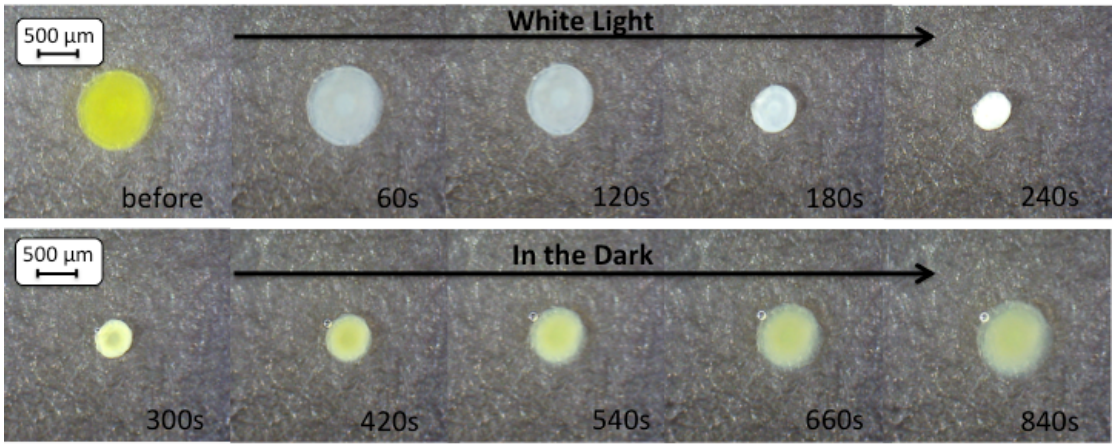

Figure A1.16. Microscope images (magnification X60) of the 1:1 Dioxane: DI water hydrogel during a shrinking and reswelling cycle.

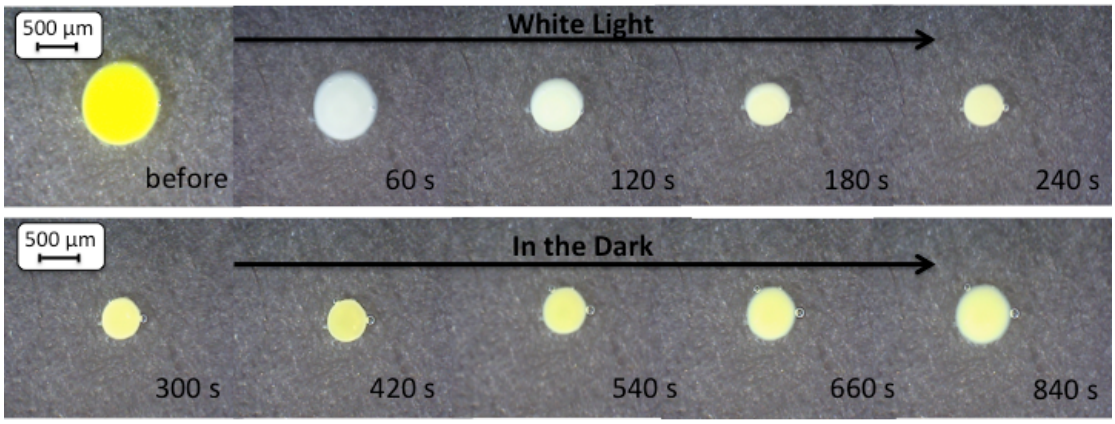

Figure A1.17. Microscope images (magnification X60) of the 4:1 Acetone: DI water hydrogel during a shrinking and reswelling cycle.

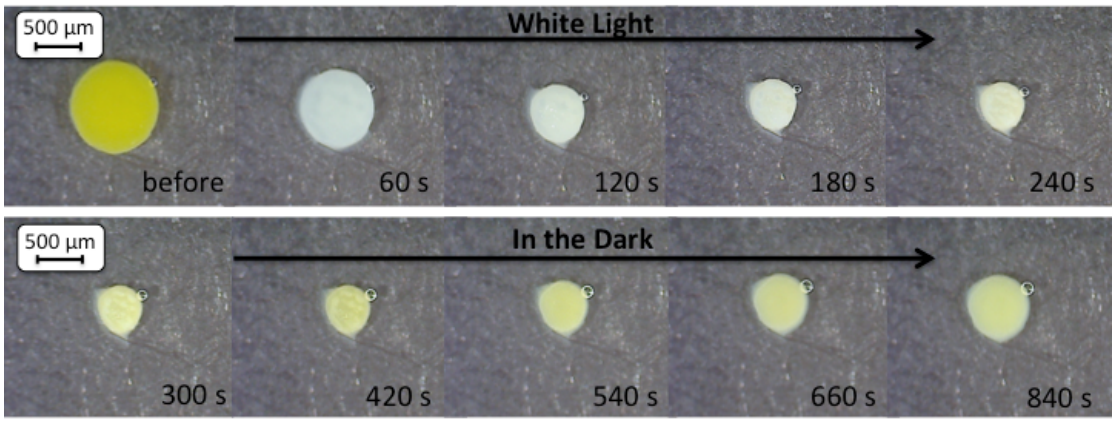

Figure A1.18. Microscope images (magnification X60) of the 2:1 Acetone: DI water hydrogel during a shrinking and reswelling cycle.

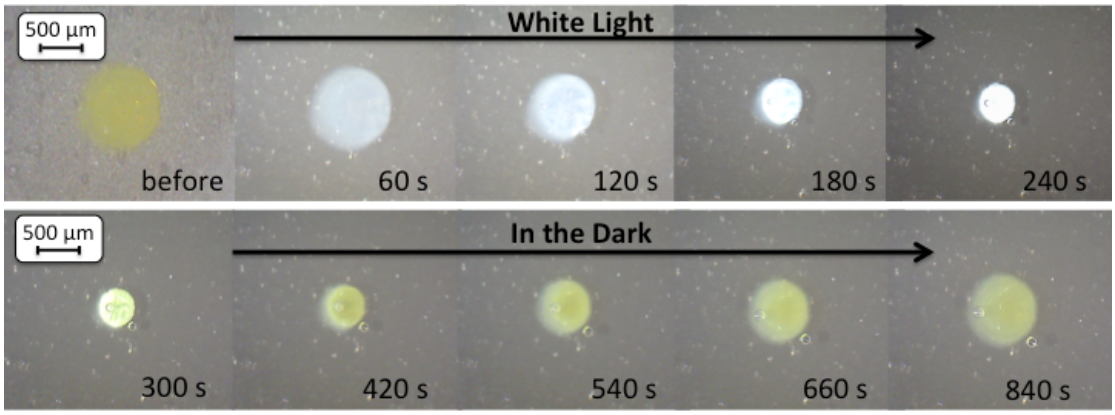

Figure A1.19. Microscope images (magnification X60) of the 1:1 Acetone: DI water hydrogel during a shrinking and reswelling cycle.

Photo-actuation measurements:

The area measurements of the freestanding hydrogel discs were done using Image J (1.47v) software. Three different hydrogels (n=3) were measured for each point and the relative area % was calculated as the ratio between the hydrogel area at specific times (A_t) and the area measurement of the hydrogel before actuation (A_0) as described in the following equation:

$$\text{Relative area \%} = \frac{A_t}{A_o} \times 100$$

A_t = measured area at time t

A_o = measured area of fully hydrated hydrogel.

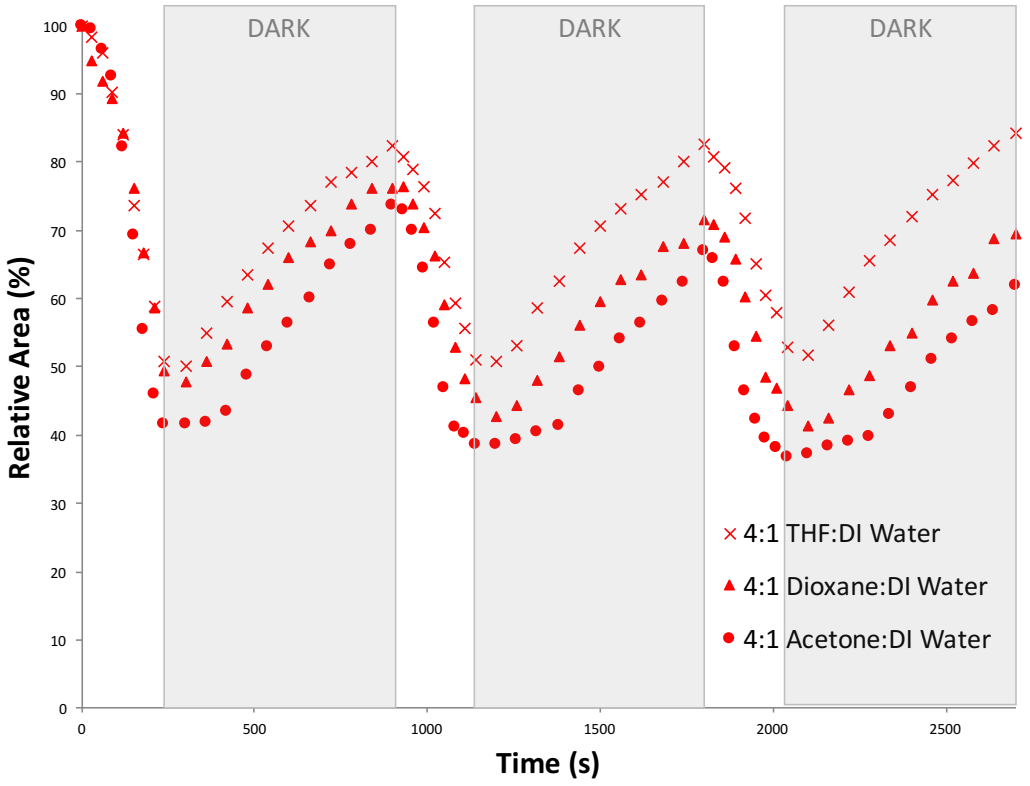

Figure A1.20. Photo-actuation cycles of hydrogels produced when the polymerisation solvent was 4:1 (V:V) organic solvent (THF, dioxane and acetone, respectively) : deionised water, in real time.

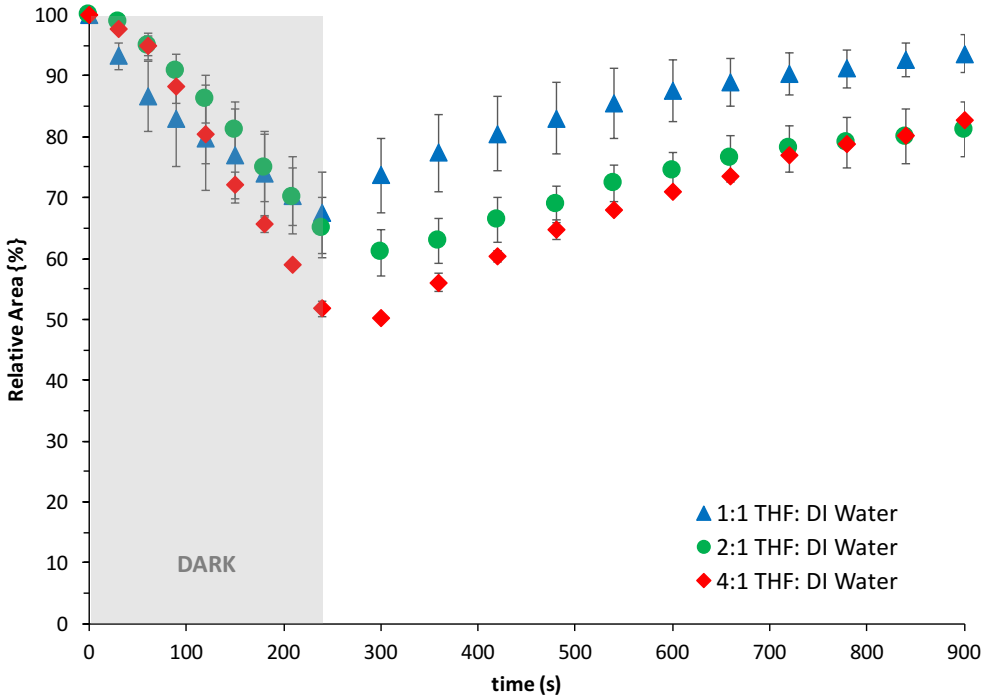

Figure A1.21. Single photo-actuation cycle of three different hydrogels produced when the polymerisation solvent was THF: DI water, in real time.

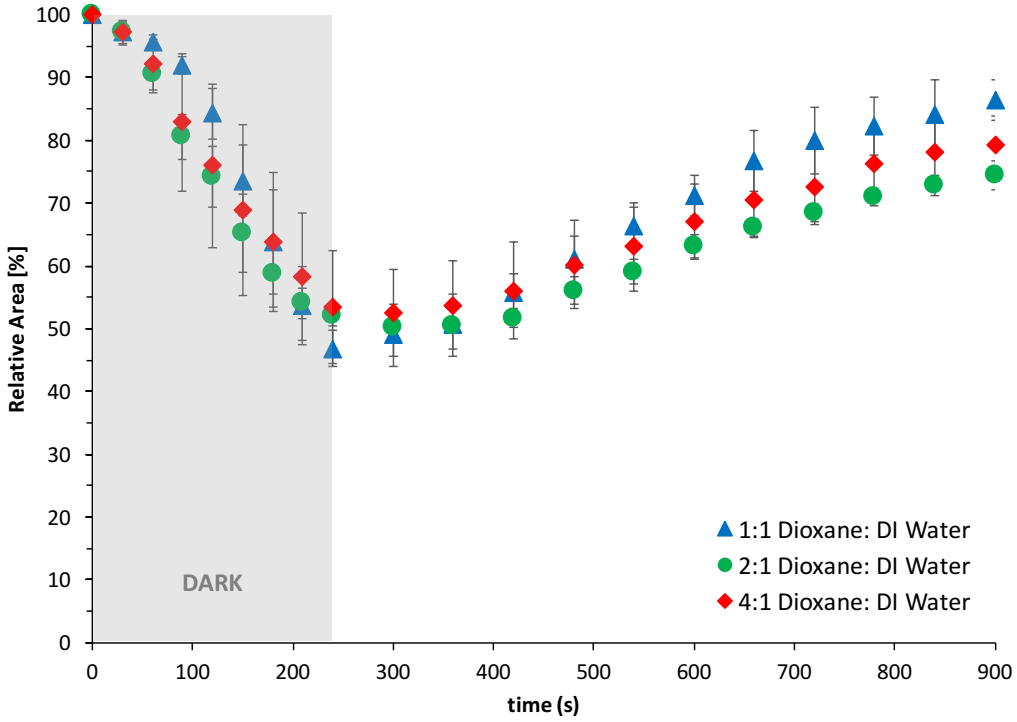

Figure A1.22. Single photo-actuation cycle of three different hydrogels produced when the polymerisation solvent was Dioxane: DI water, in real time.

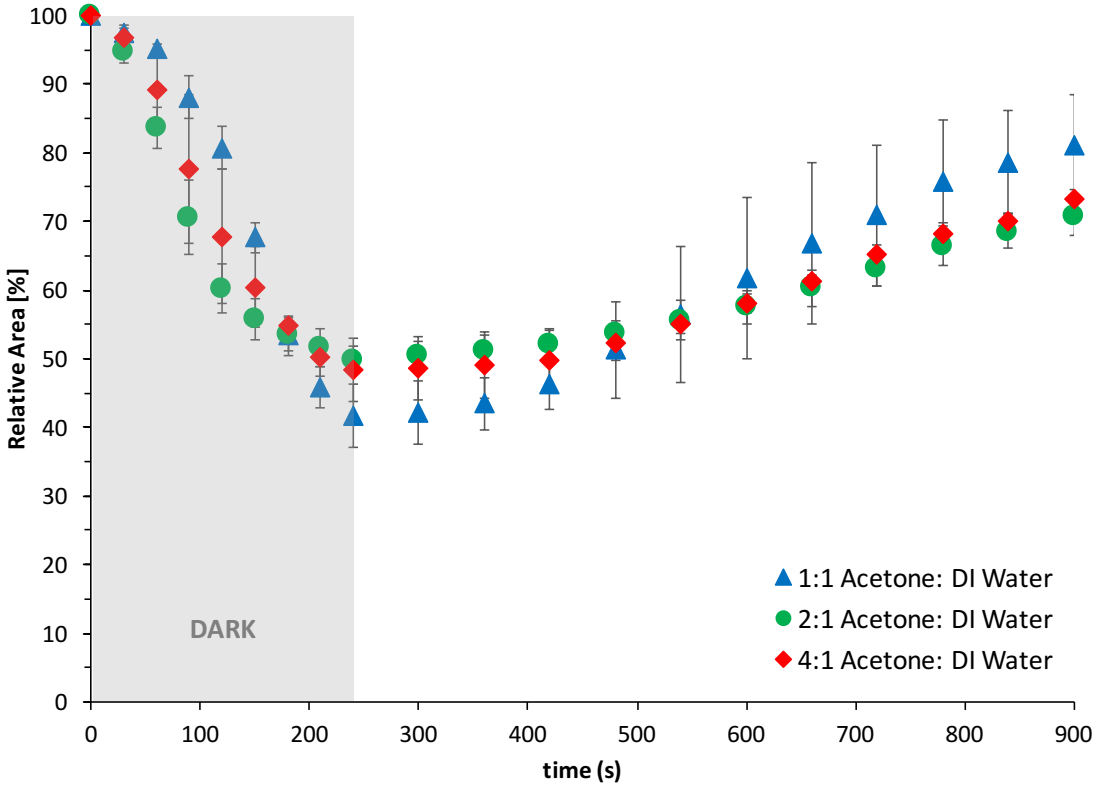

Figure A1.23. Single photo-actuation cycle of three different hydrogels produced when the polymerisation solvent was Acetone: DI water, in real time.

Appendix 2

Supporting Information for

Spiropyran Based Hydrogel Actuators – Walking in the Light*

***Spiropyran Based Hydrogels Actuators − Walking in the Light**, Wayne Francis, Aishling Dunne, Colm Delaney, Larisa Florea*, Dermot Diamond, *Sensors and Actuators B: Chem.* 250 (2017): 608-616.

Rheology:

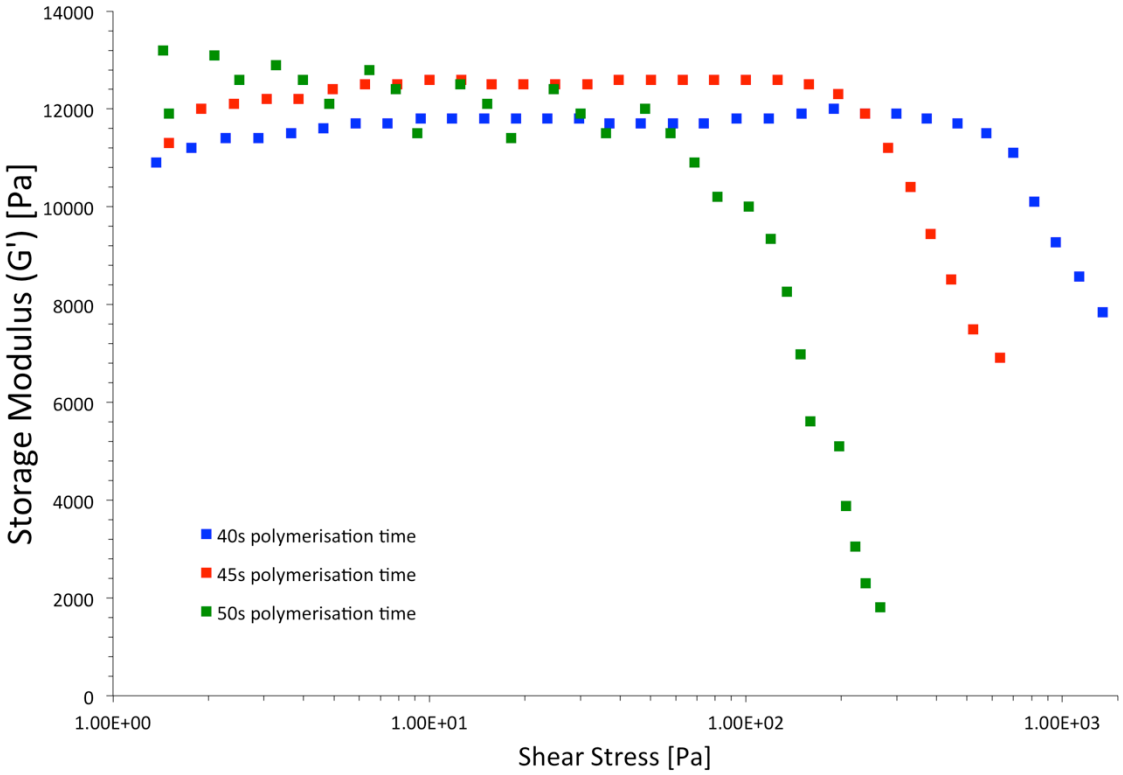

Figure A2.1. Storage moduli versus shear stress of the hydrated hydrogels polymerised during 40 s, 45 s and 50 s of white light irradiation, respectively, using a strain amplitude sweep with a normal force of 1 N.

Hydrogel Walker Actuation:

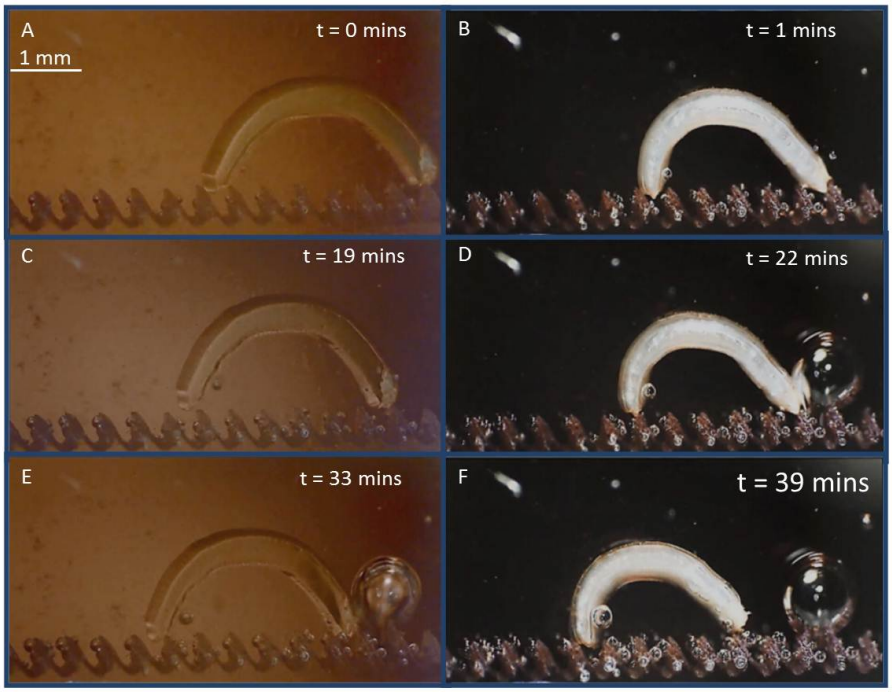

Figure A2.2*. Series of snapshots showing the walking behaviour of the hydrogel (**Video S2**); A - shows the initial position of the hydrogel before any white irradiation; B, D and F show the contraction of the trailing leg during respective white light irradiation phases. C and E show how the swelling in the dark (after the respective white light irradiation phases) results in the forward leg being pushed over the ratchet.*

Videos:

Video A2.1 demonstrates the observed locomotion of the p(NIPAAm-*co*-SP-*co*-AA) hydrogels. The ratcheted channels in this video are filled with deionised water. Once the hydrogel had been securely placed onto the ratchet, it was irradiated with white light (~305 kLux). After the trailing leg had been dragged across at least one of ratcheted steps, the light was removed. When the leading leg had been pushed over at least one of the ratchet steps the light was re-introduced. This was repeated until the walker moved out of frame, resulting in a walking motion across 5 ratchet steps. For convenience the speed of the video was increased by a factor of 64.

Video A2.2 shows another example of the walking motion of a p(NIPAAm-*co*-SP-*co*-AA) hydrogel. The channel was again filled with DI water. Similarly to the above example, the walker was irradiated with white light (~305 kLux) until the trailing leg had been dragged across at least one of the walker steps. The white light was then removed and the walker was monitored in real time until the leading leg had been pushed across at least one of the ratchet steps. This was repeated until the walker got dislodged from the ratchet. The walker in this video completed three full cycles of white light irradiation and walked across 7 of the ratchet steps. For convenience the speed of the video was increased by a factor of 64.

Appendix 3

Supporting Information for

Micro-capillary Coatings Based on Spiropyran Polymeric Brushes for Metal Ion Binding, Detection and Release in Continuous Flow*

***Micro-Capillary Coatings Based on Spiropyran Polymeric Brushes for Metal Ion Binding, Detection, and Release in Continuous Flow**, Aishling Dunne, Colm Delaney, Aoife McKeon, Pavel Nesterenko, Brett Paull, Fernando Benito-Lopez, Dermot Diamond, Larisa Florea*, *Sensors,* 2018, 18(4), 1083 – 1095.

polySP polymeric brushes functionalised micro-capillary:

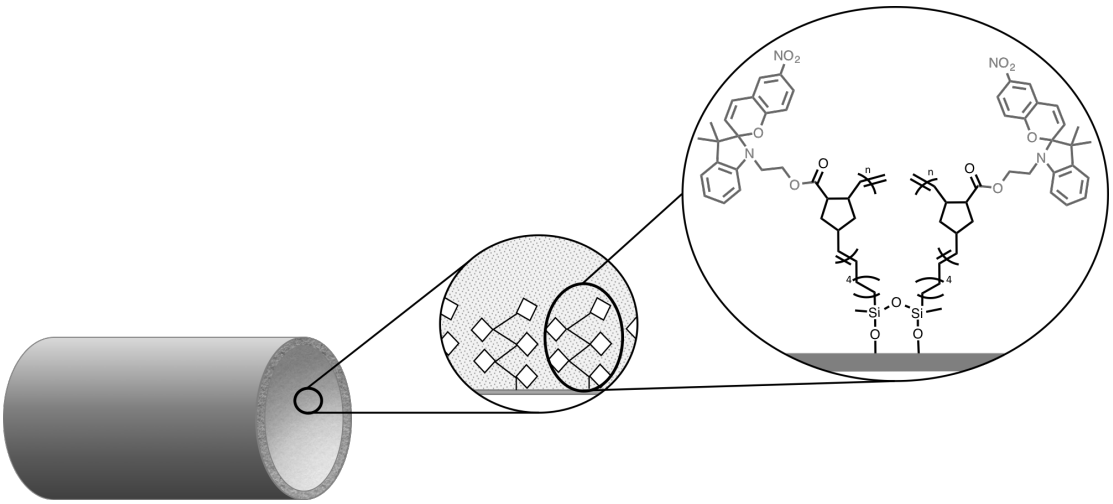

Figure A3.1. Schematic representation of the polySP polymeric brush structure and functionalised micro-capillary.

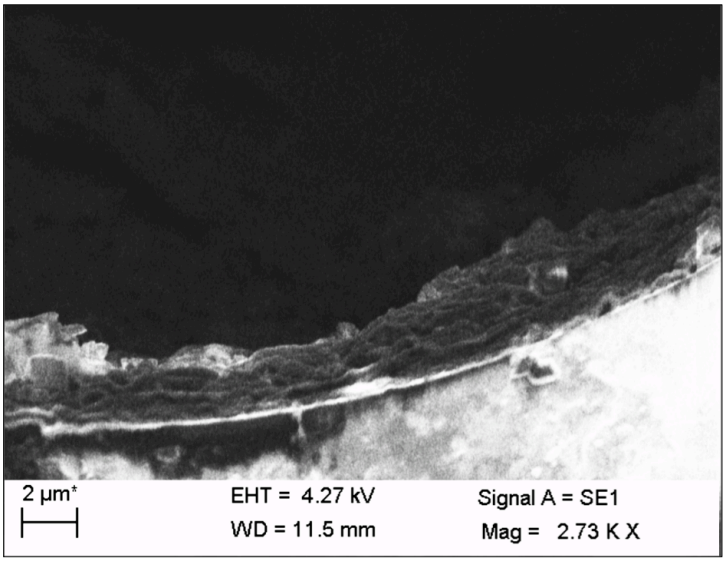

Figure A3.2. Scanning Electron Microscopy image of the polySP polymeric brushes functionalised micro-capillary.

Set-up for absorbance measurements of micro-capillaries:

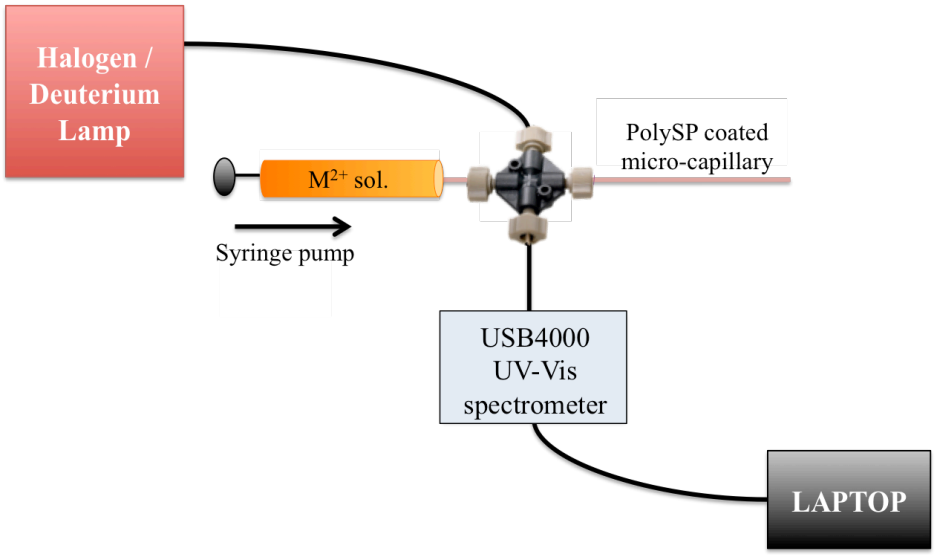

Figure A3.3. Set-up used to study the absorbance spectra of the micro-capillary when M^{2+} solutions (in ACN) are passed through the micro-capillary in continuous flow. The set-up is composed of a two fiber-optic light guides connected to a light source and a Miniature Fiber Optic Spectrometer (USB4000, Ocean Optics) and aligned using a cross-shaped cell. The M^{2+} solution (in ACN) is passed through the micro-capillary using a syringe pump.

Photo-induced binding and releasing of metal ions:

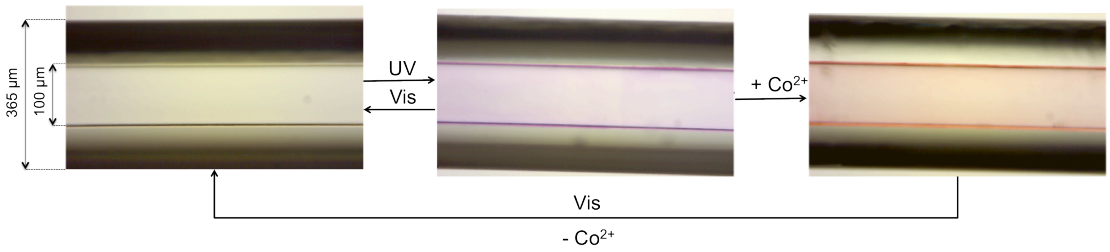

Figure A3.4. Microscopy photos of a section of a micro-capillary modified with spiropyran polymer brushes (polySP) before (left) and after irradiation for 20 s with UV light (middle) followed by the addition of Co^{2+} (right). The micro-capillary returns to colourless (due to the conversion of the polyMC to polySP) after irradiation with white light for 1 min, resulting in the release of Co^{2+} ions.

In order to prove the release of the bound metal ion from the SP-polymer brushes coated micro-capillary through irradiation with white light, the release of metal ion

was demonstrated in the case of Co^{2+} through detection post modified micro-capillary using a chelating reagent, 4-(2-pyridylazo)resorcinol (PAR). PAR can coordinate to metal ions through a heterocyclic nitrogen group, azo group, and *o*-hydroxyl group, as shown in Figure A3.5 [1-3].

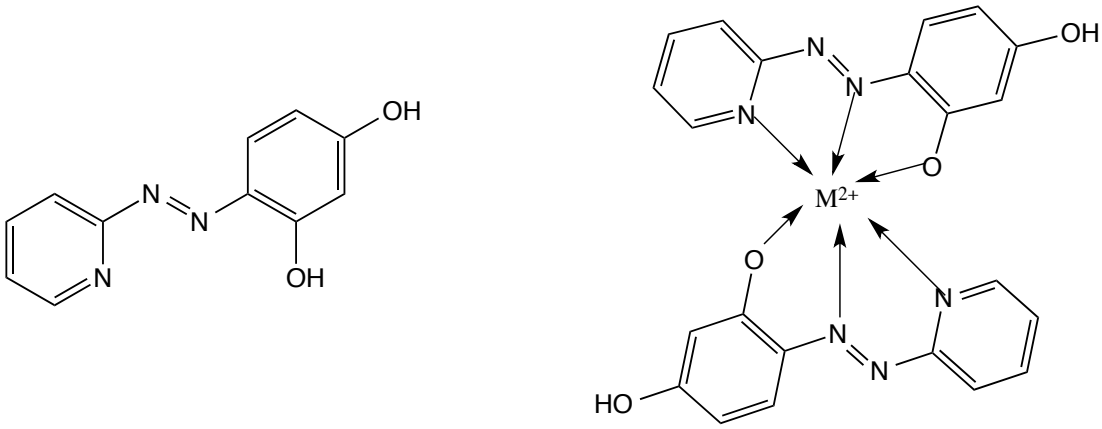

Figure A3.5. Chemical structures of 4-(2-pyridylazo) resorcinol (left) and metal complexed 4-(2-pyridylazo) resorcinol (right).

Firstly, the absorbance spectra of the chelating reagent (PAR) and its Co^{2+} complex were recorded (Figure A3.6) by passing a solution of PAR (1 mM) and PAR-Co^{2+} (PAR: Co^{2+} 1:1) through an unmodified glass micro-capillary at 2 µL min^{-1}. The spectra (Figure A3.6) show the typical absorbance bands corresponding to PAR (black) and PAR-Co^{2+} (red). The absorbance maximum for PAR-Co^{2+} was recorded at ~ 510 nm.

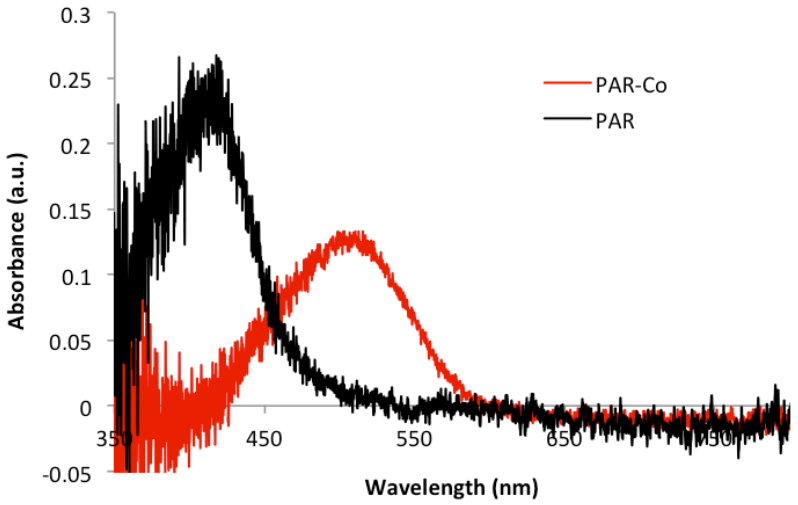

Figure A3.6. Absorbance spectra of the chelating reagent (PAR) and its Co^{2+} complex.

For the detection of the photo-released Co^{2+}, the previous set-up (Figure A3.6) was modified (Figure A3.7) to include the injection of Co^{2+} solution in ACN (1 mM), and the following steps were undertaken:

1. The pump (left) was turned on (flow rate = 20 µL min^{-1}; mobile phase = ACN).
2. The syringe pump (right) was turned on (flow rate = 20 µL min^{-1}; mobile phase = post column reagent PAR 0.1 M).
3. The polySP modified micro-capillary was irradiated with UV light for 20 s.
4. Co^{2+} solution (1 mM) from the injection loop was injected in the system at a flow rate of 20 µL min^{-1} for approximately 5 min.
5. When all the expected Co^{2+} solution left the detection area, both pumps (ACN and PAR) were turned *OFF* and the while light was turned *ON*.
6. After about 5 min, both pumps (ACN and PAR) were turned back *ON*.
7. The absorbance at λ_{max} specific for PAR-Co^{2+} (510 nm) was recorded during the whole experiment (steps 1-6) and plotted in Figure A3.8.

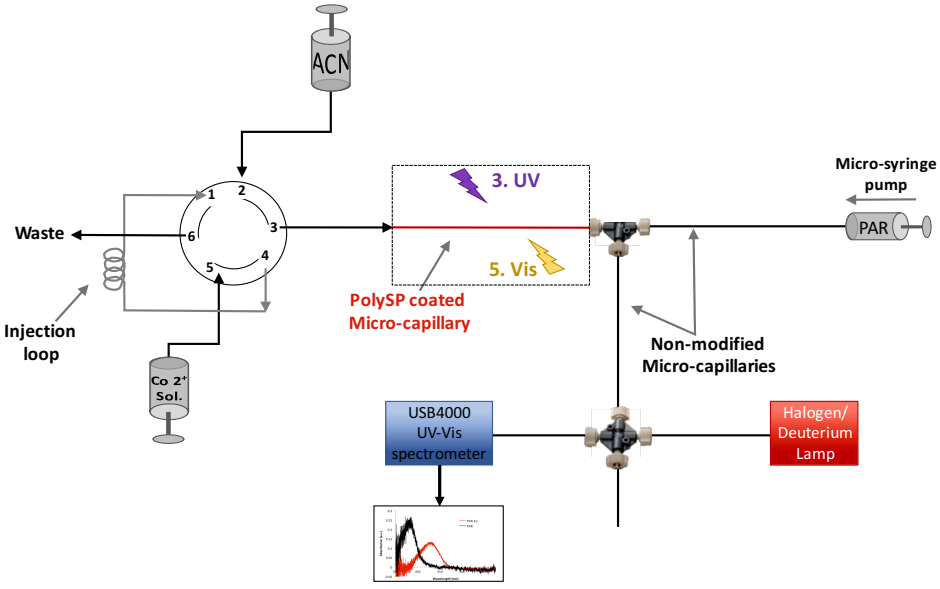

Figure A3.7. Scheme of the set-up used for the determination of metal ions photo-released from the polySP modified micro-capillary using PAR. Step 3 (irradiation of the spiropyran modified micro-capillary with UV light) and 5 (irradiation of spiropyran modified micro-capillary with white light) are depicted in the scheme.

It is expected that, after the irradiation of the micro-capillary with white light (step 5), the Co^{2+} ions will be released and then, with both pumps turned ON, the two

confluent flows will react and PAR-Co^{2+} will be formed. When reaching the detection area, PAR-Co^{2+} will generate a change in the absorption spectra, generating a new absorbance band at 510 nm. This absorbance band (Figure A3.8) was recorded during the experiment (steps 1 to 6) and shows an increase in the absorbance band at 510 nm when both the PAR flow (step 2) and Co^{2+} flow (step 4) are turned ON. When the Co^{2+} flow is turned OFF (step 5), a decrease in the band at 510 nm is observed until this reaches an absorbance of ~0 a.u. indicating that all Co^{2+} has exited the detection area. Following this, the PAR flow is also switched OFF and the SP-M polymeric brushes functionalised micro-capillary is irradiated with white light for 5 minutes. Finally, the ACN and PAR flows are switched ON. This causes an increase in the band at 510 nm (Figure A3.8, step 6) indicating that indeed Co^{2+} was released upon white light irradiation from the modified micro-capillary.

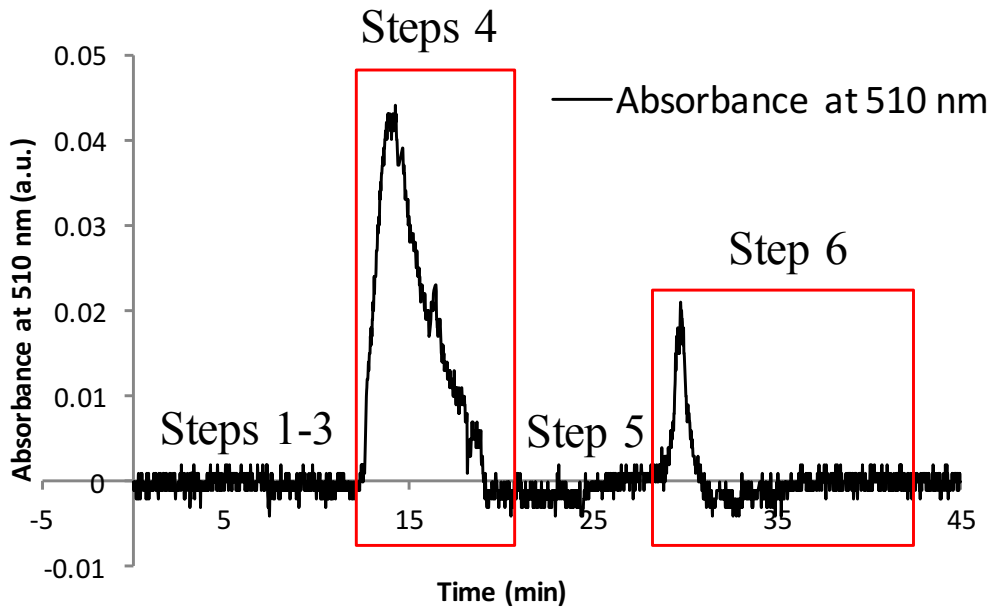

Figure A3.8. Absorbance at 510nm recorded on a USB400 spectrometer using the set-up depicted in Figure A3.7 during experimental steps 1-6. The increase of the absorbance band centred at 510nm indicates the presence of PAR-Co^{2+} complex.

Videos:

Video A3.1 shows in real time the colour change of the spiropyran norbornene monomer crystals under different illumination conditions. In the video, the UV light was turned ON at 0:45 and switched OFF after ~ 2 min (time 2:49), followed by ~ 3

min of white light irradiation (white light ON at 5:13 and switched OFF at 8:21). The video was recorded on a benchtop Aigo digital Microscope GE5, at a magnification of 180x.

References:

1. Ghasemi, J.; Niazi, A.; Maeder, M. Spectrophotometric studies on the protonation and nickel complexation equilibria of 4-(2-pyridylazo) resorcinol using global analysis in aqueous solution. *Journal of the Brazilian Chemical Society* **2007**, *18*, 267-272.
2. Ghasemi, J.; Peyman, H.; Meloun, M. Study of complex formation between 4-(2-pyridylazo) resorcinol and Al^{3+}, Fe^{3+}, Zn^{2+}, and Cd^{2+} ions in an aqueous solution at 0.1 m ionic strength. *J. Chem. Eng. Data* **2007**, *52*, 1171-1178.
3. Chen, Q.; Feng, Y.; Zhang, D.; Zhang, G.; Fan, Q.; Sun, S.; Zhu, D. Light‐triggered self‐assembly of a spiropyran‐functionalized dendron into nano‐/micrometer‐sized particles and photoresponsive organogel with switchable fluorescence. *Advanced Functional Materials* **2010**, *20*, 36-42.